MULTINUCLEAR COPPER(I) AND SILVER(I) PYRAZOLATES:

SYNTHESIS, LUMINESCENCE, AND CATALYSIS

by

MONIKA R. PATTERSON

DISSERTATION

Submitted in partial fulfillment of the requirements
for the degree of Doctor of Philosophy at
The University of Texas at Arlington
December 2021

Arlington, Texas

Committee:
Rasika Dias, Supervising Professor
Frederick MacDonnell
Robin Macaluso
Kayunta Johnson-Winters

Acknowledgements

I would like to express my sincerest gratitude to Dr. Rasika Dias for his mentorship and support throughout my graduate studies. His guidance, insights, patience, motivation, and financial support has greatly enriched my research experience. I would also like to thank my dissertation committee members, Dr. Frederick MacDonnell, Dr. Robin Macaluso, and Dr. Kayunta Johnson-Winters, for their insight and suggestions. I would also like to acknowledge the Department of Chemistry and Biochemistry at the University of Texas at Arlington, Robert A. Welch Foundation, and National Science Foundation for financial support.

I am extremely grateful to the Dias group members, both past and present, for being both my friends and colleagues and for their support and help throughout my graduate studies – Dr. Devaborniny Parasar, Anurag Noonikara Poyil, Adway O. Zacharias, Brandon T. Watson, Dr. Mukundam Vanga, Deepika Karade, and Vo Quang Huy Phan. I would like to additionally thank the faculty members and staff of the Department of Chemistry and Biochemistry, and all my collaborators.

Most importantly, I would like to thank my amazing family. My husband, Trae Patterson, my parents, Ross and Kathy Hailey, my sister, Emily Walker, and grandparents, Herbert and Antoinette Critser and Christine Hailey, for all their support, love, and encouragement. All of you have believed in me and helped me fulfill this dream to get where I am today. I am forever grateful.

November 15, 2021

Abstract

MULTINUCLEAR COPPER(I) AND SILVER(I) PYRAZOLATES: SYNTHESIS, LUMINESCENCE, AND CATALYSIS

Monika Rose Patterson, Ph.D.

The University of Texas at Arlington, 2021

Supervising Professor: H. V. Rasika Dias

Copper and silver pyrazolate complexes have numerous fascinating properties such as luminescence, catalytic ability, and complexation with small molecules. Using both more widely studied non-fluorinated pyrazolates and less common highly fluorinated pyrazolates as supporting ligands, we successfully synthesized and investigated several new coinage metal complexes. Synthetic details, structures, and properties i.e., luminescence and catalytic ability, have been studied.

Chapter 2 of this research describes the synthesis of a new pyrazole with highly fluorinated aryl groups and corresponding trinuclear copper(I), silver(I), and gold(I) complexes. All three metal complexes exhibit bright blue luminescence under exposure to UV light. Additionally, the copper(I) complex proved to be an excellent catalyst in azide-alkyne cycloadditions.

Chapter 3 discusses the synthesis and characterization of four new non-fluorinated copper(I) and silver(I) pyrazolates with ethyl ester substituents on the pyrazole ligand. These complexes were investigated as potentially cheaper

and more common alternatives to highly fluorinated coinage metal complexes. Despite the electronic and steric similarities, these new non-fluorinated trimers were not found to exemplify the same properties as the previously reported fluorinated analogs.

Chapter 4 compares several trinuclear and tetranuclear copper(I) pyrazolates in copper catalyzed azide-alkyne cycloaddition reactions (CuAAC). Previous work has shown copper(I) trimers with fluorinated pyrazoles are excellent stand-alone catalysts for these reactions. In this chapter we found copper(I) trimers with less or non-fluorinated pyrazolates are poor catalyst. However, copper(I) tetramers, even with electron donating alkyl substituents on the pyrazole, are excellent catalysts. To gain further understanding, the solution behavior of several copper(I) trimers and tetramers are studied using vapor pressure osmometry and some kinetic experiments were performed.

Chapter 5 describes the synthesis of heteroleptic complexes using {[3,5-$(CF_3)_2$Pz]Cu}$_3$ and bis(diphenylphosphinomethane). The resulting copper(I) pyrazolate complexes with bis(diphenylphosphinomethane) have interesting luminescent properties that could provide potential applications as an inorganic LED.

Table of Contents

List of Figures

List of Tables

Chapter 1

Introduction

1.1 Pyrazole Ligand

Pyrazoles are an important class of molecules containing five-membered heterocyclic rings with three carbon atoms and two adjacent nitrogen atoms (Figure 1.1). One of the most attractive features of pyrazoles is that they are easily tunable ligands. By simply changing the substituents on the 3-, 4-, and 5-positions of the pyrazole ring, the steric and electronic properties of this ligand can be changed. This tunability at three possible positions allows for pyrazoles to be a highly versatile ligand with applications across inorganic, bioinorganic, and organometallic chemistry.[1, 2]

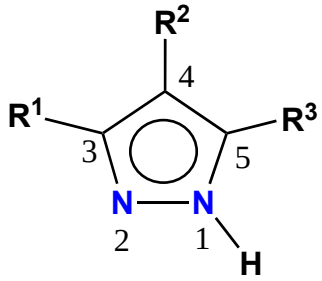

Figure 1.1 Pyrazole Ligand

These molecules are well-known nitrogen donors and can behave as monodentate or bidentate ligands after deprotonation of the N1-*H*. Upon deprotonation, the pyrazolate ion can coordinate to metals in several different ways, such as a bridging ligand using both nitrogen donor sites in both an *exo*- and *endo*- manner. This versatility has allowed pyrazolates to be a useful ligand for most metals across the periodic table.[3] A focus of our laboratory has been the synthesis and study of coinage metal complexes, often with pyrazolate ligands. These ligands can strongly bind to coinage metal ions Cu(I), Ag(I), and

Au(I) in a neutral monodentate, anionic monodentate, or as previously mentioned, *exo*/*endo*-bidentate fashion (Figure 1.2).[4] Depending on the substituents on the pyrazolate backbone and the reaction conditions, these coinage metal complexes can adopt many conformations such as monomers, dimers, trimers, tetramers, hexamers, and polymers. The degree to which the complexes aggregate can be manipulated by changing the pyrazolate substituents and reaction conditions.

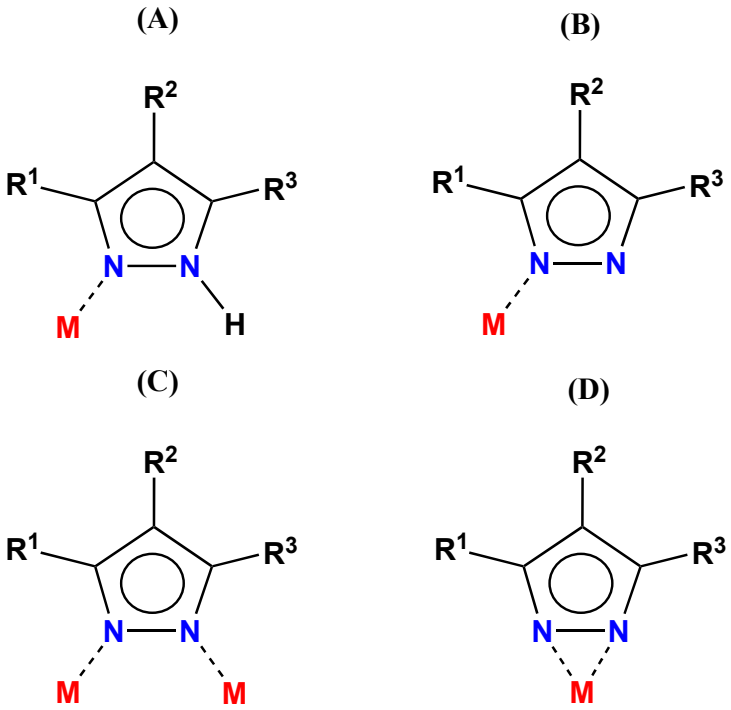

Figure 1.2 Coordination modes of pyrazole ligand. (A) neutral monodentate, (B) anionic monodentate, (C) exo-bidentate, and (D) endo-bidentate.

For example, when using pyrazole with hydrogen atoms on the 3-, 4-, and 5- positions, a polymeric copper complex is formed, $[Cu(Pz)]_n$.[3, 4] Increasing the steric demand of the pyrazolate causes an increase in nuclearity as seen in the trimeric $\{[3,5\text{-}(i\text{-}Pr)_2Pz]Cu\}_3$,[5-7] tetrameric $\{[(3,5\text{-}(t\text{-}Bu)_2Pz]Ag\}_4$,[6, 8] and hexameric $\{[3,5\text{-}(Ph)_2Pz]Au\}_6$.[9] The nuclearity is also dependent on the size of

the coinage metal used, as observed when using 3-(*i*-Pr)-5-(*t*-Bu)PzH. The copper and gold complexes with this pyrazolate adopts a tetrameric structure, {[3-(*i*-Pr)-5-(*t*-Bu)Pz]Cu}$_4$ and {[3-(*i*-Pr)-5-(*t*-Bu)Pz]Au}$_4$, while the silver complex forms a trimeric structure, {[3-(*i*-Pr)-5-(*t*-Bu)Pz]Ag}$_3$.[6, 10, 11] For this study, we focused on only the *exo*-bidentate coordination mode to allow for the formation of multinuclear coinage metal complexes, such as the ones previously mentioned.

A literature search of previous complexes with pyrazolate ligands indicates that most work with metal ions has been limited to the parent ligand, $[Pz]^-$, and electron-rich alkyl and aryl pyrazolates such as $[3,5\text{-}(CH_3)_2Pz]^-$ and $[3,5\text{-}(Ph)_2Pz]^-$.[6] Comparatively less work has been done on pyrazolate ligands with fluorinated substituents, despite the interesting properties fluorine endows on molecules..[5, 12, 13] The presence of C-F bonds on the pyrazole moiety significantly modifies the electronic properties of the ligand by making it more electron-deficient. This, in turn, provides the complexes of these pyrazolates with interesting properties such as high oxidative resistance, thermal stability, higher volatility, longer shelf life, and interesting photophysical and catalytic properties.[1, 14] Several of these fluorinated pyrazolates have been studied in our laboratory, such as $[3,5\text{-}(CF_3)_2Pz]^-$. However, these fluorinated pyrazolates are less common than their non-fluorinated counterparts.[5] So, while the fluorinated analogs afford many attractive properties, the non-fluorinated analogs are more economically practical in some cases. For this study we examine both fluorinated and non-fluorinated pyrazolates for various applications, such as luminescent materials and catalysts, to further expand the relatively less studied fluorinated pyrazolate complexes while also studying non-fluorinated

pyrazolate complexes in hopes of finding a more common, but equally active, complex.

1.2 Coinage metal metallacycles

One of the main focuses of research in our laboratory is the study of coinage metal (Cu, Ag, and Au) complexes with pyrazole ligands. Several coinage metal pyrazolates have been reported in the literature with *exo*-bidentate coordination ranging from trimers to polymers, Figure 1.3.

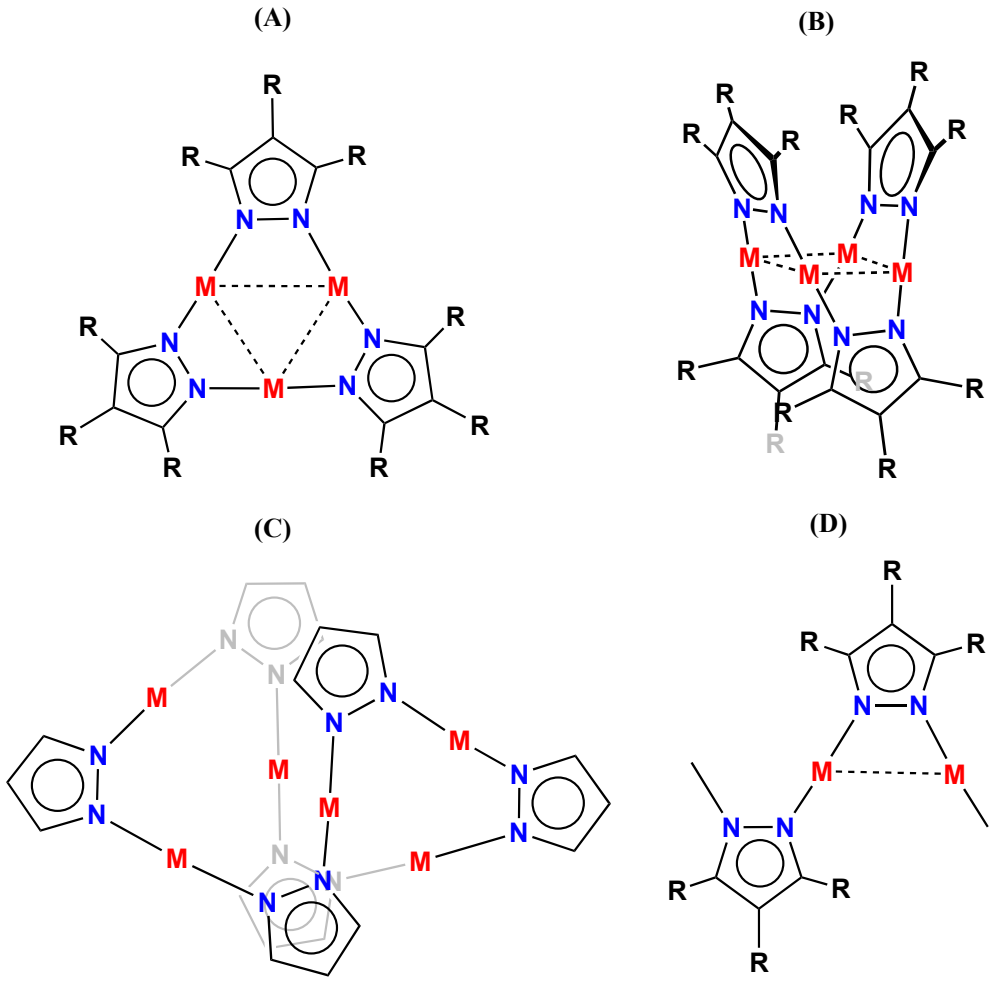

Figure 1.3 Coinage metal pyrazolates with varying levels of aggregation. (A) trimeric, (B) tetrameric, (C) hexameric, pyrazolate substituents removed for clarity, and (D) polymeric.

For example, several trimeric copper(I) pyrazolates, such as {[3,5-$(CH_3)_2$Pz]Cu}$_3$[5] and {[3,5-(*i*-Pr)$_2$Pz]Cu}$_3$,[5] have been previously reported. Additionally, tetrameric copper(I) pyrazolates, such as {[3,5-(*t*-Bu)$_2$Pz]Cu}$_4$[11] and {[3,5-(dcsb)$_2$Pz]Cu}$_4$ (dscb = dicarbo-*sec*-butyoxy),[11] and polymeric, such as [Cu(Pz)]$_n$,[3, 4] have also been reported. Similarly, several trimeric silver(I) pyrazolates are known, such as {[3,5-(*i*-Pr)$_2$Pz]Ag}$_3$[6, 15] and {[4-(NO_2)-3,5-(*i*-Pr)$_2$Pz]Ag}$_3$,[15] while fewer tetrameric, {[3,5-(*t*-Bu)$_2$Pz]Ag}$_4$,[8] and hexameric, {[4-(^{t}BuCO$_2$)-3,5-(Ph)$_2$Pz]Ag}$_6$,[16] are known. Additionally, some work has been done on gold(I) pyrazolates and trimeric, {[3,5-(*i*-Pr)$_2$Pz]Au}$_3$[6] and {[3,5-(CO_2Et)$_2$Pz]Au}$_3$,[17] tetrameric, {[3,5-(*t*-Bu)$_2$Pz]Au}$_4$,[6] and hexameric, {[3,5-(Ph)$_2$Pz]Au}$_6$ [9] are known. Relatively less work has been done on fluorinated analogs of coinage metal pyrazolates, however.[12]

In 2000, our group introduced a convenient synthetic route copper(I) and silver (I) complexes containing the highly fluorinated pyrazolate, [3,5-$(CF_3)_2$Pz]$^-$.[12] By combining the pyrazole and corresponding metal oxide, i.e. copper(I) oxide or silver(I) oxide, in benzene or toluene followed by heating, the desired trimeric complexes, {[3,5-$(CF_3)_2$Pz]Cu}$_3$ and {[3,5-$(CF_3)_2$Pz]Ag}$_3$ were obtained, Figure 1.4.

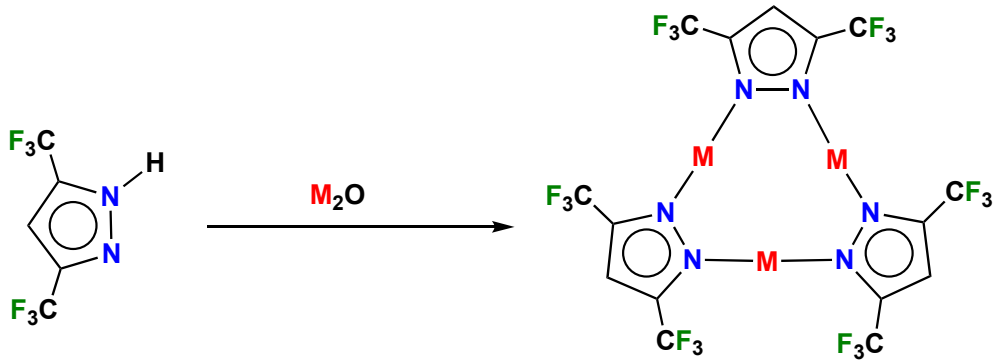

Figure 1.4 Synthesis of trimeric copper(I) or silver(I) pyrazolates.

Later, using a similar approach, our group reported several more trinuclear copper(I) complexes with fluorinated pyrazolates: {[3-(CF_3)Pz]Cu}$_3$, {[3-(CF_3)-5-(CH_3)Pz]Cu}$_3$, {[3-(CF_3)-5-(Ph)Pz]Cu}$_3$, {[4-Br-3,5-(CF_3)$_2$Pz]Cu}$_3$, {[4-Cl-3,5-(CF_3)$_2$Pz]Cu}$_3$, and {[3,4,5-(CF_3)$_3$Pz]Cu}$_3$.[5, 18, 19] Our group has also reported the synthesis of additional fluorinated trinuclear silver(I) pyrazolates using an analogs method to {[3,5-(CF_3)$_2$Pz]Ag}$_3$ to obtain the trinuclear complexes {[3-(CF_3)Pz]Ag}$_3$, {[3-(CF_3)-5-(CH_3)Pz]Ag}$_3$, {[3-(CF_3)-5-(Ph)Pz]Ag}$_3$, and {[3-(CF_3)-5-(*t*-Bu)Pz]Cu}$_3$, {[3-(C_3F_7)-5-(*t*-Bu)Pz]Cu}$_3$.[13] Much less work has been done on gold(I) complexes with fluorinated pyrazolates, however. Based on a literature search, there have only been two previously reported fluorinated trimeric gold(I) pyrazolates, {[3,5-(CF_3)$_2$Pz]Au}$_3$[20] and {[3-(CF_3)-5-(CH_3)Pz]Au}$_3$.[21] Regardless of the coinage metal used or pyrazolate substituents, these trimeric complexes adopt a triangular conformation with a M_3N_6 metallacyclic core.

Many of the complexes also exhibit remarkable photophysical properties and donor-accepter chemistry.[5, 6, 13, 20, 22] For example, our group has shown many copper complexes have phosphorescent emissions under UV excitation at both room temperature and frozen solutions. These emissions can be easily tuned by changing solvent, temperature, excitation wavelength, and substituents on the pyrazolate backbone.[5] For example, {[3,5-(CF_3)$_2$Pz]Cu}$_3$ exhibits orange luminescence at room temperature that shifts to red once the sample is cooled to 77 K. If one of the trifluoromethyl groups on the pyrazolate is replaced with a phenyl group, the corresponding copper(I) trimer exhibits no luminescence at room temperature. But, upon cooling to 77 K, this trimer exhibits dark blue/purple or light blue emissions, depending on the excitation wavelength

used. When solutions of {[3,5-$(CF_3)_2$Pz]Cu}$_3$ are frozen the luminescent emissions vary in color from red when dissolved in benzene, to green when dissolved in toluene, to blue when dissolved in acetonitrile, exhibiting the remarkable solvatochromism of this trimer. The silver and gold analogs of this trimer also show interesting thermochromism properties.[13, 20] The photoluminescent properties of these fluorinated coinage metal trimeric complexes makes them potential candidates to be used in molecular light emitting devices (MOLEDs).

These fluorinated coinage metal complexes also serve as π-acids, forming adducts with π-bases like benzene, toluene, mesitylene, and naphthalene as well as forming diverse supramolecular aggregates with C_{60}.[5, 23] These properties provide an interesting potential application for coinage metal pyrazolates as sensors for the detection of often harmful aromatic hydrocarbons, such as benzene and toluene. Using the silver trimer {[3,5-$(CF_3)_2$Pz]Ag}$_3$, our group and others showed that the presence of benzene, toluene, or mesitylene could be sensed by monitoring the luminescence of the silver trimer.[24]

More recently, the copper trimer {[3,5-$(CF_3)_2$Pz]Cu}$_3$ has been shown to readily react and form complexes with carbon monoxide, ethylene, and alkynes to form various dinuclear and tetranuclear species.[19, 25-28] These ligands coordinate to the copper center in a manner consistent with the Dewar-Chatt-Duncanson Model, Figure 1.5, illustrated for an olefin.

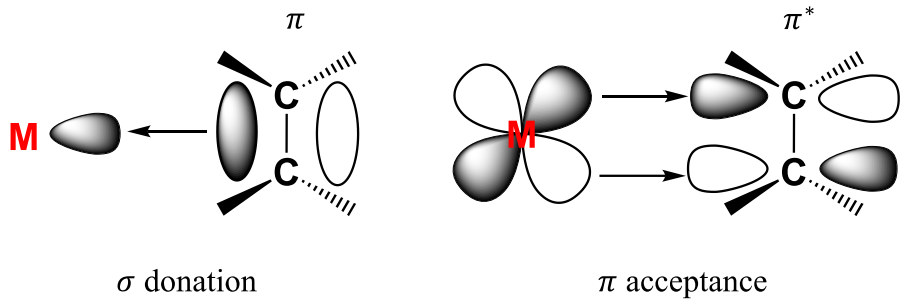

Figure 1.5 Dewar Chatt Duncanson Model

Based on the ability of {[3,5-$(CF_3)_2$Pz]Cu}$_3$ to form complexes with these types of molecules, our group and others probed various applications in which this complex could be used. It was found that this copper trimer has many interesting applications including, olefin-paraffin separation,[19, 28] small molecule sensing via photoluminescence,[14, 25] and catalytic transformations.[26]

Tetranuclear coinage metal pyrazolate complexes are notably less common than trinuclear complexes, and fluorinated analogs are even less studied.[11, 22] Previous work has been done on non-fluorinated copper(I) tetramers such as, {[3,5-$(Ph)_2$Pz]Cu}$_4$,[11] {[3,5-(t-Bu)$_2$Pz]Cu}$_4$,[6, 11] and {[3-(i-Pr)-5-(t-Bu)Pz]Cu}$_4$.[6] Much more recently, our group reported the synthesis and luminescent properties of the tetranuclear copper(I) pyrazolates {[3-(CF_3)-5-(t-Bu)Pz]Cu}$_4$ and {[4-Br-3,5-(i-Pr)$_2$Pz]Cu}$_4$.[22] Significantly less work has been done on tetrameric silver(I) pyrazolates. The only known tetrameric silver(I) complexes reported, based on a literature search, are with non-fluorinated pyrazolates, i.e. {[3,5-(t-Bu)$_2$Pz]Ag}$_4$.[6, 8] Work done by our group found that even when using a pyrazolate ligand with two large groups on the pyrazole ring, such as [3-(C_3F_7)-5-(t-Bu)Pz]$^-$, the silver complex still trimerizes, although the Ag_3N_6 core does significantly distort from the usual planarity.[13] This work

exemplified that silver pyrazolates are able to accommodate larger substituents on the pyrazole ring than copper or gold analogs, due to the size of the coinage metal ion. Silver is the largest of the coinage metals, as shown by the covalent radii of two-coordinate Cu(I), Ag(I), and Au(I) as 1.11, 1.33, and 1.25 Å, respectively.[29] Tetrameric gold(I) pyrazolates are known, such as {[3,5-(*t*-Bu)$_2$Pz]Au}$_4$ and {[3-(*i*-Pr)-5-(*t*-Bu)Pz]Au}$_4$.[6] However, similarly to the case with silver, tetrameric gold(I) complexes have only been reported with non-fluorinated pyrazolates. Regardless of the coinage metal used, tetrameric complexes adopt a basket shaped structure in which two pyrazolyl rings lie above and two below the plane created by the M$_4$ core, see Figure 1.3 (B).

Tetrameric copper(I) pyrazolates, {[3-(CF$_3$)-5-(*t*-Bu)Pz]Cu}$_4$ and {[4-Br-3,5-(*i*-Pr)$_2$Pz]Cu}$_4$,[22] were found to have interesting photoluminescent properties, similarly to the trimeric analogs. In the solid state these tetramers exhibited bright luminescence that showed solvatochromism when in frozen toluene solutions. However, despite these positive findings, much less work has been done to study the potential application of tetrameric coinage metal pyrazolates.

Considering the fascinating properties of coinage metal pyrazolates, we set out to expand the work done on fluorinated pyrazolates and their coinage metal complexes, further probe the catalytic ability of tri- and tetranuclear copper pyrazolates and explore alternatives to highly fluorinated pyrazolate complexes for equally efficient applications. In chapter 2 the synthesis, luminescence, and catalytic ability of new coinage metal pyrazolates containing highly fluorinated aryl substituents is discussed. And while these new highly fluorinated trimers show interesting properties, similar to previously reported fluorinated coinage

metal complexes, in chapter 3 we investigated a potential non-fluorinated alternative. Two copper(I) and two silver(I) complexes were synthesized using diethyl 3,5-dicarboxylate pyrazole and 4-bromo diethyl 3,5-dicarboxylate pyrazole. Although ethyl ester groups have similar electronics to trifluoromethyl groups,[30] we found the corresponding copper(I) and silver(I) complexes did not exhibit the same positive properties as the highly fluorinated analogs, further discussed in chapter 3. The catalytic ability of trinuclear and tetranuclear copper(I) pyrazolates, both fluorinated and non-fluorinated, in copper catalyzed azide-alkyne cycloaddition (CuAAC) reactions was investigated in chapter 4. We found electron rich copper trimers are poor catalysts, while the previously reported highly fluorinated copper trimers are excellent stand-alone catalysts. Additionally, we found both fluorinated and non-fluorinated copper tetramers were excellent catalysts in CuAAC reactions and further investigated these complexes. Chapter 5 looks at the synthesis and luminescence of coinage metal complexes of $[3,5\text{-}(CF_3)_2Pz]^-$ and bis(diphenylphosphino) methane as potential candidates for inorganic LEDs. Finally, chapter 6 is devoted to the experimental details of each chapter and appendix A-D include the corresponding spectroscopic data for each chapter. Further details about this research work can be found in the related chapters herein.

Chapter 2

Coinage metal metallacycles involving a fluorinated 3,5-diarylpyrazolate

Jaspreet S. Lakhi, Monika R. Patterson, H. V. Rasika Dias

This work has been published in New J. Chem., 2020, 44, 14814-14822[31]

2.1 Abstract

Copper(I) and silver(I) pyrazolate complexes {[3,5-(3,5-$(CF_3)_2Ph)_2Pz$]Cu}$_3$ and {[3,5-(3,5-$(CF_3)_2Ph)_2Pz$]Ag}$_3$ have been synthesized using the fluorinated 3,5-(diaryl)pyrazole 3,5-(3,5-$(CF_3)_2Ph)_2PzH$ and copper(I) oxide and silver(I) oxide, respectively. The gold(I) analog was obtained from a reaction between Au(THT)Cl and [3,5-(3,5-$(CF_3)_2Ph)_2Pz$]H/NaH. The X-ray crystal structures show that the coinage metal complexes {[3,5-(3,5-$(CF_3)_2Ph)_2Pz$]M}$_3$ (M = Cu, Ag, Au) are trinuclear in the solid state. They feature, distorted nine-membered M_3N_6 metalacyclic cores. The M-N distances follow Cu < Au < Ag, which is the trend expected from covalent radii of the corresponding coinage metal ions. The 3,5-(3,5-$(CF_3)_2Ph)_2PzH$ forms hydrogen bonded trimers in the solid state that are further organized by π-stacking between aryl rings. Solid samples of {[3,5-(3,5-$(CF_3)_2Ph)_2Pz$]M}$_3$ display blue photoluminescence. The copper complex {[3,5-(3,5-$(CF_3)_2Ph)_2Pz$]Cu}$_3$ is an excellent catalyst for mediating azide-alkyne cycloaddition chemistry.

2.2 Introduction

Pyrazolate complexes of monovalent coinage metals (Cu(I), Ag(I), Au(I)) represent an important class of coordination compounds whose significance spans multiple areas of chemistry, including acid/base and host/guest chemistry, metallophilic d^{10}-d^{10} interactions, supramolecular assemblies, M-M bonded excimers and exciplexes, luminescence,[3, 4, 6, 20, 32-43] as well as catalysis.[26, 40, 44-46] Trinuclear structures are the most common motif among homoleptic coinage metal pyrazolates while tetranuclear, hexanuclear and polymeric complexes are also known to a lesser degree.[6, 8, 22, 32, 46-48] For example, a search of Cambridge Structural Database (CSD)[49] for 3,5-diphenylpyrazolate ligand based copper,

silver and gold complexes shows that {[3,5-(Ph)$_2$Pz]M}$_3$ (Figure 2.1, **1**, M = Cu, Ag, Au; X = H),[9, 50] {[4-Cl-3,5-(Ph)$_2$Pz]M}$_3$ (Figure 2.1, **1**, M = Cu, Ag, Au; X = Cl),[48, 51, 52] {[4-Br-3,5-(Ph)$_2$Pz]M}$_3$ (Figure 2.1, **1**, M = Ag, Au; X = Br),[53] {[4-I-3,5-(Ph)$_2$Pz]M}$_3$ (Figure 2.1, **1**, M = Ag, Au; X = I),[52] {[4-Me-3,5-(Ph)$_2$Pz]Ag}$_3$[52] are known and feature trinuclear structures. In addition, a few tetramers {[3,5-(Ph)$_2$Pz]Cu}$_4$,[46] {[4-Cl-3,5-(Ph)$_2$Pz]Cu}$_4$,[51] {[4-(^{t}BuCO$_2$)-3,5-(Ph)$_2$Pz]Ag}$_4$,[16] and hexamers {[3,5-(Ph)$_2$Pz]Au}$_6$,[9] and {[4-(^{t}BuCO$_2$)-3,5-(Ph)$_2$Pz]Ag}$_6$[16] resulting from the same or similar pyrazolate ligands have also been observed, depending on the method of synthesis and crystallization.

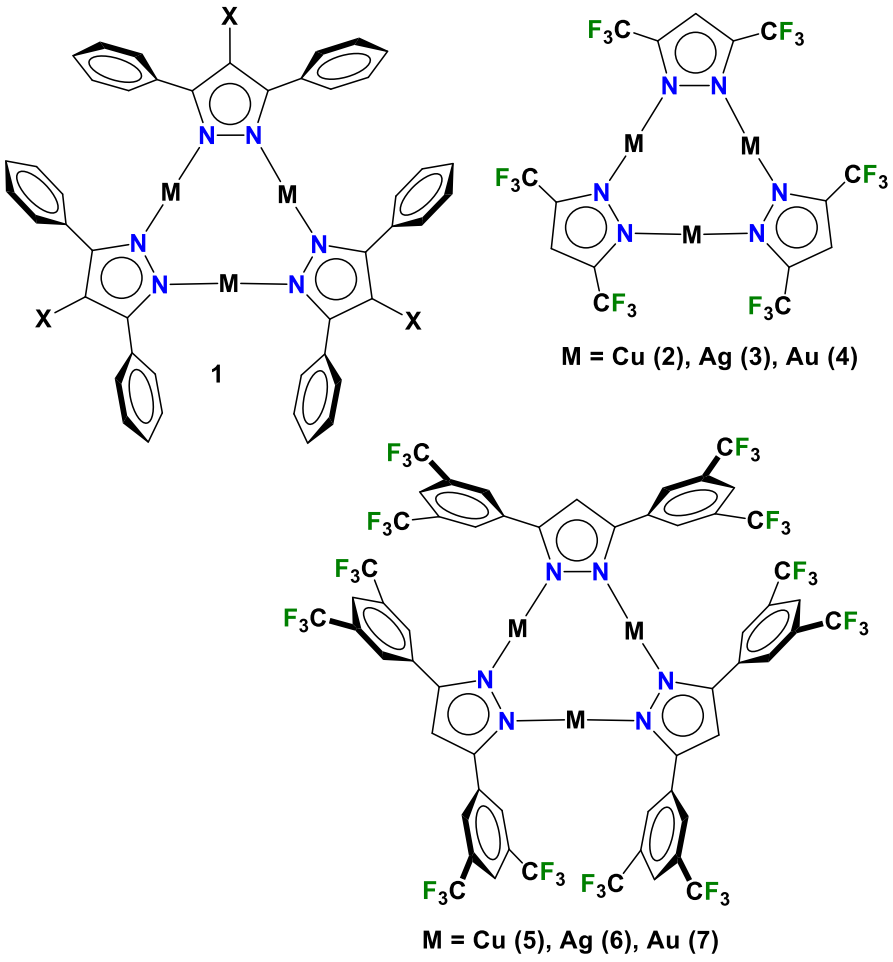

Figure 2.1 Several coinage metal complexes involving pyrazolate ligand support.

An area of research activity in our laboratory concerns the chemistry of copper, silver and gold complexes of highly fluorinated pyrazolates.[5, 13, 14, 18-20, 23, 24, 27, 54-58] Several years ago, we reported a convenient synthetic route to copper(I) and silver(I) adducts $\{[3,5\text{-}(CF_3)_2Pz]Cu\}_3$ (**2**) and $\{[3,5\text{-}(CF_3)_2Pz]Ag\}_3$ (**3**) using $[3,5\text{-}(CF_3)_2Pz]H$ and the corresponding metal(I) oxides (Figure 2.1).[12, 20] These trinuclear d^{10} pyrazolates and the related $\{[3,5\text{-}(CF_3)_2Pz]Au\}_3$ (**4**) show remarkable photophysical properties and donor-acceptor chemistry.[5, 13, 14, 20, 56, 59, 60] For example, the copper complex $\{[3,5\text{-}(CF_3)_2Pz]Cu\}_3$ exhibits bright phosphorescent emissions both in the solid state and in frozen solutions under UV excitation that can be easily fine- and coarse-tuned to multiple visible colors by varying the solvent, copper adduct concentration, temperature, and the excitation wavelength.[5, 14] These coinage metal complexes **2-4** serve as π-acids, and form adducts with π-bases like benzene, toluene, mesitylene and naphthalene as well as with C_{60} forming diverse supramolecular aggregates.[13, 23, 24, 59, 60] The silver complex $\{[3,5\text{-}(CF_3)_2Pz]Ag\}_3$ also serves as an excellent sensor for the detection of volatile aromatic hydrocarbons such as benzene and toluene.[56] In addition, the trinuclear $\{[3,5\text{-}(CF_3)_2Pz]Cu\}_3$ complex readily reacts with alkynes and CO forming dinuclear and tetranuclear species.[25-27] It is also an excellent catalyst for azide-alkyne Click-chemistry.[26] Various other groups have also investigated the interesting chemistry of $\{[3,5\text{-}(CF_3)_2Pz]M\}_3$ (**2-4**, M = Cu, Ag, Au).[32, 33, 37, 42, 61-63]

Structurally authenticated coinage metal pyrazolates such as $\{[3,5\text{-}(CF_3)_2Pz]M\}_3$ with fluoro alkyl substituents are noticeably less common,[49] and fluorinated aryl groups are barely explored compared to those featuring

hydrocarbon substituents (e.g., Me, *i*-Pr, *t*-Bu, Ph) on the pyrazolate ligand backbone. Considering current interest in metal pyrazolates and in particular, the attractive features of the fluorinated analogs, we embarked on a project to develop fluorinated diarylpyrazolate ligands such as $[3,5\text{-}(3,5\text{-}(CF_3)_2Ph)_2Pz]^-$ and investigate their chemistry. Here we report the synthesis of $3,5\text{-}(3,5\text{-}(CF_3)_2Ph)_2PzH$, and the isolation of coinage metal complexes $\{[3,5\text{-}(3,5\text{-}(CF_3)_2Ph)_2Pz]M\}_3$ (Figure 2.1, **5-7**; M = Cu, Ag, Au), as well as their X-ray crystal structural data and preliminary photophysical and catalytic properties.

2.3 Results and Discussion

The diketone 1,3-bis(3,5-bis(trifluoromethyl)phenyl)propane-1,3-dione was synthesized from a mixture of 3,5-bis(trifluoromethylbenzoate and 3,5-bis(trifluoromethyl)acetophenone under basic conditions using a modified literature method utilized in the synthesis of somewhat related 1,3-bis(4-methylphenyl)propane-1,3-dione.[64] It was isolated as a white solid in 87% yield. The ^{1}H NMR spectrum of $3,5\text{-}(3,5\text{-}(CF_3)_2PhCO)_2CH_2$ in $CDCl_3$ suggest the presence of enol form, 1,3-bis(3,5-bis(trifluoromethyl)phenyl)-3-hydroxyprop-2-en-1-one in solution. The pyrazole $3,5\text{-}(3,5\text{-}(CF_3)_2Ph)_2PzH$ was synthesized by a cyclocondensation reaction involving 1,3-bis(3,5-bis(trifluoromethyl)phenyl)-3-hydroxyprop-2-en-1-one and hydrazine monohydrate, and isolated as a colorless crystalline solid in 87% yield. The $3,5\text{-}(3,5\text{-}(CF_3)_2Ph)_2PzH$ is soluble in acetone and tetrahydrofuran at room temperature and in hot benzene and hot chloroform. It was characterized by several methods including X-ray crystallography. The ^{1}H NMR spectrum in $CDCl_3$ includes three peaks assignable to $3,5\text{-}(CF_3)_2Ph$ protons (δ 8.18 and 7.87

ppm) and CH of the pyrazole (δ 7.11 ppm) ring. ^{19}F NMR spectrum displayed a singlet at δ -63.23 ppm.

The analysis of the crystals obtained from $CHCl_3$ by single crystal X-ray diffraction show that 3,5-(3,5-$(CF_3)_2$Ph)$_2$PzH forms hydrogen bonded trimers in the solid state (Figure 2.2) that are further organized by π-stacking between aryl rings (with centroid to centroid distances ranging from 3.70-3.87 Å). The trimeric form is unexpected considering the steric demands of the bulky aryl groups at the 3- and 5-positions, facing each other in a planar arrangement. The aggregate accommodates that encounter by twisting pyrazolyl planes and placing aryl groups above and below each other (Figure 2.2). The nitrogen atoms of the trimeric core form a distorted chair configuration with N•••N distances (the distances between donor and acceptor nitrogen atoms of the hydrogen bond) of 2.85 Å. Solid state structures of NH-pyrazoles have indeed attracted interest as they show diverse structures ranging from dimers, trimers, tetramers, hexamers, and polymers (catemers) and due to the tautomerism.[65-67] They are also of interest because binary group 11 metal pyrazolates (in-which N-H is replaced by N-M; M = Cu, Ag, Au) also show some parallels as noted earlier. Among 1,3-diarylpyrazoles,[49] the dimeric form appears to be the most common (e.g., in 4-(CF_3)-3,5-(Ph)$_2$PzH,[68] 4-(NC)-3,5-(Ph)$_2$PzH,[69] 4-(Br)-3,5-(Ph)$_2$PzH,[65] 3-(4-(CF_3)Ph)-5-(Ph)PzH[70]) while examples of tetramers (e.g., 3,5-(Ph)$_2$PzH)[71] and polymers (e.g., 3,5-(4-Cl-Ph)$_2$PzH,[72] 3,5-(4-NC-Ph)$_2$PzH,[73]) are also known.

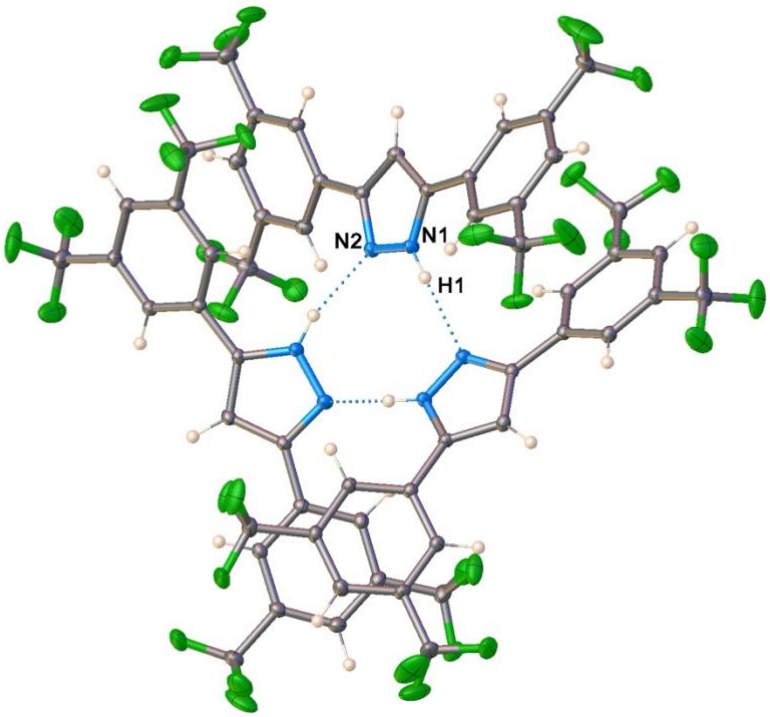

Figure 2.2 Molecular structure of 3,5-(3,5-$(CF_3)_2Ph)_2PzH$ showing the trimers resulting from NH•••N hydrogen bonding.

The trinuclear {[3,5-(3,5-$(CF_3)_2Ph)_2Pz]Cu\}_3$ (**5**) was synthesized by using copper(I) oxide and 3,5-(3,5-$(CF_3)_2Ph)_2PzH$ via a method similar to that reported for {[3,5-$(CF_3)_2Pz]Cu\}_3$.[12] However, unlike the 3,5-trifluoromethyl pyrazole analog, it was found that the formation of **5** did not take place when benzene was used as a solvent but works well when higher boiling toluene was used. The Cu(I) oxide/pyrazole mixture in toluene was refluxed under nitrogen overnight and filtered while maintaining the solution temperature above 90 ℃ to remove the excess metal oxide. It was found that if the solution was allowed to cool below 90 ℃, the product began to precipitate. The hot-filtered clear solution was allowed to slowly come to room temperature to obtain colorless needles. ^{1}H NMR spectrum of these crystals in $CDCl_3$ showed an upfield shifted C*H* resonance of the pyrazolyl rings (δ 7.00 ppm) with respect to the starting

material (δ 7.11 ppm), indicating the formation of the trinuclear complex {[3,5-(3,5-$(CF_3)_2Ph)_2Pz$]Cu}$_3$. The ^{1}H NMR also indicated the inclusion of some toluene molecules in the crystalline copper complex. The trapped toluene can be removed by drying the crystals under vacuum at 90 ℃ for about 4 hours. It was found that the toluene-free crystals were much less soluble in solvents such as $CDCl_3$.

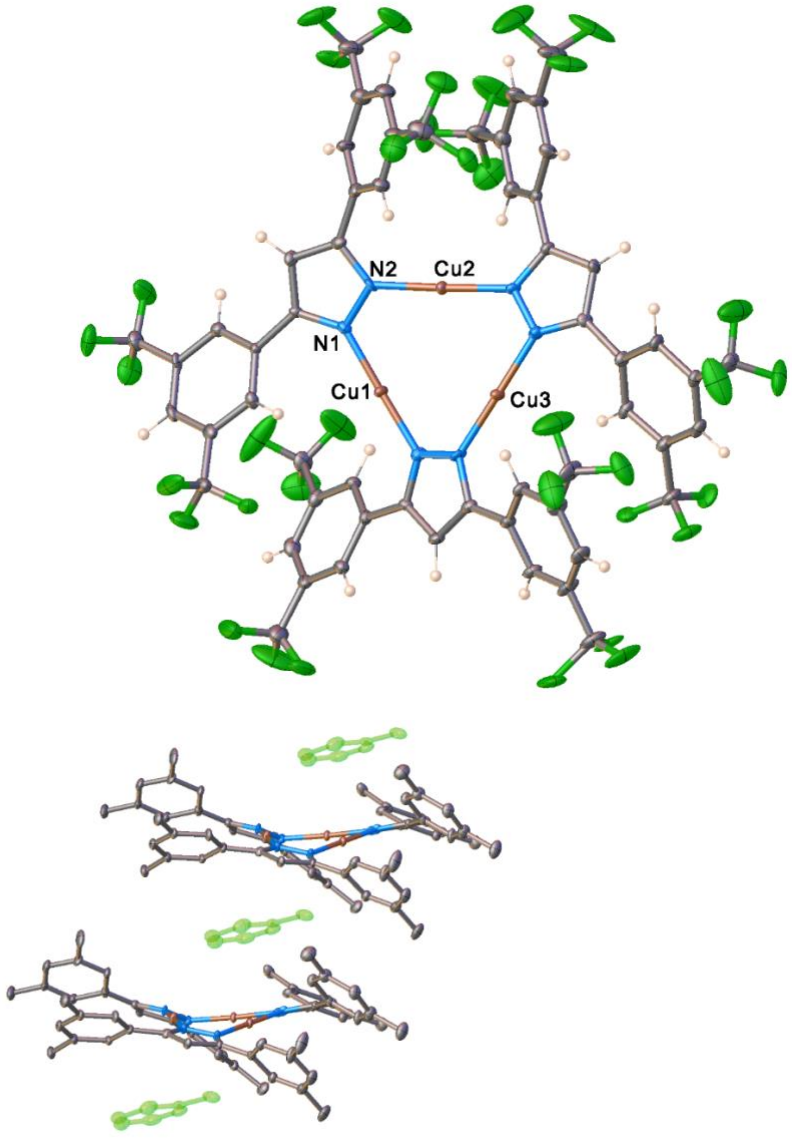

Figure 2.3 Top: Molecular structure of {[3,5-(3,5-$(CF_3)_2Ph)_2Pz$]Cu}$_3$ (toluene molecules in the crystal lattice have been omitted for clarity), and **Bottom**: A

view showing intercalation of toluene molecules between {[3,5-(3,5-$(CF_3)_2Ph)_2Pz]Cu\}_3$ (hydrogen and fluorine atoms have been omitted for clarity).

Table 2.1 Selected bond distances (Å) and angles (º) of trinuclear copper(I), silver(I) and gold(I) complexes supported by pyrazolates with 3,5-diaryl groups on the pyrazolyl rings. M = Cu, Ag or Au

Metal pyrazolate	M-N	N-M-N	M•••M (intra-trimer)	M•••M (inter trimer)	Ref
$\{[3,5\text{-}(Ph)_2Pz]Cu\}_3$	2.041(7)-2.105(7)	169.2(3)-178.6(3)	3.280-3.406	over 5	[50]
{[4-Cl-3,5-$(Ph)_2Pz]Cu\}_3$	1.849(2)-1.867(2)	173.22(9)-178.42(9)	3.140-3.251	4.704	[51]
$\{[3,5\text{-}(3,5\text{-}(CF_3)_2Ph)_2Pz]Cu\}_3$	1.843(7)-1.869(7)	175.2(3)-178.1(3)	3.133-3.285	over 5	This work
$\{[3,5\text{-}(Ph)_2Pz]Ag\}_3$	2.073(4)-2.106(4)	171.17(17)-172.30(16)	3.357-3.525	2.979	[74]
{[4-Cl-3,5-$(Ph)_2Pz]Ag\}_3$	2.082(10)-2.112(11)	175.6(4)-177.8(4)	3.469-3.549	over 5	[52]
{[4-Br-3,5-$(Ph)_2Pz]Ag\}_3$	2.054(10)-2.132(10)	170.1(4)-178.4(4)	3.312-3.632	over 5	[53]
{[4-I-3,5-$(Ph)_2Pz]Ag\}_3$	2.074(5)-2.093(5)	173.6(2)-174.8(2)	3.414-3.596	over 5	[52]
{[4-(Me)-3,5-$(Ph)_2Pz]Ag\}_3$	2.059(3)-2.092(3)	169.85(14)-175.95(15)	3.342-3.573	3.937	[52]
$\{[3,5\text{-}(3,5\text{-}(CF_3)_2Ph)_2Pz]Ag\}_3$	2.072(4)-2.088(5)	174.2(2)-177.1(2)	3.368-3.433	over 5	This work
$\{[3,5\text{-}(Ph)_2Pz]Au\}_3$	1.978(9)	179.6(3)	3.368	over 5	[9]
{[4-Cl-3,5-$(Ph)_2Pz]Au\}_3$	1.997(7)-2.009(6)	178.2(3)-179.2(3)	3.340-3.386	4.387	[52]
{[4-Br-3,5-$(Ph)_2Pz]Au\}_3$	1.998(6)-2.016(6)	178.1(2)-179.6(3)	3.348-3.379	4.442	[53]
{[4-I-3,5-$(Ph)_2Pz]Au\}_3$	2.003(15)-2.045(13)	175.4(6)-178.0(6)	3.347-3.455	over 5	[52]
$\{[3,5\text{-}(3,5\text{-}(CF_3)_2Ph)_2Pz]Au\}_3$	1.996(3)-2.013(3)	176.66(14)-177.28(14)	3.288-3.369	over 5	This work

For comparison, the van der Waals contact distance of two metal atoms based on values suggested by Bondi[29] and Alvarez[75] are: for Cu•••Cu = 2.80 and 4.76 Å, Ag•••Ag = 3.44 and 5.06 Å, and Au•••Au = 3.32 and 4.64 Å, respectively.

The copper(I) complex {[3,5-(3,5-$(CF_3)_2$Ph)$_2$Pz]Cu}$_3$ (**5**) was re-crystallized from toluene. The X-ray crystal structure of **5** shows that it crystallizes with 1.5 molecules of toluene in the asymmetric unit. One of these toluene molecules and {[3,5-(3,5-$(CF_3)_2$Ph)$_2$Pz]Cu}$_3$ forms extended columns as illustrated in Figure 2.3, with closest Cu•••C(toluene) separations of 3.32 and 3.47 Å. These distances are slightly longer than sum of the Bondi's van der Waals radii of copper and carbon 1.40 + 1.70 = 3.10 Å.[29] However, more recent work from Alveraz[75] places van der Waals contact distance of copper and carbon at 4.15 Å implying noteworthy interactions between these moieties. This tendency of {[3,5-(3,5-$(CF_3)_2$Ph)$_2$Pz]Cu}$_3$ to intercalate arenes is similar to that observed with {[3,5-$(CF_3)_2$Pz]Cu}$_3$ (**2**).[24] The partially occupied (second) toluene molecule occupies the space between these columns. Selected bond distances and angles of {[3,5-(3,5-$(CF_3)_2$Ph)$_2$Pz]Cu}$_3$ are given in Table 2.1. It is a trinuclear species with a somewhat twisted Cu_3N_6 metallacyclic core.

The silver(I) complex {[3,5-(3,5-$(CF_3)_2$Ph)$_2$Pz]Ag}$_3$ (**6**), was synthesized using a method similar to that used for {[3,5-$(CF_3)_2$Pz]Ag}$_3$ using the appropriate pyrazole 3,5-(3,5-$(CF_3)_2$Ph)$_2$PzH and silver(I) oxide.[12] Similarly to the copper analog, it was found that the higher boiling toluene (instead of benzene) is needed for the efficient reaction. The {[3,5-(3,5-$(CF_3)_2$Ph)$_2$Pz]Ag}$_3$ was isolated as a white solid in moderate yield (51%). The ^{1}H NMR spectrum of the solid samples indicated the presence of some trapped toluene, which was removed by drying the solids under vacuum at 60 ℃ overnight. These solids were then recrystallized from dichloromethane/hexanes (4:1) at -20 ℃ to give colorless needle-like crystals. It is soluble in most common organic solvents

such benzene, dichloromethane, acetonitrile, toluene, and tetrahydrofuran and in hot hexane.

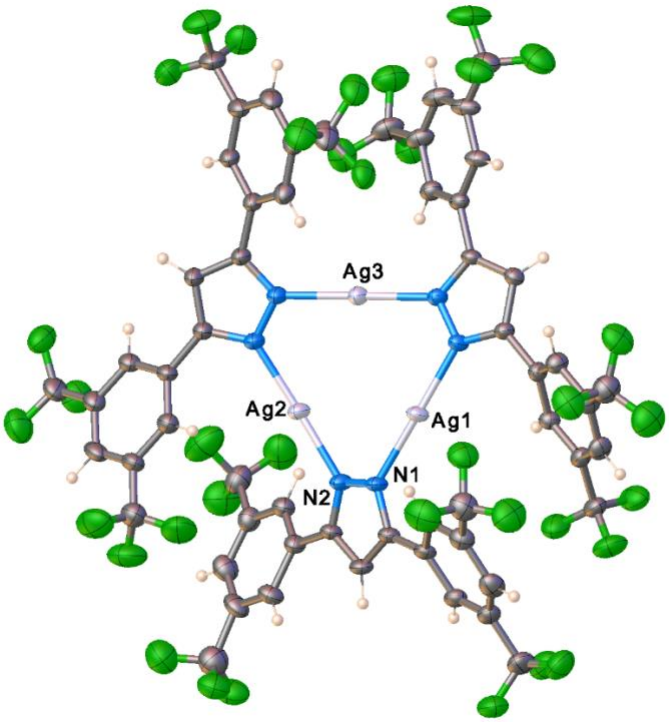

Figure 2.4 Molecular structure of {[3,5-(3,5-$(CF_3)_2$Ph)$_2$Pz]Ag}$_3$ (dichloromethane molecules in the crystal lattice have been omitted for clarity).

The silver(I) complex {[3,5-(3,5-$(CF_3)_2$Ph)$_2$Pz]Ag}$_3$ (**6**) crystallizes with molecules of dichloromethane the asymmetric unit. The molecular structure of {[3,5-(3,5-$(CF_3)_2$Ph)$_2$Pz]Ag}$_3$ (Figure 2.4) shows that it is a trinuclear species and forms a somewhat twisted Ag_3N_6 core to avoid unfavorable steric interactions of 3,5-aryl groups of the neighboring pyrazolates in **6**. There are no close inter-trimer Ag•••Ag contacts as seen with several trinuclear silver pyrazolates bearing alkyl substituents[13, 15, 48] and in some analogs with 3,5-diarylated pyrazolates (Table 2.1). The bulky aryl groups in {[3,5-(3,5-$(CF_3)_2$Ph)$_2$Pz]Ag}$_3$ likely hinder the close face-to-face approach of neighboring

trimers from above and below the trimer-plane to form inter-trimer argentophilic contacts.

The synthesis of the trinuclear pyrazolate complex of gold(I), {[3,5-(3,5-$(CF_3)_2Ph)_2Pz$]Au}$_3$ (**7**) involved the reaction between [3,5-(3,5-$(CF_3)_2Ph)_2Pz$]Na (prepared from NaH and 3,5-(3,5-$(CF_3)_2Ph)_2PzH$) and Au(THT)Cl in THF. The product {[3,5-(3,5-$(CF_3)_2Ph)_2Pz$]Au}$_3$ was found to be light sensitive and generates the starting pyrazole ligand back upon prolonged exposure to light (~ 2 days). The molecular structure of the gold(I) complex {[3,5-(3,5-$(CF_3)_2Ph)_2Pz$]Au}$_3$ (**7**) is illustrated in Figure 2.4. It is also a trinuclear species similar to the lighter coinage metal adduct analogs **5** and **6**. It has a relatively less twisted (more planar) M_3N_6 core. For example, there are 3, 6, and 5 nitrogen or metal atoms with deviations over 0.2 Å (largest 0.26, 0.34 and 0.29 Å) from mean-plane of M_3N_6 core of the Au, Ag, and Cu adducts **7-5**, respectively. Table 2.1 summarizes selected bond distances and angles for {[3,5-(3,5-$(CF_3)_2Ph)_2Pz$]Au}$_3$ in addition to other related systems. The M-N distances of **5-7** follow the trend expected from covalent radii of the corresponding coinage metal ions,[20, 76] with longest and shortest M-N distances observed in the silver(I) and copper(I) complexes, respectively.

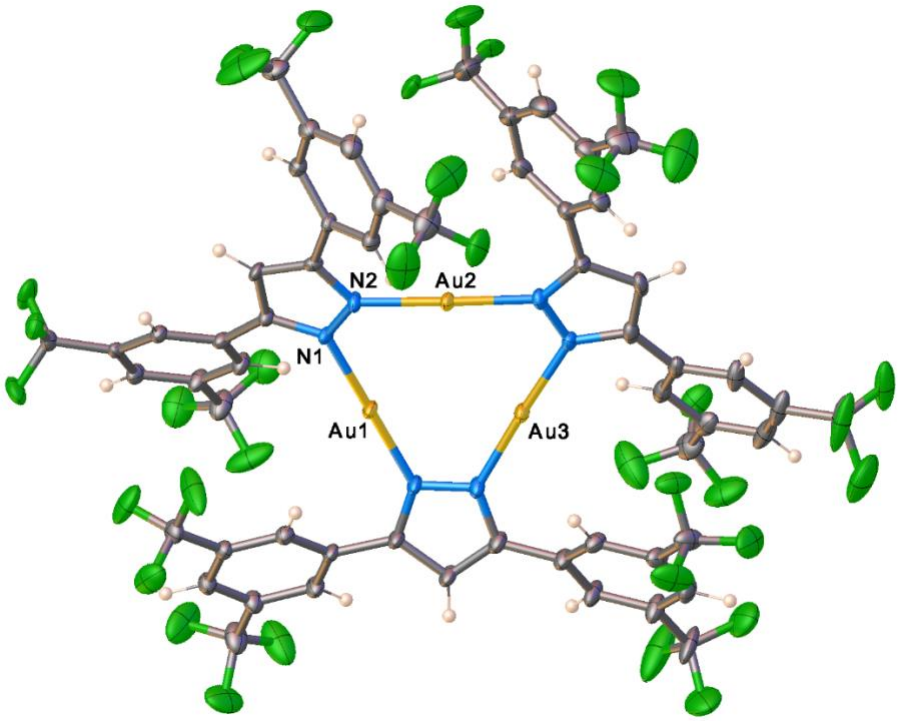

Figure 2.5 Molecular structure of {[3,5-(3,5-$(CF_3)_2$Ph)$_2$Pz]Au}$_3$ (7).

2.4 Photophysical Properties

All three metal pyrazolates **5-7** exhibited blue luminescence upon exposure to UV radiation. The copper and silver analogs exhibited luminescence only at lower temperatures (e.g., 77 K), while the gold analog display luminescence at both at room temperature and lower temperatures. For example at 77 K, {[3,5-(3,5-$(CF_3)_2$Ph)$_2$Pz]Cu}$_3$ (**5**) displayed a light blue luminescence under UV radiation with an excitation maximum at 315 nm and emission maximum at 460 nm, with a Stokes Shift of ~8200 cm^{-1} (Figure 2.6). The gold(I) complex, {[3,5-(3,5-$(CF_3)_2$Ph)$_2$Pz]Au}$_3$ emitted bright blue light under UV light with an excitation maximum at 310 nm and emission maximum at 460 nm, with a Stokes shift of ~8500 cm^{-1}. (Figure 2.6). As noted above, these {[3,5-(3,5-$(CF_3)_2$Ph)$_2$Pz]M}$_3$ complexes do not show close inter-trimer metallophilic interactions in the solid state. The somewhat similar blue emissions observed in these three coinage metal complexes {[3,5-(3,5-$(CF_3)_2$Ph)$_2$Pz]M}$_3$ supported

by 3,5-diaryl substituted pyrazolates (featuring extended aromatic systems) are likely a result of pyrazole ligand centered luminescence[70] that are sensitized via internal heavy atom effect. We have observed similar emissions in {[3-(CF_3),5-(Ph)Pz]Cu}$_3$.[5]

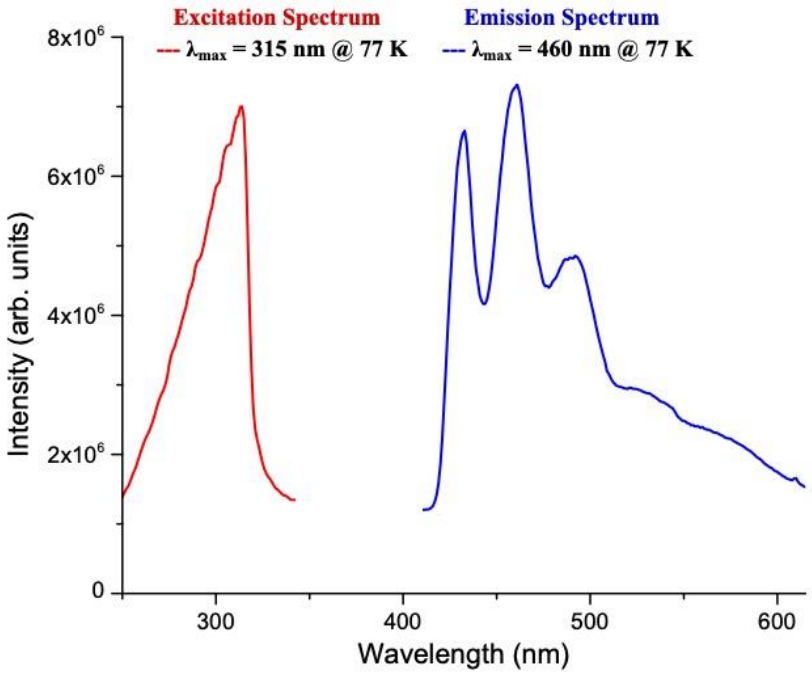

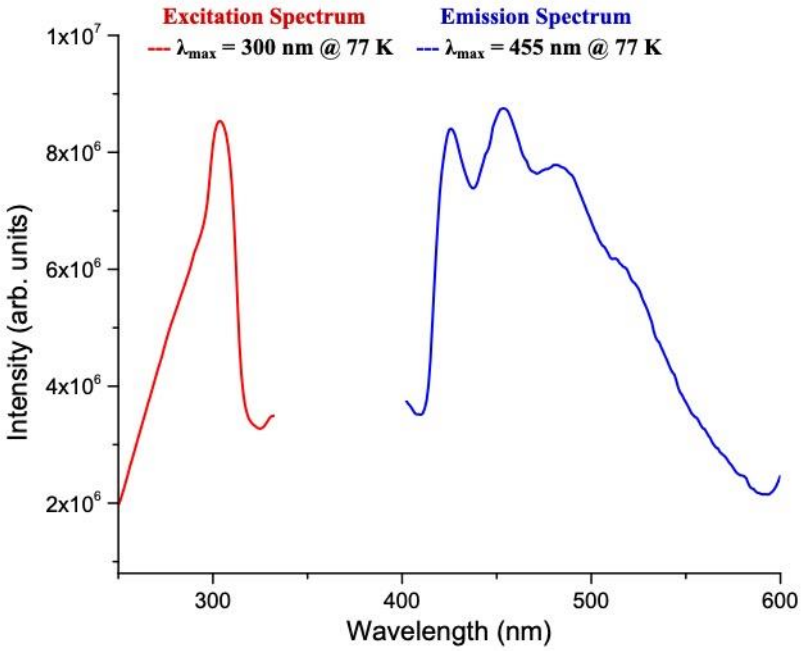

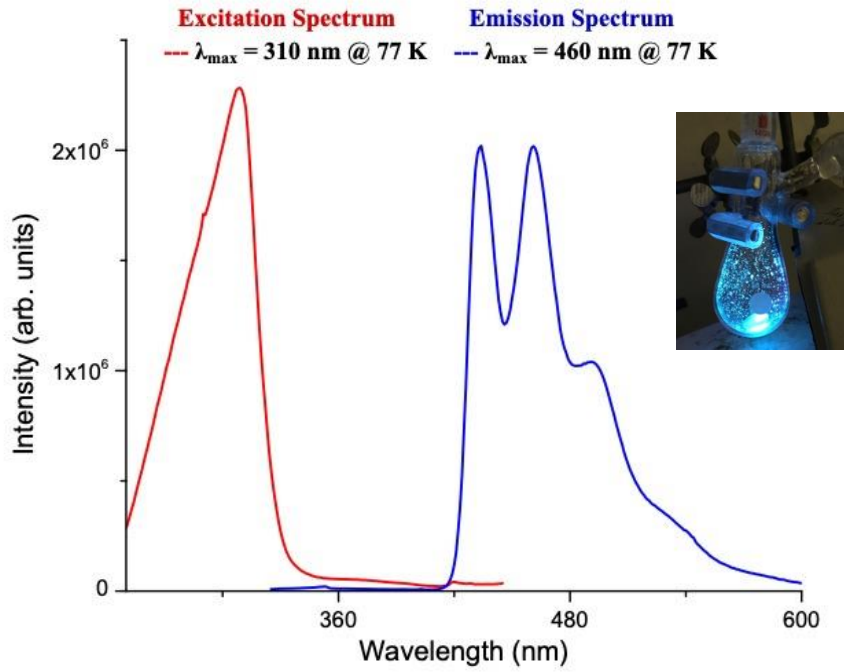

Figure 2.6 Emission and excitation spectra of crystalline solid samples of {[3,5-(3,5-$(CF_3)_2$Ph)$_2$Pz]Cu}$_3$ (top) and {[3,5-(3,5-$(CF_3)_2$Ph)$_2$Pz]Ag}$_3$ (middle) and {[3,5-(3,5-$(CF_3)_2$Ph)$_2$Pz]Au}$_3$ (bottom) at 77 K. Bottom insert: a photo showing the emission color of the gold complex under UV exposure.

2.5 Catalysis

Copper catalyzed synthesis of 1,2,3-triazoles via the cycloaddition of azides to triple bonds of alkynes is a very important process involving copper and alkynes.[77-82] The standard catalytic system uses copper(II) salts such as copper sulfate pentahydrate in the presence of a reducing agent, such as sodium ascorbate.[78] Recently, we and others reported that {μ-[3,5-$(CF_3)_2$Pz]Cu}$_3$ is an excellent, stand-alone catalyst for the cycloaddition of azides to terminal alkynes.[26, 45] In an attempt to extend this work to other copper(I) pyrazolates,

we probed the viability of {[3,5-(3,5-$(CF_3)_2$Ph)$_2$Pz]Cu}$_3$ as a catalyst in azide-cycloaddition of alkynes.

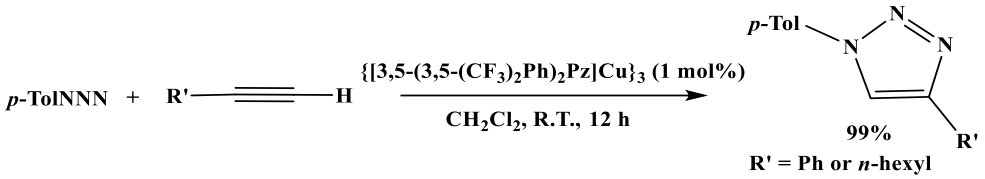

Scheme 1. The {[3,5-(3,5-$(CF_3)_2$Ph)$_2$Pz]Cu}$_3$ catalyzed alkyne-azide cycloaddition of terminal alkynes and p-tolylazide.

Indeed, {[3,5-(3,5-$(CF_3)_2$Ph)$_2$Pz]Cu}$_3$, is an excellent catalyst for azide-alkyne cycloaddition of *p*-tolylazide with 1-octyne or phenylacetylene (Scheme 1), leading to 1,2,3-triazoles in ≥ 99% conversion (Table 2.2), under mild conditions, without any additives, and in high isolated yields. The silver and gold analogs were inactive under similar conditions.

Table 2.2 Azide-alkyne cycloaddition chemistry. Reactions were performed at room temperature in CH_2Cl_2 using catalyst (1 mol%), alkyne (1.5 mmol), *p*-tolylazide (1.5 mmol)

Entry	Catalyst	Alkyne	Percent Conversion	Isolated Yield
1	{[3,5-(3,5-$(CF_3)_2$Ph)$_2$Pz]Cu}$_3$	1-octyne	99 %	94 %
2	{[3,5-(3,5-$(CF_3)_2$Ph)$_2$Pz]Ag}$_3$	1-octyne	0 %	N/A
3	{[3,5-(3,5-$(CF_3)_2$Ph)$_2$Pz]Au}$_3$	1-octyne	0 %	N/A
4	{[3,5-(3,5-$(CF_3)_2$Ph)$_2$Pz]Cu}$_3$	phenylacetylene	100 %	97 %

Cyclopropanation of olefins is also an important reaction.[83, 84] Previous reports indicate that tetranuclear copper(I) pyrazolate complexes, {[3,5-(Ph)$_2$Pz]Cu}$_4$, {[3,5-(*t*-Bu)$_2$Pz]Cu}$_4$, and {[3,5-(*sec*-BuCO$_2$)$_2$Pz]Cu}$_4$ catalyze the cyclopropanation of alkenes in high *trans:cis* ratios and conversion yields.[11] We also investigated the ability of the copper(I) complex {[3,5-(3,5-(CF$_3$)$_2$Ph)$_2$Pz]Cu}$_3$ to catalyze the cyclopropanation of alkenes, but found the cyclopropane yields to be low. For example, 3 mol% of {[3,5-(3,5-(CF$_3$)$_2$Ph)$_2$Pz]Cu}$_3$ catalyzes the reaction of styrene (in excess) with ethyl diazoacetate (EDA) in dichloromethane (catalyst:EDA:styrene molar ratio of 1:33:100) to afford ethyl-2-phenylcyclopropane-1-carboxylate in 45% yield. The *trans*-diastereomer is found in moderately greater excess in the product mixture (similar to the previous report).[11] The {[3,5-(CF$_3$)$_2$Pz]Cu}$_3$ also catalyzes the same process affording slightly lower yield of the cyclopropane (37%) product. Although we did not optimize the reaction conditions, this preliminary work shows that trinuclear {[3,5-(3,5-(CF$_3$)$_2$Ph)$_2$Pz]Cu}$_3$ and {[3,5-(CF$_3$)$_2$Pz]Cu}$_3$ are capable of mediating carbene transfer to olefins (Table 2.3).

Table 2.3 Cyclopropanation catalyzed by copper(I) trimers.

Entry	Catalyst	EDA addition time (hours)	*trans:cis**	Cyclopropane yield %*
1	{[3,5-(3,5-(CF$_3$)$_2$Ph)$_2$Pz]Cu}$_3$	10	73:27	45
2	{[3,5-(CF$_3$)$_2$Pz]Cu}$_3$	10	61:39	37

*Calculated from ^{1}H NMR, using an internal standard of dimethylformamide.

In summary, we have successfully synthesized a useful fluorinated pyrazole, 3,5-(3,5-(CF$_3$)$_2$Ph)$_2$PzH and utilized it in the preparation of homoleptic,

copper(I), silver(I) and gold(I) complexes {[3,5-(3,5-$(CF_3)_2Ph)_2Pz$]M}$_3$ (**5-7**). X-ray crystal structures of the precursor pyrazole and {[3,5-(3,5-$(CF_3)_2Ph)_2Pz$]M}$_3$ are also reported. They all feature trimeric structures. These complexes **5-7** displayed solid state photoluminescence at lower temperature for the copper and silver, and both at lower and room temperature for the gold adduct. The {[3,5-(3,5-$(CF_3)_2Ph)_2Pz$]Cu}$_3$ is an excellent catalyst for azide-alkyne cycloaddition chemistry. It can also mediate olefin cyclopropanations. We are currently expanding this work to other fluorinated aryl pyrazolates and applications.

2.6 Acknowledgments

This material is based upon the work supported by the Robert A. Welch Foundation Grant Y-1289 and partially by the National Science Foundation under Grant No. NSF grant 1954456. We are grateful for Dr. Roy N. McDougald Jr. for his support for photo luminescence data collection.

Chapter 3

Non-fluorinated trinuclear coinage metal metallacycles: synthesis and luminescence

Monika R. Patterson, and H. V. Rasika Dias

`

3.1 Abstract

Four new coinage metal complexes were synthesized: {[3,5-$(CO_2Et)_2Pz$]Cu}$_3$, {[3,5-$(CO_2Et)_2Pz$]Ag}$_3$, {[4-Br-3,5-$(CO_2Et)_2Pz$]Cu}$_3$, and {[4-Br-3,5-$(CO_2Et)_2Pz$]Ag}$_3$. These coinage metal complexes were synthesized by using the appropriate metal(I) oxide, Cu_2O or Ag_2O and pyrazole combination and were characterized with NMR, IR, and HRMS. Both silver trimers show luminescence in the solid state at room temperature and 77 K. Although the pyrazoles used, 3,5-$(CO_2Et)_2PzH$ and 4-Br-3,5-$(CO_2Et)_2PzH$, are electronically similar to 3,5-$(CF_3)_2PzH$, the corresponding coinage metal complexes have very different properties.

3.2 Introduction

Coinage metal pyrazolates have been a major area of focus in our laboratory for many years. Pyrazoles with alkyl groups, such as 3,5-$(CH_3)_2PzH$ and 3,5-(*t*-Bu)$_2$PzH, aryl groups, such as 3,5-$(Ph)_2PzH$, and fluorinated groups, such as 3,5-$(CF_3)_2PzH$, have been studied as ligands in coinage metal complexes.[5, 6] Our group and others have found many advantageous properties of fluorinated complexes over non-fluorinated. [5, 13, 14, 18-20, 23, 24, 27, 54-58] For example, fluorinated copper(I) trimers exhibit luminescent properties that could potentially be used in sensing or OLED applicaitons,[5] were found to successfully separate olefins from olefin/paraffin mixtures,[19, 28] and are excellent catalysts in reactions such as azide-alkyne cycloadditions.[26] Despite the numerous positive properties of complexes with fluorinated pyrazoles, these ligands are less common and more expensive than most non-fluorinated pyrazoles. For example, 3,5-$(CF_3)_2PzH$ is approximately 12 times more expensive than the non-fluorinated 3,5-$(CH_3)_2PzH$ (Table 3.1).

`

Table 3.1 Price per gram of various pyrazoles.

Pyrazole	Price per gram
3,5-$(CF_3)_2$PzH	$80.60
3,5-$(CH_3)_2$PzH	$6.52
3,5-(*i*-Pr)$_2$PzH	$67.10
3,5-$(Ph)_2$PzH	$49.85
3,5-$(CO_2Et)_2$PzH	$68.30
3,5-(*t*-Bu)$_2$PzH	$306.00
2,2,6,6-tetramethyl-3,5-heptanedione	$8.22

When looking for a non-fluorinated pyrazole that would provide similar properties as a ligand in coinage metal complexes, the sterics and electronics of the substituents on the pyrazole were considered. Although 3,5-(*i*-Pr)$_2$PzH is sterically similar to 3,5-$(CF_3)_2$PzH,[85] the electronics of *iso*-propyl and trifluoromethyl groups are very different.[30] This electronic difference is evident when comparing the chemical shift of the C(4)-*H* proton in ^{1}H NMR and in the different synthetic methods of the corresponding copper(I) trimers. The C(4)-*H* proton of 3,5-$(CF_3)_2$PzH is observed at 6.9 ppm, while the same proton of 3,5-(*i*-Pr)$_2$PzH is observed more upfield, at 5.9 ppm. When using 3,5-$(CF_3)_2$PzH, the trimeric copper complex is obtained by refluxing the pyrazole with Cu_2O in benzene or toluene.[5] The electron-withdrawing trifluoromethyl groups make the N-H proton quite acidic to react with copper(I) oxide. However, this method does not work when using pyrazoles with electron-donating substituents. When using pyrazole with *iso*-propyl groups, a stronger base must be used to deprotonate the N-H proton,[5, 6] Figure 3.1.

`

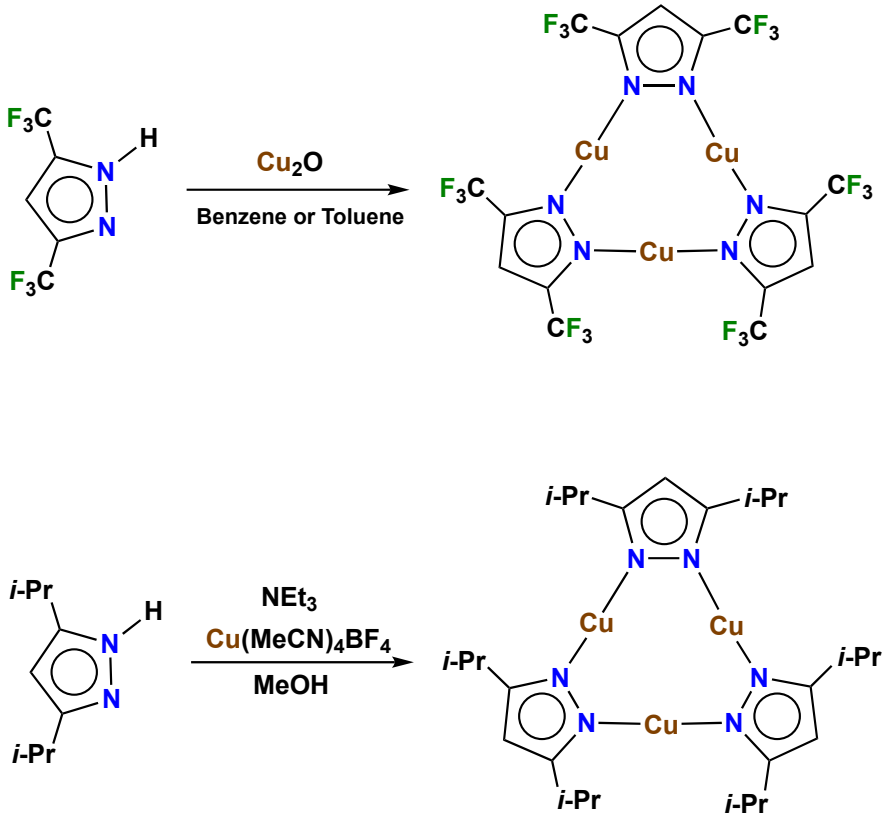

Figure 3.1 Synthesis of {[3,5-$(CF_3)_2$Pz]Cu}$_3$ and {[3,5-(*i*-Pr)$_2$Pz]Cu}$_3$.

When looking for a pyrazole that has similar electronics as 3,5-$(CF_3)_2$PzH we looked at other fluorinated pyrazoles, such as 3,5-(3,5-$(CF_3)_2$Ph)$_2$PzH mentioned in chapter 2. The NMR of this pyrazole has a chemical shift for the C(4)-*H* proton of 7.1 ppm, almost matching the chemical shift of the C(4)-*H* for 3,5-$(CF_3)_2$PzH. Additionally, both pyrazoles can be synthesized using an identical procedure of refluxing with copper(I) oxide in toluene.[5, 31] The identical C(4)-*H* chemical shifts and synthetic methods suggest these pyrazoles are very similar electronically. However, the -CF_3 groups are much less sterically demanding than -Ph(3,5-$(CF_3)_2$) groups making this pyrazole not an ideal substitute.

Another pyrazole investigated was 3,5-$(CO_2Et)_2$PzH. Ethyl ester groups have similar electronics to trifluoromethyl groups,[30] while also being sterically

`

similar.[85] The C(4)-*H* proton of 3,5-$(CO_2Et)_2$PzH is observed at 7.34 ppm which is closer to the chemical shift of 3,5-$(CF_3)_2$PzH than the *iso*-propyl analog. The A-value, i.e. the conformational free energy difference (ΔG, kcal/mol) for mono-substituted cyclohexane, of -CO_2Et substituents is 1.2 kcal/mol compared to the A-value of -CF_3, 2.1 kcal/mol. However, this is still closer sterically than 3,5-(3,5-$(CF_3)_2$Ph)$_2$PzH, as unsubstituted -Ph groups have an A-value of 3 kcal/mol. Another attractive feature of this pyrazole is that it is cheaper than 3,5-$(CF_3)_2$PzH and can also be easily synthesized from the very cheap 3,5-$(CH_3)_2$PzH,[86] Figure 3.2.

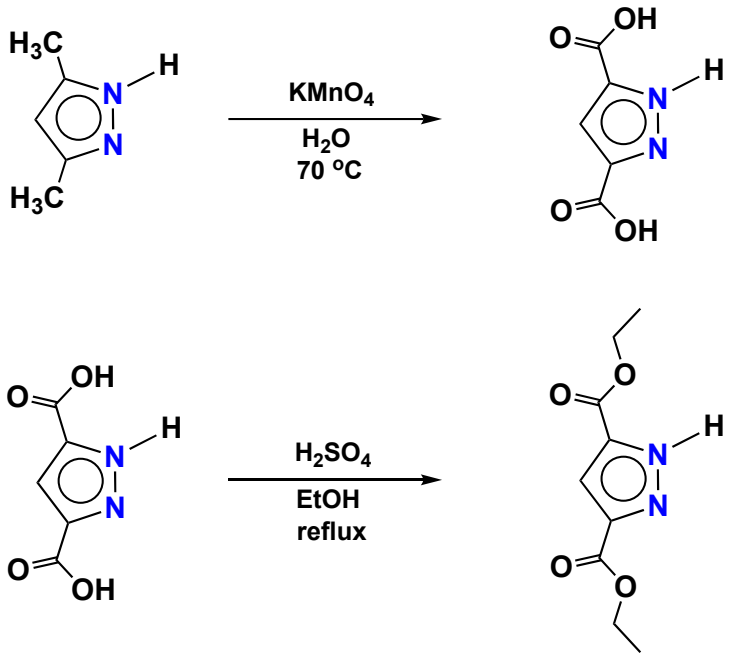

Figure 3.2 Synthesis of 3,5-$(CO_2Et)_2$PzH from 3,5-$(CH_3)_2$PzH.[86]

All of these features make 3,5-$(CO_2Et)_2$PzH a promising cheaper substitute for 3,5-$(CF_3)_2$PzH to be used as a ligand in coinage metal complexes, and potentially exhibit the same positive applications. Using the pyrazole 3,5-$(CO_2Et)_2$PzH and related 4-Br-3,5-$(CO_2Et)_2$PzH, four new coinage metal metallacycles, {[3,5-$(CO_2Et)_2$Pz]Cu}$_3$, {[3,5-$(CO_2Et)_2$Pz]Ag}$_3$, {[4-Br-3,5-

`

$(CO_2Et)_2Pz]Cu\}_3$, and $\{[4\text{-Br-}3,5\text{-}(CO_2Et)_2Pz]Ag\}_3$, Figure 3.3, were synthesized and investigated for their luminescence and catalytic abilities.

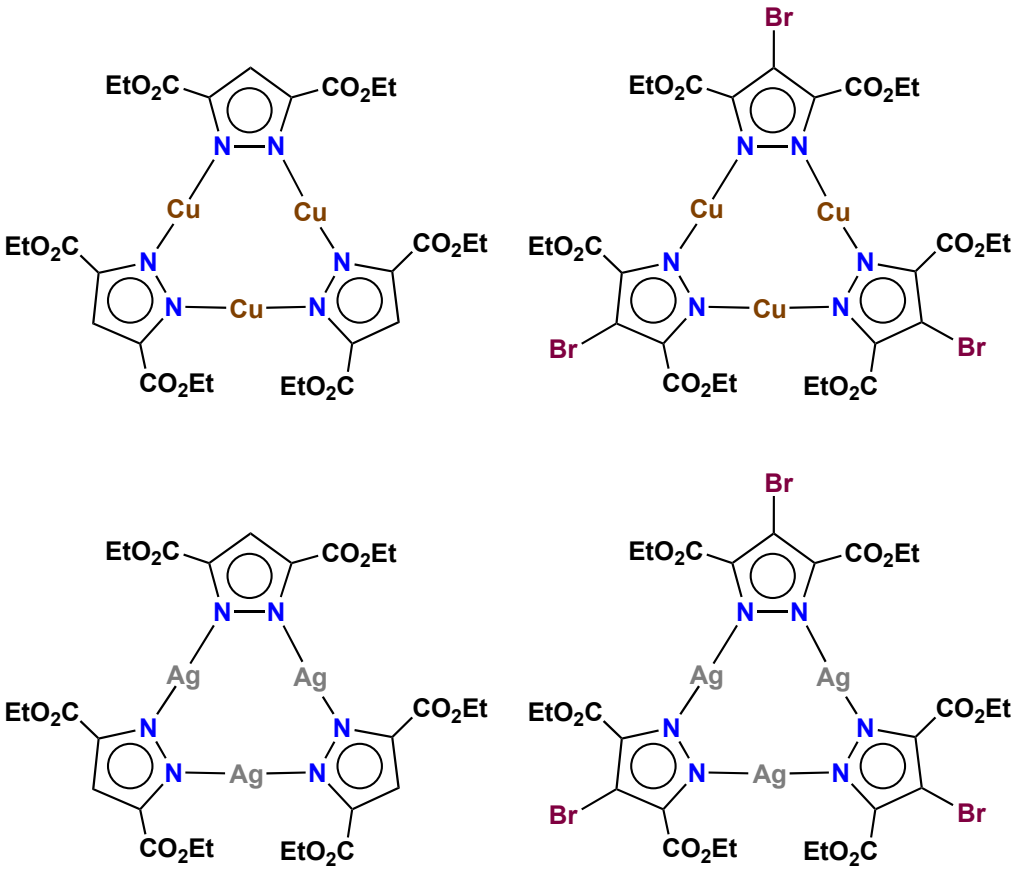

Figure 3.3 Four new coinage metal complexes with ethyl ester substituents on the pyrazolate backbone.

3.3 Results and discussion

Diethyl 3,5-dicarboxylate pyrazole was synthesized by a previously reported method.[86] The starting 3,5-dimethylpyrazole was oxidized with potassium permanganate and heated to 70 ℃ in water followed by a Fischer esterification with sulfuric acid in ethanol, heated to reflux. The crude product was purified via column chromatography (diethyl ether/hexanes, 2:1) to afford pure pyrazole in 63% yield. The ^{1}H NMR spectrum was consistent with previous reports.[86] The diethyl 4-bromo-3,5-dicarboxylate pyrazole was

`

synthesized from diethyl 3,5-dicarboxylate pyrazole in an analogous method to the synthesis of 4-bromo-3,5-bis(trifluoromethyl)pyrazole.[87] N-bromosuccinimide and diethyl 3,5-dicarboxylate pyrazole were combined and dissolved in N,N-dimethylformamide. The resulting solution was stirred at 130 °C overnight. The crude product was purified by column chromatography (ethyl acetate/hexanes, 1:1) to obtain pure pyrazole in 65% yield.

The trinuclear copper(I) pyrazolate, $\{[3,5\text{-}(CO_2Et)_2Pz]Cu\}_3$ was synthesized by combining the corresponding pyrazole with copper(I) oxide via a similar method to that reported for $\{[3,5\text{-}(CF_3)_2Pz]Cu\}_3$.[12] After refluxing the pyrazole and copper(I) oxide mixture overnight, the solution was filtered through Celite and dried to obtain a green oil. The oil was washed with hexanes to precipitate a pale green solid in 54% yield, $\{[3,5\text{-}(CO_2Et)_2Pz]Cu\}_3$. To remove toluene, the solids were heated under vacuum at 80 °C. The formation of $\{[3,5\text{-}(CO_2Et)_2Pz]Cu\}_3$ was confirmed by ^{1}H NMR. The starting pyrazole has a broad N-H singlet at 11.18 ppm that is absent in the spectrum of the copper(I) trimer, as expected. Additionally, there is a small shift in the singlet corresponding to C(4)-*H* from 7.34 ppm to 7.32 ppm, the quartet from the CH_2 of the ethyl group from 4.42 ppm to 4.34 ppm, and the triplet from the CH_3 hydrogens from 1.41 to 1.28 ppm. This solid is soluble in common organic solvents such as toluene, dichloromethane, chloroform, and tetrahydrofuran. However, crystals were not able to be obtained of this complex. The infrared spectrum of this solid was also examined and compared to the spectrum of the free ligand. The free ligand has one strong carbonyl absorption at 1729 cm^{-1} while the copper(I) trimer has a relatively less strong and sharp carbonyl absorption at 1718 cm^{-1}. This relatively weaker and broader peak could be

`

attributed to a weak interaction between some of the carbonyl oxygens and copper atoms.[11] However, the very slight shift in wavenumber more likely suggests the majority of the carbonyl groups are not coordinated to the copper(I) metal centers.

HRMS (ESI/TOF) data was obtained for $\{[3,5\text{-}(CO_2Et)_2Pz]Cu\}_3$ and the $[M+H]^+$ peaks were observed. As expected, multiple peaks are seen due to the isotopic distribution of copper, Cu^{63} and Cu^{65}, in 69.17% and 30.83% abundance, respectively. Additionally, due to the nuclearity, there are four $[M+H]^+$ peaks, corresponding to all possible combinations of copper isotopes. Based on the data three of these $[M+H]^+$ were observed, Table 3.2

Table 3.2 HRMS data for $\{[3,5\text{-}(CO_2Et)_2Pz]Cu\}_3$.

Ion	Calculated (m/z)	Found (m/z)
1. $C_{27}H_{34}Cu_3N_6O_{12}^+$ $[M+H]^+$		
1a. $[(Cu^{63})_3+H]^+$	823.0114	823.0062
1b. $[(Cu^{63})_2 + Cu^{65}+H]^+$	825.0096	825.0050
1c. $[Cu^{63} + (Cu^{65})_2+H]^+$	827.0078	827.0077
2. $C_{18}H_{24}CuN_4O_8^+$ [PzCu + PzH + H]$^+$		
2a. $[PzCu^{63} + PzH + H]^+$	487.0890	487.0872
2b. $[PzCu^{65} + PzH + H]^+$	489.0872	489.0833
3. $C_9H_{12}CuN_2O_4^+$ [PzCu + H]$^+$		
3a. $[PzCu^{63} + H]^+$	275.0093	275.0070
3b. $[PzCu^{65} + H]^+$	273.0075	273.0062

The trinuclear copper(I) pyrazolate, $\{[4\text{-Br-}3,5\text{-}(CO_2Et)_2Pz]Cu\}_3$ was synthesized in an analogous method to the preparation of $\{[3,5\text{-}(CO_2Et)_2Pz]Cu\}_3$ to afford a pale yellow-green solid in 40% yield. The starting pyrazole has a broad N-H peak in the ^{1}H NMR at 11.90 ppm. This peak, as expected, is absent in the ^{1}H NMR of the copper(I) trimer. Additionally, the ethyl CH_2 and CH_3 peaks shifted slightly from 4.42 ppm and 1.41 ppm to 4.38

`

ppm and 1.32 ppm, respectively. These shifted trimer peaks are broader than the free pyrazole peaks which may be attributed to some of the carbonyl oxygens interacting with the copper(I) metal center of the trimer and therefore those ethyl group being in a slightly different electronic environment than the groups not interacting with copper. Due to the large bromine atom in the 4-position on the pyrazole, the ethyl ester groups on the 3- and 5-position are pushed closer to the copper metal centers, so it is consistent that this trimer would have more carbonyl-metal interactions than the 4-hydro analog. However, crystals were not able to be obtained of this complex to confirm. The infrared spectrum of the free starting pyrazole has a single strong carbonyl absorption at 1723 cm^{-1}. The infrared spectrum of $\{[4\text{-Br-}3,5\text{-}(CO_2Et)_2Pz]Cu\}_3$ has multiple weaker carbonyl peaks at 1734, 1717, and 1696 cm^{-1}. These multiple peaks could correspond to a varying number of interactions between carbonyl oxygens and copper(I) metal centers.[11]

HRMS (ESI/TOF) data was obtained for $\{[4\text{-Br-}3,5\text{-}(CO_2Et)_2Pz]Cu\}_3$ and multiple $[M]^+$ peaks were present. These multiple peaks are seen due to the isotopic distribution of copper, Cu^{63} and Cu^{65}, in 69.17% and 30.83% abundance, respectively, and of bromine, Br^{79} and Br^{81}, in 50.69% and 49.31%, respectively. Additionally, due to the nuclearity, there are sixteen potential $[M]^+$ peaks, of which five were observed, Table 3.3.

`

Table 3.3 HRMS of {[4-Br-3,5-$(CO_2Et)_2$Pz]Cu}$_3$.

Ion	Calculated (m/z)	Found (m/z)
1. $C_{27}H_{30}Cu_3N_6O_{12}Br_3^+$ [M]$^+$		
1a. $[(Cu^{63})_2 + Cu^{65} + (Br^{79})_3 + H]^+$	1057.7333	1057.7343
1a. $[(Cu^{63})_3 + (Br^{79})_2 + Br^{81} + H]^+$	1057.7331	
1b. $[Cu^{63} + (Cu^{65})_2 + (Br^{79})_3 + H]^+$	1059.7315	1059.7273
1b. $[(Cu^{63})_3 + (Br^{79})_2 + Br^{81} + H]^+$	1059.7313	
1b. $[(Cu^{63})_2 + Cu^{65} + Br^{79} + (Br^{81})_2 + H]^+$	1059.7313	
1c. $[(Cu^{65})_3 + (Br^{79})_3 + H]^+$	1061.7297	1061.7360
1c. $[(Cu^{63})_3 + (Br^{81})_3 + H]^+$	1061.7291	
1c. $[(Cu^{63})_2 + Cu^{65} + (Br^{79})_2 + Br^{81} + H]^+$	1061.7293	
1c. $[Cu^{63} + (Cu^{65})_2 + (Br^{79})_2 + Br^{81} + H]^+$	1061.7294	
1d. $[(Cu^{63})_2 + Cu^{65} + (Br^{81})_3 + H]^+$	1063.7273	1063.7301
1d. $[Cu^{63} + (Cu^{65})_2 + Br^{79} + (Br^{81})_2 + H]^+$	1063.7275	
1d. $[(Cu^{65})_3 + (Br^{79})_2 + Br^{81} + H]^+$	1063.7277	
1e. $[Cu^{63} + (Cu^{65})_2 + (Br^{81})_3 + H]^+$	1065.7255	1065.7213
1e. $[(Cu^{65})_3 + Br^{79} + (Br^{81})_2 + H]^+$	1065.7257	

The trinuclear silver(I) pyrazolate, {[3,5-$(CO_2Et)_2$Pz]Ag}$_3$ was synthesized by combining the corresponding pyrazole with silver(I) oxide via a similar method to that reported for {[3,5-$(CF_3)_2$Pz]Ag}$_3$.[12] After refluxing the pyrazole and silver(I) oxide mixture overnight, the solution was filtered through Celite while hot and dried under vacuum to obtain a white solid in 49% yield, {[3,5-$(CO_2Et)_2$Pz]Ag}$_3$. This trinuclear silver(I) complex was only found to be soluble in hot chloroform and hot toluene and crystals were unable to be obtained. When comparing the ^{1}H NMR of the trimer to the free ligand, the N-*H* peak at 11.18 ppm was no longer present, the C(4)-*H* shifted from 7.34 ppm to 7.39 ppm, the CH_2 peak shifted slightly from 4.42 ppm to 4.46 ppm, and the CH_3 peak shifted from 1.41 ppm to 1.39 ppm. HRMS (ESI/TOF) data was obtained and confirmed the compound to be {[3,5-$(CO_2Et)_2$Pz]Ag}$_3$ due to the presence of $[M+H]^+$ peaks. As expected, multiple peaks are seen due to the

`

isotopic distribution of silver, Ag^{107} and Ag^{109}, in 51.84% and 48.16% abundance, respectively. Additionally, due to the nuclearity, there are four $[M+H]^+$ peaks, corresponding to all possible combinations of silver isotopes. This was observed for the corresponding fragments as well, Table 3.4.

Table 3.4 HRMS Data for $\{[3,5\text{-}(CO_2Et)_2Pz]Ag\}_3$

Ion	Calculated (m/z)	Found (m/z)
1. $C_{27}H_{34}Ag_3N_6O_{12}^+$ $[M+H]^+$		
1a. $[(Ag^{107})_3 + H]^+$	954.9379	954.9358
1b. $[(Ag^{107})_2 + Ag^{109} + H]^+$	956.9376	956.9364
1c. $[Ag^{107} + (Ag^{109})_2 + H]^+$	958.9373	958.9361
1d. $[(Ag^{109})_3 + H]^+$	960.9370	960.9378
2. $C_{18}H_{23}Ag_2N_4O_8^+$ $[(PzAg)_2+H]^+$		
2a. $[2Pz + (Ag^{107})_2 + H]^+$	636.9612	636.9595
2b. $[2Pz + Ag^{107} + Ag^{109} + H]^+$	638.9609	638.9598
2c. $[2Pz + (Ag^{109})_2 + H]^+$	640.9606	640.9596
3. $C_{18}H_{24}AgN_4O_8^+$ $[PzAg + PzH + H]^+$		
3a. $[PzAg^{107} + PzH + H]^+$	531.0639	531.0628
3b. $[PzAg^{109} + PzH + H]^+$	533.0636	533.0626
4. $C_9H_{12}AgN_2O_4^+$ $[PzAg + H]^+$		
4a. $[PzAg^{107} + H]^+$	318.9845	318.9807
4b. $[PzAg^{109} + H]^+$	320.9842	320.9814

The infrared spectrum of this trinuclear silver(I) pyrazolates was compared to the free starting pyrazole and both spectra were observed to have a strong, sharp carbonyl peak. The free pyrazole carbonyl peak is observed at 1729 cm^{-1} and the peak shifts to 1711 cm^{-1} for the silver(I) trimer. Only one strong carbonyl peak observed in the trimer spectrum, found close to the wavenumber of the free ligand, suggests the carbonyl groups on both the 3- and 5-position are equivalent and likely not coordinated to the silver(I) metal center. This finding was expected as silver(I) is larger than copper(I) and thus can better accommodate the substituents.[29]

`

The trinuclear silver(I) pyrazolate, {[4-Br-3,5-$(CO_2Et)_2$Pz]Ag}$_3$ was synthesized in an analogous method to {[3,5-$(CO_2Et)_2$Pz]Ag}$_3$ to obtain a white solid in 49% yield. This trinuclear silver(I) complex was also found to be only soluble in very hot chloroform and hot toluene and crystals were unable to be obtained. The ^{1}H NMR of the trimer showed a slight shift in peaks from free ligand, 4.42 ppm and 1.41 ppm to 4.41 ppm and 1.39 ppm. The product peaks were also observed to be much broader than those of the free ligand. Despite silver(I) being a larger metal ion,[29] the bromine atoms push the ester groups towards the metal. The peak broadening may then be due to some of the carbonyl oxygens interacting with the silver(I) metal centers of the trimer and therefore the ethyl group being in a slightly different electronic environment, just as seen with the 4-bromo copper analog.[11] HRMS (ESI/TOF) data was obtained and confirmed the compound to be {[4-Br-3,5-$(CO_2Et)_2$Pz]Ag}$_3$ due to the presence of $[M+H]^+$ peaks. Similarly to {[3,5-$(CO_2Et)_2$Pz]Ag}$_3$, multiple peaks are seen due to the isotopic distribution of silver, Ag^{107} and Ag^{109}, in 51.84% and 48.16% abundance, respectively. The isotopic distribution of bromine, Br^{79} and Br^{81}, in 50.69% and 49.31%, respectively, further contributes to additional $[M+H]^+$ peaks. Finally, the nuclearity of this trimer affords 16 isotopic combinations, of which four $[M+H]^+$ peaks were observed. Multiple peaks due to varying isotopes and combinations were observed for the corresponding fragments as well, Table 3.5.

`

Table 3.5 HRMS Data for {[4-Br-3,5-$(CO_2Et)_2$Pz]Ag}$_3$

Ion	Calculated (m/z)	Found (m/z)
1. $C_{27}H_{31}Ag_3N_6O_{12}Br_3^+$ [M+H]$^+$		
1a. [Ag^{107} + $(Ag^{109})_2$ + $(Br^{79})_3$ +H]$^+$	1192.6688	1192.6822
1a. [$(Ag^{107})_3$ + Br^{79} + $(Br^{81})_2$ +H]$^+$	1192.6654	
1a. [$(Ag^{107})_2$ + Ag^{109} + $(Br^{79})_2$ + Br^{81} +H]$^+$	1192.6671	
1b. [$(Ag^{109})_3$ + $(Br^{79})_3$ +H]$^+$	1194.6685	1194.6522, 1194.6906
1b. [$(Ag^{107})_2$ + Ag^{109} + Br^{79} + $(Br^{81})_2$ +H]$^+$	1194.6651	
1b. [$(Ag^{107})_3$ + $(Br^{81})_3$ +H]$^+$	1194.6634	
1b. [Ag^{107} + $(Ag^{109})_2$ + $(Br^{79})_2$ + Br^{81} +H]$^+$	1194.6668	
1c. [$Ag_2{}^{107}$ + Ag^{109} + $Br_3{}^{81}$ + H]$^+$	1196.6665	1196.6758

The infrared spectrum of this trinuclear silver(I) pyrazolates was compared to the free starting pyrazole. The spectrum of the starting pyrazole has a strong, sharp carbonyl peak at 1723 cm^{-1}. The silver(I) trimer, however, has multiple weaker and broader peaks at 1727 cm^{-1}, 1696 cm^{-1}, and 1686 cm^{-1}, similar to the spectrum observed in the case of {[4-Br-3,5-$(CO_2Et)_2$Pz]Cu}$_3$. Again, the multiple peaks could correspond to a varying number of interactions between carbonyl oxygens and silver(I) metal centers, due to the bromine atom on the 4-position pushing the ethyl ester groups closer to the metal centers.

3.4 Photophysical properties

All four coinage metal trimers were check for photoluminescence using UV light. Neither copper(I) pyrazolate showed luminescence, at room temperature or low temperature. However, both silver pyrazolates showed luminescence at room temperature and low temperature (77 K). The 4-bromo analog shows light green emission at room and low temperatures while the 4-hydro analog shows blue emission at both temperatures. However, the room temperature

`

luminescence in both cases was too dim to obtain good spectra, so only the low temperature luminescence spectra were obtained. At 77 K, {[3,5-$(CO_2Et)_2Pz$]Ag}$_3$ displayed blue luminescence under UV radiation with an excitation maximum at 287 nm and emission maximum at 370 nm and 390 nm, with a Stokes Shift of ~8300 cm^{-1}, Figure 3.4. The 4-bromo analog, {[4-Br-3,5-$(CO_2Et)_2Pz$]Ag}$_3$, at 77 K displayed light green luminescence under UV radiation with an excitation maximum of 384 nm and emission maximum at 542 nm, with a Stokes Shift of ~14000 cm^{-1}, Figure 3.5.

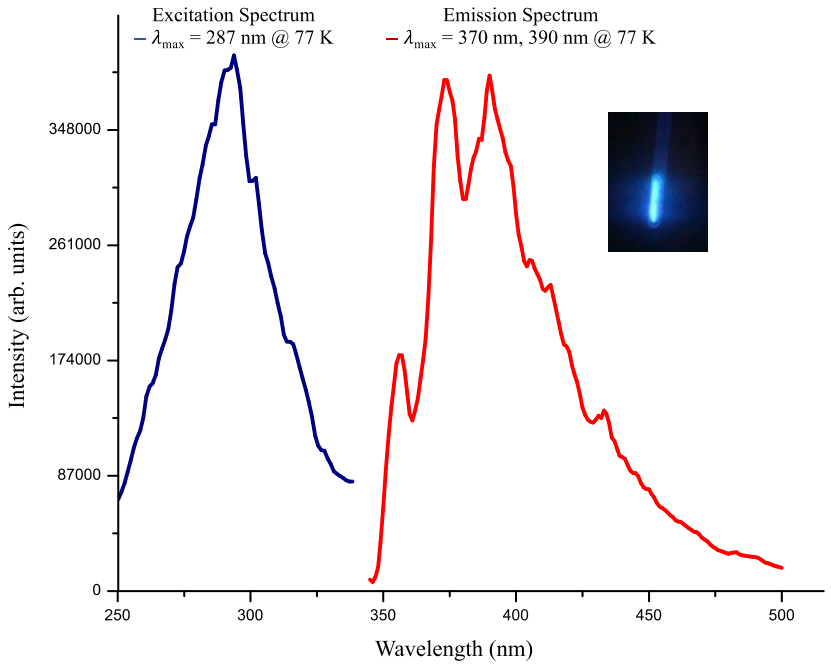

Figure 3.4 Luminescence spectrum of {[3,5-$(CO_2Et)_2Pz$]Ag}$_3$ at 77 K.

`

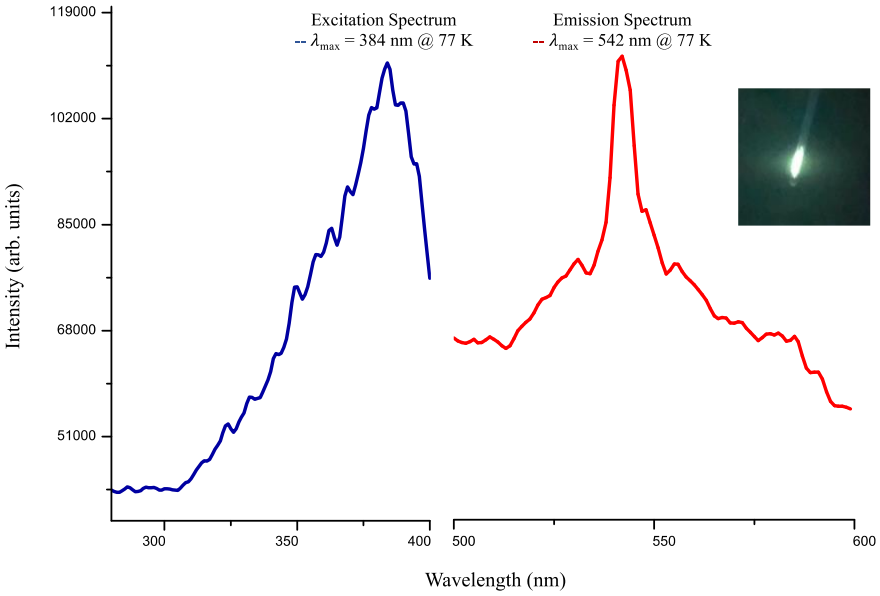

Figure 3.5 Luminescence spectrum of $\{[4\text{-Br-}3,5\text{-}(CO_2Et)_2Pz]Ag\}_3$ at 77 K.

3.5 Catalysis

Copper catalyzed azide-alkyne cycloadditions (CuAAC) are a very important process with many biological and medicinal applications.[79, 82, 88, 89] The standard catalytic system for these reactions is a copper(II) salt and reducing agent, such as copper sulfate pentahydrate and sodium ascorbate.[77, 90] Recently, our group and others reported excellent stand-alone trinuclear copper catalysts, $\{[3,5\text{-}(CF_3)_2Pz]Cu\}_3$ and $\{[3,5\text{-}(3,5\text{-}(CF_3)_2Ph)_2Pz]Cu\}_3$.[26, 31] However, both catalysts mentioned are highly fluorinated and therefore more expensive than non-fluorinated trinuclear copper(I) pyrazolates. In an attempt to extend this work and find a cheaper catalytic alternative, both $\{[3,5\text{-}(CO_2Et)_2Pz]Cu\}_3$ and $\{[4\text{-Br-}3,5\text{-}(CO_2Et)_2Pz]Cu\}_3$ were tested as catalysts in copper catalyzed azide-alkyne cycloadditions (CuAAC). As previously mentioned, the ethyl ester groups are electronically similar to trifluoromethyl groups[30] so we were hopeful that these new trimers would perform as equally excellent catalysts. In an identical method to previous work, 1 mol percent of

`

catalyst was added to a mixture of 100 mg of *p*-tolylazide, 1 equivalent of alkyne, and 5 mL of dichloromethane. The resulting mixture was stirred at room temperature for 12 hours. An aliquot was then taken and ^{1}H NMR was run to check for the presence of the desired 1,4-disubstituted 1,2,3-triazole. Based on the NMR spectra, it was observed that neither trimer catalyzed these cycloadditions effectively, with percent conversions of only 2-15%, Table 3.6.

Table 3.6 Azide-alkyne cycloadditions using {[3,5-$(CO_2Et)_2$Pz]Cu}$_3$ and {[4-Br-3,5-$(CO_2Et)_2$Pz]Cu}$_3$. Reactions were done at room temperature, with 1 mol % catalyst loading, and stirred for 12 hours.

Entry	Catalyst	Alkyne	% Conversion
1	[{3,5-$(CO_2Et)_2$Pz}Cu]$_3$	1-octyne	4
2	[{3,5-$(CO_2Et)_2$Pz}Cu]$_3$	phenylacetylene	15
3	[{4-Br-3,5-$(CO_2Et)_2$Pz}Cu]$_3$	1-octyne	2

Both catalysts tested are electronically similar to {[3,5-$(CF_3)_2$Pz]Cu}$_3$ so the poor catalytic ability likely cannot be attributed to the electronics of the catalysts. Rather, the poor catalytic ability could be due to the sterics of the ethyl ester groups. However, previous work by our group had shown trinuclear copper(I) pyrazolates with very sterically demanding substituents, i.e. {[(3,5-$(CF_3)_2$Ph)$_2$Pz]Cu}$_3$, can effectively catalyze these cycloadditions.[31] While the ethyl ester groups are not extremely bulky, the do contain oxygen atoms that could interact with the metal centers. The 4-bromo analog even more so causes the ester groups to be pushed towards the metal thereby increasing the likelihood of Cu-O interactions. Additionally, as previously mentioned, the IR spectra of both complexes showed broader, weaker C=O stretching frequencies, possibly indicating such interactions are present.[11] A recent study from

`

Larionov, Titov and coworkers reported a mechanism for the {[3,5-$(CF_3)_2$Pz]Cu}$_3$ mediated azide-alkyne cycloaddition reaction.[91] In this work, they propose the first step of the catalytic cycle is coordination between the metal center and alkyne. If the ester groups from these two new copper(I) trimers are indeed blocking the copper(I) metal centers, or even interacting with the copper metal centers themselves, this would cause alkyne coordination to be much more difficult and therefore lower the catalytic ability of the complexes. Based on previous discussion, it would be expected that {[4-Br-3,5-$(CO_2Et)_2$Pz]Cu}$_3$ would have greater Cu-O interactions than {[3,5-$(CO_2Et)_2$Pz]Cu}$_3$ and would be expected to be a less effective catalyst. In accordance with this logic, {[4-Br-3,5-$(CO_2Et)_2$Pz]Cu}$_3$ was found to catalyze the reaction between *p*-tolylazide and 1-octyne in half the percent conversion compared to {[3,5-$(CO_2Et)_2$Pz]Cu}$_3$, Table 3.6.

3.6 Conclusions

We synthesized four non-fluorinated coinage metal pyrazolates: {[3,5-$(CO_2Et)_2$Pz]Cu}$_3$, {[4-Br-3,5-$(CO_2Et)_2$Pz]Cu}$_3$, {[3,5-$(CO_2Et)_2$Pz]Ag}3, and {[4-Br-3,5-$(CO_2Et)_2$Pz]Ag}$_3$. Although the ethyl ester groups are electronically very similar and sterically somewhat similar to trifluoromethyl, it was observed that these newly synthesized trimers do not have the same attractive properties as the bis(trifluoromethyl) analogs. The silver(I) trinuclear pyrazolates exhibit luminescence but the copper(I) trimers do not. The copper(I) complexes were also observed to be poor catalysts in copper catalyzed azide-alkyne cycloaddition reactions (CuAAC). This could be attributed to the ethyl ester groups interacting with the coinage metal centers. In conclusion, despite numerous similarities between 3,5-$(CO_2Et)_2$PzH and 3,5-$(CF_3)_2$PzH, the

`

corresponding coinage metal complexes exhibit very different properties that do not allow for 3,5-$(CF_3)_2$PzH to be interchanged for the cheaper 3,5-$(CO_2Et)_2$PzH.

`

Chapter 4

Tetranuclear and trinuclear copper(I) pyrazolates as catalysts in copper catalyzed azide-alkyne cycloadditions (CuAAC)

Monika R. Patterson, Devaborniny Parasar, and H. V. Rasika Dias

Part of this work has been published in *Dalton Trans.*, 2021, DOI: 10.1039/D1DT04026J [92]

`

4.1 Abstract

1,2,3-triazoles have been a highly researched topic due to their biological applications. The 1,4-disubstituted isomers have particular biological interest due to their therapeutic potential in areas such as antitumor, anticancer, and anti-HIV. Various methods to synthesize these heterocycles have been developed such as Huisgen cycloaddition and Sharpless's click chemistry reaction using a copper catalyst. More recently, our group successfully isolated the 1,4-disubstituted product in excellent yields and mild conditions using standalone, highly fluorinated, trinuclear copper(I) catalysts, $\{[3,5\text{-}(CF_3)_2Pz]Cu\}_3$ and $\{[3,5\text{-}(3,5\text{-}(CF_3)_2Ph)_2Pz]Cu\}_3$. In this chapter we further investigated the catalytic ability of other trinuclear and tetranuclear copper(I) pyrazolates, $\{[3,5\text{-}(i\text{-}Pr)_2Pz]Cu\}_3$, $\{[3\text{-}(CF_3)\text{-}5\text{-}(CH_3)Pz]Cu\}_3$, $\{[3,5\text{-}(t\text{-}Bu)_2Pz]Cu\}_4$, $\{[3\text{-}(CF_3)\text{-}5\text{-}(t\text{-}Bu)Pz]Cu\}_4$, $\{[4\text{-}Br\text{-}3,5\text{-}(i\text{-}Pr)_2Pz]Cu\}_4$, and the newly synthesized $\{[4\text{-}NO_2\text{-}3,5\text{-}(CF_3)_2Pz]Cu\}_3$. It was found that the homoleptic tetranuclear copper(I) pyrazolates are excellent stand-alone catalysts for azide-alkyne cycloaddition reactions (CuAAC). This work demonstrates that a range of pyrazolates, including those with electron donating and electron-withdrawing groups to sterically demanding substituents on the pyrazolyl backbones, can serve as effective ligand supports on tetranuclear copper catalysts. However, in contrast to the tetramers and also highly fluorinated $\{[3,5\text{-}(CF_3)_2Pz]Cu\}_3$, trinuclear copper(I) complexes such as $\{[3,5\text{-}(i\text{-}Pr)_2Pz]Cu\}_3$ and $\{[3\text{-}(CF_3)\text{-}5\text{-}(CH_3)Pz]Cu\}_3$ supported by relatively electron rich pyrazolates display poor catalytic activity in CuAAC. The behavior and degree of aggregation of several of these copper(I) pyrazolates in solution were examined using vapor pressure osmometry. Copper(I) complexes such as $\{[3,5\text{-}(CF_3)_2Pz]Cu\}_3$ and $\{[3\text{-}(CF_3)\text{-}$

`

5-(*t*-Bu)Pz]Cu}$_4$ with electron withdrawing pyrazolates were found to break up in solution to different degrees producing smaller aggregates while those such as {[3,5-(*i*-Pr)$_2$Pz]Cu}$_3$ and {[3,5-(*t*-Bu)$_2$Pz]Cu}$_4$ with electron rich pyrazolates remain intact. In addition, kinetic experiments were performed to understand the unusual activity of tetranuclear copper(I) pyrazolate systems..

4.2 Introduction

Triazoles represent an important class of heterocyclic ring structures due to their extensive biological and therapeutic applications.[93] Two possible isomers exist of triazoles, namely 1,2,3-triazoles and 1,2,4-triazoles. The 1,2,3-triazoles are of particular interest between these because of their stability towards oxidative and reductive conditions and hydrolysis.[94, 95] Additionally, the 1,4-disubstituted version of 1,2,3-triazoles can serve as good models for bioactive amides due to its strong dipole moment, planarity, hydrogen bond donor/acceptor characters, and other features, Figure 4.1. For example, the lone pair on the nitrogen of the triazole mimics the hydrogen bond accepting character of the carbonyl on the amide, while the triazole C(5)-H mimics the hydrogen bond donor character of the amide N-H.

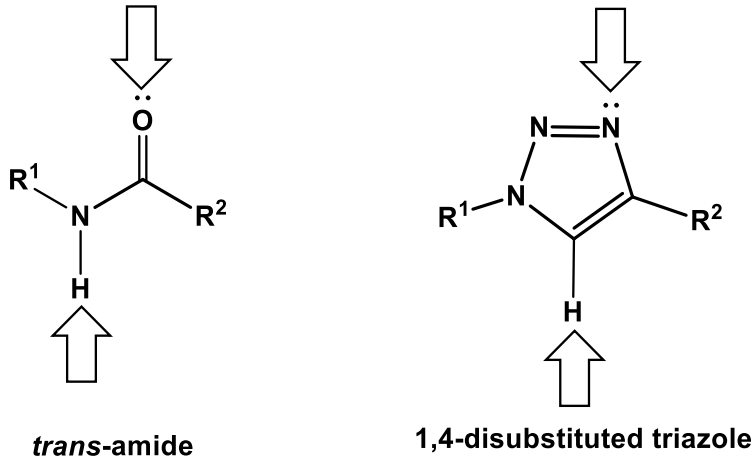

Figure 4.1 Similarities between trans-amide and 1,4-disubstituted triazoles.

`

Due to the importance and wide utility, there has been much effort focused on the efficient synthesis 1,2,3-triazole. One of the earliest and most effective methods is the Huisgen cycloaddition where an azide and terminal alkyne are combined and heated.[96] However, this method yields a mixture of 1,4-disubstituted and 1,5-disubstituted isomers, Figure 4.2. Furthermore, the need for elevated temperature and low yields makes Huisgen cycloaddition less than ideal for wider synthetic purposes.[88] Later, Sharpless and Meldal improved on this reaction and used a copper catalyst to obtain only the 1,4-substituted isomer, Figure 4.2.[90, 97] Using this copper-catalyzed azide–alkyne cycloaddition (CuAAC) chemistry route, many 1,4-disubstituted 1,2,3-triazoles could be synthesized in high yields, under milder conditions, and with easily removable solvents and byproducts.[89, 90, 98, 99] However, these reactions often require the use of a reducing agent such as sodium ascorbate to reduce the copper source (e.g., commonly utilized copper sulfate pentahydrate) to the catalytically active copper(I) species.

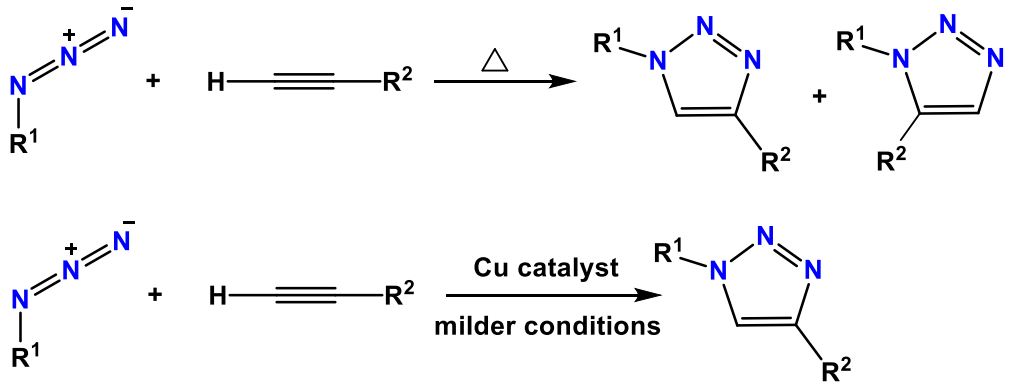

Figure 4.2 Huisgen cycloaddition (top) leading to the 1,4- and 1,5-regioisomers of 1,2,3-triazoles; Sharpless and Meldal, copper-catalyzed azide-alkyne cycloaddition (CuAAC) reaction affording the 1,4-regioisomer of 1,2,3-triazole (bottom)

`

More recently our group[26] and Titov, Larionov, and co-workers[45] found that the need for a reducing agent could be eliminated by using the trinuclear copper(I) pyrazolates {[3,5-$(CF_3)_2$Pz]Cu}$_3$ (Figure 4.3, **1**)[12] and {[3,5-(3,5-$(CF_3)_2$Ph)$_2$Pz]Cu}$_3$ as catalysts.[31] These reactions are quite attractive as they are mediated by standalone copper pyrazolates, which serve as a bifunctional catalytic system providing copper source and Bronsted base, operate at room temperature, and afford only the 1,4-isomer in essentially quantitative yields.

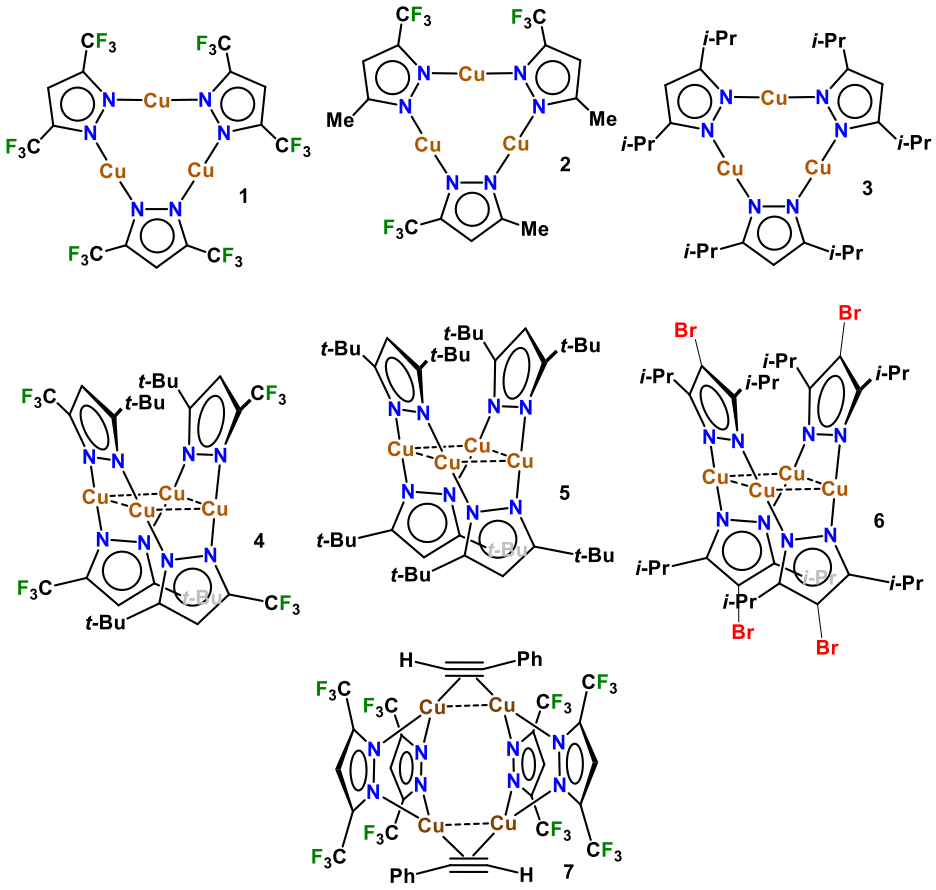

Figure 4.3 Structure of selected trinuclear and tetranuclear copper(I) pyrazolate catalysts and the proposed reaction intermediate in copper pyrazolate mediated CuAAC reactions.

There are a variety of copper(I) pyrazolates known in the literature.[3, 100, 101] Among these, highly fluorinated copper(I) pyrazolates are relatively more

`

expensive and less common than their non-fluorinated analogs.[5] Encouraged by the catalytic ability of these trinuclear copper(I) pyrazolates, we set out to investigate if other copper(I) pyrazolates such as trimers and tetramers supported by more electron-rich, non-fluorinated analogs were similarly effective in mediating the azide-alkyne cycloaddition chemistry. Specifically, we investigated the catalytic ability of the trinuclear copper(I) pyrazolates {[3-(CF_3)-5-(CH_3)Pz]Cu}$_3$ (**2**), {[3,5-(*i*-Pr)$_2$Pz]Cu}$_3$ (**3**) and the tetranuclear copper(I) pyrazolates {[3-(CF_3)-5-(*t*-Bu)Pz]Cu}$_4$ (**4**), {[3,5-(*t*-Bu)$_2$Pz]Cu}$_4$ (**5**), and {[4-Br-3,5-(*i*-Pr)$_2$Pz]Cu}$_4$ (**6**), and uncovered some unique reactivity of tetranuclear species in CuAAC chemistry.[5, 11, 22] We also synthesized, characterized, and tested the catalytic ability of {[4-NO_2-3,5-(CF_3)$_2$Pz]Cu}$_3$ to further compare highly fluorinated trinuclear complexes against non-fluorinated analogs.

4.3 Results and discussion

Catalysis

As noted above, the highly fluorinated {[3,5-(CF_3)$_2$Pz]Cu}$_3$ (**1**) catalyzes azide-alkyne cycloadditions very effectively (Table 4.1, entries 1-4), affording ≥ 99% conversion at room temperature using only 1 mol percent of catalyst.[26, 31, 91] We found that the less fluorinated {[3-(CF_3)-5-(CH_3)Pz]Cu}$_3$ (**2**) and non-fluorinated {[3,5-(*i*-Pr)$_2$Pz]Cu}$_3$ (**3**) catalyze the reaction between 1-octyne or phenylacetylene with *p*-tolylazide, under similar conditions, but only very sluggishly, giving disappointingly low product yields (entries 5-8). Although the percent conversion slightly improved when benzyl azide was used due to increased azide reactivity (entries 9-10),[102-104] they remained significantly lower

`

than those observed with highly fluorinated catalysts. When using the sterically hindered 1-adamantyl azide, the percent conversion was zero at room temperature and only slightly increased when the reaction was heated in chloroform at 60 ℃.

Table 4.1 Azide-alkyne cycloadditions with trinuclear copper(I) catalysts. Reactions were performed at room temperature in dichloromethane with 1 mol% catalyst loading. *reaction done in chloroform at 60℃. #reaction done in THF due to poor catalyst solubility.

Entry	Catalyst	Reaction Time	Alkyne	Azide	% Conversion	Ref
1	{[3,5-$(CF_3)_2$Pz]Cu}$_3$ (**1**)	12 hrs	1-octyne	*p*-tolylazide	99	105
2			phenylacetylene	*p*-tolylazide	99	105
3		4 hrs	1-octyne	benzylazide	> 99	106
4			phenylacetylene	benzylazide	> 99	106
5	{[3-(CF_3)-5-(CH_3)Pz]Cu}$_3$ (**2**)	12 hrs	1-octyne	*p*-tolylazide	12	This work
6			phenylacetylene	*p*-tolylazide	6	This work
7	{[3,5-(*i*-Pr)$_2$Pz]Cu}$_3$ (**3**)	12 hrs	1-octyne	*p*-tolylazide	13	This work
8			phenylacetylene	*p*-tolylazide	12	This work
9			1-octyne	benzylazide	15	This work
10			phenylacetylene	benzylazide	40	This work
11			phenylacetylene	1-adamantyl azide	0	This work
12			phenylacetylene	1-adamantyl azide	2*	This work
13		36 hrs	phenylacetylene	1-adamantyl azide	6*	This work
14	{[4-NO_2-3,5-$(CF_3)_2$Pz]Cu}$_3$	12 hrs	1-octyne	benzylazide	43#	This work
15			phenylacetylene	benzylazide	100#	This work

The {[3,5-(*i*-Pr)$_2$Pz]Cu}$_3$ (**3**) and {[3,5-(CF_3)$_2$Pz]Cu}$_3$ (**1**) have sterically similar (the CF_3 group is considered as sterically similar to the *iso*-propyl group)[107, 108] but electronically very different[30] substituents. Therefore, the

`

sluggish catalytic activity of {[3,5-(*i*-Pr)$_2$Pz]Cu}$_3$ (**3**) may not be a simple result of steric effects. On the other hand, the pyrazolate ligands bearing *iso*-propyl and methyl groups are significantly better donors than weakly donating [3,5-(CF$_3$)$_2$Pz]$^-$. For example, copper(I) carbonyl complexes supported by tris(pyrazolyl)borates [HB(3,5-(*i*-Pr)$_2$Pz)$_3$]$^-$, [HB(3-(CF$_3$)-5-(Me)Pz)$_3$]$^-$, and [HB(3,5-(CF$_3$)$_2$Pz)$_3$]$^-$ show their CO stretching frequencies at 2056, 2107, and 2137 cm^{-1}, respectively.[109-111] This could result in relatively strong Cu-N interactions and less electrophilic copper sites in {[3,5-(*i*-Pr)$_2$Pz]Cu}$_3$ (**3**) and {[3-(CF$_3$)-5-(CH$_3$)Pz]Cu}$_3$ (**2**).

To further confirm these findings, we synthesized a new copper(I) trinuclear complex using a highly fluorinated and electron-withdrawing pyrazole, 4-NO$_2$-3,5-(CF$_3$)$_2$PzH. This copper complex was synthesized in an analogous method to {[3,5-(CF$_3$)$_2$Pz]Cu}$_3$ (**1**) by combining pyrazole and copper(I) oxide in toluene and refluxing the resulting mixture overnight.[5, 12] After cooling, tetrahydrofuran is added due to the product insolubility in toluene and then the mixture is filtered through Celite to remove excess copper(I) oxide. The solvent was removed to obtain {[4-NO$_2$-3,5-(CF$_3$)$_2$Pz]Cu}$_3$ as a yellow solid in 90% yield. The copper complex was re-crystallized from tetrahydrofuran at -20 ℃. The X-ray crystal structure shows this trimer crystallizes with one coordinated tetrahydrofuran molecule, Figure 4.4.

`

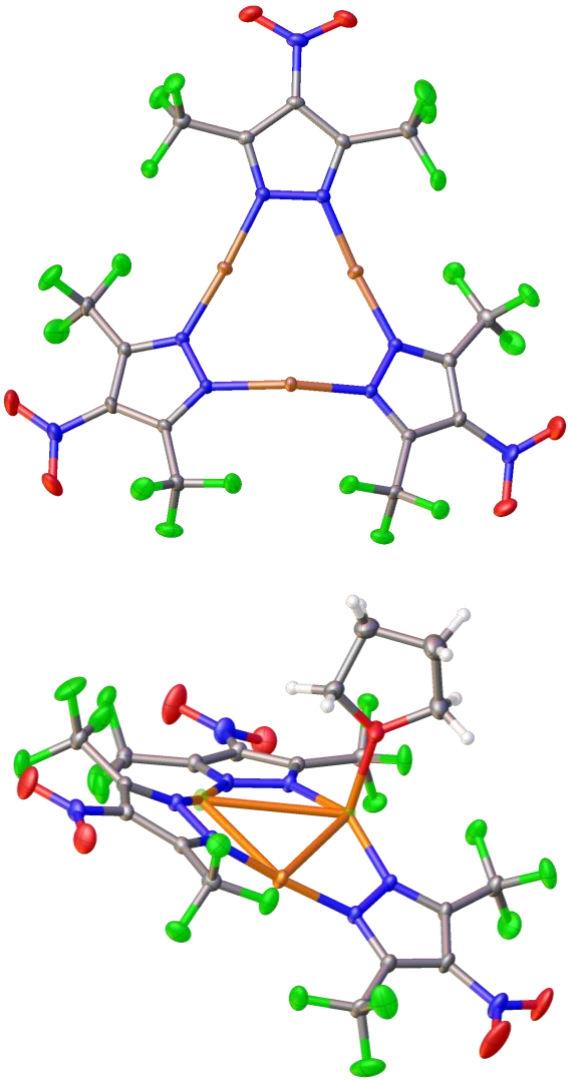

Figure 4.4 XRD structure of {[4-NO_2-3,5-$(CF_3)_2$Pz]Cu}$_3$ with coordinated THF omitted for clarity (top) and {[4-NO_2-3,5-$(CF_3)_2$Pz]Cu}$_3$·THF (bottom).

When performing azide-alkyne cycloadditions of benzylazide and 1-octyne or phenylacetylene with this catalyst in identical conditions, stirred for 12 hours at room temperature with 1 mol percent catalyst in dichloromethane, the percent conversion was surprisingly low. However, it was observed that {[4-NO_2-3,5-$(CF_3)_2$Pz]Cu}$_3$ was insoluble in dichloromethane. The catalysis reactions were repeated in tetrahydrofuran, a solvent the catalyst fully dissolves in, and the percent conversion increased, (entries 14-15).

`

Recently, Larionov, Titov and coworkers reported a mechanism for the {[3,5-$(CF_3)_2$Pz]Cu}$_3$ mediated CuAAC reaction in which a tetranuclear copper(I) pyrazolate-alkyne complexes are believed to play a major role as intermediates in the catalytic cycle.[91] They proposed that {[3,5-$(CF_3)_2$Pz]Cu}$_3$ interacts with the triple bond of the alkyne via η^2-coordination to form the catalytically active "bis-butterfly" tetranuclear complex Cu_4(pyrazolate)$_4$(RC≡CH)$_2$ (Figure 4.3, **7**). Indeed, it is possible to break up the trinuclear {[3,5-$(CF_3)_2$Pz]Cu}$_3$ with alkynes and form such tetranuclear intermediates, further supporting this proposed mechanism.[87] Thus, it is likely that the poor catalytic ability of {[3,5-(*i*-Pr)$_2$Pz]Cu}$_3$ (**3**) and {[3-(CF_3)-5-(CH_3)Pz]Cu}$_3$ (**2**) may be a result of stronger Cu-N bonds making the structure reorganization and tetranuclear intermediate (or even a more common dinuclear copper intermediate complex)[82, 112-115] formation more difficult through interactions with weak alkyne nucleophiles. We were able to isolate a similar dinuclear complex with {[4-NO_2-3,5-$(CF_3)_2$Pz]Cu}$_3$ and phenylacetylene, Cu_2(4-NO_2-3,5-$(CF_3)_2$Pz)$_2$(PhC≡CH)$_2$. X-ray quality crystals of this complex were obtained from dichloromethane at -20 ℃, Figure 4.5. This structure contributes to a library of similar structures obtained by our group previously.[26]

`

1

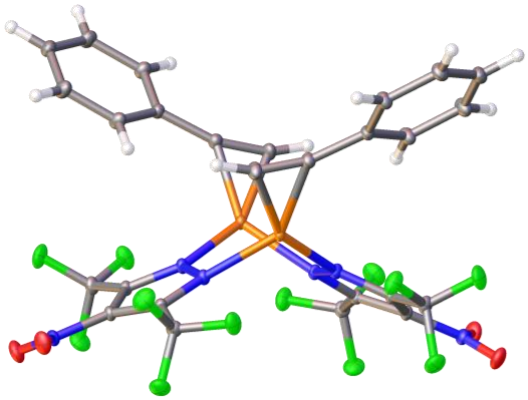

2

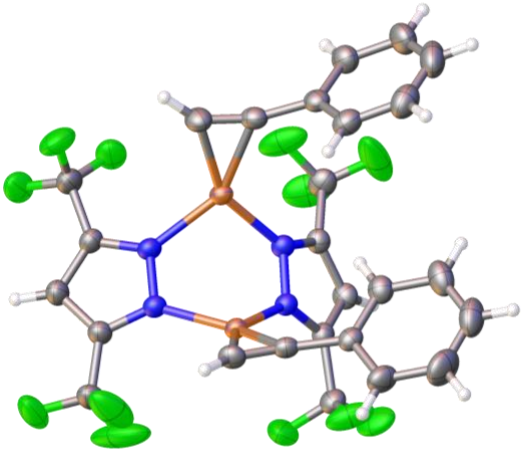

Figure 4.5 XRD structure of $Cu_2(4\text{-}NO_2\text{-}3,5\text{-}(CF_3)_2Pz)_2(PhC{\equiv}CH)_2$ (**1**) and $Cu_2(3,5\text{-}(CF_3)_2Pz)_2(PhC{\equiv}CH)_2$ (**2**).

Interestingly, this crystal structure is slightly different than the previously reported complex using $\{[3,5\text{-}(CF_3)_2Pz]Cu\}_3$ (**1**). In the previous crystal structure, the orientation of phenyl groups point in the same direction[26], while in this new complex the phenyl groups point in opposite directions. The bond lengths and angles were also compared between **1** and **2** and can be found in Table 4.2. Despite the difference in orientation of phenylacetylene, all bond lengths and angles are very similar between the two complexes.

`

Table 4.2 Selected bond lengths (Å) and angles (°) for Cu_2(4-NO_2-3,5-(CF_3)$_2$Pz)$_2$(PhC≡CH)$_2$ (**1**) and Cu_2(3,5-(CF_3)$_2$Pz)$_2$(PhC≡CH)$_2$ (**2**)

Parameter\complex	**1**	**2**[26]
Av. Cu-C(H)≡	1.960	1.943
Av. Cu-C(C)≡	2.001	1.996
Av. C≡C	1.239	1.226
Av. Cu-N	1.987	1.971
Shortest Cu···Cu	3.033	3.161
Av. C-Cu-C	36.43	36.23
Av. C-C≡C	160.2	161.4
Av N-Cu-N	99.74	100.05

After observing disappointing outcomes from these less fluorinated and non-fluorinated copper(I) trimers, we turned our attention to the related tetranuclear species. Trinuclear copper(I) pyrazolates are the most common structural type of homoleptic copper pyrazolates and have a planar geometry (see **1**-**3**). Tetranuclear copper(I) pyrazolate complexes (e.g., **4**-**6**), in contrast, feature saddle-shaped structures.[6, 22, 100] Furthermore, trinuclear species tend to aggregate as a result of multiple inter-trimer cuprophilic Cu•••Cu interactions,[5, 101] whereas the tetramers usually remain as discrete entities in the solid.[6, 22] Therefore, we anticipated we could observe different reactivity in tetranuclear copper(I) pyrazolates.

The activity of three different tetranuclear copper(I) pyrazolates, {[3-(CF_3)-5-(*t*-Bu)Pz]Cu}$_4$ (**4**), {[3,5-(*t*-Bu)$_2$Pz]Cu}$_4$ (**5**), and {[4-Br-3,5-(*i*-Pr)$_2$Pz]Cu}$_4$ (**6**) in CuAAC were investigated. These catalysts were tested under identical conditions to previous trials using dichloromethane as a solvent and stirring at room temperature for 12 hours. Contrary to the trend found in trinuclear copper complexes, both electron deficient and electron rich tetranuclear copper pyrazolates were excellent catalysts (Table 4.3). It was observed that the

`

percent conversion improved to > 99% (entries 18-19, 22-23, 27-28) when using the relatively more reactive benzyl azide instead of the *p*-tolylazide.[102-104] The percent conversion is somewhat lower when reacting phenylacetylene with *p*-tolylazide (entries 17, 21). This can be attributed to the increased steric bulk of the phenyl ring on the alkyne making coordination to the copper center of the catalysts more difficult. However, even with this increase in steric strain, the percent conversion remains much higher than those observed with electron rich copper(I) trimers. In contrast to trinuclear {[3,5-(*i*-Pr)$_2$Pz]Cu}$_3$ (**3**), tetranuclear {[3,5-(*t*-Bu)$_2$Pz]Cu}$_4$ (**5**) is also effective in the CuAAC involving highly sterically hindered 1-adamantyl, albeit at a higher temperature of 60 ℃, providing the desired triazole.

Table 4.3. Azide-alkyne cycloadditions with copper(I) tetranuclear catalysts. Reactions in dichloromethane, 12 h at room temperature, with 1 mol% catalyst loading. *Reaction done in chloroform at 60 ℃.

Entry	Catalyst	Reaction Time	Alkyne	Azide	% Conversion
16	{[3-(CF_3)-5-(*t*-Bu)Pz]Cu}$_4$ (**4**)	12 hrs	1-octyne	*p*-tolylazide	97
17			phenylacetylene	*p*-tolylazide	77
18			1-octyne	benzylazide	>99
19			phenylacetylene	benzylazide	>99
20	{[3,5-(*t*-Bu)$_2$Pz]Cu}$_4$ (**5**)	12 hrs	1-octyne	*p*-tolylazide	98
21			phenylacetylene	*p*-tolylazide	63
22			1-octyne	benzylazide	>99
23			phenylacetylene	benzylazide	>99
24			phenylacetylene	1-adamantyl azide	4
25			phenylacetylene	1-adamantyl azide	28*
26		36 hrs	phenylacetylene	1-adamantyl azide	60*
27	{[4-Br-3,5-(*i*-Pr)$_2$Pz]Cu}$_4$ (**6**)	12 hrs	1-octyne	benzylazide	>99
28			phenylacetylene	benzylazide	>99

`

Vapor Pressure Osmometry

The excellent catalytic ability of all three tetranuclear copper(I) pyrazolates prompted a further investigation into the solution behavior of these complexes using Vapor Pressure Osmometry (VPO), Table 4.4. The electron rich complex {[3,5-(*t*-Bu)$_2$Pz]Cu}$_4$ (**5**) was investigated at a concentration range of 4-12 mmol/kg and found to remain unchanged when dissolved in chloroform. For example, the experimentally observed molecular weight of 985 g/mol corresponded closely to the actual molecular weight of the complex, 970 g/mol indicating that this molecule exists as a tetramer in solution.

Table 4.4 Experimentally determined average molecular weights of the solution species of copper pyrazolate catalysts using Vapor Pressure Osmometry (VPO).

Catalyst	Concentration range (mmol/kg)	Actual MW (g/mol)	Observed MW (g/mol)
{[3,5-(*t*-Bu)$_2$Pz]Cu}$_4$ (**5**)	4-12	971	985
{[3-(CF$_3$)-5-(*t*-Bu)Pz]Cu}$_4$ (**4**)	4-10	1019	900
{[4-Br-3,5-(*i*-Pr)$_2$Pz]Cu}$_4$ (**6**)	4-12	1174	1058
{[3,5-(*i*-Pr)$_2$Pz]Cu}$_3$(**3**)	4-10	644	685
{[3,5-(CF$_3$)$_2$Pz]Cu}$_3$ (**1**)	4-10	800	529

The solution behavior of {[3-(CF$_3$)-5-(*t*-Bu)Pz]Cu}$_4$ (**4**) containing a relatively more electron deficient pyrazolate was also examined. In the concentration range 4-10 mmol/kg, the molecular weight was found to be 900 g/mol. Previous NMR studies of this complex showed an equilibrium between two species, likely a trimer and tetramer in approximately a 1:1.52 ratio at low concentrations, Figure 4.6.[22] This corresponds to a calculated average weight of 917 g/mol, and agrees well with VPO study results, indicating the presence of a

`

mixture of trinuclear and tetranuclear copper pyrazolates at approximately the same ratio.

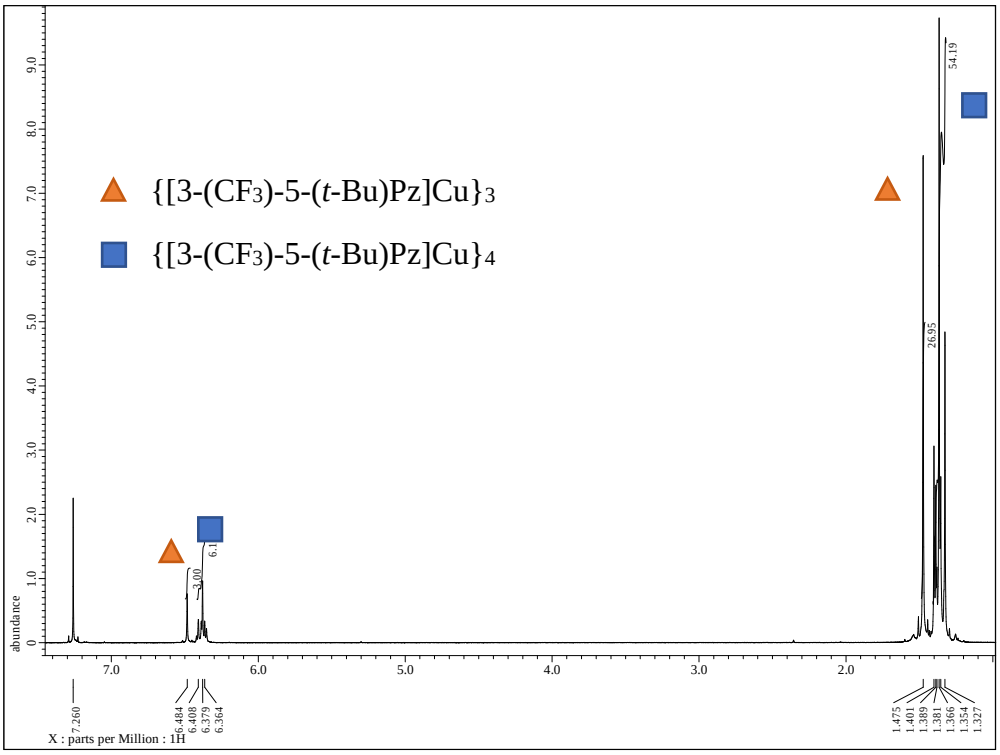

Figure 4.6 1H NMR spectrum of 6 mmol/kg solution of {[3-(CF_3)-5-(*t*-Bu)Pz]Cu}$_4$ in $CDCl_3$ at room temperature.

The ^{1}H NMR spectrum for {[3-(CF_3)-5-(*t*-Bu)Pz]Cu}$_4$ in $CDCl_3$, Figure 4.6, has a singlet at 6.48 ppm (3.00 H) and a multiplet in the region 6.36-6.41 ppm (6.13 H). Both of these correspond to the hydrogen on C4 of the pyrazolates, and were attributed to two isomers of the complex. Similarly two sets of peaks were seen in the ^{1}H NMR at 1.33-1.47 ppm corresponding to the *tert*-butyl CH_3 peaks for two isomers of the complex. Using this information combined with the calculated molecular weight in chloroform from VPO data, we were able to assign the singlets at 6.48 ppm and 1.47 ppm, notated with triangles, to the trinuclear isomer and the peaks at 6.36-6.41 ppm and 1.33-1.40 ppm, notated with squares, to the tetranuclear isomer (Calculation 1).

`

This provides a calculated molecular weight based on NMR of 917 g/mol and observed molecular weight (based on VPO) of 900 g/mol. Similar results were obtained when calculations were done using the peak integration values for the *tert*-butyl CH_3 peaks. As a further confirmation, when molecular weights were calculated using the opposite NMR peak assignments (i.e., a ratio of 2.6 Cu_3 : 1 Cu_4 is used), a molecular weight of 834 g/mol was obtained, which does not agree with the observed molecular weight based on VPO. Overall, VPO results are in good agreement with NMR data. In agreement with previous NMR data.[22]

Calculation 1. Assuming the peak at 6.48 (3.00 H) corresponds to the trinuclear isomer, and the peaks at 6.36-6.41 (6.13 H) correspond to the tetranuclear isomer.

$$\frac{3.00\ H}{3\ H} = 1\ Cu_3 \qquad \frac{6.13\ H}{4\ H} = 1.5\ Cu_4$$

$$\mathbf{1\ Cu_3 : 1.5\ Cu_4}$$

$$Calculated\ molecular\ weight\ using\ this\ ratio:$$

$$Molecular\ weight\ of\ Cu_3 = 764.2\frac{g}{mol} \quad Molecular\ weight\ of\ Cu_4$$

$$= 1018.9\frac{g}{mol}$$

$$\frac{\left(1 \times 764.2\ \frac{g}{mol}\right) + \left(1.5 \times 1018.9\frac{g}{mol}\right)}{(1 + 1.5)} = \mathbf{917}\frac{\boldsymbol{g}}{\boldsymbol{mol}}$$

The {[4-Br-3,5-(*i*-Pr)$_2$Pz]Cu}$_4$ also displayed similar solution behavior at low concentrations. Within the concentration range 4-12 mmol/kg, the VPO gave a molecular weight of 1058 g/mol. NMR data indicated the presence of

`

two species at approximately 1:1.5 ratio, Figure 4.7.[22] A mixture of trinuclear and tetranuclear species at that ratio indeed corresponds to a calculated average molecular weight of 1057 g/mol, which is in excellent agreement with the VPO results.

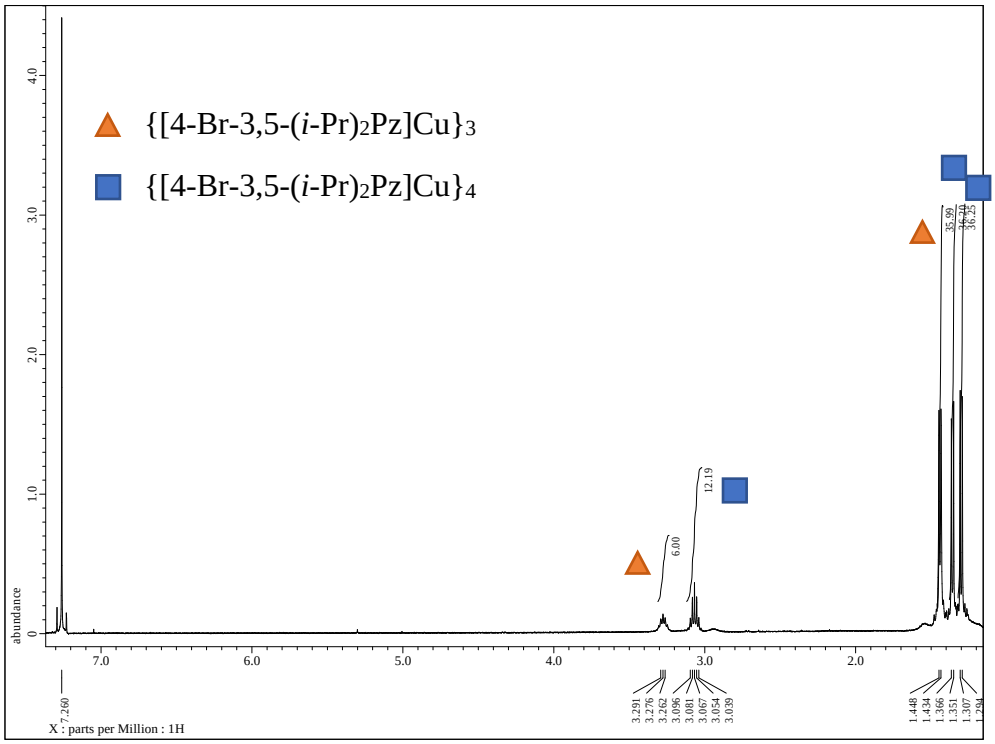

Figure 4.7 ^{1}H NMR spectrum of 6 mmol/kg solution of {[4-Br-3,5-(*i*-Pr)$_2$Pz]Cu}$_4$ in $CDCl_3$, at room temperature.

The ^{1}H NMR spectrum for {[4-Br-3,5-(*i*-Pr)$_2$Pz]Cu}$_4$ in $CDCl_3$, Figure 4.7, indicates that there is a mixture of isomers present. There is a septet at 3.28 ppm (6.00 H) and a second septet at 3.07 ppm (12.2 H), in agreement with previous NMR data.[22] They correspond to the C*H* hydrogen of the *iso*-propyl groups on the pyrazolates. There are also doublets at 1.44 ppm (36 H), 1.35 ppm (36 H), and 1.30 ppm (36 H). Using this information combined with the molecular weight in chloroform from VPO data, we were again able to assign the peaks at 3.28 ppm and 1.44 ppm, notated with triangles, to the trinuclear isomer and the

`

peaks at 3.07 ppm, 1.35 ppm and 1.30 ppm, notated with squares, to the tetranuclear isomer (Calculation 2). This provides a calculated molecular weight of 1057 g/mol based on NMR data and observed molecular weight of 1058 g/mol based on VPO data, which is a remarkably close agreement. These calculations were also done using the peak integration values for the *iso*-propyl CH_3 signals, giving very similar results. As a final confirmation, when molecular weight was calculated using the opposite peak assignments (i.e., a ratio of $2.65\ Cu_3 : 1\ Cu_4$), a molecular weight of 960 g/mol was obtained, which does not correspond closely to the observed molecular weight.

Calculation 2. Assuming the peak at 3.28 (6.00 H) corresponds to the trinuclear isomer, and the peak at 3.07 (12.2 H) corresponds to the tetranuclear isomer.

$$\frac{6.00\ H}{6\ H} = 1\ Cu_3 \qquad \frac{12.2\ H}{8\ H} = 1.5\ Cu_4$$

$$\mathbf{1\ Cu_3 : 1.5\ Cu_4}$$

$$Calculated\ molecular\ weight\ using\ this\ ratio:$$

$$Molecular\ weight\ of\ Cu_3 = 881.0\frac{g}{mol} \quad Molecular\ weight\ of\ Cu_4$$

$$= 1174.7\frac{g}{mol}$$

$$\frac{\left(1 \times 881.0\ \frac{g}{mol}\right) + \left(1.5 \times 1174.7\frac{g}{mol}\right)}{(1 + 1.5)} = \mathbf{1057}\frac{\boldsymbol{g}}{\boldsymbol{mol}}$$

We have also examined the solution behavior of trinuclear copper complexes {[3,5-$(CF_3)_2$Pz]Cu}$_3$ (**1**) and {[3,5-(*i*-Pr)$_2$Pz]Cu}$_3$ (**3**). The fluorinated, trinuclear copper catalyst {[3,5-$(CF_3)_2$Pz]Cu}$_3$ at a concentration range of 4-10 mmol/kg, produced a VPO based molecular weight of 529 g/mol. This weight closely corresponds to the molecular

`

weight of a dinuclear copper complex, 533 g/mol. These results align with work previously done by our group illustrating the different levels of aggregation of $\{[3,5\text{-}(CF_3)_2Pz]Ag\}_3$ at various concentrations.[57] For example, $\{[3,5\text{-}(CF_3)_2Pz]Ag\}_3$ displayed different degrees of aggregation, including dimers, at different concentrations.

Finally, the solution behavior of $\{[3,5\text{-}(i\text{-}Pr)_2Pz]Cu\}_3$ (**3**) was also investigated in a concentration range of 4-10 mmol/kg. The observed molecular weight of 685 g/mol closely corresponds to the actual molecular weight of a trinuclear species, 644 g/mol, indicating that it essentially exists as a trimer in solution. It is also interesting to note that $\{[3,5\text{-}(i\text{-}Pr)_2Pz]Cu\}_3$ (**3**) exists as a dimer of trimer with two short coprophilic (Cu•••Cu) inter-trimer interactions in the solid state.[5] In fact, the observed molecular weight does match more closely to a mixture consisting of 13:1 trimer to dimer of trimer (which represent an average molecular weight of 689 g/mol). This work shoes that the majority of inter-trimer Cu•••Cu contacts of this molecule do not survive in solution under the tested conditions. One could argue that tetramers in combination with trimers could also lead to similar average molecular weights (e.g., 8:2 mixture of $\{[3,5\text{-}(i\text{-}Pr)_2Pz]Cu\}_3$ (**3**) and "$\{[3,5\text{-}(i\text{-}Pr)_2Pz]Cu\}_4$"). Although that is a remote possibility, ^{1}H NMR data of $\{[3,5\text{-}(i\text{-}Pr)_2Pz]Cu\}_3$ (in contrast to **4** and **6**) do not show signs of such a mixture.

Overall, VPO data indicate that the fluorinated copper trimer $\{[3,5\text{-}(CF_3)_2Pz]Cu\}_3$ (**1**) and the relatively weakly donating pyrazolate supported tetramers $\{[3\text{-}(CF_3)\text{-}5\text{-}(t\text{-}Bu)Pz]Cu\}_4$ (**4**) and $\{[4\text{-}Br\text{-}3,5\text{-}(i\text{-}Pr)_2Pz]Cu\}_4$ (**6**) exist with their smaller aggregates in $CHCl_3$ solution.

`

They have relatively weaker Cu-N interactions and more Lewis acidic copper sites relative to {[3,5-(*i*-Pr)$_2$Pz]Cu}$_3$ (**3**) and {[3,5-(*t*-Bu)$_2$Pz]Cu}$_4$ (**5**), and could breakup more easily to smaller copper pyrazolate entities aided by solvents. Their ability to dissociate and structural flexibility in solution may contribute to the excellent catalytic ability displayed by these molecules in CuACC as the formation of reaction intermediates and establishment of equilibria with substrates, alkynes and organic azides, are easier. These observations also explain the notably low catalytic activity of {[3,5-(*i*-Pr)$_2$Pz]Cu}$_3$ (**3**) since it does not break-up easily in $CHCl_3$, making the formation of catalytically active intermediates (e.g., copper acetylides or alkyne complexes) by interactions with CuACC substrates more difficult.

However, strong Cu-N interactions and the apparent structural integrity do not hinder the ability of {[3,5-(*t*-Bu)$_2$Pz]Cu}$_4$ (**5**) to facilitate the azide–alkyne cycloaddition chemistry as evident from the catalytic data. Trinuclear copper(I) pyrazolate, {[3,5-(CF$_3$)$_2$Pz]Cu}$_3$ (**1**) mediated CuAAC believed to proceed via a key tetranuclear reaction intermediate.[91] Perhaps having preassembled tetranuclear species as in {[3,5-(*t*-Bu)$_2$Pz]Cu}$_4$ (**5**) facilitate the formation of such catalytic intermediate quite easily, because, only minimum structural rearrangement is required (see **5** and **7**, Figure 4.3). Furthermore, analysis of solid state X-ray structural data show that tetramers like {[3,5-(*t*-Bu)$_2$Pz]Cu}$_4$ (**5**), {[4-Br-3,5-(*i*-Pr)$_2$Pz]Cu}$_4$ (**6**) and {[3-(CF$_3$)-5-(*t*-Bu)Pz]Cu}$_4$ (**4**) have somewhat closer intra-trimer Cu•••Cu contacts (shortest Cu•••Cu separation of 2.96, 2.90 and 2.91 Å, respectively) than the corresponding separation

`

observed in trimers like {[3,5-(*i*-Pr)$_2$Pz]Cu}$_3$ (3.19 Å).[49] In addition, Cu$_4$ framework in these molecules can adopt shapes ranging from nearly square to rhombus (e.g., Cu••Cu••Cu angles of {[3,5-(*t*-Bu)$_2$Pz]Cu}$_4$ (**5**), {[4-Br-3,5-(*i*-Pr)$_2$Pz]Cu}$_4$ (**6**) and {[3-(CF$_3$)-5-(*t*-Bu)Pz]Cu}$_4$ (**4**) span 69.5°- 109.3°, 66.1°-113.4°, and 79.8°-99.1°), while Cu$_3$ core in systems like {[3,5-(*i*-Pr)$_2$Pz]Cu}$_3$ (**3**) is essentially equilateral triangles. Such flexible and closely held copper sites in Cu$_4$ systems could facilitate the CuAAC even if catalytic moiety involves two or more cooperating copper sites, such as the commonly reported bimetallic σ, π-alkynyl reaction intermediate and bridging acetylides.[115-118]

Kinetics

Mechanistic and kinetic studies of copper catalyzed azide-alkyne cycloadditions have shown that alkyne (and to a lesser degree the organoazide)[119, 120] coordination is an important earlier step in the catalytic cycle.[91, 121, 122] In addition, broken orders, as well as zero and first order rate dependance with respect to azide and alkyne under various conditions have been observed.[91, 113, 123] The catalytic intermediate based on copper could be mono, di, tri, tetra or poly-nuclear although most reports suggest that the catalytic process benefits from the participation of at least two copper centers. [91, 112, 115, 117, 123-126]

We also wanted to get additional insights to the mechanism by investigating the reaction kinetics mediated by copper(I) pyrazolates. The reactions of 1-octyne and benzylazide with tetranuclear catalysts {[3-(CF$_3$)-5-(*t*-Bu)Pz]Cu}$_4$ (**4**) and {[3,5-(*t*-Bu)$_2$Pz]Cu}$_4$ (**5**), and trinuclear catalysts {[3,5-(CF$_3$)$_2$Pz]Cu}$_3$ (**1**) and {[3,5-(*i*-Pr)$_2$Pz]Cu}$_3$ (**3**) were

`

compared and monitored to investigate the rate of reaction of copper tetramers in comparison to copper trimers. An aliquot of each reaction mixture was analyzed via NMR and the percent conversion was calculated for each hour, Figure 4.8.

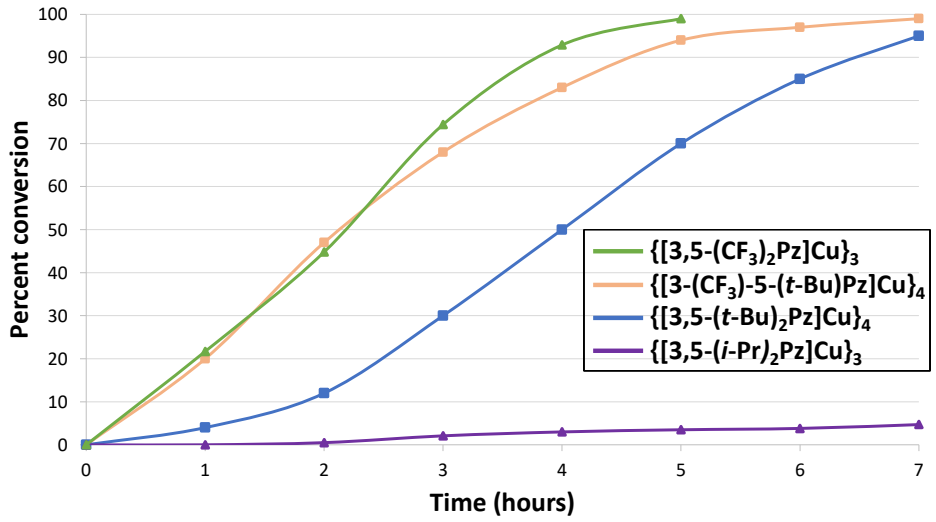

Figure 4.8 Percent conversion vs. time for copper(I) pyrazolate mediated CuAAC reaction at room temperature with 1-octyne and benzylazide.

Table 4.5 Reaction conversion measured after each hour for copper(I) pyrazolates.

	{[3-(CF_3)-5-(*t*-Bu)Pz]Cu}$_4$ (**4**)	{[3,5-(*t*-Bu)$_2$Pz]Cu}$_4$ (**5**)	{[3,5-(CF_3)$_2$Pz]Cu}$_3$ (**1**)	{[3,5-(*i*-Pr)$_2$Pz]Cu}$_3$ (**3**)
Time (hr)	% conversion	% conversion	% conversion	% conversion
1	20	7	22	0
2	47	17	45	0.5
3	68	34	74	2
4	80	56	93	3
5	93	77	>99	3.5
6	97	89	-	4
7	>99	95	-	4.7

Results show that among the molecules tested at room temperature, **1** and **4** are the most active, closely followed by **5**, while **3** is essentially inactive. For example, the fluorinated trimer, {[3,5-(CF_3)$_2$Pz]Cu}$_3$ (**1**),

`

afforded >99% conversion to product after five hours, while the non-fluorinated trimer, {[3,5-(*i*-Pr)$_2$Pz]Cu}$_3$ (**3**), gave only 5% conversion even after seven hours. This large difference in conversion may also be attributed to the ability to dissociate in solution, as indicated by vapor pressure osmometry data, and the facile formation of transition states. It is commonly accepted that the π-complex formation of copper(I) centers with alkyne substrate is a key initial step, in order to form the related σ-complex through deprotonation.[117] Generation of coordinatively unsaturated metal sites through ligand dissociation or disaggregation would facilitate such reactions. Furthermore, recent work suggests that weaker Lewis base supporting ligands are beneficial for the rate of CuAAC reaction, perhaps through lowering of the activation barrier for the protonolysis triazolide of by the terminal alkyne.[123]

When comparing the rate of product formation with tetramer catalysts, it was found that the more electron rich tetramer, {[3,5-(*t*-Bu)$_2$Pz]Cu}$_4$ (**5**) initially produced the desired 1,2,3-triazole somewhat slowly. However, in contrast to the electron-rich trinuclear species, {[3,5-(*t*-Bu)$_2$Pz]Cu}$_4$ catalyst still afforded the product in high (95%) conversion after 7 hours, suggesting the pyrazolate basicity plays a much smaller but clear role (see Figure 3) in tetranuclear copper complexes. Additionally, this shows again the apparent lack of dissociation in solution of this tetramer does not affect its catalytic efficacy.

`

Table 6.6 Overview of the conditions for the order determination of the various components of the reaction between 1-octyne and benzylazide using [{3,5-(*t*-Bu)$_2$Pz}Cu]$_4$ (**5**), {[3-(CF$_3$)-5-(*t*-Bu)Pz]Cu}$_4$ (**4**), or {[3,5-(CF$_3$)$_2$Pz]Cu}$_3$ (**1**).

Entry	Component	1-octyne (equiv)	Benzylazide (equiv)	Cu cat.	Cu complex (equiv)	Rate order
1	Cu$_4$ (**5**)	1	1	**5**	0.01 – 0.05	1.05
2	Cu$_4$ (**4**)	1	1	**4**	0.01 – 0.05	0.87
3	Cu$_3$ (**1**)	1	1	**1**	0.01 – 0.05	1.63
4	1-octyne	1 – 5	1	**5**	0.01	0.95
5	1-octyne	20 – 40	1	**5**	0.01	0.68
6	1-octyne	1-5	40	**5**	0.01	1.09
7	BnN$_3$	1	1 – 5	**5**	0.01	0.79
8	BnN$_3$	1	20 – 40	**5**	0.01	0.02
9	BnN$_3$	40	1-5	**5**	0.01	0.74

To further probe the kinetics of tetranuclear copper(I) pyrazolate catalysts, experiments were performed on the reaction of 1-octyne and benzylazide with {[3,5-(*t*-Bu)$_2$Pz]Cu}$_4$ (**5**). Aliquots of the reaction mixture were taken at intervals and analyzed via ^{1}H NMR to calculate percent conversion to the desired 1,2,3-triazole. Reactions were carried out with different equivalents of each substrate while maintaining other components at constant concentration. An approximately first-order dependency on copper(I) tetramer concentration was observed, when it was maintained at catalytic levels (<5 mol%, Table 4.6, entry 1). The reaction order for another copper(I) tetramer, [{3-(CF$_3$)-5-(*t*-Bu)Pz}Cu]$_4$ (**4**), was also observed to be approximately first-order, see supplementary information for details. This may indicate that an undissociated copper(I) tetramers are involved in the rate determining step.[123] The observed first

`

order dependency on copper tetramers also supports the hypothesis that a preassembled tetranuclear structure could contribute to the excellent catalytic ability of these copper(I) tetramers. When using the trinuclear copper(I) pyrazolate {[3,5-$(CF_3)_2$Pz]Cu}$_3$ an approximately second order dependency is observed, see supplementary information for details. Based on the data from vapor pressure osmometry presented in this work, {[3,5-$(CF_3)_2$Pz]Cu}$_3$ exists as a dinuclear species in solution. This second order dependency seen by our work and others[91] on this molecule could be attributed to two dimers involved in the rate determining step to form the required tetranuclear reaction intermediate. Most mechanistic studies on CuAAC imply the participation of two copper sites in the catalytically active intermediate,[112, 114] which is also possible from a Cu_4 system.

4.4 Conclusions

In summary, unlike the highly fluorinated, electron deficient trinuclear copper(I) pyrazolate complexes, the electron rich analogs such as {[3,5-(*i*-Pr)$_2$Pz]Cu}$_3$ containing strongly donating pyrazolates, are less effective in CuAAC. This may be a consequence of stronger Cu-pyrazolate interactions making the breakup of planar nine-membered framework by alkynes, and the formation of catalytically active intermediates, more difficult. Tetranuclear copper(I) pyrazolates however, were found to be excellent catalysts even with electron donating and bulkier substituents on the pyrazolate ligands, which is probably due to the ease of attaining the possible tetranuclear reaction intermediates via the pre-formed tetranuclear catalyst precursors. Also, saddle-shaped tetramers have somewhat closely situated copper sites and a flexible Cu_4 framework

`

relative to planar copper trimers, which may be an important feature that can facilitate reactions that involve multi-nuclear catalytic centers. The VPO data indicate the generation of smaller copper pyrazolate aggregates in solutions relative to their solid-state versions, when supported by relatively weakly donating pyrazolates. The activity of the non-fluorinated tetranuclear $\{[3,5\text{-}(t\text{-Bu})_2\text{Pz}]\text{Cu}\}_4$ complex is particularly noteworthy as it shows the ability to use more widely available, non-fluorinated pyrazolates in catalyst design for CuAAC chemistry.

4.5 Acknowledgments

Authors acknowledge the financial support by the National Science Foundation (CHE-1954456, HVRD) and Robert A. Welch Foundation (Grant Y-1289, HVRD).

`

Chapter 5

Heteroleptic complexes with $\{[3,5\text{-}(CF_3)_2Pz]Cu\}_3$

Mohammad A. Omary, John J. Determan, Chammi S. Palehepitiya Gamage, Pankaj Sinha, Shan Li, Monika R. Patterson, Vladimir N. Nestero, Angela K. Wilson & H. V. Rasika Dias

This work has been published in Comments on Inorganic Chemistry, 40, 2020, 1, 1-24. [127]

`

5.1 Abstract

Herein, the dinuclear complexes {Cu[3,5-$(CF_3)_2$Pz](μ-dppm)}$_2$ and {Cu[3,5-$(CF_3)_2$Pz](μ-dppm)}$_2$•3THF, were synthesized. Both copper complexes were studied structurally, spectroscopically and via density functional theory (DFT). They were synthesized by reacting bis(diphenylphosphino)methane (dppm) with the cyclic trinuclear complex {μ-[3,5-$(CF_3)_2$Pz]Cu}$_3$ to effect nuclearity reduction. Two forms of crystalline solids, {Cu[3,5-$(CF_3)_2$Pz](μ-dppm)}$_2$ and {Cu[3,5-$(CF_3)_2$Pz](μ-dppm)}$_2$•3THF have been obtained using different recrystallization conditions. The {Cu[3,5-$(CF_3)_2$Pz](μ-dppm)}$_2$ complex was found through DFT computations to undergo a distortion from a Y-shaped coordination sphere in the S_0 ground state towards a T-shape in the T_1 photoexcited, lowest-lying, phosphorescent state. The distortion also causes the copper-copper bond length to contract and form an excimer bond ($d_{Cu\text{-}Cu}$ = 2.577 Å). Experimentally, the presence of THF in the crystal was found to cause a blue shift, effecting a change in emission color from teal to blue to the naked eye, with a near-unity quantum yields (93%), rendering the latter solid suitable for inorganic LED applications but not OLEDs, as thin films exhibit a reduced quantum yield. Crystallographic evidence suggests that THF leads to a more compact lattice that makes the complexes more rigid and thus hinder the excited state distortions vs unsolvated crystals. Greater distortion leads to a lower energy radiative emission and thus a red shift in the emission color. Films were also studied and found to undergo further red shifting as a result of less rigidity in the media and more surface molecules susceptible to distortion, hence manifesting the luminescence rigidochromism optical phenomenon in the solid state as opposed to the

`

traditional manifestation in frozen vs fluid solution. Photobleaching was studied in both the film and powder to assess photostability, which was superior in neat vs doped solids, which is also favorable for LED applications.

5.2 Introduction

Manufacturing of white organic light-emitting devices (OLEDs) requires materials that emit in the blue (~450-470 nm), green (~500-550 nm) and red (~650-700 nm) color spectra. While green and red emitting materials are relatively abundant, efficient blue emitting materials with high stability have proven to be more challenging to produce.[128, 129] In addition to requiring materials that span the visible region of the spectra, materials for white OLEDs should have phosphorescent emissions, as these emissions can be up to four times more efficient than fluorescent materials.[130] Statistically, recombination of electrons and holes in the emitting layer will be favor phosphorescent emission (75% chance) over fluorescence (25% chance). Devices which incorporate triplet emission (phosphorescent emission) are known as phosphorescent organic light emitting diodes (PhOLEDs) and have the possibility of 100% internal quantum efficiency.[130-133]

Incorporation of transition metal complexes into OLED materials has been shown to increase the efficiency of these devices, as these complexes increase the probability of spin-forbidden triplet state phosphorescent transitions to the ground state due to spin-orbit coupling and heavy atom effects.[54, 134-137] In particular, many efficient electroluminescent devices utilize metal-to-ligand charge transfer (MLCT) excited states.[138] Additionally, metal-centered emissions have been used in many electroluminescent devices. These devices tend to be based on d^6 and d^8 metal complexes, including Ir(III),[129, 133, 139-142]

`

Ru(II),[143, 144] Re(I),[145] Os(II),[129, 146, 147] and Pt(II)[129, 148, 149] complexes. While these compounds have been studied extensively for use in lighting applications due to fairly high external quantum efficiencies near 20% on glass substrates, the limited natural abundance and high cost of these metals make exploration of materials made with more abundant metals (e.g., copper among coinage metals) a worthwhile endeavor.

Previous crystallographic studies have found aurophillic Au(I) dimers to exhibit stronger than expected interactions, which result in short Au(I)•••Au(I) distances in ground state compounds.[150, 151] Upon photoexcitation to the lowest phosphorescent states, closed-shell d^{10} metal-metal interactions have been found to contract as the bond strength increases.[152] Excited state distortions in Au(I)-Au(I) interactions has been characterized by photoluminescence[152] and the nature of excited state distortion of the lowest phosphorescent exited state of dinulear cationic phosphine complexes has been studied computationally.[153] It was determined that the Au(I)-Au(I) bond length undergoes a contraction upon photoexcitation. Jahn-Teller distortions from a Y-shape to a T-shaped molecule structure has also been determined for similar complexes in computational studies.[154]

Copper(I)-phosphine complexes have garnered intense attention in recent years in part due to their utilization in OLEDs besides possessing intriguing photophysical properties.[155-166] Multinuclear Cu(I) phosphine complexes have demonstrated similar structural and luminescence properties as the analogous Au(I) complexes.[167-170] These Cu(I) complexes have weak Cu(I)•••Cu(I) interactions in the ground state and bright phosphorescent emissions. Common among the multinuclear Cu(I) complexes is a 3-coordinate, nearly trigonal

`

planar symmetry of monomeric sub-units within the complex. The excited state distortions of 3-coordinate Cu(I) complexes have not been studied as extensively as have 3-coordinate Au(I) complexes. Within these dinuclear Cu(I) complexes, the primary types of distortions upon photoexcitation are: 1) M-M excimer formation, 2) T-shape distortion of a single metal center, or 3) T-shape distortion in both metal centers; experimental/computational studies of the sort herein are needed for such complexes to understand their excited state structure like the case for other classes of Cu(I) species extensively studied in the literature such as tetranuclear copper iodide clusters whose electronic structure was delineated by the Ford group.[171-180] Each of the aforementioned distortions can occur and are not necessarily mutually exclusive. For example, Cu(I)-Cu(I) excitation and T-shape distortion may be common in both metal centers upon photoexcitation.[170] In addition to greater abundance and lower cost, comparison of photophysics of Cu(I) diphosphine complexes to the greatly studied Au(I) diphosphine complexes will reveal more information on the role of spin-orbit coupling and thermally-activated delayed fluorescence phenomena.[181]

Recent studies of multinuclear copper(I) complexes have suggested high quantum efficiency at room temperature.[5, 12, 14, 20, 54] These promising quantum efficiency results have led to further investigations into the properties that afford these highly efficient luminescent materials including the variation of supporting ligand and the investigation of packing effects caused by various solvents used for recrystallization of materials. In this regards, we have synthesized a dinuclear copper complex {Cu[3,5-$(CF_3)_2$Pz](μ-dppm)}$_2$ (**1**) and evaluated it as a potential blue emitting material for use in OLEDs or inorganic

`

LEDs. Furthermore, we show the effects of crystallization method on X-ray crystal structures and luminescence spectra. Recrystallization of {Cu[3,5-$(CF_3)_2$Pz](μ-dppm)}$_2$ from a dichloromethane solution led to an unsolvated {Cu[3,5-$(CF_3)_2$Pz](μ-dppm)}$_2$ structure (**1**) while recrystallization of the product from a slow cooling in tetrahydrafuran solvent favored a {Cu[3,5-$(CF_3)_2$Pz](μ-dppm)}$_2$•3THF structure (**1**•3THF). Crystals or powders of **1**•3THF and **1** are found to have blue (472 nm) and teal (477 nm) emissions, respectively, upon photoexcitation. Materials are also evaluated by lifetime and quantum yield for use in (O)LEDs. Materials are drop-cast into films to study changes in emission energies and quantum yields that will occur in the OLED manufacturing process.

5.3 Results & Discussion

Crystal Structures. The molecular structure of {Cu[3,5-$(CF_3)_2$Pz](μ-dppm)}$_2$ is shown in Figure 5.1 while Tables 5.1 and 5.2 provide a summary of crystal data and selected bond distances/angles, respectively. Molecules of {Cu[3,5-$(CF_3)_2$Pz](μ-dppm)}$_2$ crystallize in the *C*2/c space group and sit on a center of inversion. The [3,5-$(CF_3)_2$Pz]$^-$ serves as a κ^1-ligand, as it coordinates to copper via only one of the pyrazolyl nitrogen atoms. Two dppm ligands act as bridging ligands that bridge two copper sites. The copper centers adopt a trigonal planar geometry. The intra-molecular Cu•••Cu separation is 3.3880(9) Å, which is significantly longer than the Bondi's van der Waals contact radius of copper (2.80Å). Inter-molecular Cu-Cu separations are very long with the closest at 10.394 Å.

`

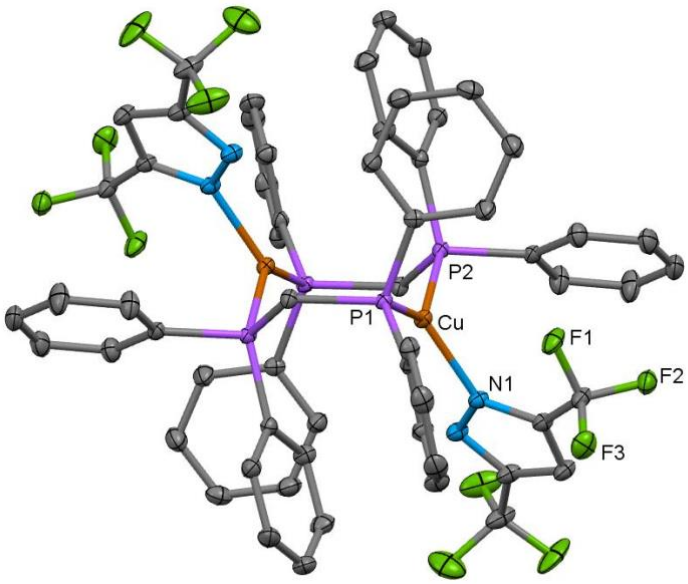

Figure 5.1 Molecular structure of {Cu[3,5-(CF3)2Pz](μ-dppm)}2 (1). Thermal ellipsoids are shown at 50% level and hydrogen atoms have been omitted for clarity.

`

Table 5.1 Sample and crystal data for {Cu[3,5-(CF3)2Pz](μ-dppm)}2 (1).

Empirical formula	$C_{60}H_{46}Cu_2F_{12}N_4P_4$
Formula weight	1301.97
Temperature/K	100(2)
Crystal system	Monoclinic
Space group	C2/c
a/Å	23.2128(19)
b/Å	20.4041(17)
c/Å	12.2228(10)
α/°	90
β/°	102.5470(10)
γ/°	90
Volume/Å^3	5650.9(8)
Z	4
$\rho_{calc/}$ g/cm^3	1.530
Independent reflections	5550 [R_{int} = 0.0237, R_{sigma} = 0.0187]
Goodness-of-fit on F^2	1.062
Final R indexes [I>=2σ (I)]	R_1 = 0.0260, wR_2 = 0.0702
Final R indexes [all data]	R_1 = 0.0268, wR_2 = 0.0707

Table 5.2 Selected bond lengths (Å) and angles (°) for 1.

		P1	Cu	P2	133.653(16)
		N1	Cu	P1	127.14(4)
Cu P1	2.2177(5)	N1	Cu	P2	97.48(4)
Cu P2	2.2578(5)	N2	N1	Cu	117.52(9)
Cu N1	2.0109(13)				

The {Cu[3,5-$(CF_3)_2$Pz](μ-dppm)}$_2$•3THF crystals are stable only at lower temperatures. There are two chemically similar, but crystallographically different molecular halves of {Cu[3,5-$(CF_3)_2$Pz](μ-dppm)}$_2$ in the asymmetric unit of the THF solvate. They sit on centers of inversion. The inter-molecular Cu-Cu separations of {Cu[3,5-$(CF_3)_2$Pz](μ-dppm)}$_2$•3THF are very long, with closest at 10.149 Å. The intra-molecular Cu•••Cu separation of these molecules

`

are 3.299(2) and 3.2276(18) Å. They are significantly shorter compared to that observed for the molecules of the THF-free {Cu[3,5-$(CF_3)_2$Pz](μ-dppm)}$_2$. This is perhaps a result of distortions caused by the packing effects of lattice THF. A comparison of void spaces of {Cu[3,5-$(CF_3)_2$Pz](μ-dppm)}$_2$•3THF and {Cu[3,5-$(CF_3)_2$Pz](μ-dppm)}$_2$ crystal unit cells indicates that the latter has about 130 Å^3 voids for 1Å probe radius (~2.3% unit cell volume) while the former has no void space. Also as seen in Figures 5.2 and 5.3, the arrangements of the molecules themselves are dependent on the packing of the crystal. In the {Cu[3,5-$(CF_3)_2$Pz](μ-dppm)}$_2$ crystal, molecules arrange themselves in a manner that leaves some space between molecules, particularly in between the phenyl rings of the diphenylphosphinomethane ligand. This is also evident from the void space estimate noted above. The molecules of {Cu[3,5-$(CF_3)_2$Pz](μ-dppm)}$_2$•3THF are arranged in a manner that cause some distortions at the {Cu[3,5-$(CF_3)_2$Pz](μ-dppm)}$_2$ core (e.g., intramolecular Cu-Cu distances as noted above), as well as causing the phenyl rings of the diphenylphosphinomethane to be sterically hindered from free vibrations due to the inclusion of the THF molecules. This hindrance will impart greater rigidity in the molecule, disallowing distortion from occurring upon photoexcitation.

`

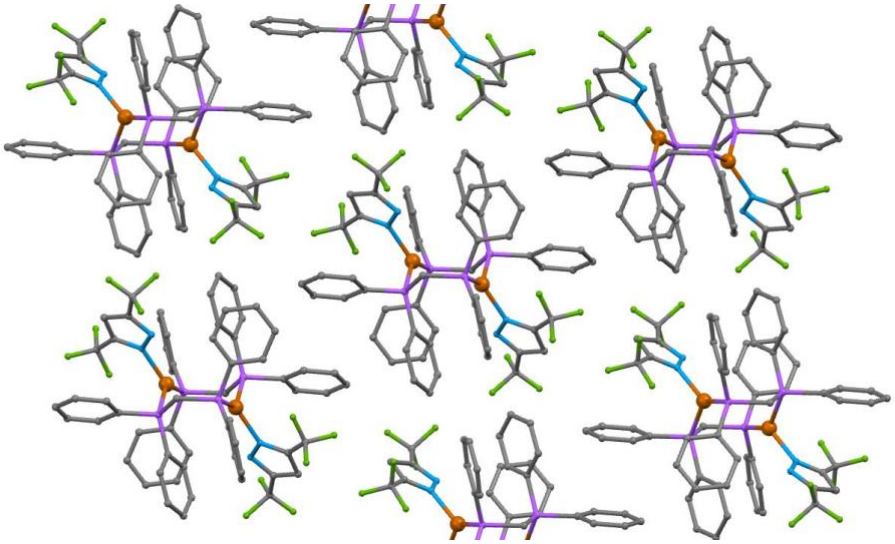

Figure 5.2 A view showing crystal packing in {Cu[3,5-(CF3)2Pz](μ-dppm)}2. Hydrogen atoms have been omitted for clarity.

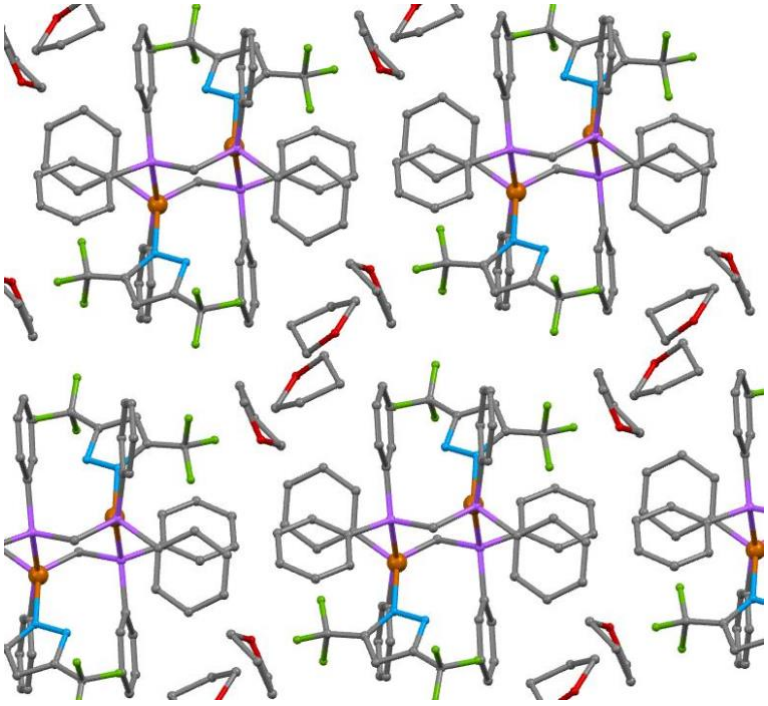

Figure 5.3 A view of crystal packing in {Cu[3,5-(CF3)2Pz](μ-dppm)}2•3THF and the placement of THF molecules in the crystal lattice. Hydrogen atoms have been omitted for clarity.

`

DFT-Predicted Changes in {Cu[3,5-$(CF_3)_2$Pz](μ-dppm)}$_2$ Structure Upon Photoexcitation. DFT computations for the S_0 singlet ground state and T_1 lowest triplet excited state of {Cu[3,5-$(CF_3)_2$Pz](μ-dppm)}$_2$ models have been carried out starting with the crystal structure of **1**, as shown in Figure 5.4. The structure was optimized using the B3PW91/aug-LANL2DZ combination that is described in the methods section. Bond lengths and angles are compared to the experimental structure in Table 5.3. One structural parameter that is notably different in the computational result as compared to the crystal structure is bond length *g*, or the distance between the copper atoms of the {Cu[3,5-$(CF_3)_2$Pz](μ-dppm)}$_2$ complex. The difference between the computed and experimental value, 0.368 Å, can be attributed to the choice of methodology used in the computation. While B3PW91 has been shown to give values for metal-metal bond lengths that agree well with experimental values in the excited state, which become covalent due to excimeric bonding, the method is not capable of properly describing long-range dispersion forces between Cu(I) atoms of the *ground-state* molecules, known as metallophilic interactions.[182, 183] [184] Metallophilic interactions are caused by correlation effects that are strengthened by relativistic effect.[185] These interactions cause the copper-copper interaction of the complex to be stronger than van der Waals only interactions and thus the bond lengths are shorter as a result. The bond strength will be underestimated with convention density functional methods, such as B3PW91 and thus the bonds will be longer than experimental values. The predicted proximity between the two Cu(I) atoms even as it is, within ~0.4 Å, is largely due to the dppm bridging ligand's bite size than the method's description of cuprophilic bonding.

`

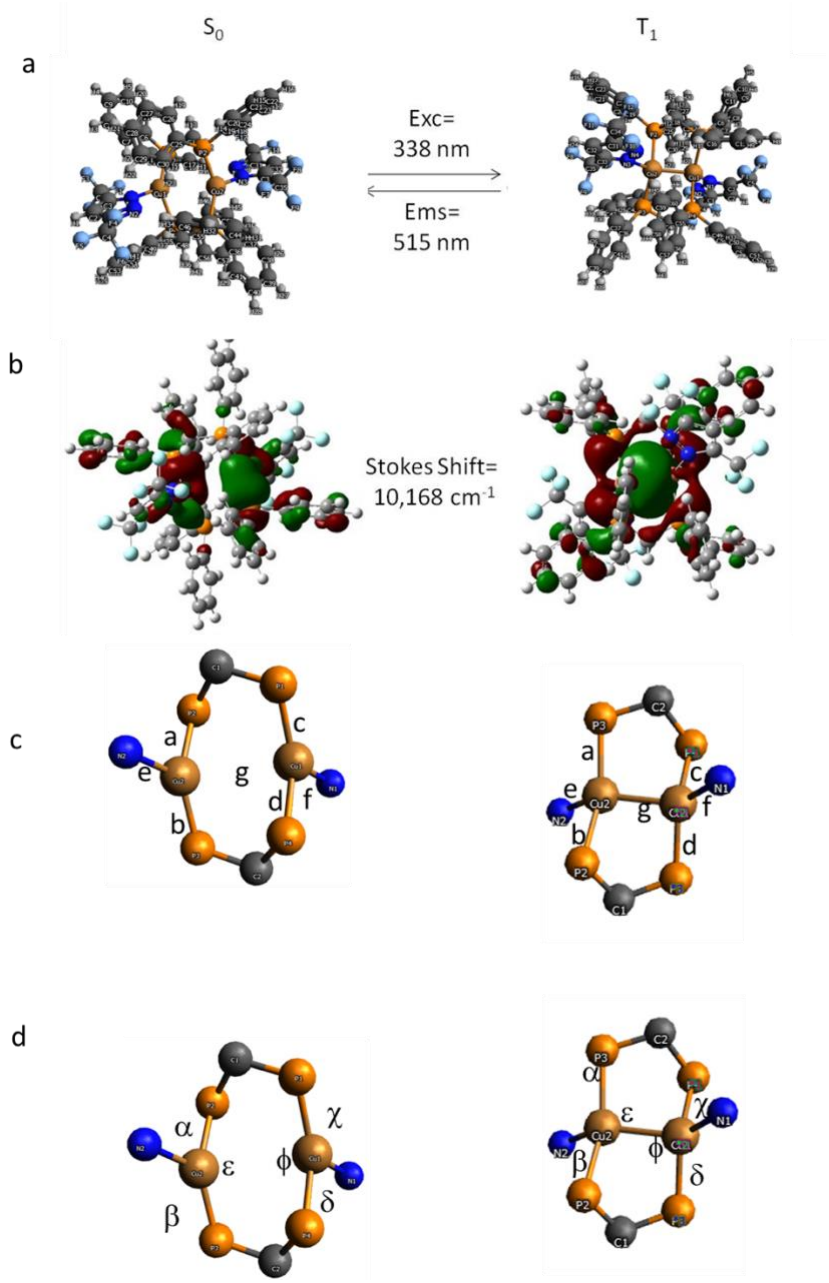

Figure 5.4 B3PW91/aug-LANL2DZ computed (a) full (including rings and H atoms of ligands) S0 and T1 geometries (b) HOMO contours of {Cu(μ-[3,5-$(CF_3)_2$Pz])(μ-dppm)}$_2$ (c) bonds of S0 and T1 with rings and H atoms removed (d) angles of S0 and T1 with rings and H atoms.

`

Table 5.3 Geometry parameters ((a) bond lengths (angstroms) and (b) bond angles (degrees) of 1 computed with B3PW91/aug-LANL2DZ.

(a)

	a	***b***	***c***	***d***	***e***	***f***	***g***
Expt.	2.251	2.213	2.213	2.251	2.011	2.011	3.388
S_0	2.324	2.281	2.281	2.324	2.024	2.024	3.645
T_1	2.396	2.368	2.368	2.396	2.036	2.036	2.577
T_1-S_0	0.072	0.087	0.087	0.072	0.012	0.012	-1.068

(b)

	α	***β***	***χ***	***δ***	***ε***	***φ***
Expt.	96.4	121.8	121.8	96.4	140.7	140.7
S_0	97.1	125.9	125.9	97.1	136.8	136.8
T_1	109.3	90.4	90.4	109.3	144.5	144.5
T_1-S_0	12.2	-35.5	-35.5	12.2	7.7	7.7

Upon photoexcitation, each copper center is seen to undergo a distortion from a distorted Y-shaped structure in the ground state towards a T-shaped structure in the lowest-lying T_1 triple state, as is represented in Figure 5.4. The inside angles, *e'* and *f'* are shown to distort from 136.8° for the ground state (S_0) structure to 144.5° in the T_1 structure. As this distortion occurs, the copper-copper distance, *g*, is shown to contract from 3.645 Å in S_0 to 2.577 Å in the T_1 excited state. The reason for this large distortion, Δg = -1.068 Å, is seen in the HOMO contours shown in Figure 5.4. The HOMO in the ground state shows a sigma donation of electron density from the diphenylphosphinomethane to the

`

copper atom. The copper atoms of the dimer show no formal bond in the ground state. As the complex undergoes photoexcitation, a formal copper-copper bond is formed in the resulting triplet excimer. Electron density is shared between the copper atoms, as a covalent bond is formed and thus the copper-copper distance contracts.

The large geometric distortion of the complex corresponds to a large Stokes' shift of 10,168 cm^{-1}. This value is large as compared to the experimental value of 6,814 cm^{-1}. Both the ground state and excited state structures cause this overestimation in the Stokes' shift. The ground state has an excitation energy that is underestimated when compared to the experimental data, due to the inability of the B3PW91 method to model dispersion force interactions. As was previously mentioned in this section, underestimation of the metallophilic interactions will cause the copper-copper interactions to be underestimated and thus the excitation energy is affected by the use of a structure with a longer copper-copper bond length. The computations are approximated using a gas phase matrix for the material, while the experiment is carried out for a solid-state material. The solid-state interactions will cause the excited state distortion to be diminished, due to lattice constraints, and thus the emission energy will be red-shifted in the computations compared the experimentally found values. The combination of these errors in excitation and emission energies results in the computed Stokes' shift to be larger than the experimental Stokes' shift.

Photoluminescence and Device Screening for 1 and 1•3THF**.** As was discussed in the synthetic and crystallographic results sections, recrystallization conditions cause small differences in the structural parameters of **1** and **1**•3THF. Upon excitation with a black lamp source at 365 nm, as shown in Figure 5.5, a

`

difference in emission color is observed. The spectra obtained by excitation at λ_{max} of the **1** and **1**•3THF reveal the emission wavelengths are only 5 nm/222 cm^{-1} apart, at 477 nm and 472 nm, respectively, at room temperature, whereas the excitation range is essentially indifferent; see Figure 5.5. The subtle difference in emission maximum can be seen by the naked eye, as the shift occurs in a sensitive portion of the visible region, whereby 5 nm is the difference between a true blue emission from **1**•3THF and a teal-colored emission from **1**. Both the **1**•3THF and **1** materials have phosphorescent decay lifetimes in the microsecond region, with values of 27.7 ± 0.1 microseconds and 24.9 ± 0.3 microseconds, respectively. Quantum efficiency experiments attained a much greater photoluminescence quantum yield (PLQY) for the solvated **1**•3THF product than for the dry **1** product, with an average PLQY value of 93% versus 60%, respectively. The blue shift, higher quantum yield, and longer lifetime for the **1**•3THF crystals or crystalline powder versus the unsolvated **1** form are attributed to greater resistance to excited-state distortion due to tighter packing (see void calculations and description of a space group with tighter packing for the THF solvate vs dry crystals in the crystallographic section above).

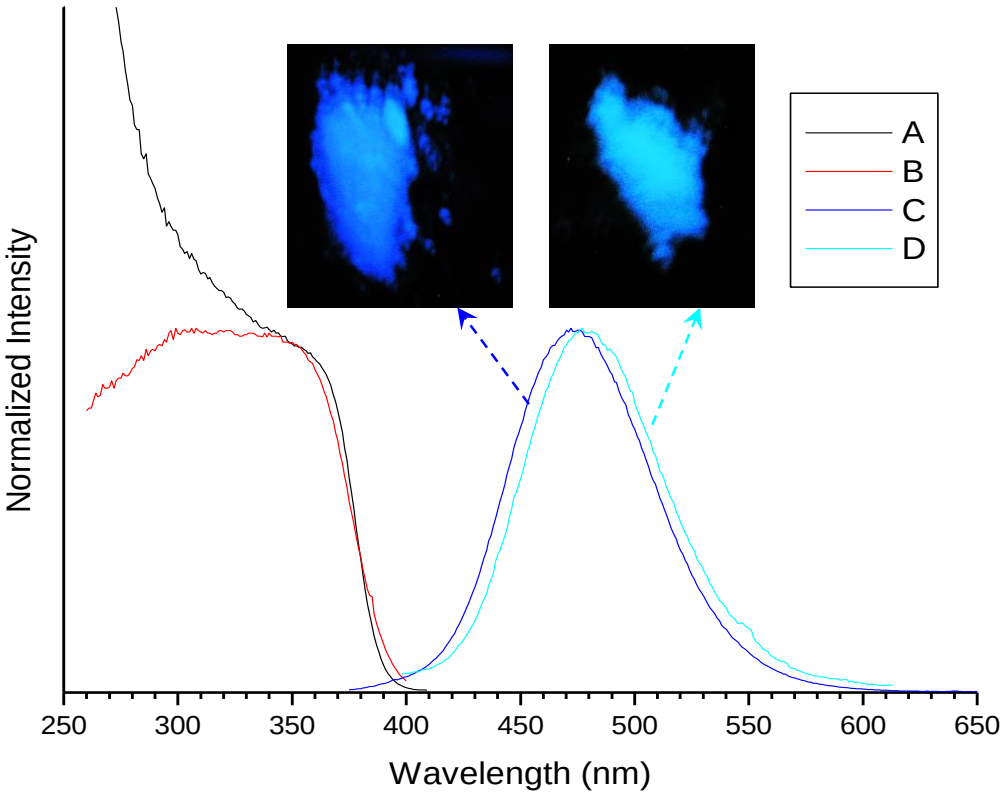

Figure 5.5 Steady-state luminescence of **1** and **1**•3THF at 298 K (A) excitation of **1**•3THF (λ_{max}=360 nm). (B) excitation of **1** (λ_{max}=360 nm). (C) emission of **1**•3THF (λ_{max}=472 nm). (D) emission of **1** (λ_{max}=477 nm). The inset shows pictures of the luminescence of **1**•3THF and **1** excited at 365 nm with a hand-held UV lamp source.

The **1**•3THF solid is shown to blue-shift to 466 nm upon cooling of the material to 90 K (Figure 5.6). This blue shift can be attributed to a reduction of the excited state distortion as the material is cooled, providing less thermal assistance for the distortion and causing a consequent reduction in the Stokes' shift. Comparison of the **1**•3THF emission at 90 K with the emission of a frozen glass of 10^{-3} M (**1** in 2-methyltetrahydrofuran, which forms a transparent glass at 77-90 K) reveals a further blue shift in emission as the amount of solvent in the frozen matrix is increased; see Figure 5.6. This phenomenon can be

`

explained by the crystal structures of the **1**•3THF and **1** complexes as well as by the computations carried out on **1**. The crystal structures reveal measurable empty space in **1**. The **1**•3THF crystal show that the tetrahydrofuran molecules reduce this void spaces and cause efficient packing. While these molecules do not directly interact with {Cu(μ-[3,5-$(CF_3)_2$Pz])(μ-dppm)}$_2$, the filling of the space between molecules hinders the distortions. This will increase the rigidity of the molecule and thus the emission will be blue-shifted and the quantum yield will be increased as the vibrations of the phenyl rings will be suppressed. Medium rigidity is well-known to cause blue shift and increased quantum yield in phosphorescent coordination compounds, owing to seminal work by Wrighton and co-workers.[186-188] However, it is usually manifested by frozen glass vs fluid solution whereas herein we manifest the latter in the solid state.

`

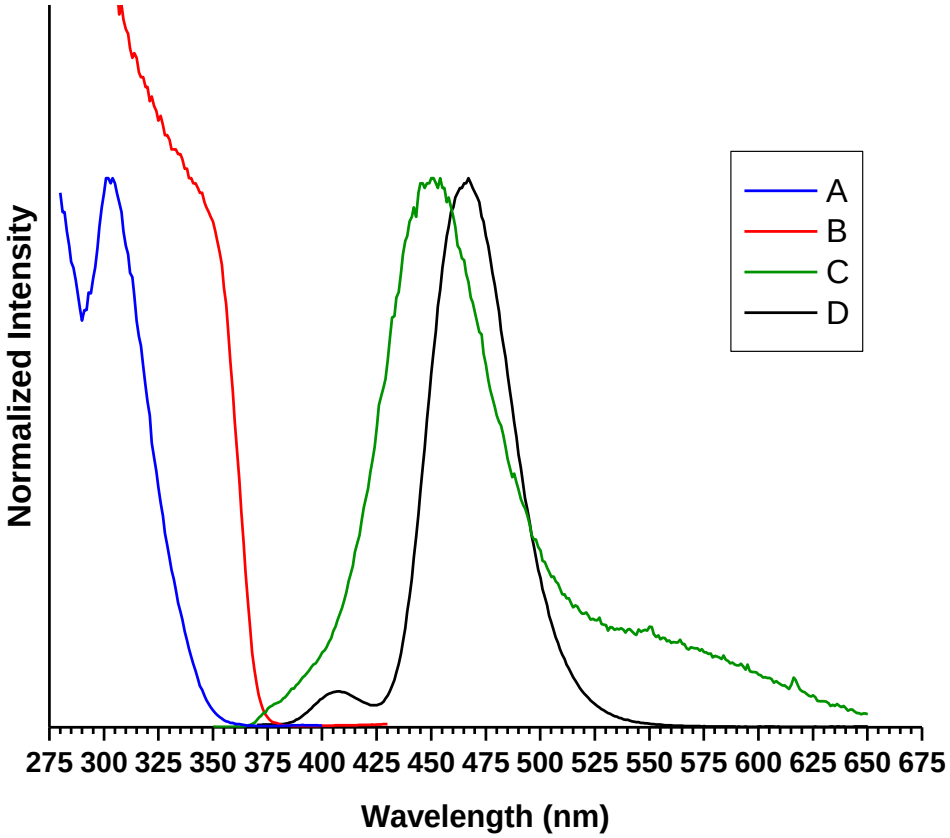

Figure 5.6 Steady-state luminescence of **1** and **1**•3THF at 90 K. (A) excitation of **1** in a 10^{-3} M glass in 2-methyltetrahydrofuran (λ_{max} = 300 nm). (B) excitation of **1**•3THF solid (λ_{max}=340 nm). (C) emission of **1** in a 10^{-3} M glass in 2-methyltetrahydrofuran (λ_{max}=450 nm). (D) emission of **1**•3THF solid (λ_{max}=466 nm).

The combination of microsecond lifetimes as well as high quantum efficiencies (93%) at a blue emission of 472 nm wavelength, makes **1**•3THF appear to be an ideal candidate for lighting or video display applications in organic or inorganic light-emitting diodes (OLEDs and LEDs, respectively). The luminescence standard quinine sulfate solution well-known to exhibit PLQY in the ~50-55% range was measured using the same technique to verify the methodology. Upon sublimation of this **1**•3THF product, however, the emission color shows a red-shift to 500 nm, in addition to the loss of the high

`

quantum efficiency seen in the **1**•3THF powder. This is probably a result of losing THF from **1**•3THF during the sublimation. Therefore, methods used to manufacture OLEDs will not be able to be utilize **1**•3THF successfully while maintaining the desired characteristics of this material. For LED applications with near-UV pumping, however, the solvated solid form can be conserved in the silicone host matrix. However, THF could very likely be lost at high operational temperatures and that would still lead to a compromised device efficiency. Other means besides a volatile solvent to constrain the excited-state distortion, for example by using a different ligand design that would resist the flattening of the P-Cu-P angle in the excited state, could be invoked in future designs of a similar material composition. Thompson and co-workers have recently described a series of Cu, Ag and Au complexes with bulky ligands that fit this description.[189, 190]

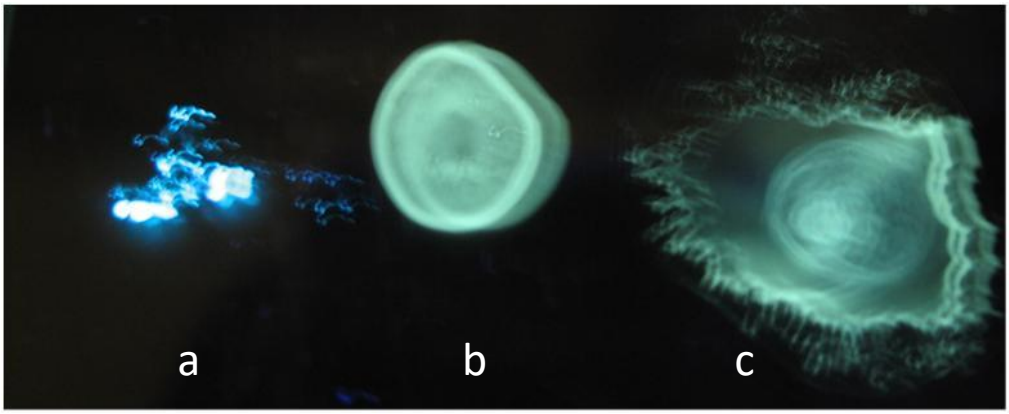

Figure 5.7 Comparison of visual emission colors of (a) **1**•3THF (b) drop-cast neat film of **1**•3THF (c) drop-cast film of PVK doped **1**•3THF.

Emissions are also seen to red-shift upon deposition of the **1** powder into either a neat film or a doped thin film. As is shown in Figure 5.7, when **1** is drop-cast onto a glass slide to make a thin film, the material is seen to shift emission color from blue to dull green. Addition of a doping material, such as

`

polyvinyl carbazole (PVK), broadens the emission as the film appears to be a whitish-green in color as seen in Figure 5.7c.

Spectra of **1** and **1**•3THF have been compared with films made by deposition of the **1** powder onto a quartz slide in Figure 5.8. The emission energies are shown to red-shift from 477 nm for the **1** powder to 496 nm for the 140 nm-thick neat thin film of **1**. Purity of the film as well as the stability of the material is monitored by infrared spectroscopy. Peaks remain consistent, indicating the powder does not decompose upon sublimation. Addition of a common OLED host, 1,3-bis(9-carbazolyl)benzene (mCP), causes broadening of the film's emission as well as further red-shifting the emission maximum to 513 nm. The reason for the red shifting is due to a decrease in medium rigidity as the material composition is diluted and lattice constraints are reduced versus the pure crystalline material. Crystal structures have a 3-dimensional lattice that causes steric effects to quench the excited state distortions of the material. Thin films allow for greater distortions of the material at the surface and, thus, the overall emission of the material is red-shifted. The films are less thick as compared to a neat powder and thus the matrix allows for more surface molecules, which are not hindered by surrounding molecules, allowing for greater excited-state distortions of the material. A shoulder is seen at 420 nm in the doped film. This shoulder can be attributed to emissions from the mCP host material, thus the emission covers more of the visible region and the overall emission appears as a whitish-green material. The films also show greatly reduced quantum yields of 11% and 2% for neat and doped films, respectively. As the excited-state distortions are much more allowed in the films than in the powders, more energy

`

is lost to non-radiative de-excitation decay processes, as is represented in the following equation:

$$\phi_p = (\phi_t)\ ((k_p)/(k_p+k_m))$$

where ϕ_p = phosphorescent quantum yield, ϕ_t = triplet formation efficiency, k_p = rate constant for phosphorescence, and k_m = rate constant for radiationless transition from the triplet state.[83] Given this equation, as the nonradiative emission is increased the overall phosphorescent emission efficiencies are greatly reduced. Improvement in rigidity of material will be required for efficient films to be manufactured.

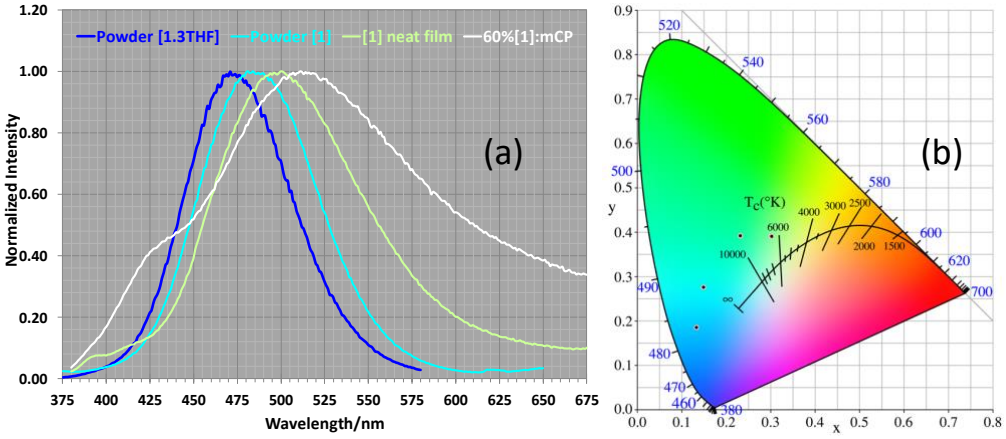

Figure 5.8 (a) Comparison of emissions of powder A = **1** (472 nm); powder B = **1**•3THF (477 nm); 140 nm thick neat film of **1** onto quartz slide (496 nm); 140 nm thick 60% **1**:mCP (deposition of 60% **1** doped with 40% 1,3-bis(9-carbazolyl)benzene = mCP) (511 nm). (b) Representation of the four spectra on the CIE color gamut; the CCT quadrants show that the 60% **1**:mCP doped film and neat film give rise to a warm-white (CCT = 6558) and cool white (CCT = 9762) color rendering, respectively.

Test of longevity have been conducted for the **1** powder, neat film and doped film. As films are exposed to an excitation source (such as a 75 W xenon arc

`

lamp in this study), the film will degrade through a process known as photobleaching.[191] Constant exposure to the excitation source will cause decomposition of the chromophores used in OLED or LED manufacturing, and thus efficiency of the device will degrade over the lifetime of the device. The amount of degradation was studied by quantum yield (%) after exposure to the xenon arc lamp excitation source. The films were made by drop-casting a solution of **1** in chloroform or a solution of 80:20 (by weight) **1**:PVK in chloroform onto a quartz slide. The films were allowed to air-dry for several hours and then were dried in a vacuum desiccator for several more hours.

Table 5.4 show the results of photobleaching experiments for a powder, a drop-cast neat thin film, and a drop-cast PVK-doped thin film of **1**, respectively. The **1** powder was first studied to show the stability of the material in the absence of the polyvinyl carbazole (PVK) host material. As shown in Table 5.4, the **1** powder is found to have 60.0 % efficiency before any exposure to the xenon arc lamp. The material is then excited at 360 nm for the reported amount of time between measurements of the quantum yield. After 120 minutes of exposure to the 75 W xenon arc lamp, the quantum efficiency is observed to be 55.4 %. The 4.6% difference in quantum efficiency is within the error of the method used; therefore, the values are not statistically different. The drop-cast neat **1** film is shown to have a lower quantum yield than the neat powder. As mentioned above, films have less hindrance in the distortion of the molecule, thus the emission peak will be red-shifted and exhibit a lower quantum yield. Compared to the neat deposited film, the neat drop-cast film exhibits a greater quantum yield. This is to be expected, as the drop-cast films are generally thicker. As the film is exposed to the xenon arc lamp, there is only a 1.8% drop

`

in quantum yield, a value that is within the error of the experiment. Statistically, the neat film is not seen to degrade with exposure to the xenon arc lamp, within the studied time. The drop-cast 80:20 **1**:PVK doped film is seen to have only 6.5% quantum efficiency at time zero. Similar to doped-films in the above studies, the matrix allows for large distortions in the material, causing a very low efficiency, even before photobleaching occurs. As the doped film is exposed to the xenon arc lamp, the efficiency drops over 60% in value to a quantum efficiency value of only 2.8%. This drop in intensity is statistically significant, as this value cannot be attributed to only the error in the experimental method. As shown in Figure 5.9, the neat PVK film is also seen degrade at a rapid rate. After exposure to the lamp intensity for an hour, a drop from 38% efficiency to only 24% efficiency is observed in the quantum yield of the film. Two additional hours of exposure of the neat PVK film to the lamp results in degradation to only a 12% quantum efficiency, less than 33% of the original intensity of the film. Photodegradation studies have shown the need for a different host material. While PVK is commonly used as a host material due to photophysical properties, large amounts of degradation are seen when the material is excited by the xenon arc lamp. The **1** sample does not experience substantial degradation and thus is shown to have stability over long-term exposure to an excitation source, which is favorable for OLEDs.

`

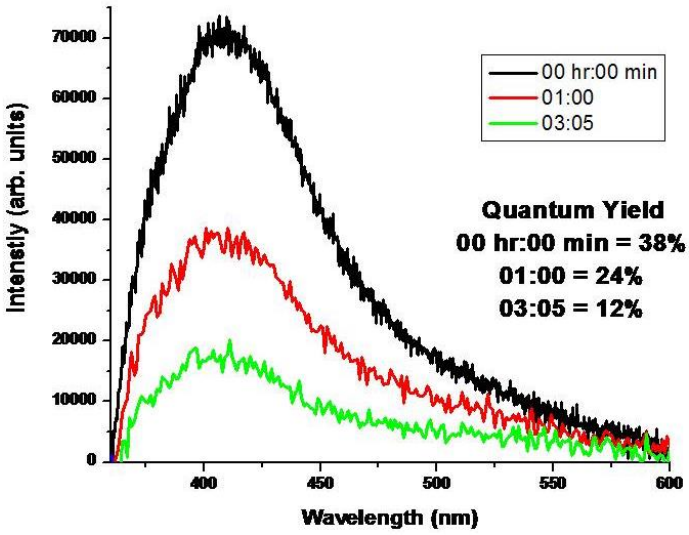

Figure 5.9 Photo-bleaching of a drop-cast neat PVK film.

Table 5.4 Time dependent (minutes exposed to a xenon arc lamp) photobleaching of (A) **1** powder, (B) drop-cast neat film of **1**, and (C) drop-cast 80:20 **1**:PVK doped film.

Time (min)	Quantum Yield A (%)	Quantum Yield B (%)	Quantum Yield C (%)
0	60.0 ± 3.0	28.5 ± 1.4	6.5 ± 0.3
15	58.8 ± 2.9	28.3 ± 1.4	2.8 ± 0.1
30	56.9 ± 2.8	27.9 ±1.4	2.7 ± 0.1
45	59.3 ± 3.0	27.8 ± 1.4	2.6 ± 0.1
60	55.5 ± 2.8	27.7 ± 1.4	2.5 ± 0.1
75	58.4 ±2.9	27.7 ± 1.4	2.5 ± 0.1
90	55.4 ± 2.8	27.4 ± 1.4	2.5 ± 0.1
120	54.8 ± 2.7	26.7 ± 1.3	2.3 ± 0.1

Overall, we conclude that the use of neat solid powders as downconversion phosphors for inorganic LEDs is more favorable than OLEDs, as the latter require thin films which exhibit reduced quantum efficiency due to less medium rigidity of molecules near the surface. Rare earth-free LED downconversion phosphors are highly desirable due to the adverse environmental impacts of lanthanide mining, besides abundance reasons.

`

5.4 Conclusion

{Cu(μ-[3,5-$(CF_3)_2$Pz])(μ-dppm)}$_2$•3THF shows high quantum efficiency of ~90% in the blue region of the visible spectrum with microsecond lifetimes. This material would be an ideal candidate for an emitting layer of an OLED, if not for the loss of rigidity upon sublimation of the material. THF-free {Cu(μ-[3,5-$(CF_3)_2$Pz])(μ-dppm)}$_2$ is shown to exhibit 60% quantum efficiency with a red-shifted emission of 477 nm. Deposition of material onto films further red-shifts the emission of the material and greatly reduce quantum efficiencies. Use of neat solid powders as down-conversion phosphors for inorganic LEDs is, however, favorable. Rigidity will need to be increased in materials to successfully produce more efficient OLED or LED phosphors. Further study of alternative host materials is also important to find materials less sensitive to photodegradation, thus increasing the longevity of OLEDs.

5.5 Acknowledgements

This research has been supported by the Welch Foundation (Grant Y-1289 to H.V.R.D. and Grant B-1542 to M.A.O.), and the U.S. National Science Foundation (Grant CHE-1413641 to M.A.O. for research support and Departmental Grants CHE-1531468 and CHE-1726652 for equipment support).

`

Chapter 6

Experimental Details

6.1 General Methods

All preparations and manipulations were carried out under an atmosphere of purified nitrogen using standard Schlenk technique. Commercially available solvents were purified and dried by standard methods and degassed twice by freeze– pump–thaw method prior to use. Glassware was oven dried overnight at 150 °C. NMR spectra were acquired at 25 °C, on a JEOL Eclipse 500 spectrometer (^{1}H, 500.16 MHz; ^{13}C, 125.78 MHz and ^{19}F, 470.62 MHz), unless otherwise noted. ^{19}F NMR values were referenced to external $CFCl_3$. Melting points were obtained on a Mel-Temp II apparatus and were not corrected. Elemental analyses were performed using a Perkin- Elmer Model 2400 CHN analyzer. Au(THT)Cl and p-tolyl azide were prepared via a reported routes.[192] Other reagents were obtained from commercial sources and used as received.

6.2 Experimental for Chapter 2

1,3-bis(3,5-bis(trifluoromethyl)phenyl)-3-hydroxyprop-2-en-1-one:

Sodium hydride (60% in mineral oil, 0.468 g, 11.72 mmol) was washed with hexanes (5 mL) at room temperature under an atmosphere of nitrogen. Anhydrous THF (20 mL) was then added. In a separate flask, 3',5'-bis(trifluoromethyl)acetophenone (2.00 g, 7.80 mmol) was combined with methyl 3,5-bis(trifluoromethyl)benzoate (2.32 g, 8.58 mmol) and added to the sodium hydride solution, dropwise. The resultant mixture was heated at reflux for 36 hours. The mixture was cooled to room temperature and ice-cold 10% hydrochloric acid (40 mL) was added dropwise to the rapidly stirred mixture,

`

forming a precipitate. Diethyl ether (25 mL) was added to dissolve the precipitate. The organic layer was isolated by extraction, dried over anhydrous Na_2SO_4, filtered and concentrated under vacuum to afford an off-white solid. This solid was recrystallized in acetone to afford the title compound as colorless needles (3.35 g, 87%). m.p. 173 °C. Anal. Calculated for $C_{19}H_8F_{12}O_2$: C, 45.99%; H, 1.62%; N, 0%. Found: C, 45.98%; H, 1.62%; N, 0%. ^{1}H NMR ($CDCl_3$, 500 MHz) δ: 16.59 (s, 1H, O*H*), 8.44 (s, 4H, ar C*H*), 8.11 (s, 2H, ar C*H*), 6.89 (s, 1H, C*H*). $^{13}C\{^1H\}$ NMR ($CDCl_3$, 500 MHz) δ: 183.5 (s, *C*=O), 137.0 (s, ar *C*), 132.8 (q, $^2J_{CF}$ = 33.6 Hz, *C*CF_3), 127.5 (s, ar *C*), 126.4 (m, $^3J_{CF}$ = 3.6 Hz, ar *C*), 123.0 (q, $^1J_{CF}$ = 274 Hz, *C*F_3), 94.0 (s, *C*H). ^{19}F NMR ($CDCl_3$, 500 MHz) δ: -63.11. We have also confirmed the identity of this molecule using X-ray crystallography but the data quality is not high enough for publication of the crystal structure. Crystal Data for $C_{19}H_8F_{12}O_2$ (*M* =496.25 g/mol): monoclinic, space group C2/c (no. 15), *a* = 24.913(6) Å, *b* = 8.3684(18) Å, *c* = 9.241(2) Å, *β* = 110.639(6)°, *V* = 1802.9(7) Å^3, *Z* = 4, *T* = 101.49 K, μ(MoKα) = 0.201 mm^{-1}, *Dcalc* = 1.828 g/cm^3.

3,5-(3,5-$(CF_3)_2$Ph)$_2$PzH:

To a solution of 1,3-bis(3,5-bis(trifluoromethyl)phenyl)-3-hydroxyprop-2-en-1-one (2.00 g, 4.04 mmol) in chloroform (40 mL), hydrazine monohydrate (303 mg, 6.06 mmol) was added, dropwise. The resulting yellow solution was refluxed overnight. Once cooled to room temperature 40 mL of H_2O was slowly added, precipitating the product. This solid was isolated by vacuum filtration, and dried under vacuum. The white solid was recrystallized from hot chloroform to give colorless cubic crystals (2.18 g, 87%). m.p. 188 °C. Anal.

`

Calculated for $C_{19}H_8F_{12}N_2$: C, 46.36%; H, 1.64%; N, 5.69%. Found: C, 46.21%; H, 1.36%; N, 5.80%. ^{1}H NMR ($CDCl_3$, 500 MHz) 8.18 (s, 4H, ar C*H*), 7.87 (s, 2H, ar C*H*), 7.11 (s, 1H, Pz*H*), could not observe the NH resonance. $^{13}C\{^1H\}$ NMR ($CDCl_3$, 500 MHz) δ: 146.8 (s, Pz*C*), 132.7 (q, $^2J_{CF}$ = 33.6 Hz, *C*CF_3), 132.7 (s, ar *C*), 125.8 (s, ar *C*), 122.4 (m, ar *C*, $^3J_{CF}$ = 3.6 Hz), 123.2 (q, $^1J_{CF}$ = 274 Hz, *C*F_3), 102.3 (s, Pz*C*H). ^{19}F NMR ($CDCl_3$, 500 MHz) δ: -63.23 ppm.

{[3,5-(3,5-(CF$_3$)$_2$Ph)$_2$Pz]Cu}$_3$ (5):

3,5-(3,5-$(CF_3)_2$Ph)$_2$PzH (200 mg, 0.41 mmol) and Cu_2O (29 mg, 0.20 mmol) are combined in a flask and 15 mL dry toluene. The resulting mixture was refluxed overnight. The mixture was filtered while still hot to remove excess Cu_2O. The resulting clear solution was allowed to slowly come to room temperature, giving colorless needles. The crystalline solid was dried under reduced pressure to obtain **5** (130 mg, 57%). Anal. Calcd for $C_{57}H_{21}Cu_3F_{36}N_6$•0.3 toluene: C, 41.95%; H, 1.39%; N, 4.97%, Found: C, 42.29%; H, 1.33%; N, 5.88%. The crystals were dried under vacuum at 90 °C for 4 hours to remove toluene. ^{1}H NMR ($CDCl_3$, 500 MHz): 8.07 (s, 4H, ar C*H*); 7.65 (s, 2H, ar C*H*); 7.00 (s, 1H, Pz*H*). ^{19}F NMR ($CDCl_3$, 500 MHz): -63.47 ppm. $^{13}C\{^1H\}$ NMR ($CDCl_3$, 500 MHz) on sample containing some toluene: 153.2 (s, Pz*C*), 132.6 (q, $^2J_{CF}$ = 34.8 Hz, *C*CF_3), 126.3 (s, ar *C*), 125.9 (s, ar *C*), 123.1 (q, $^1J_{CF}$ = 274 Hz, *C*F_3), 122.2 (s, ar *C*), 104.5 (Pz*C*H), and toluene peaks present (toluene free product is not very soluble in $CDCl_3$). X-ray quality crystals were obtained by cooling a warm solution of **5** in toluene.

{[3,5-(3,5-(CF$_3$)$_2$Ph)$_2$Pz]Ag}$_3$ (6):

`

3,5-(3,5-$(CF_3)_2$Ph)$_2$PzH (500 mg, 1.01 mmol) and Ag_2O (118 mg, 0.51 mmol) were combined in a flask and 20 mL dry toluene was added. This solution was protected from light and refluxed overnight. After cooling to room temperature, the mixture was filtered through Celite to obtain a colorless solution. This solution was dried under reduced pressure to yield a white solid. Trapped toluene was removed by drying the solids under vacuum at 60 ^{0}C overnight, 310 mg, 51% yield. Anal. Calcd for $C_{57}H_{21}Ag_3F_{36}N_6$: C, 38.09%; H, 1.18%; N, 4.68%, Found: C, 38.33%; H, 1.39%; N, 4.19%. ^{1}H NMR ($CDCl_3$, 500 MHz): 8.08 (s, 4H, ar C*H*); 7.77 (s, 2H, ar C*H*); 7.06 (s, 1H, Pz*H*). ^{19}F NMR ($CDCl_3$, 500 MHz): -63.52 ppm. ^{13}C{^{1}H} NMR ($CDCl_3$, 500 MHz): 151.9 (br s, Pz*C*), 134.3 (s, ar *C*), 132.5 (q, $^2J_{CF}$ = 33.6 Hz, *C*CF_3), 126.0 (s, ar *C*), 123.0 (q, $^1J_{CF}$ = 272 Hz, *C*F_3), 122.1 (s, ar *C*), 103.2 (Pz*C*H). The product was recrystallized from dichloromethane: hexane (4:1) at -20 °C to give colorless needle-like crystals of **6**.

{[3,5-(3,5-$(CF_3)_2$Ph)$_2$Pz]Au}$_3$ (7):

NaH (8.9 mg, 0.22 mmol, 60% in oil) was washed free from oil with dry hexanes (2 mL). In a separate flask, (3,5-$(CF_3)_2$Ph)$_2$PzH (100 mg, 0.20 mmol) was dissolved in 10 mL dry THF. This solution was then slowly added dropwise to the NaH solution, at 0 °C. The resulting mixture was allowed to stir for 1 hour. This sodium salt of pyrazolate was filtered to remove any excess NaH and then added to Au(THT)Cl (64 mg, 0.20 mmol) in 5 mL dry THF. The resulting solution was stirred for 6 hours at room temperature, protected from light by aluminum foil. The solution was filtered through Celite and the filtrate was pumped dried to obtain **7** as a white solid (82 mg, 57%). Anal. Calcd for

`

$C_{57}H_{21}Au_3F_{36}N_6$: C, 33.16%; H, 1.03%; N, 4.07%, Found: C, 33.32%; H, 0.88%; N, 3.98%. ^{1}H NMR ($CDCl_3$, 500 MHz): 8.15 (s, 4H, ar C*H*); 7.72 (s, 2H, ar C*H*); 7.17 (s, 1H, Pz*H*). ^{19}F NMR ($CDCl_3$, 500 MHz): -63.59 ppm. ^{13}C{^{1}H} NMR ($CDCl_3$, 500 MHz): 151.6 (s, Pz*C*), 133.6 (s, ar *C*), 132.2 (q, $^{2}J_{CF}$ = 33.6 Hz, *C*CF_3), 127.2 (s, ar *C*), 122.8 (q, $^{1}J_{CF}$ = 274 Hz, *C*F_3), 122.4 (m, ar *C*), 106.3 (Pz*C*H). Solid samples of **7** was recrystallized from toluene to obtain X-ray quality crystals.

General procedure for Azide-Alkyne Cycloaddition:

The catalyst (0.015 mmol, 1 mol% based on *p*-tolylazide) was dissolved in CH_2Cl_2 (5 mL) under a nitrogen atmosphere at room temperature. The alkyne (1.5 mmol) was slowly added, followed by *p*-tolylazide (1.5 mmol). The mixture was stirred at room temperature overnight, under a nitrogen atmosphere. The crude mixture was analyzed using ^{1}H NMR, to check for the presence of the desired triazole.

General procedure for cyclopropanation:

The catalyst (0.023 mmol, 3 mol% based on ethyl diazoacetate, EDA) was dissolved in CH_2Cl_2 (10 mL) under a nitrogen atmosphere at room temperature. Styrene (2.25 mmol) was added, followed by slow addition over 10 hours of EDA (0.75 mmol). The mixture was stirred at room temperature overnight, under a nitrogen atmosphere, while EDA was added. After complete addition, the mixture was stirred for 1 day at room temperature. The crude mixture was analyzed using ^{1}H NMR, to check for the presence of cyclopropane. Percent yield and percentage of cis/trans isomers were calculated using ^{1}H NMR and an

`

internal standard of dimethylformamide. The ^{1}H NMR also shows peaks corresponding to diethyl maleate and diethyl fumarate.

Photophysical properties.

The steady state photoluminescence of the three complexes (white microcrystalline powders packed into 5 mm quartz tubes) were recorded using the FluoroMax-3 spectrofluorometer (Horiba Jobin Yvon, France) with the DataMax software (Horiba, Japan). Excitation and Emission spectra were recorded in the range of 250–600 nm with a bandpass of 1 nm. The resulting spectra were corrected to the background intensity of the 150W Xe arc lamp. The 77 K photoluminescence data were collected by submerging the sample in liquid nitrogen using a Suprasil quartz liquid nitrogen dewar.

X-ray Structure Determinations.

A suitable crystal covered with a layer of hydrocarbon/Paratone-N oil was selected and mounted on a Cryo-loop, and immediately placed in the low temperature nitrogen stream. The X-ray intensity data were measured on a Bruker D8 Quest with a Photon 100 CMOS detector equipped with an Oxford Cryosystems 700 series cooler, a Triumph monochromator, and a MoKα fine-focus sealed tube (λ = 0.71073 Å). Intensity data were processed using the Bruker Apex program suite. Absorption corrections were applied using SADABS. Initial atomic positions were located by direct methods using XT, and the structures of the compounds were refined by the least-squares method using SHELXL[193] within Olex2[194] GUI. The {[3,5-(3,5-$(CF_3)_2Ph)_2Pz$]Cu}$_3$ (**5**) crystallizes in Triclinic P-1 space group with 1.5 molecules of toluene.

`

Compound {[3,5-(3,5-$(CF_3)_2$Ph)$_2$Pz]Ag}$_3$ (**6**) crystallizes with 2 molecules of dichloromethane in the crystal lattice. Crystals tend to crack at low temperature and therefore data were collected at room temperature. One of the CH_2Cl_2 molecules show significant disorder and a quite a few fluorine atoms of CF_3 groups show positional disorder. The disordered CH_2Cl_2 was removed using MASK routine in Olex2. Positional disorder of fluorine atoms were managed by SHELX constraints. All these issues lower the structure quality somewhat and therefore metrical parameters of {[3,5-(3,5-$(CF_3)_2$Ph)$_2$Pz]Ag}$_3$ should be treated with care. In {[3,5-(3,5-$(CF_3)_2$Ph)$_2$Pz]Au}$_3$ (**7**), a highly disordered solvent molecule was removed using the PLATON SQEEZE routine. All the non-hydrogen atoms were refined anisotropically. Hydrogen atoms were included at calculated positions and refined riding on corresponding carbons. X-ray structural figures were generated using Olex2. CCDC 2012029-2012032 files contain the supplementary crystallographic data. These data can be obtained free of charge via http://www.ccdc.cam.ac.uk/conts/retrieving.html or from the Cambridge Crystallographic Data Centre (CCDC), 12 Union Road, Cambridge, CB2 1EZ, UK). Additional details are provided in supporting information section.

Crystal Data for 3,5-(3,5-$(CF_3)_2$Ph)$_2$PzH, $C_{19}H_8F_{12}N_2$ (M =492.27 g/mol): trigonal, space group R-3 (no. 148), a = 17.7048(6) Å, c = 31.8231(11) Å, V = 8638.8(7) Å^3, Z = 18, T = 99.99 K, μ(MoKα) = 0.184 mm^{-1}, *Dcalc* = 1.703 g/cm^3, 36951 reflections measured (5.466° ≤ 2Θ ≤ 59.264°), 5428 unique (R_{int} = 0.0228, R_{sigma} = 0.0144) which were used in all calculations. The final R_1 was 0.0332 (I > 2σ(I)) and wR_2 was 0.0900 (all data).

`

Crystal Data for {[3,5-(3,5-$(CF_3)_2$Ph)$_2$Pz]Cu}$_3$•1.5(toluene), $C_{67.5}H_{33}Cu_3F_{36}N_6$ (*M* =1802.62 g/mol): triclinic, space group P-1 (no. 2), *a* = 8.4054(10) Å, *b* = 19.555(2) Å, *c* = 21.674(2) Å, *α* = 107.382(2)°, *β* = 91.600(2)°, *γ* = 98.226(2)°, *V* = 3355.4(7) Å^3, *Z* = 2, *T* = 100.01 K, μ(MoKα) = 1.091 mm^{-1}, *Dcalc* = 1.784 g/cm^3, 30015 reflections measured (5.654° ≤ 2Θ ≤ 52°), 13114 unique (R_{int} = 0.0440, R_{sigma} = 0.0620) which were used in all calculations. The final R_1 was 0.0864 (I > 2σ(I)) and wR_2 was 0.2592 (all data).

Crystal Data for {[3,5-(3,5-$(CF_3)_2$Ph)$_2$Pz]Ag}$_3$•CH_2Cl_2, $C_{58}H_{23}Ag_3Cl_2F_{36}N_6$ (*M* =1882.33 g/mol): triclinic, space group P-1 (no. 2), *a* = 8.6941(5) Å, *b* = 15.8573(8) Å, *c* = 26.1433(13) Å, *α* = 89.287(2)°, *β* = 85.728(2)°, *γ* = 87.428(2)°, *V* = 3590.5(3) Å^3, *Z* = 2, *T* = 299.06 K, μ(MoKα) = 1.019 mm^{-1}, *Dcalc* = 1.741 g/cm^3, 37199 reflections measured (5.768° ≤ 2Θ ≤ 52.998°), 14836 unique (R_{int} = 0.0332, R_{sigma} = 0.0407) which were used in all calculations. The final R_1 was 0.0615 (I > 2σ(I)) and wR_2 was 0.1945 (all data).

Crystal Data for {[3,5-(3,5-$(CF_3)_2$Ph)$_2$Pz]Au}$_3$, $C_{57}H_{21}Au_3F_{36}N_6$ (*M* =2064.70 g/mol): monoclinic, space group $P2_1/c$ (no. 14), *a* = 8.3667(5) Å, *b* = 31.7232(19) Å, *c* = 25.7197(15) Å, *β* = 91.507(2)°, *V* = 6824.1(7) Å^3, *Z* = 4, *T* = 100.0 K, μ(MoKα) = 6.573 mm^{-1}, *Dcalc* = 2.010 g/cm^3, 89629 reflections measured (5.694° ≤ 2Θ ≤ 60.054°), 19862 unique (R_{int} = 0.0345, R_{sigma} = 0.0273) which were used in all calculations. The final R_1 was 0.0317 (I > 2σ(I)) and wR_2 was 0.0702 (all data).

`

6.3 Experimental for Chapter 3

Diethyl 3,5-dicarboxylate pyrazole:

The starting pyrazole was synthesized from 3,5-dimethylpyrazole and purified via a previously reported method[86] to yield the pure diethyl 3,5-dicarboxylate pyrazole in 63% yield. M.p.: 52-54 °C. NMR data is consistent with the previous report. ^{1}H NMR ($CDCl_3$): δ (ppm) = 11.18 (s, 1H, N*H*), 7.34 (s, 1H, Pz*H*), 4.42 (q, 4H, CH_2, J = 7.5 Hz), 1.41 (t, 6H, CH_3, J = 7.5 Hz). ^{13}C{^{1}H} ($CDCl_3$): δ (ppm) 160.5, 139.9, 111.4, 61.8, 14.3.

Diethyl 4-bromo-3,5-dicarboxylate pyrazole:

This starting pyrazole was synthesized in an analogous method to the previously reported 4-bromo-3,5-trifluoromethyl pyrazole.[195] Diethyl 3,5-dicarboxylate pyrazole (1.0 g, 4.7 mmol) and NBS (924 mg, 5.2 mmol) were combined in a round bottom flask to which DMF (20 mL) was added. The solution was stirred at 130 °C overnight. After stirring overnight, the solution was allowed to cool to room temperature and water (20 mL) was added followed by extraction of product with ethyl acetate. The organic layers were combined, dried over Na_2SO_4, filtered and the solvent was removed under reduced pressure to obtain a light brown oil. The oil was purified via column chromatography (1:1, hexanes: ethyl acetate) to obtain a white solid in 65% yield. M.p.: 92-95 °C. NMR data is consistent with previous report.[4] ^{1}H NMR ($CDCl_3$): δ (ppm) = 11.90 (s, 1H, N*H*), 4.46 (q, 4H, CH_2, J = 6.5 Hz), 1.43 (t, 6H, CH_3, J = 6.5 Hz). ^{13}C{^{1}H} ($CDCl_3$): δ (ppm) = 159.5, 138.3, 100.7, 62.1, 14.3.

`

{[3,5-(CO_2Et)$_2$Pz]Cu}$_3$:

Diethyl 3,5-dicarboxylate pyrazole (1.0 g, 4.71 mmol) and Cu_2O (354 mg, 2.48 mmol) were combined in a Schlenk flask and toluene (25 mL) was added. The resulting mixture was refluxed for 24 hours, under nitrogen. The mixture was cooled to room temperature and filtered through Celite to remove excess copper(I) oxide. The green solution was pumped dry to obtain a green oil. This oil was washed with hexanes to precipitate a pale green solid. The solid was dried under vacuum at 80 °C to remove toluene (710 mg, 54 %). M.p.: 146-150 °C. ^{1}H NMR ($CDCl_3$): δ (ppm) = 7.32 (s, 1H, Pz*H*), 4.34 (q, 4H, C*H*$_2$, J = 6.87 Hz), 1.28 (t, 6H, C*H*$_3$, J = 6.87 Hz). $^{13}C\{^1H\}$ ($CDCl_3$): δ (ppm) = 161.8, 144.8, 110.6, 61.4, 14.3. Anal. Calculated for $C_{27}H_{33}Cu_3N_6O_{12}$: C, 39.35%; H, 4.04%; N, 10.16%. Found: C, 39.55%; H, 4.19%; N, 9.70%.

{[3,5-(CO_2Et)$_2$Pz]Ag}$_3$:

Diethyl 3,5-dicarboxylate pyrazole (1.0 g, 4.71 mmol) and Ag_2O (575 mg, 2.48 mmol) were combined in a Schlenk flask and toluene (25 mL) was added. The mixture was refluxed overnight under nitrogen atmosphere, while protecting from light using aluminum foil. The mixture was then cooled to room temperature and filtered through Celite to remove excess silver(I) oxide. The clear solution was dried under vacuum to obtain a white solid (840 mg, 56 %). M.p.: 252-255 °C (decomposition). ^{1}H NMR ($CDCl_3$): δ (ppm) = 7.40 (s, 1H, Pz*H*), 4.46 (q, 4H, C*H*$_2$, J = 6.5 Hz), 1.39 (t, 6H, C*H*$_3$, J = 6.5 Hz). $^{13}C\{^1H\}$ ($CDCl_3$): δ (ppm) = 162.44, 145.15, 110.18, 61.18, 14.51. Anal. Calculated for

`

$C_{27}H_{33}Ag_3N_6O_{12}$: C, 33.88%; H, 3.48%; N, 8.78%. Found: C, 35.12%; H, 3.46%; N, 8.32%.

{[4-Br-3,5-(CO_2Et)$_2$Pz]Cu}$_3$:

Prepared in an analogous procedure to diethyl 3,5-dicarboxylate pyrazolate copper trimer synthesis. Diethyl 4-bromo-3,5-dicarboxylate pyrazole (200 mg, 0.69 mmol) was combined with Cu_2O (54 mg, 0.38 mmol) and toluene (15 mL) was added. The resulting mixture was refluxed, under nitrogen, overnight. The reaction mixture was then allowed to cool to room temperature and filtered through Celite to remove excess Cu_2O and afford a clear, light green solution. The solvent was removed under reduced pressure to obtain a green oil. This oil was washed with hexanes to precipitate a pale yellow-green solid in 40 % yield. M.p.: 200-204 °C. ^{1}H NMR ($CDCl_3$): δ (ppm) = 4.38 (br q, 4H, C*H*$_2$, J = 6.9 Hz), 1.32 (br t, 6H, C*H*$_3$). ^{13}C{^{1}H} ($CDCl_3$): δ (ppm) = 161.3, 142.7, 99.4, 61.9, 14.3. Anal. Calculated for $C_{27}H_{30}Cu_3Br_3N_6O_{12}$ + 0.25 toluene: C, 32.20%; H, 3.00%; N, 7.74%. Found: C, 32.54%; H, 3.09%; N, 8.13%.

{[4-Br-3,5-(CO_2Et)$_2$Pz]Ag}$_3$:

Prepared in an analogous procedure to diethyl 3,5-dicarboxylate pyrazolate silver trimer synthesis. Diethyl 4-bromo-3,5-dicarboxylate pyrazole (200 mg, 0.69 mmol) was combined in a Schlenk flask with Ag_2O (88 mg, 0.38 mmol) and toluene (15 mL). The resulting mixture was refluxed, under nitrogen, overnight while protected from the light. The solution was cooled to room temperature and filtered through Celite to afford a colorless solution. The solvent was removed under vacuum to obtain a white solid in 49 % yield. ^{1}H

`

NMR ($CDCl_3$): δ (ppm) = 4.41 (br q, 4H, C*H*$_2$), 1.39 (br t, 6H, CH_3). $^{13}C\{^1H\}$ ($CDCl_3$): δ (ppm) = 161.7, 142.9, 99.2, 61.7, 14.4. Anal. Calculated for $C_{27}H_{30}Ag_3Br_3N_6O_{12}$: C, 27.16%; H, 2.53%; N, 7.04%. Found: C, 28.06%; H, 2.75%; N, 6.96%.

`

6.4 Experimental for Chapter 4

General Procedure:

Benzyl azide, p-tolyl azide, 1-adamantyl azide, {[3,5-(*i*-Pr)$_2$Pz]Cu}$_3$, {[3-(CF$_3$)-5-(CH$_3$)Pz]Cu}$_3$, {[3,5-(*t*-Bu)$_2$Pz]Cu}$_4$, {[3-(CF$_3$)-5-(*t*-Bu)Pz]Cu}$_4$, and {[4-Br-3,5-(*i*-Pr)$_2$Pz]Cu}$_4$ were prepared via reported routes.[5, 11, 22, 192, 196, 197] Solvents were purchased from commercial sources and purified before use. All other reagents were obtained from commercial sources and used as received.

{[4-NO$_2$-3,5-(CF$_3$)$_2$Pz]Cu}$_3$:

4-NO$_2$-3,5-(CF$_3$)$_2$PzH (0.300 g, 1.204 mmol) and Cu$_2$O (0.138 g, 0.963 mmol) were taken in a high pressure Schlenk flask and vacuum dried for ~30 mins. Toluene (~12 mL) was added to the flask under nitrogen and the reaction mixture was heated to 120-125 °C overnight. The solution was then cooled to room temperature, tetrahydrofuran was added to it and finally filtered through Celite. The solvent was removed under reduced pressure to obtain {[4-NO$_2$-3,5-(CF$_3$)$_2$Pz]Cu}$_3$ as yellow colored solid. X-ray quality crystals were grown from tetrahydrofuran at -20°C. Yield: 90%. M.p.: 340-342 °C (decomposition). ^{19}F NMR ((CD$_3$)$_2$CO): δ (ppm) = -62.61 (s). ^{13}C{^{1}H} NMR (CDCl$_3$/THF, 0.25:1): δ (ppm) = 137.6 (br q, *C*CF$_3$), 130.0 (s, *C*-4 Pz), 117.8 (q, ^{1}J$_{C\text{-}F}$ = 275 Hz, *C*F$_3$). In the ^{13}C{^{1}H} NMR, a peak at 127.1 (s) was also observed. This peak is also found when taking a ^{13}C{^{1}H} NMR of only THF in CDCl$_3$, so the peak corresponds to a small impurity in the distilled THF. IR (cm^{-1}, selected peaks): 1515, 1366, 1231, 1170, 1144, 1027. Raman (cm^{-1}): 1526, 1367, 1264, 1153,

`

1063, 841. Anal. Calculated for $C_{15}Cu_3N_9O_6F_{18}$ · THF: C, 22.66%; H, 0.80%, N, 12.52%. Found: C, 22.84%; H, 1.00%; N, 14.70%.

$Cu_2(\mu$-[4-NO_2-3,5-$(CF_3)_2$Pz])$_2$(HC≡CPh)$_2$:

Phenylacetylene (0.035 mL, 0.321 mmol) was added to a solution of {[4-NO_2-3,5-$(CF_3)_2$Pz]Cu}$_3$ (100 mg, 0.107 mmol) in THF (5 mL) at room temperature. The reaction mixture was stirred for 4 hours under nitrogen and then solvent was removed under reduced pressure to obtain $Cu_2(\mu$-[4-NO_2-3,5-$(CF_3)_2$Pz])$_2$(HC≡CPh)$_2$ as a pale yellow solid. X-ray quality crystals were grown from dichloromethane at -20 °C. Yield: 92%. M.p.: 145-148 °C (decomposition). ^{1}H NMR ($CDCl_3$): δ (ppm) = 7.41 (m, J = 4.2 Hz, 2H, ar C*H*), 7.27 (m, 3H, ar C*H*), 5.16 (brs, 1H, ≡C*H*). $^{13}C\{^1H\}$ ($CDCl_3$): δ (ppm) = 138.9 (q, $^2J_{C\text{-}F}$ =38 Hz, *C*CF_3), 131.1 (s, ar-*C*H), 130.6 (br s, ar-*C*), 129.1 (s, ar-*C*), 120.9 (s, ar-*C*), 118.9 (q, $^1J_{C\text{-}F}$ =269 Hz, *C*F_3), 78.5 (brs, C≡*C*H). The peak of the quaternary carbon atom of the phenylacetylene triple bond was not observed, and the broad singlet at 130.6 is likely two overlapping aromatic carbon peaks. ^{19}F NMR ($CDCl_3$) δ (ppm) = -61.5 (s, C*F*$_3$). IR (cm^{-1}, selected peaks): 3184 (C≡CH), 2919, 1977 (C≡C), 1511, 1365, 1223, 1163, 1132, 1014. Anal. Calculated for $C_{26}H_{12}Cu_2N_6O_4F_{12}$: C, 37.74%; H, 1.46%, N, 10.16%. Found: C, 37.33%; H, 1.35%; N, 10.72%.

`

Materials and Methods for Catalysis

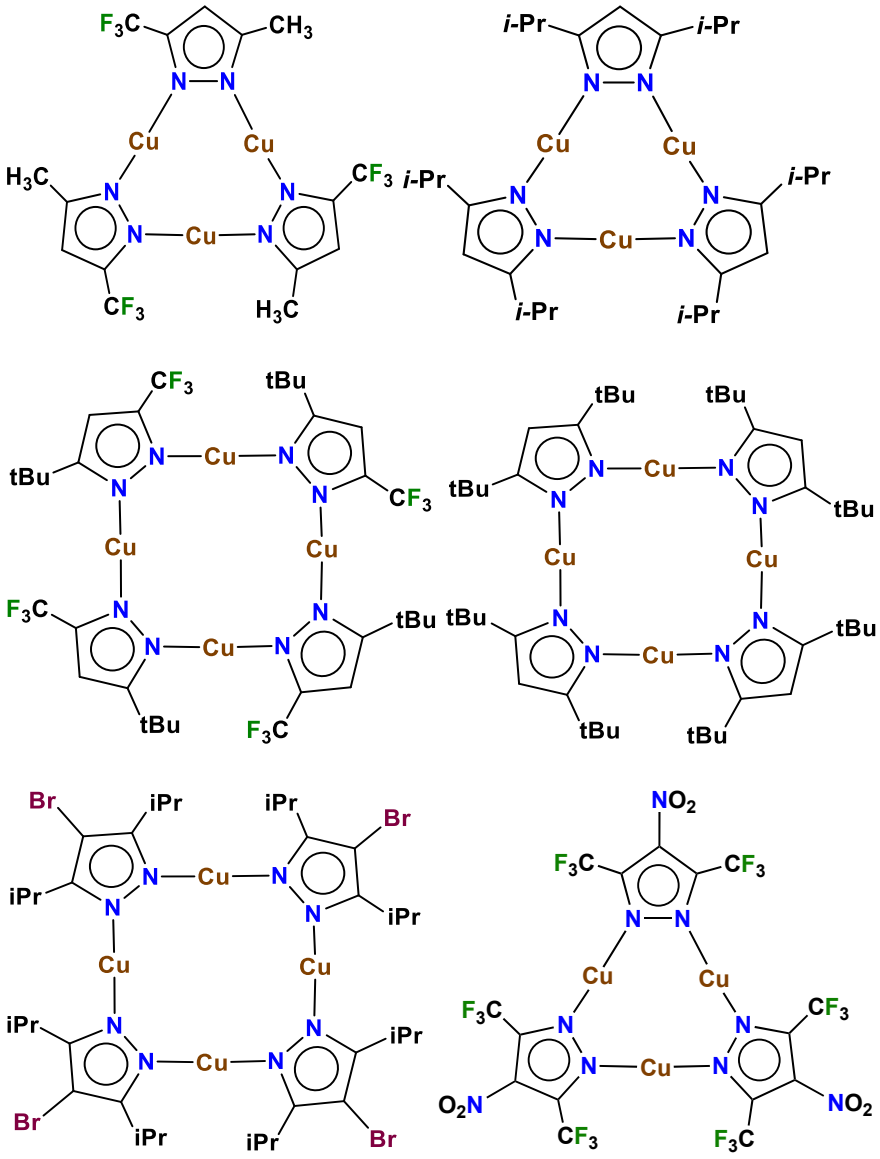

Figure 6.4.1. Catalysts used in this work

`

General procedure for azide-alkyne cycloadditions

Benzyl azide, p-tolyl azide, 1-adamantyl azide, {[3,5-(*i*-Pr)$_2$Pz]Cu}$_3$, {[3-(CF$_3$)-5-(CH$_3$)Pz]Cu}$_3$, {[3,5-(*t*-Bu)$_2$Pz]Cu}$_4$, {[3-(CF$_3$)-5-(*t*-Bu)Pz]Cu}$_4$, and {[4-Br-3,5-(*i*-Pr)$_2$Pz]Cu}$_4$ were prepared via reported routes.[111-116] All other reagents were obtained from commercial sources and used as received. For all reactions, 1 mol percent of the catalyst was added to a vial, open to air, containing 100 mg of azide, 1 equiv. of alkyne, and 5 mL dried dichloromethane. The vials were closed, and the resulting solutions were stirred at room temperature for 12 hours. Approximately 0.1 mL of the crude mixtures were taken in an NMR tube and CDCl$_3$ was added. Samples were analyzed using NMR and acquired at 25 °C on a JEOL Eclipse 500 spectrometer (^{1}H, 500.16 MHz; ^{13}C, 125.78 MHz), in CDCl3, to check for the presence of the desired triazole. The percent conversion was calculated by comparing the peaks of the desired 1,2,3-triazole with the peaks of the starting azide. No by-products were observed.

1-(*p*-tolyl)-4-hexyl-1*H*-1,2,3-triazole

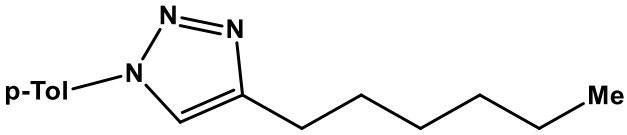

^{1}H NMR (CDCl$_3$, 500 MHz): 7.67 (s, 1H), 7.55 (d, 2H, J = 6.87 Hz), 7.23 (d, 2H, J = 6.87 Hz), 2.73 (t, 2H, J = 7.45 Hz), 2.35 (s, 3H), 1.65-1.71 (m, 2H), 1.33-1.37 (m, 2H), 1.26-1.29 (m, 4H), 0.85 (t, 3H, J = 6.87 Hz). ^{13}C{^{1}H} NMR (CDCl$_3$, 500 MHz): 149.0, 138.4, 135.0, 130.1, 120.2, 118.8, 31.6, 29.4, 29.0, 25.7, 22.6, 21.0, 14.1.

Reference: Devaborniny, P.; Ponduru, T.; Noonikara-Poyil, A.; Jayaranta, N.; Dias, H.V.R.; Acetylene and terminal alkyne complexes of copper(I) supported fluorinated pyrazolates: synthesis, structures, and transformations. *Dalton Transactions.* **2019**, *48*, 15782-15794.

`

1-(*p*-tolyl)-4-phenyl-1*H*-1,2,3-triazole

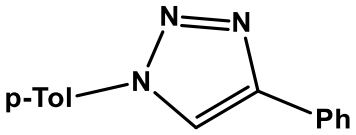

^{1}H NMR ($CDCl_3$, 500 MHz): 8.15 (s, 1H), 7.90 (d, 2H, J = 7.45 Hz), 7.65 (d, 2H, J = 8.60 Hz), 7.45 (t, 2H, J = 7.45 Hz), 7.30-7.36 (m, 3H), 2.42 (s, 3H). ^{13}C{^{1}H} NMR ($CDCl_3$, 500 MHz): 148.3, 139.0, 134.8, 130.4, 129.0, 128.4, 125.9, 120.5, 117.8, 21.2.

Reference: Meng, X.; Xu, X.; Gao, T.; Chen, B.; *Eur. J. Org. Chem.* **2010**, *2010*, 5409-5414

1-(benzyl)-4-hexyl-1*H*-1,2,3-triazole

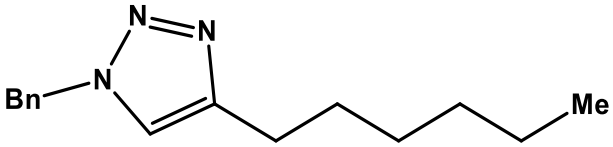

^{1}H NMR ($CDCl_3$, 500 MHz): 7.32-7.38 (m, 3H), 7.23-7.27 (m, 2H), 7.17 (s, 1H), 5.49 (s, 2H), 2.68 (t, J=7.5 Hz, 2H), 1.63 (quint, J=7.5 Hz, 2 H), 1.26-1.36 (m, 6H), 0.86 (t, J = 7.0 Hz, 3H). ^{13}C{^{1}H} NMR ($CDCl_3$, 500 MHz): 149.2, 135.2, 129.2, 128.8, 128.1, 120.6, 54.1, 31.7, 29.5, 29.1, 25.9, 22.7, 14.2.

Reference: Iwasaki, M., Yorimitsu, H., and Oshima, K.; *Chem. Asian J.* **2007**, *2*, 1430-1435.

1-(benzyl)-4-phenyl-1*H*-1,2,3-triazole

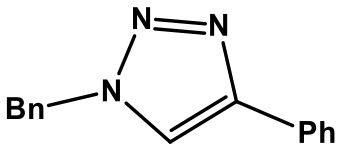

^{1}H NMR ($CDCl_3$, 500 MHz): 7.77 (m, 2H), 7.65 (s, 1H), 7.32 (m, 8H), 5.53 (s, 2H). ^{13}C{^{1}H} NMR ($CDCl_3$, 500 MHz): 161.1, 140.2, 133.6, 134.5, 129.3, 129.2, 128.3, 127.3, 54.5, 54.2.

Reference: Jlalia, I., Meganem, F., Herscovici, J., Girard, C.; *Molecules.* **2009**, *14*, 528-539.

`

1-(adamantyl)-4-phenyl-1*H*-1,2,3-triazole

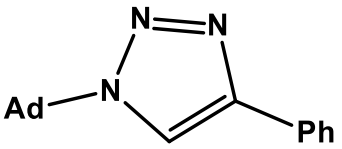

^{1}H NMR ($CDCl_3$, 500 MHz): 7.84 (d, 2H, J = 7.6 Hz), 7.83 (s, 1H), 7.41 (t, 2H, J = 7.6 Hz), 7.31 (t, 1H, J = 7.6 Hz), 2.29 (s, 9H), 1.82 (s, 6H).

Reference: Chtchigrovsky, M., Primo, A., Gonzalez, P., Molvinger, K., Robitzer, F. Q., Taran, F.; *Angewandte Chemie International Edition*. **2009**, *48*, 5916-5920.

Vapor Pressure Osmometry

Molecular weight data were obtained using a KNAUER Vapor Pressure Osmometer K-7000 with EuroOsmo 7000 software. A reference measurement was run before performing all sample measurements by attaching a droplet pure solvent on each thermistor and performing AUTOZERO. To run a sample measurement, a droplet of solution was placed on one thermistor while pure solvent remained on the other. The concentration of each sample was entered for every single run and at least three osmograms were recorded at each concentration. The software automatically calculated an average value once two or more readings were selected. To avoid contamination, it was also important to rinse the sample thermistor with pure solvent when moving from one concentration to another. The drop size was kept as constant and equal as possible on both thermistors. To provide saturated atmosphere around the thermistors, the chamber contained a reservoir and wick. The difference in vapor pressure between the two droplets caused in the difference in temperature at each thermistor.

`

Commercially available chloroform was used as the solvent, without further purification. The instrument was operated at 30 °C (the minimum working temperature suggested for the solvent) and benzil was used as the standard for calibration. A calibration curve was constructed by measuring prepared solutions of benzil in chloroform in the concentration range 5-50 mmol/kg. The minimum concentration was always kept above the suggested minimum value (3 mmol/kg) given in the manual (K-7000 VPO). EuroOsmo software was used to draw graphs and calculate the calibration constant (K_{calib}).

A similar procedure was followed to obtain measurements and calculate a sample constant (K_{sample}) for copper pyrazolate samples. The sample concentration was entered for each run and at least three concentrations were examined within each range. At least three measurements from each concentration were used in calculations to calculate the molecular weight. Since VPO is a sensitive instrument, other thermal sources and losses could contribute to the observed results. Electrical current flowing through the thermistors results in self-heating, which is kept as small as possible but cannot be eliminated entirely. To minimize the error, each sample measurement was repeated at least four times. Additionally, each entire experiment was repeated at least twice to confirm the accuracy of the values. Due to instrument limitations, the concentration range examined in VPO is higher than the actual catalyst concentration used in the reactions. However, we observed in ^{1}H NMR the ratio of isomers, 1 Cu_3 : 1.5 Cu_4, is the same at both the higher VPO concentrations and lower catalytic concentration. Thus, the VPO data serves as a good model for the solution behavior of the catalysts despite the concentration differences.

`

Kinetics General Methods

In a method similar to previous reports[91, 123], the desired amount of 1-octyne (0.75, 1.5, 3.75, 15.0, or 30.0 mmol) was added to the corresponding equivalent of benzyl azide (0.75, 1.5, 3.75, 15.0, or 30.0 mmol) in a vial, under air, and the appropriate volume of dried dichloromethane to reach a total volume of 5 mL. The copper(I) pyrazolate catalyst was then added in the desired mol percent (0.0075 mmol – 0.0375 mmol). The resulting mixtures were stirred in a room temperature, 16 °C, water bath and an approximately 0.1 mL aliquot was taken into an NMR tube every 30 minutes and $CDCl_3$ was added. Samples were analyzed via ^1H NMR for the presence of the desired 1,2,3-triazole.

Dependence on {[3,5-(*t*-Bu)$_2$Pz]Cu}$_4$ concentration

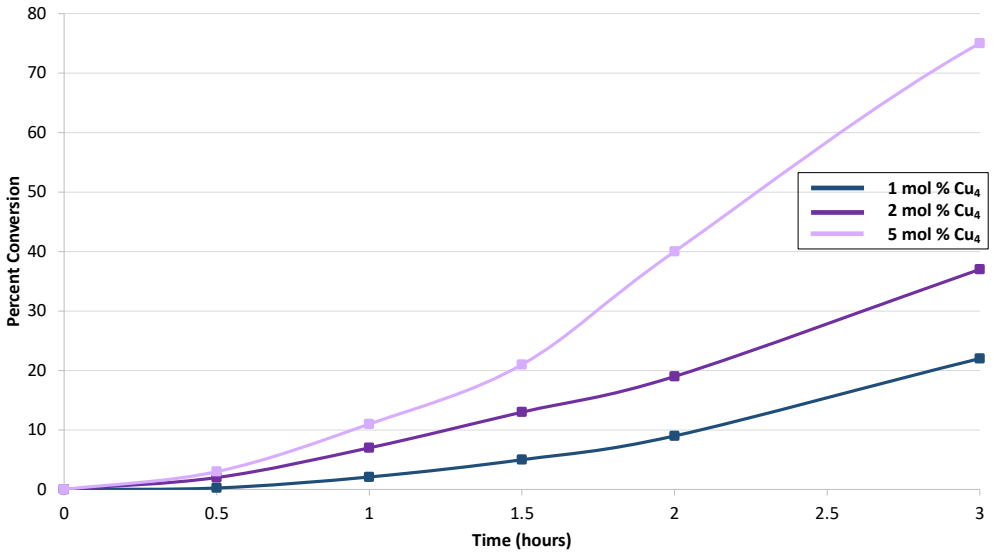

Figure 6.4.2. Percent conversion vs. time for reactions with 0.75 mmol benzyl azide, 0.75 mmol 1-octyne, and 1 – 5 mol percent of {[3,5-(*t*-Bu)$_2$Pz]Cu}$_4$ catalyst.

`

Table 6.4.1: Rate calculations for various equivalents of {[3,5-(*t*-Bu)$_2$Pz]Cu}$_4$ at t = 1 hour where [Benzyl azide] = 0.15 M, [1-octyne] = 0.15 M, and total volume is 5 mL.

Entry	[Cu$_4$] (M)	Percent Conv.	[Triazole] (M) = [Benzyl azide]*((% conv.)/100)	Rate = d[Triazole]/dt
1	0.0015	2.1	0.0032	0.0032
2	0.0030	3.7	0.0071	0.0071
3	0.0075	10	0.0165	0.0165

Calculation of order in [Cu$_4$] 0.0075 mmol – 0.0375 mmol (1 – 5 mol percent).

$$\frac{rate_1}{rate_2} = \frac{[Cu_4]_1^z}{[Cu_4]_2^z} \equiv \frac{0.0032}{0.0071} = \frac{[0.0015]^z}{[0.0030]^z}$$

$$\ln\left(\frac{0.0032}{0.0071}\right) = z \ln\left(\frac{0.0015}{0.0030}\right)$$

$$z = 1.16$$

$$\frac{rate_2}{rate_5} = \frac{[Cu_4]_2^z}{[Cu_4]_5^z} \equiv \frac{0.0071}{0.0165} = \frac{[0.0030]^z}{[0.0075]^z}$$

$$\ln\left(\frac{0.0071}{0.0165}\right) = z \ln\left(\frac{0.0030}{0.0075}\right)$$

$$z = 0.93$$

$$z_{average} = 1.05$$

`

Confirmation by graphing ln(rate) vs. ln([Cu$_4$]) for 1 – 5 mol percent, where slope = z (order with respect to Cu$_4$)

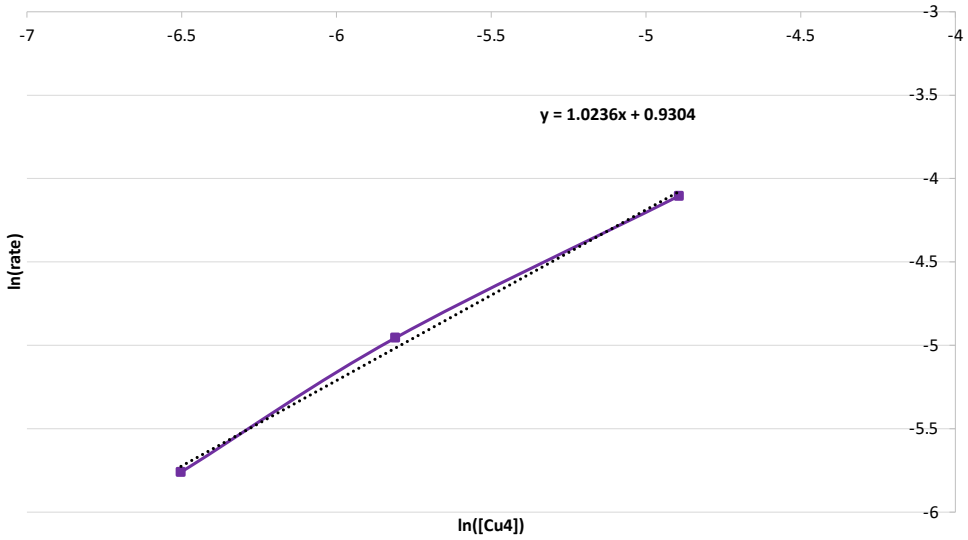

Figure 6.4.3. ln(rate) vs. ln([Cu$_4$]) for reactions with 0.75 mmol benzyl azide, 0.75 mmol 1-octyne, and 1 – 5 mol percent of {[3,5-(*t*-Bu)$_2$Pz]Cu}$_4$ catalyst.

`

Dependence on 1-octyne concentration

Percent conversion vs. time using various amounts (1 – 40 equivalents) of 1-octyne.

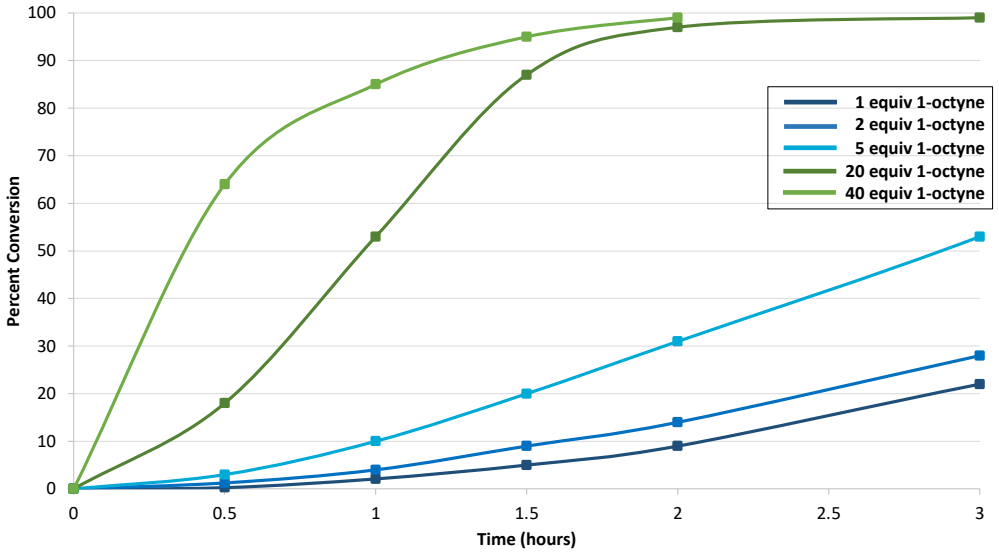

Figure 6.4.4. Percent conversion vs. time for reactions with 0.75 mmol benzyl azide, 0.0075 mmol of {[3,5-(*t*-Bu)$_2$Pz]Cu}$_4$ catalyst, and 0.75 – 30 mmol of 1-octyne.

Table 6.4.2. Rate calculations for various equivalents of 1-octyne at t = 1 hour where [Benzyl azide] = 0.15 M, [Cu$_4$] = 0.0015 M, and total volume is 5 mL.

Entry	[1-octyne] (M)	Percent Conv.	[Triazole] (M) = [Benzyl azide]*((% conv.)/100)	Rate = d[Triazole]/dt
1	0.15	2.1	0.0032	0.0032
2	0.30	3.7	0.0056	0.0056
3	0.75	10	0.015	0.015
4	3.0	53	0.0795	0.0795
5	6.0	85	0.128	0.128

`

Calculation of order in [1-octyne] 0.75 mmol – 3.75 mmol (1 – 5 equivalents).

$$\frac{rate_1}{rate_2} = \frac{[alkyne]_1^y}{[alkyne]_2^y} \equiv \frac{0.0032}{0.0056} = \frac{[0.15]^y}{[0.30]^y}$$

$$\ln\left(\frac{0.0032}{0.0056}\right) = y \ln\left(\frac{0.15}{0.30}\right)$$

$$y = 0.82$$

$$\frac{rate_2}{rate_5} = \frac{[alkyne]_2^y}{[alkyne]_5^y} \equiv \frac{0.0056}{0.015} = \frac{[0.30]^y}{[0.75]^y}$$

$$\ln\left(\frac{0.0056}{0.015}\right) = y \ln\left(\frac{0.30}{0.75}\right)$$

$$y = 1.09$$

$$y_{average} = 0.95$$

Confirmation by graphing ln(rate) vs. ln([alkyne]) for 1 – 5 equivalents, where slope = y (order with respect to alkyne)

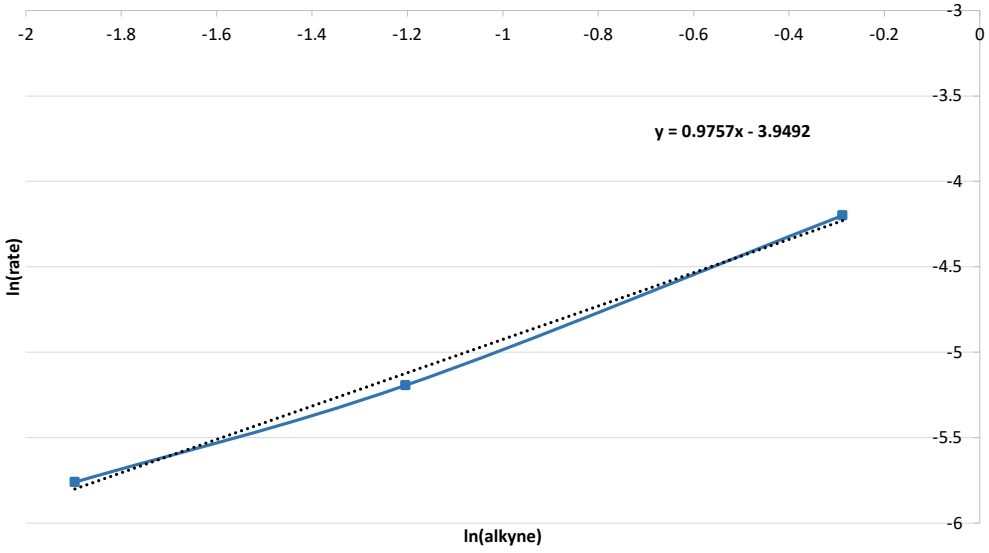

Figure 6.4.5. ln(rate) vs. ln([1-octyne]) for reactions with 0.75 mmol benzyl azide, 0.0075 mmol of {[3,5-(*t*-Bu)$_2$Pz]Cu}$_4$ catalyst, and 0.75 – 3.75 mmol of 1-octyne.

`

Table 6.4.3. Confirmation of 1-octyne order under pseudo first order conditions: [benzylazide] = 6.0 M, [Cu_4] = 0.0015 M, and total volume is 5 mL.

Entry	[1-octyne] (M)	Percent Conv.	[Triazole] (M) = [1-octyne]*((% conv.)/100)	Rate = d[Triazole]/dt
1	0.15	1.5	0.0023	0.0023
2	0.30	1.7	0.0051	0.0051
3	0.75	1.75	0.0131	0.0131

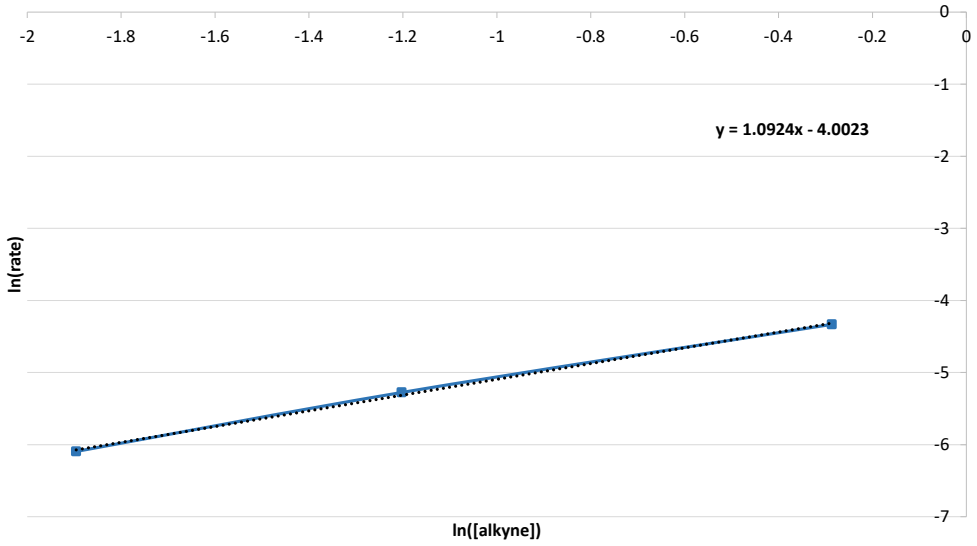

Figure 6.4.6. ln(rate) vs. ln([1-octyne]) for reactions with 30.0 mmol benzyl azide, 0.0075 mmol of {[3,5-(*t*-Bu)$_2$Pz]Cu}$_4$ catalyst, and 0.75 – 3.75 mmol of 1-octyne.

`

Calculation of order in [1-octyne] 15 mmol – 30 mmol (20 – 40 equivalents).

$$\frac{rate_{20}}{rate_{40}} = \frac{[alkyne]_{20}^{y}}{[alkyne]_{40}^{y}} \equiv \frac{0.080}{0.128} = \frac{[3.0]^{y}}{[6.0]^{y}}$$

$$\ln\left(\frac{0.080}{0.128}\right) = y \ln\left(\frac{3.0}{6.0}\right)$$

$$y = 0.68$$

Confirmation by graphing ln(rate) vs. ln([alkyne]) for 20 – 40 equivalents, where slope = y (order with respect to alkyne)

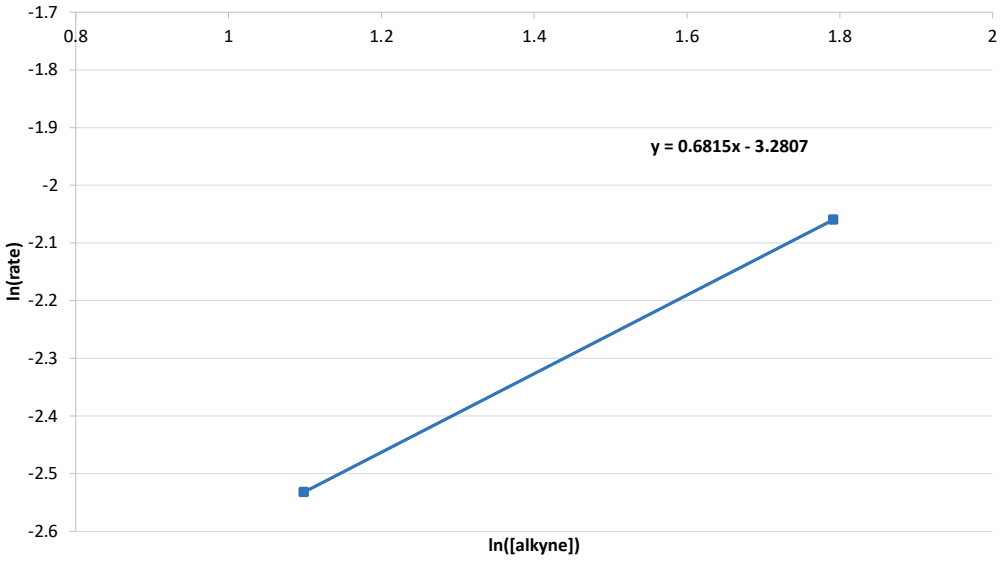

Figure 6.4.7. ln(rate) vs. ln([1-octyne]) for reactions with 0.75 mmol benzyl azide, 0.0075 mmol of {[3,5-(*t*-Bu)$_2$Pz]Cu}$_4$ catalyst, and 15.0 – 30.0 mmol of 1-octyne.

`

Dependence on benzyl azide concentration

Percent conversion vs. time using various amounts (1 – 40 equivalents) of benzyl azide.

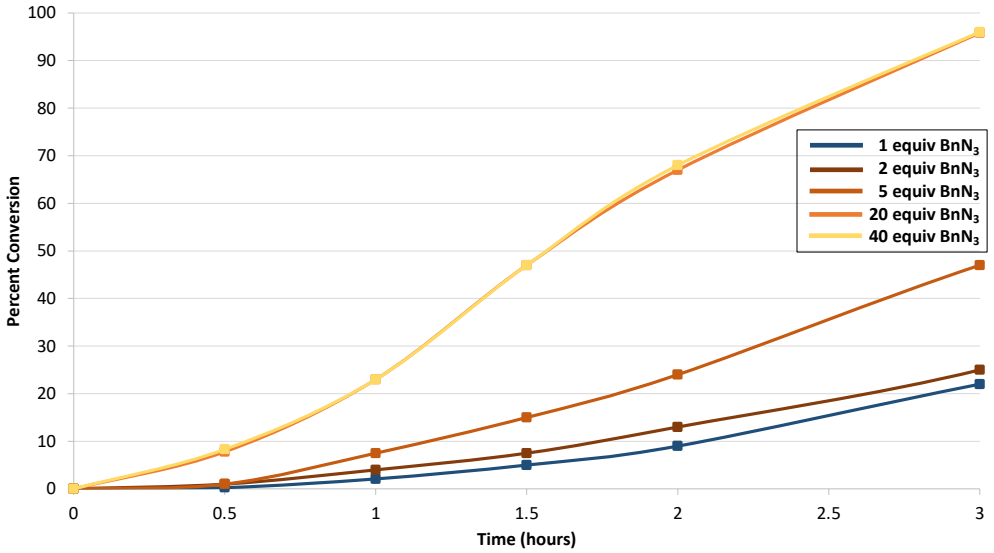

Figure 6.4.8. Percent conversion vs. time for reactions with 0.75 mmol 1-octyne, 0.0075 mmol of {[3,5-(*t*-Bu)$_2$Pz]Cu}$_4$ catalyst, and 0.75 – 30 mmol of benzyl azide.

Table 6.4.4. Rate calculations for various equivalents of benzyl azide at t = 1 hour where [1-octyne] = 0.15 M, [Cu$_4$] = 0.0015 M, and total volume is 5 mL.

Entry	[Benzyl azide] (M)	Percent Conv.	[Triazole] (M) = [1-octyne]*((% conv.)/100)	Rate = d[Triazole]/dt
1	0.15	2.1	0.0032	0.0032
2	0.30	3.7	0.0056	0.0056
3	0.75	7.5	0.0113	0.0113
4	3.0	23	0.0341	0.0341
5	6.0	23	0.0345	0.0345

`

Calculation of order in [Benzylazide] 0.75 mmol – 3.75 mmol (1 – 5 equivalents).

$$\frac{rate_1}{rate_2} = \frac{[azide]_1^x}{[azide]_2^x} \equiv \frac{0.0032}{0.0056} = \frac{[0.15]^x}{[0.30]^x}$$

$$\ln\left(\frac{0.0032}{0.0056}\right) = x \ln\left(\frac{0.15}{0.30}\right)$$

$$x = 0.82$$

$$\frac{rate_2}{rate_5} = \frac{[azide]_2^x}{[azide]_5^x} \equiv \frac{0.0056}{0.0113} = \frac{[0.30]^x}{[0.75]^x}$$

$$\ln\left(\frac{0.0056}{0.0113}\right) = x \ln\left(\frac{0.30}{0.75}\right)$$

$$x = 0.77$$

$$x_{average} = 0.79$$

Confirmation by graphing ln(rate) vs. ln([azide]) for 1 – 5 equivalents, where slope = x (order with respect to azide)

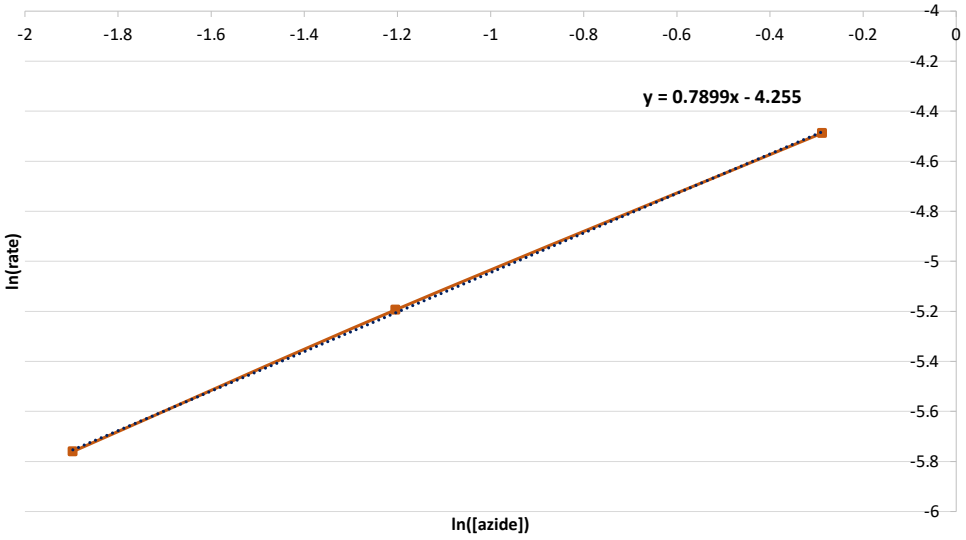

Figure 6.4.9. ln(rate) vs. ln([benzyl azide]) for reactions with 0.75 mmol 1-octyne, 0.0075 mmol of {[3,5-(*t*-Bu)$_2$Pz]Cu}$_4$ catalyst, and 0.75 – 3.75 mmol of benzyl azide.

`

Table 6.4.5. Confirmation of benzyl azide order under pseudo first order conditions: [1-octyne] = 6.0 M, [Cu_4] = 0.0015 M, and total volume is 5 mL.

Entry	[Benzylazide] (M)	Percent Conv.	[Triazole] (M) = [benzylazide]*((% conv.)/100)	Rate = d[Triazole]/dt
1	0.15	4.5	0.0034	0.0032
2	0.30	4	0.0060	0.0056
3	0.75	3	0.0113	0.0113

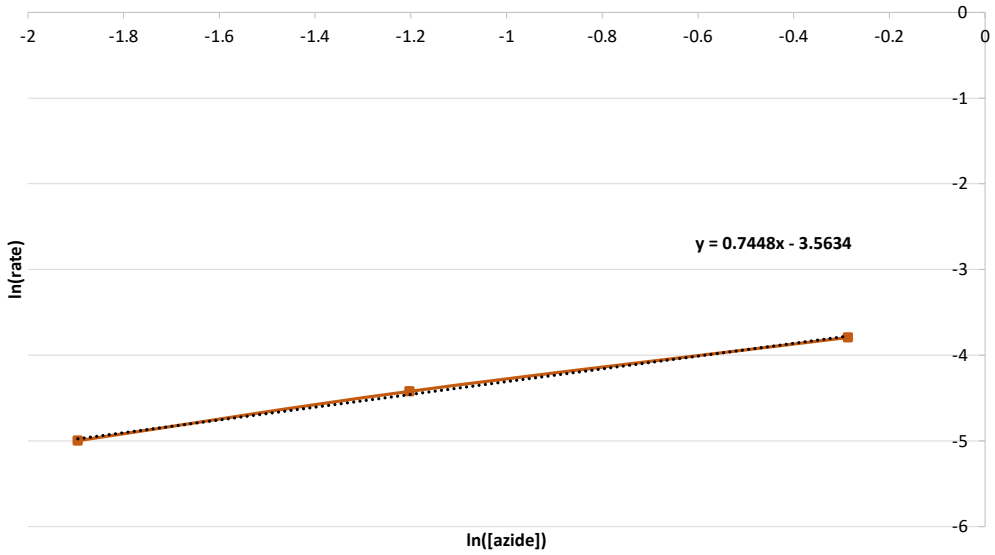

Figure 6.4.10. ln(rate) vs. ln([benzyl azide]) for reactions with 30.0 mmol 1-octyne, 0.0075 mmol of {[3,5-(*t*-Bu)$_2$Pz]Cu}$_4$ catalyst, and 0.75 – 3.75 mmol of benzyl azide.

`

Calculation of order in [Benzylazide] 15 mmol – 30 mmol (20 – 40 equivalents).

$$\frac{rate_{20}}{rate_{40}} = \frac{[azide]_{20}^{x}}{[azide]_{40}^{x}} \equiv \frac{0.0341}{0.0345} = \frac{[3.0]^{x}}{[6.0]^{x}}$$

$$\ln\left(\frac{0.0341}{0.0345}\right) = x \ln\left(\frac{3.0}{6.0}\right)$$

$$x = 0.02$$

Confirmation by graphing ln(rate) vs. ln([azide]) for 20 – 40 equivalents, where slope = x (order with respect to azide)

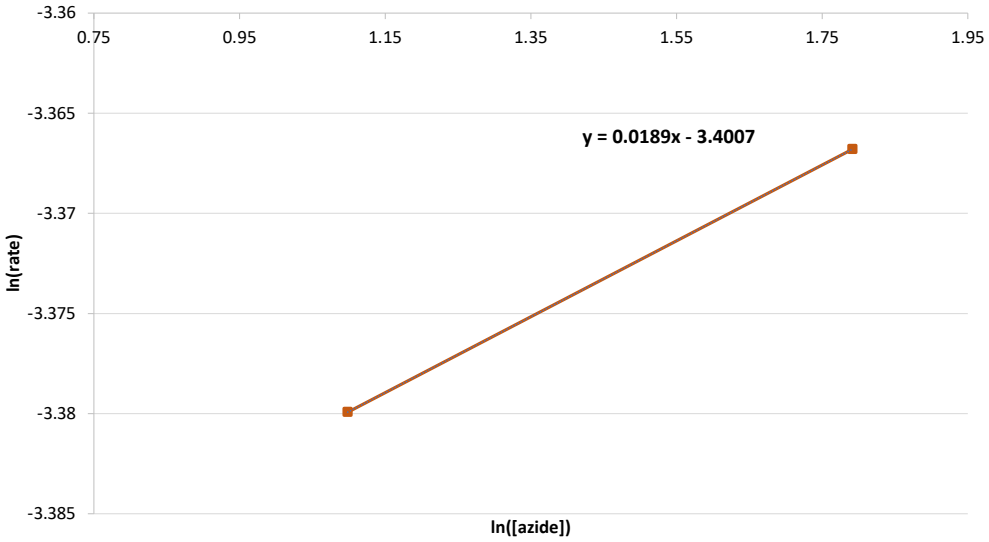

Figure 6.4.11. ln(rate) vs. ln([benzyl azide]) for reactions with 0.75 mmol 1-octyne, 0.0075 mmol of {[3,5-(*t*-Bu)$_2$Pz]Cu}$_4$ catalyst, and 15.0 – 30.0 mmol of benzyl azide.

`

Dependence on {[3-(CF_3)-5-(*t*-Bu)Pz]Cu}$_4$ concentration

Table 6.4.6. Rate calculations for various equivalents of {[3-(CF_3)-5-(*t*-Bu)Pz]Cu}$_4$ at t = 1 hour where [Benzyl azide] = 0.15 M, [1-octyne] = 0.15 M, and total volume is 5 mL.

Entry	[Cu_4] (M)	Percent Conv.	[Triazole] (M) = [Benzyl azide]*((% conv.)/100)	Rate = d[Triazole]/dt
1	0.0015	17	0.023	0.023
2	0.0030	32	0.048	0.048
3	0.0075	69	0.104	0.104

Calculation of order in [Cu_4] 0.0075 mmol – 0.0375 mmol (1 – 5 mol percent).

$$\frac{rate_1}{rate_2} = \frac{[Cu_4]_1^z}{[Cu_4]_2^z} \equiv \frac{0.023}{0.048} = \frac{[0.0015]^z}{[0.0030]^z}$$

$$\ln\left(\frac{0.023}{0.048}\right) = z \ln\left(\frac{0.0015}{0.0030}\right)$$

$$z = 0.91$$

$$\frac{rate_2}{rate_5} = \frac{[Cu_4]_2^z}{[Cu_4]_5^z} \equiv \frac{0.048}{0.104} = \frac{[0.0030]^z}{[0.0075]^z}$$

$$\ln\left(\frac{0.048}{0.104}\right) = z \ln\left(\frac{0.0030}{0.0075}\right)$$

$$z = 0.84$$

$$z_{average} = 0.88$$

`

Confirmation by graphing ln(rate) vs. ln([Cu_4]) for 1 – 5 mol percent, where slope = z (order with respect to Cu_4)

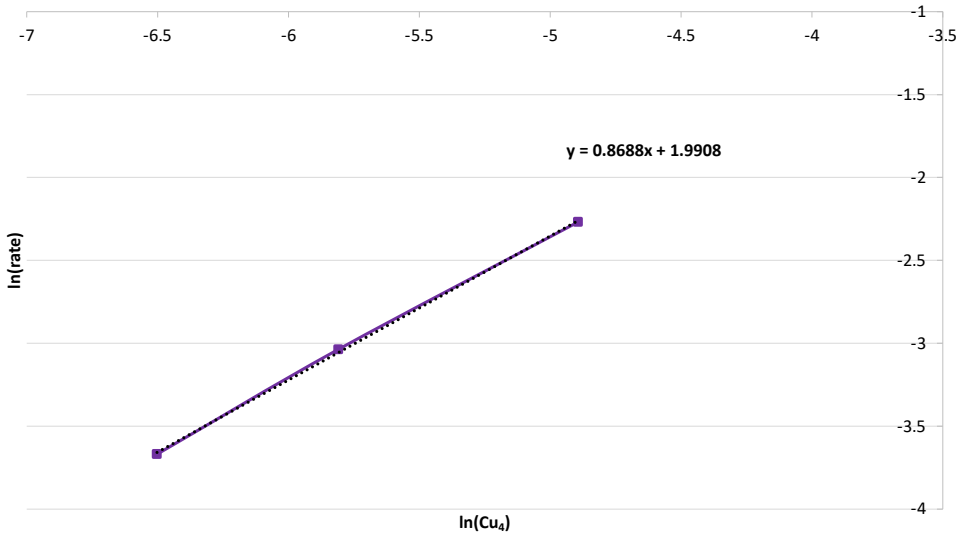

Figure 6.4.12. ln(rate) vs. ln([Cu_4]) for reactions with 0.75 mmol 1-octyne, 0.75 mmol of benzyl azide, and 1 – 5 mol percent of {[3-(CF_3)-5-(*t*-Bu)Pz]Cu}$_4$ catalyst.

`

Dependence on {[3,5-$(CF_3)_2$Pz]Cu}$_3$ concentration

Table 6.4.7. Rate calculations for various equivalents of {[3,5-$(CF_3)_2$Pz]Cu}$_3$ at t = 1 hour where [Benzyl azide] = 0.15 M, [1-octyne] = 0.15 M, and total volume is 5 mL.

Entry	[Cu_3] (M)	Percent Conv.	[Triazole] (M) = [Benzyl azide]*((% conv.)/100)	Rate = d[Triazole]/dt
1	0.0015	1	0.0045	0.0045
2	0.0030	4	0.0165	0.0165
3	0.0075	13	0.0630	0.0630

Calculation of order in [Cu_4] 0.0075 mmol – 0.0375 mmol (1 – 5 mol percent).

$$\frac{rate_1}{rate_2} = \frac{[Cu_4]_1^z}{[Cu_4]_2^z} \equiv \frac{0.0045}{0.0165} = \frac{[0.0015]^z}{[0.0030]^z}$$

$$\ln\left(\frac{0.0045}{0.0165}\right) = z \ln\left(\frac{0.0015}{0.0030}\right)$$

$$z = 1.87$$

$$\frac{rate_2}{rate_5} = \frac{[Cu_4]_2^z}{[Cu_4]_5^z} \equiv \frac{0.0165}{0.0630} = \frac{[0.0030]^z}{[0.0075]^z}$$

$$\ln\left(\frac{0.0165}{0.0630}\right) = z \ln\left(\frac{0.0030}{0.0075}\right)$$

$$z = 1.46$$

$$z_{average} = 1.67$$

`

Confirmation by graphing ln(rate) vs. ln([Cu_3]) for 1 – 5 mol percent, where slope = z (order with respect to Cu_3)

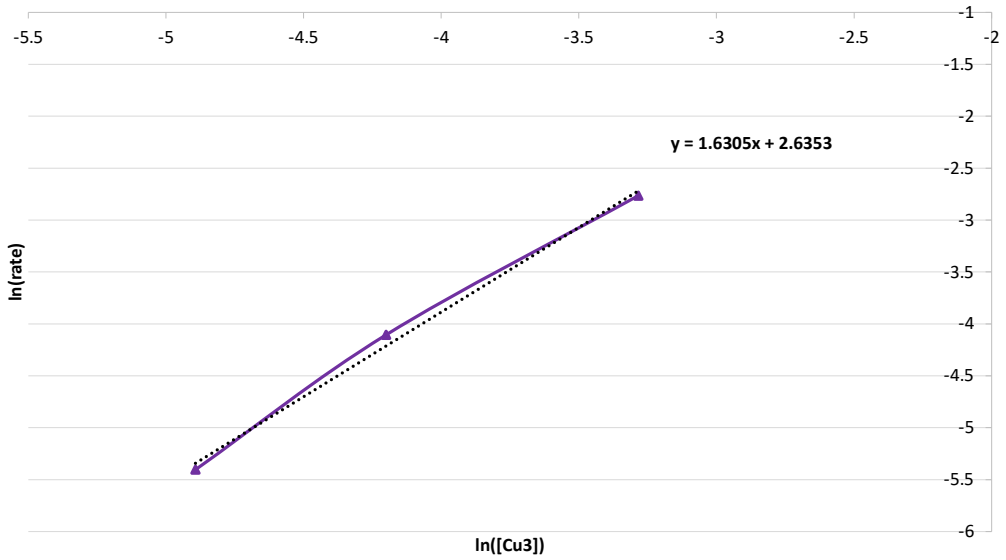

Figure 6.4.13. ln(rate) vs. ln([Cu_3]) for reactions with 0.75 mmol 1-octyne, 0.75 mmol of benzyl azide, and 1 – 5 mol percent of {[3,5-$(CF_3)_2$Pz]Cu}$_3$ catalyst.

`

6.5 Experimental for Chapter 5.1

Computational Details. All calculations were run using the Gaussian software program.[198] Calculations for $\{Cu[3,5\text{-}(CF_3)_2Pz](\mu\text{-}dppm)\}_2$ were performed for the S_0 ground state and the T_1 lowest energy excited states. Calculations of the copper complexes were optimized using the density functional, B3PW91.[199-203] Optimizations were carried out for both states using no predetermined restrictions on geometry to obtain a global minimum. Triplet state computations were performed as spin-unrestricted calculations. Absorptions and emissions were computed by modeling vertical transitions based on the Franck-Condon principle.[204] The LANL2DZ basis set[205] was used in all of the calculations with augmentation of *p*-type functions[206] for copper and a *d*-type polarization function[207] ($\xi_d = 0.55$) for phosphorus.

General Synthetic Procedures. Reactions were carried out using standard Schlenk techniques under an argon or nitrogen atmosphere. Solvents were purchased from commercial sources and dried by distilling over standard drying agents. Glassware was oven-dried at 150 °C overnight. NMR spectra were recorded at 25 ºC on a JEOL Eclipse 500 spectrometer (^{1}H, 500.16 MHz, ^{13}C, 125.78 MHz, ^{19}F, 470.62 MHz, ^{31}P, 202.46 MHz) or on a JEOL 300 Eclipse spectrometer (^{1}H, 300.53 MHz, ^{13}C, 75.57 MHz, ^{19}F, 282.78 MHz, ^{31}P, 121.66 MHz). Proton and carbon chemical shifts are reported in parts per million versus Me_4Si. ^{19}F and ^{31}P chemical shifts are referenced relative to external $CFCl_3$ and 85% H_3PO_4 respectively. $\{\mu\text{-}[3,5\text{-}(CF_3)_2Pz]Cu\}_3$ was synthesized using reported procedure by Dias *et al.*[12]

`

Materials and Syntheses.

Preparation of {Cu[3,5-$(CF_3)_2$Pz](μ-dppm)}$_2$:

{ μ-[3,5-$(CF_3)_2$Pz]Cu}$_3$ (0.50 g, 0.63 mmol) and $(PPh_2)_2CH_2$ (0.73 g, 1.90 mmol) were mixed in toluene/THF (1:1 V/V, 50 mL) at room temperature under nitrogen. The mixture was stirred for 5 hours at 40 °C. The clear solution was allowed to cool to room temperature. The solvent was removed under reduced pressure to obtain a white solid. X-ray quality crystals of {Cu(μ-[3,5-$(CF_3)_2$Pz])(μ-dppm)}$_2$ were obtained from dichloromethane at -4°C. Yield: 93%. Mp. 217-220 °C; ^{1}H NMR ($CDCl_3$): δ 3.86 (br s, C*H*$_2$, 4H), 6.63 (s, Pz-*H*, 2H), 7.06-7.20 (m, Ph-*H*, 40H); ^{19}F NMR ($CDCl_3$): δ –59.5 (s, C*F*$_3$); ^{31}P{^{1}H} NMR ($CDCl_3$): δ –9.6 (s); ^{13}C{^{1}H} NMR ($CDCl_3$): δ 141.9 (q, $^2J_{CF}$ = 36 Hz, *C*CF$_3$), 132.9 (s, Ph), 129.9 (s, Ph), 128.6 (s, Ph), 122.5 (q, $^1J_{CF}$ = 268 Hz, *C*F$_3$), 102.1 (s, *C*H), 27.4 (br s, *C*H$_2$), *Ci* (Ph) could not be assigned unambiguously. IR (KBr; cm^{-1}): 3056, 2894, 1960, 1891, 1587, 1485, 1436, 1341, 1256, 1209, 1116, 1000, 974, 846, 779, 738, 720, 694, 509, 472; Anal. Calc. for $C_{60}H_{46}Cu_2F_{12}N_4P_4$: C, 55.35; H, 3.56; N, 4.30; found: C, 55.29; H, 3.61; N, 4.35.

{Cu[3,5-$(CF_3)_2$Pz](μ-dppm)}$_2$•3THF:

The {Cu(μ-[3,5-$(CF_3)_2$Pz])(μ-dppm)}$_2$ was synthesized as noted above. Crystals of the THF solvate were obtained by slow cooling of a dilute solution of {Cu[3,5-$(CF_3)_2$Pz](μ-dppm)}$_2$ in THF. Mp: 228-231°C ; ^{1}H NMR ($CDCl_3$): δ 1.86 (m, THF, C*H*$_2$), 3.75 (m, THF, CH$_2$), 3.86 (br s, C*H*$_2$, 4H), 6.63 (s, Pz-*H*, 2H), 7.06-7.20 (m, Ph-*H*, 40H); ^{13}C{^{1}H} NMR ($CDCl_3$): δ 141.9 (q, $^2J_{CF}$ = 36 Hz, *C*CF$_3$), 132.8 (s, Ph), 129.8 (s, Ph), 128.4 (s, Ph), 122.5 (q, $^1J_{CF}$ = 268

`

Hz, *C*F_3), 101.9 (s, *C*H), 68.0 (CH_2O), 27.4 (br s, *C*H_2), 25.6 (CH_2), *Ci* (Ph) could not be assigned unambiguously. $^{31}P\{^1H\}$ NMR ($CDCl_3$, 85% H_3PO_4) δ -10.0; IR (KBr): cm^{-1} 3056, 2894, 1960, 1516, 1436, 1340, 1257, 1208, 1116, 1000, 974, 780, 739, 649, 517, 482; Anal. Calc. (Found) C, 55.86%, (55.29); H, 4.10%, (3.57); P, 9.00%, (11.12); N, 4.07%, (4.24); F, 16.57% (16.74).

X-ray Crystallography. X-ray intensity data for **1** and **1**•3THF were measured at 100(2) K on a SMART APEX II CCD area detector system equipped with a low temperature device and Mo-target X-ray tube (wavelength = 0.71073 Å) at 100(2) K. Data collection and processing and absorption correction were carried out using APEX2 software provided by BrukerAXS. Structure solution and refinement were performed by using SHELXTL software.[72] All non-hydrogen atoms were refined anisotropically. The hydrogen atoms were placed in idealized positions and were refined as riding atoms. The CCDC 1937324 contains the supplementary crystallographic data for {Cu[3,5-$(CF_3)_2$Pz](μ-dppm)}$_2$. These data can be obtained free of charge *via* http://www.ccdc.cam.ac.uk/conts/retrieving.html or from the Cambridge Crystallographic Data Centre (CCDC), 12 Union Road, Cambridge, CB2 1EZ, UK).

The {Cu[3,5-$(CF_3)_2$Pz](μ-dppm)}$_2$•3THF crystallizes in the P-1 space group with three molecules of THF in the crystal lattice. Unfortunately, it shows significant disorder in THF molecules, and at number of arene carbon and CF_3 fluorine atoms, that is challenging to model. Key core-atoms of the molecule, $NCu(PCP)_2CuN$, including copper sites however behave well. Due to this disorder, detailed analysis of metrical parameters of {Cu[3,5-$(CF_3)_2$Pz](μ-

`

dppm)}$_2$•3THF are not presented, and the data are utilized only to compare the changes to Cu—Cu distances. Crystal Data for {Cu[3,5-$(CF_3)_2$Pz](μ-dppm)}$_2$•3THF, $C_{72}H_{70}Cu_2F_{12}N_4O_3P_4$ (M =1518.28 g/mol), space group P-1 (no. 2), a = 12.773(3) Å, b = 15.071(3) Å, c = 18.746(4) Å, α = 77.181(3)°, β = 81.076(3)°, γ = 80.453(3)°, V = 3443.6(12) Å^3, Z = 2, T = 100(2) K, μ(MoKα) = 0.794 mm^{-1}, *Dcalc* = 1.464 g/cm^3, The final R_1 was 0.0921 (>2σ(I)) and wR_2 was 0.2842 (all data).

Photophysical Measurements. Luminescent measurements were carried out on purified recrystallized materials. Steady-state luminescence was recorded on a PTI QuantaMaster Model QM-4 scanning spectrofluorometer. The excitation and emission spectra are corrected for wavelength-dependent lamp intensity and detector response. Lifetimes are recorded using a PTI xenon flash and phosphorescent detector. Absorption spectra were collected using a Perkin-Elmer lambda 900 double-beam UV/VIS/NIR spectrophotometer with solutions of crystalline materials prepared using HPLC grade dichloromethane using a standard 1-cm quartz cell. ^{1}H and ^{13}C{^{1}H} NMR spectra were recorded in $CDCl_3$ at ambient temperature on a Varian spectrometer operating at 500 MHz for proton spectra. IR was recorded on a Thermo Scientific Nicolet 6700 Analytical FTIR Spectrometer.

`

`

Appendix A

Spectroscopic data of chapter 2

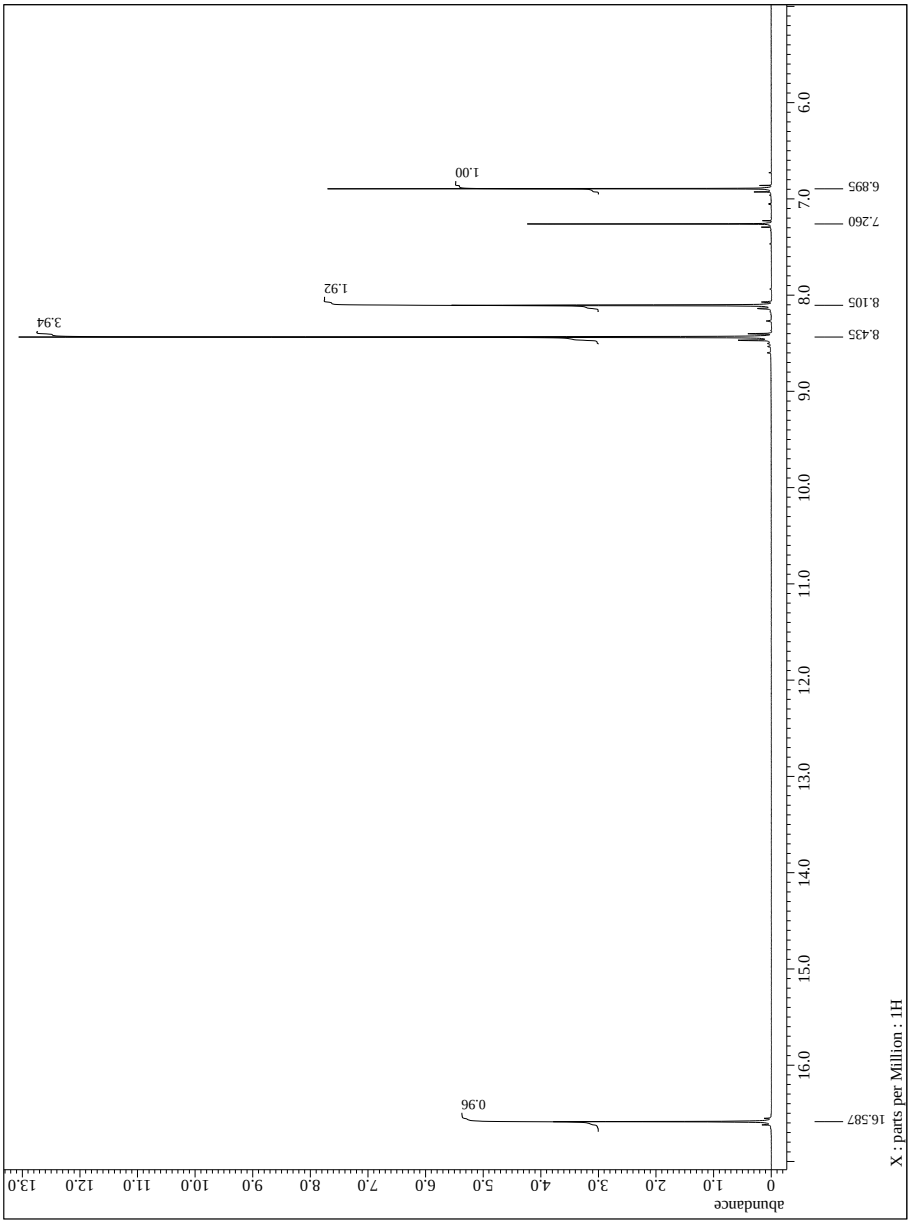

Figure A1: ^{1}H NMR of 1,3-bis(3,5-bis(trifluoromethyl)phenyl)-3-hydroxyprop-2-en-1-one.

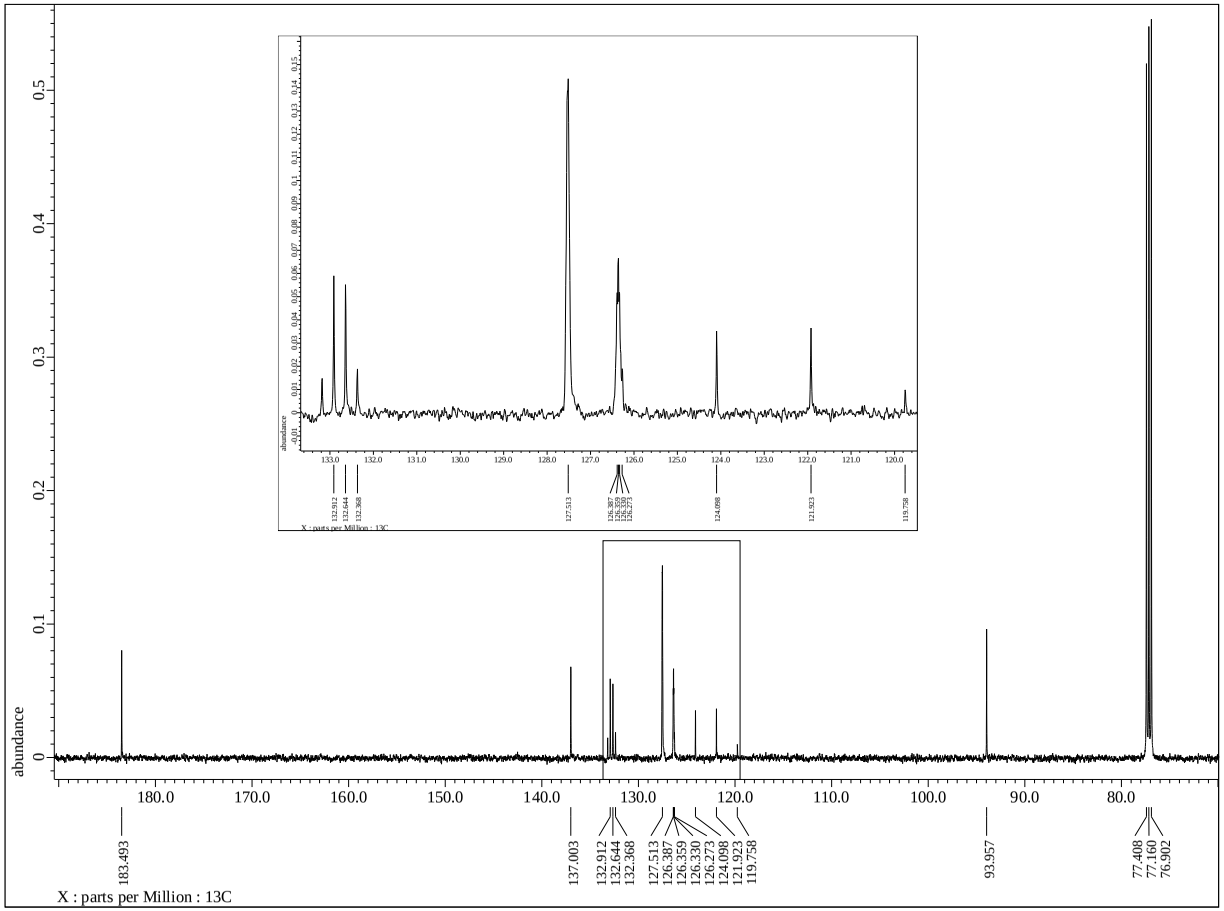

Figure A2: $^{13}C\{^{1}H\}$ NMR of 1,3-bis(3,5-bis(trifluoromethyl)phenyl)-3-hydroxyprop-2-en-1-one.

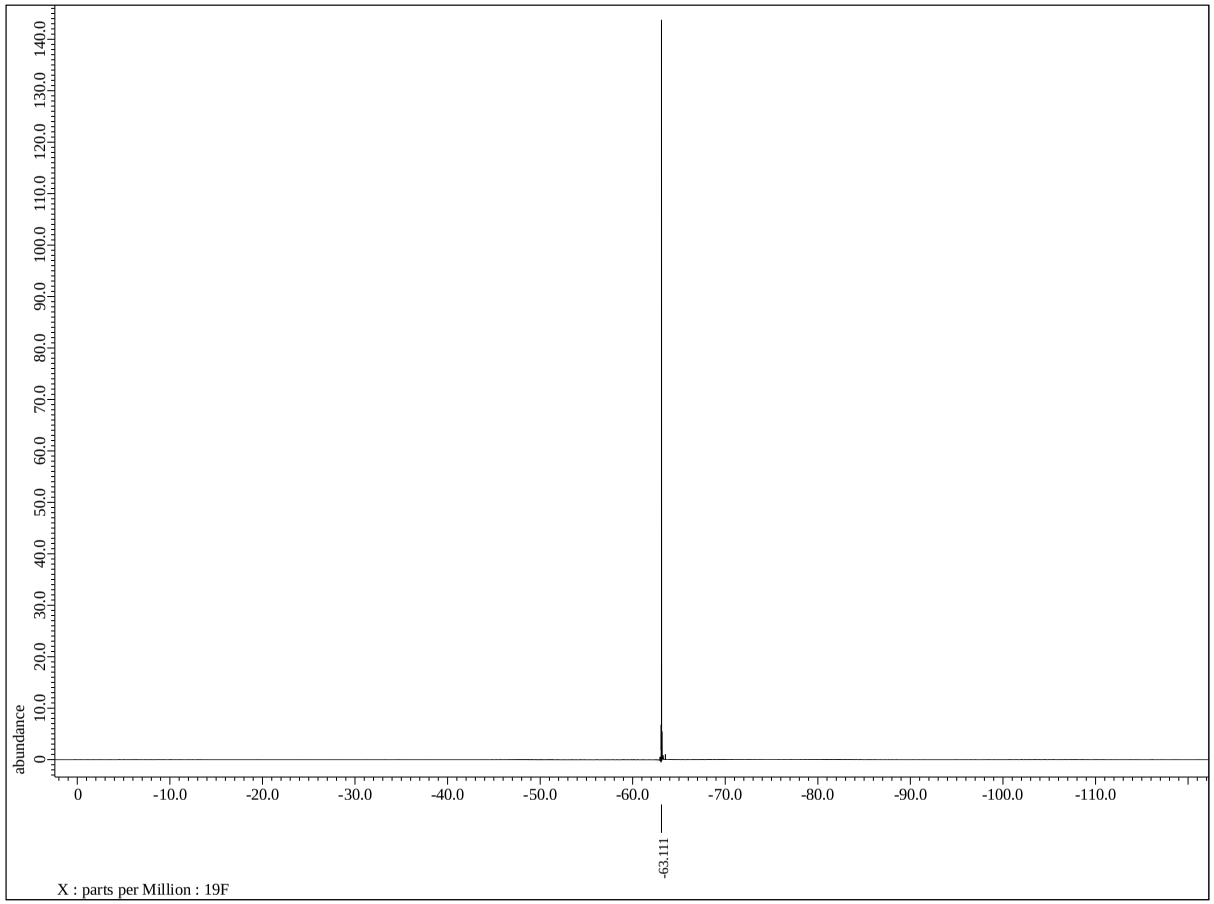

Figure A3: ^{19}F NMR of 1,3-bis(3,5-bis(trifluoromethyl)phenyl)-3-hydroxyprop-2-en-1-one.

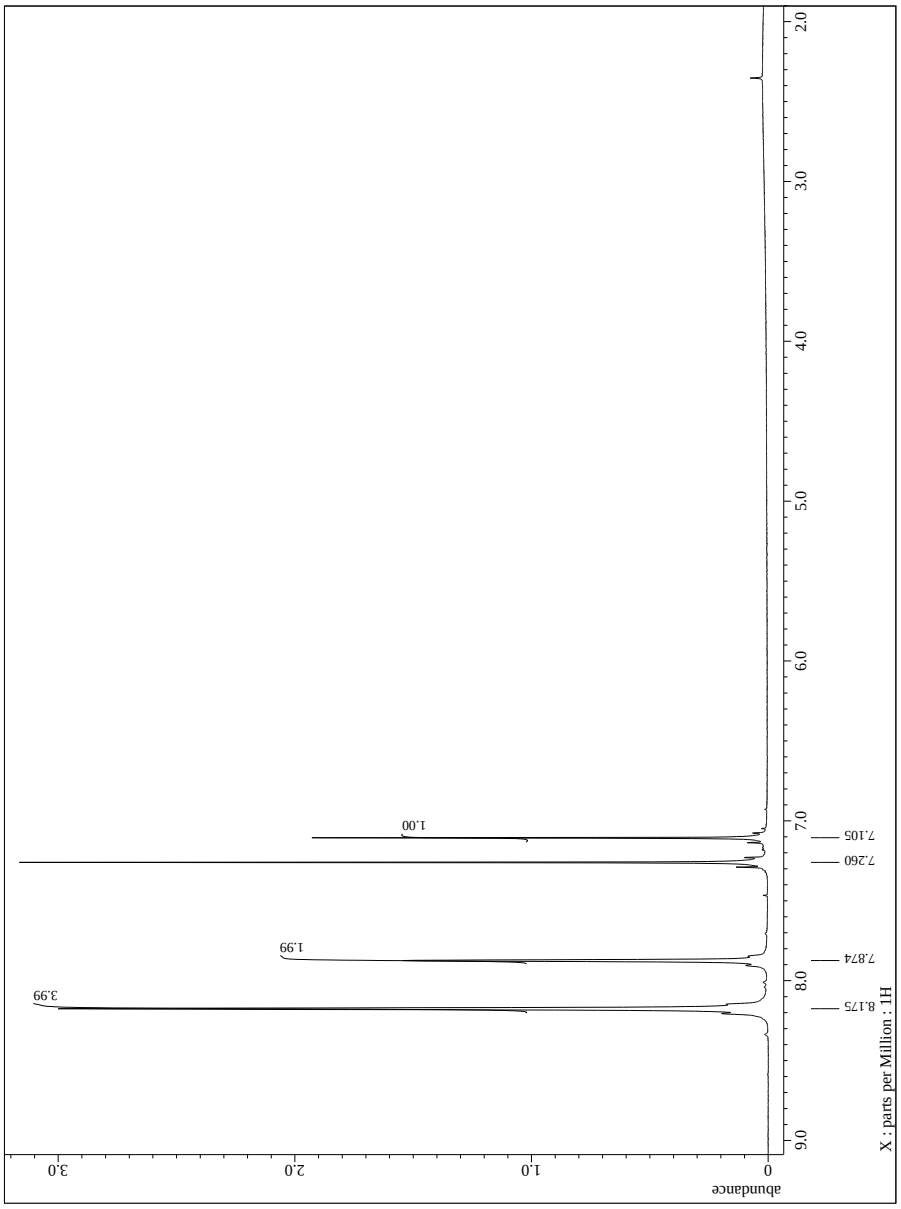

Figure A4: ^{1}H NMR of 3,5-(3,5-$(CF_3)_2$Ph)$_2$PzH.

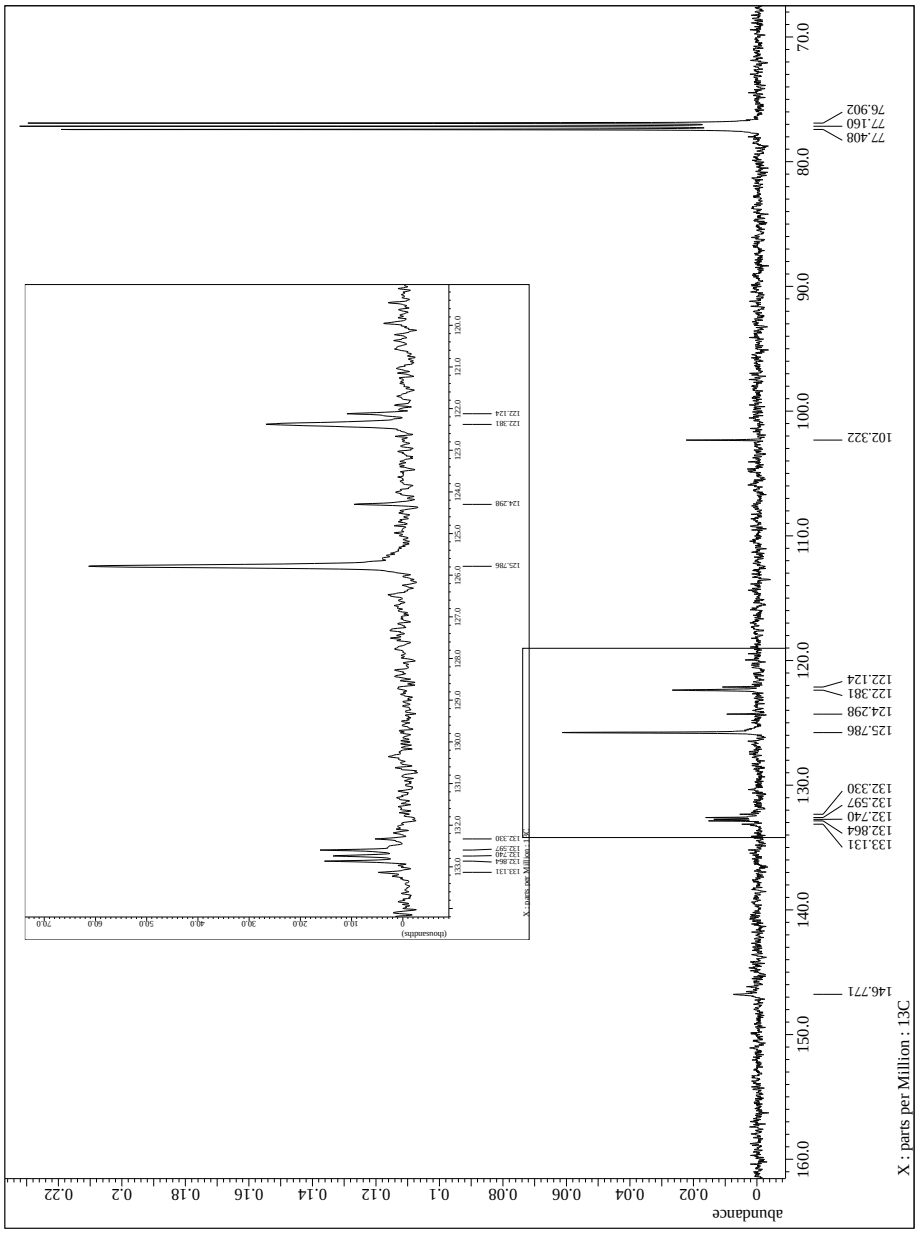

Figure A5: $^{13}C\{^{1}H\}$ NMR of 3,5-$(CF_3)_2$Ph)$_2$PzH.

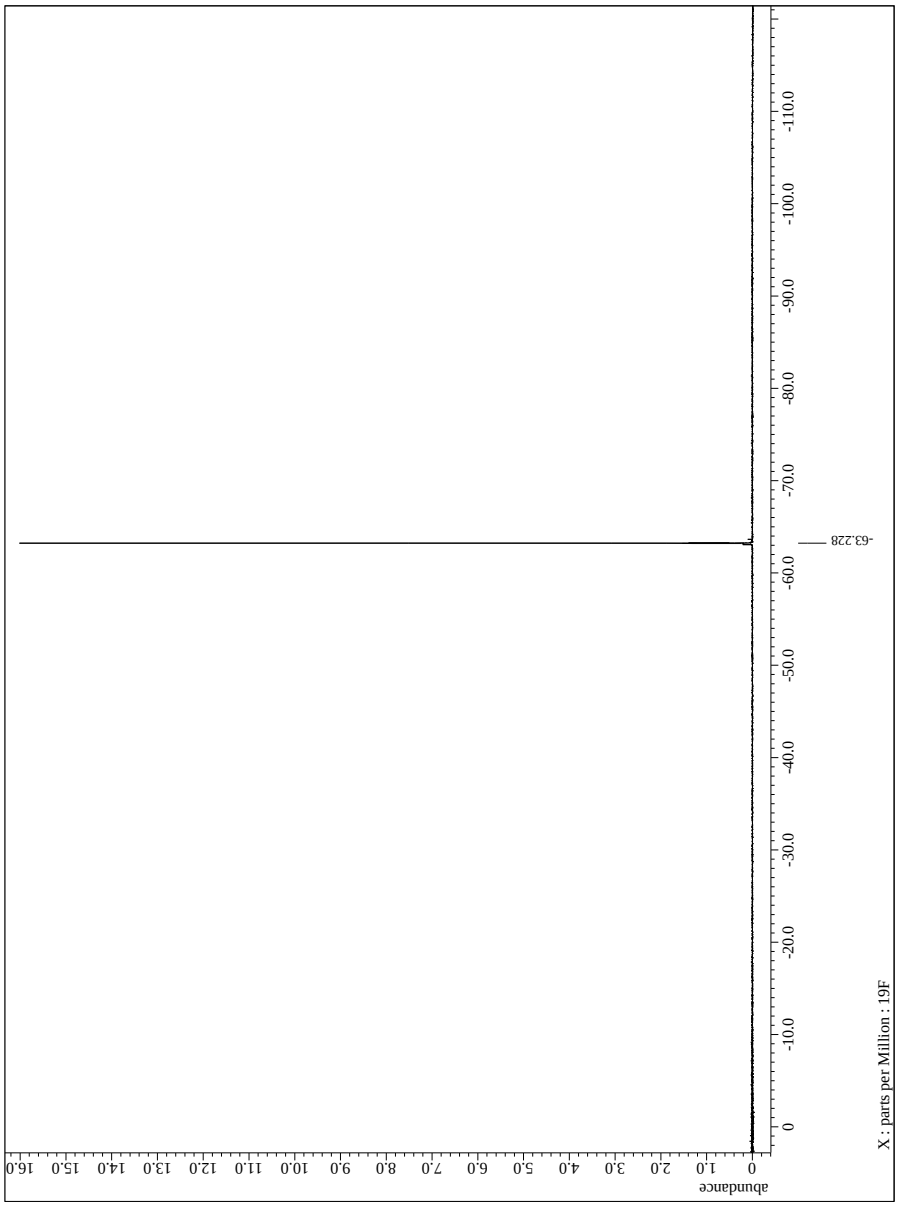

Figure A6: ^{19}F NMR of 3,5-(3,5-$(CF_3)_2Ph)_2PzH$.

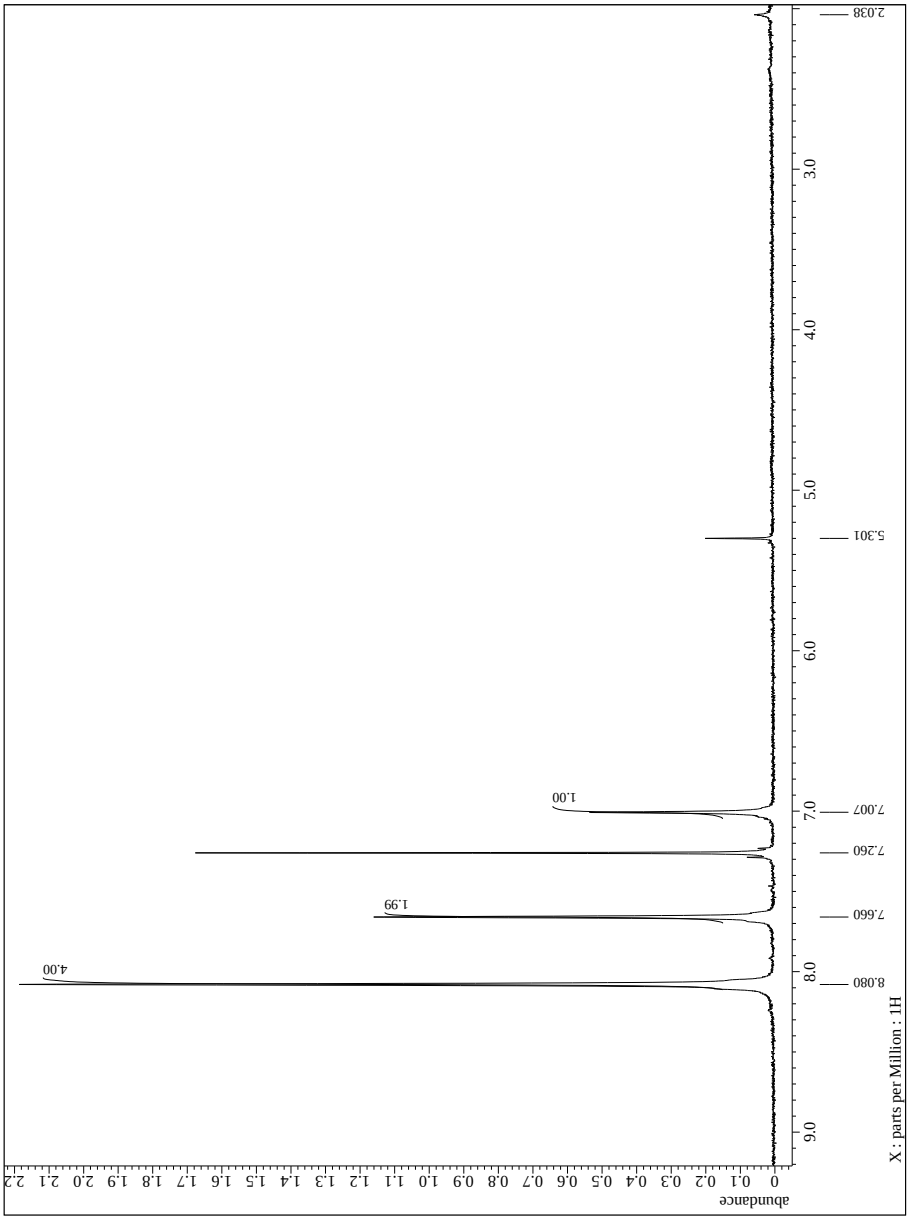

Figure A7: ^{1}H NMR of {[3,5-(3,5-(CF$_3$)$_2$Ph)$_2$Pz]Cu}$_3$.

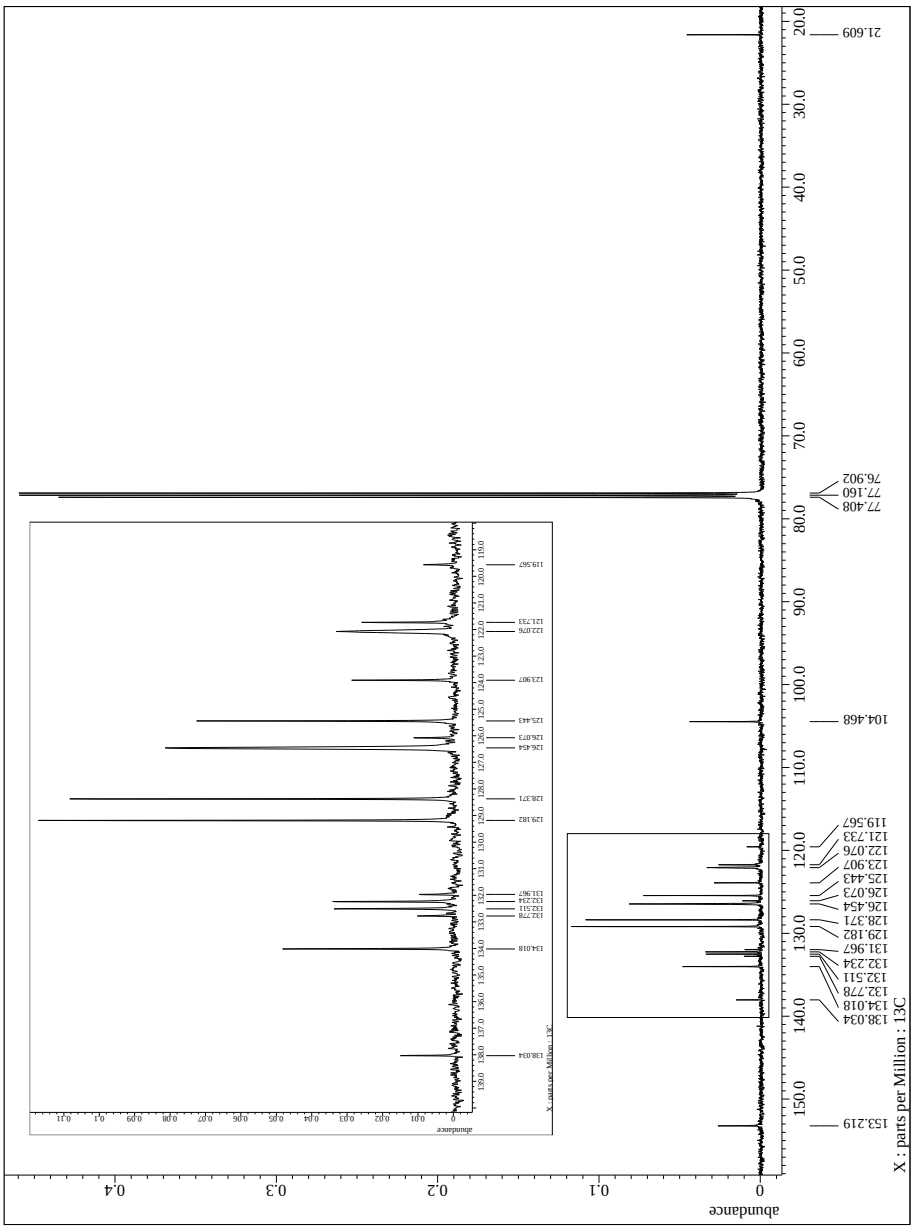

Figure A8: $^{13}C\{^{1}H\}$ NMR of $\{[3,5\text{-}(3,5\text{-}(CF_3)_2Ph)_2Pz]Cu\}_3$.

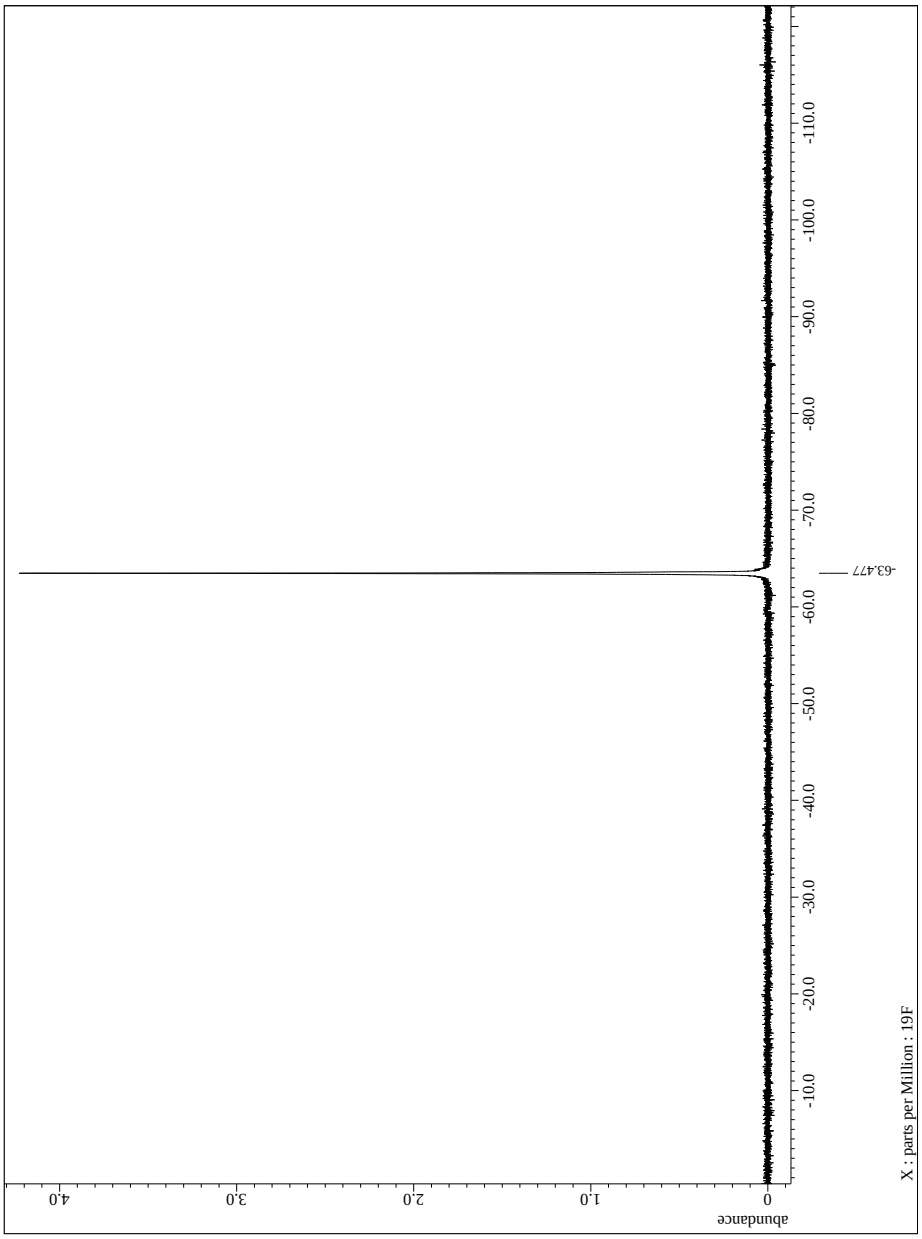

Figure A9: ^{19}F NMR of {[3,5-(CF$_3$)$_2$Ph)$_2$Pz]Cu}$_3$.

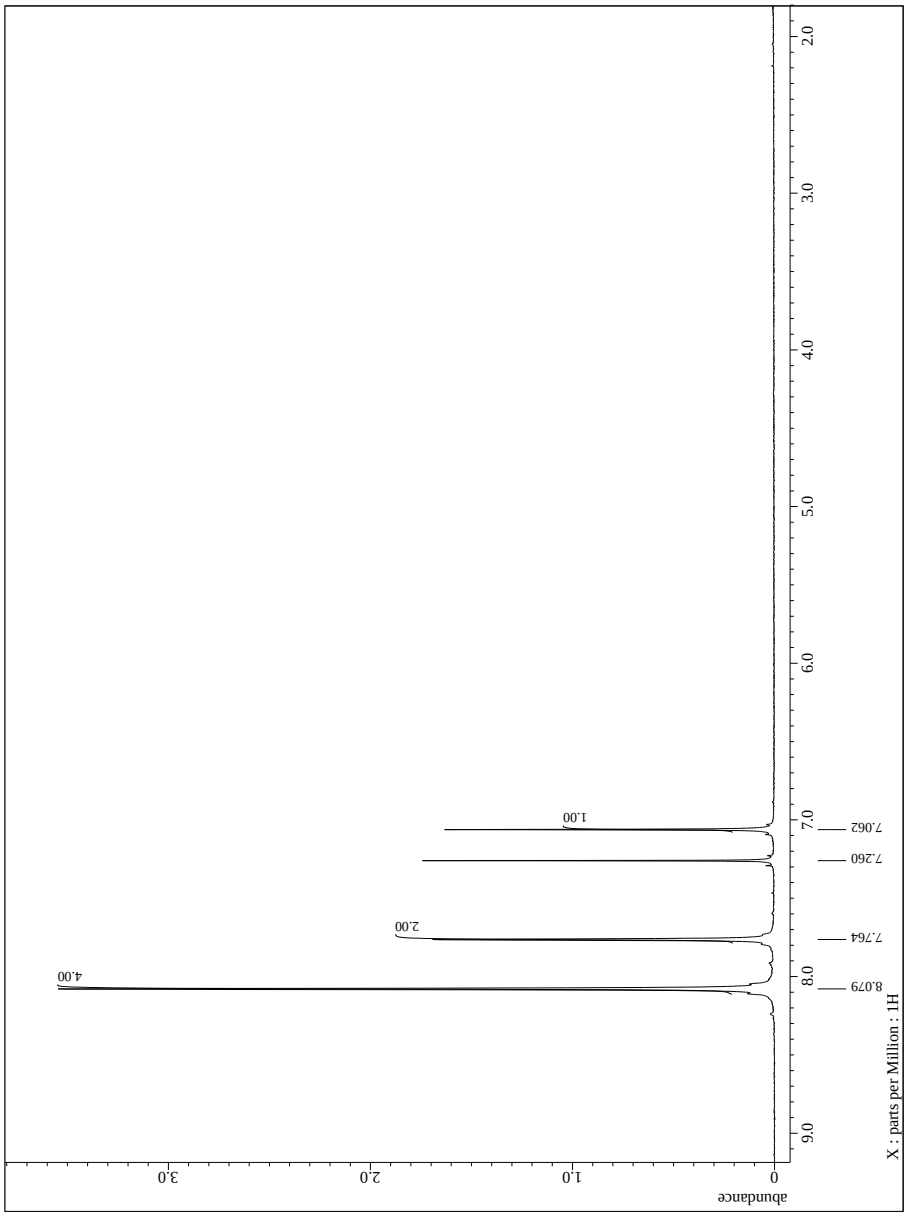

Figure A10: ^{1}H NMR of {[3,5-(3,5-$(CF_3)_2$Ph)$_2$Pz]Ag}$_3$.

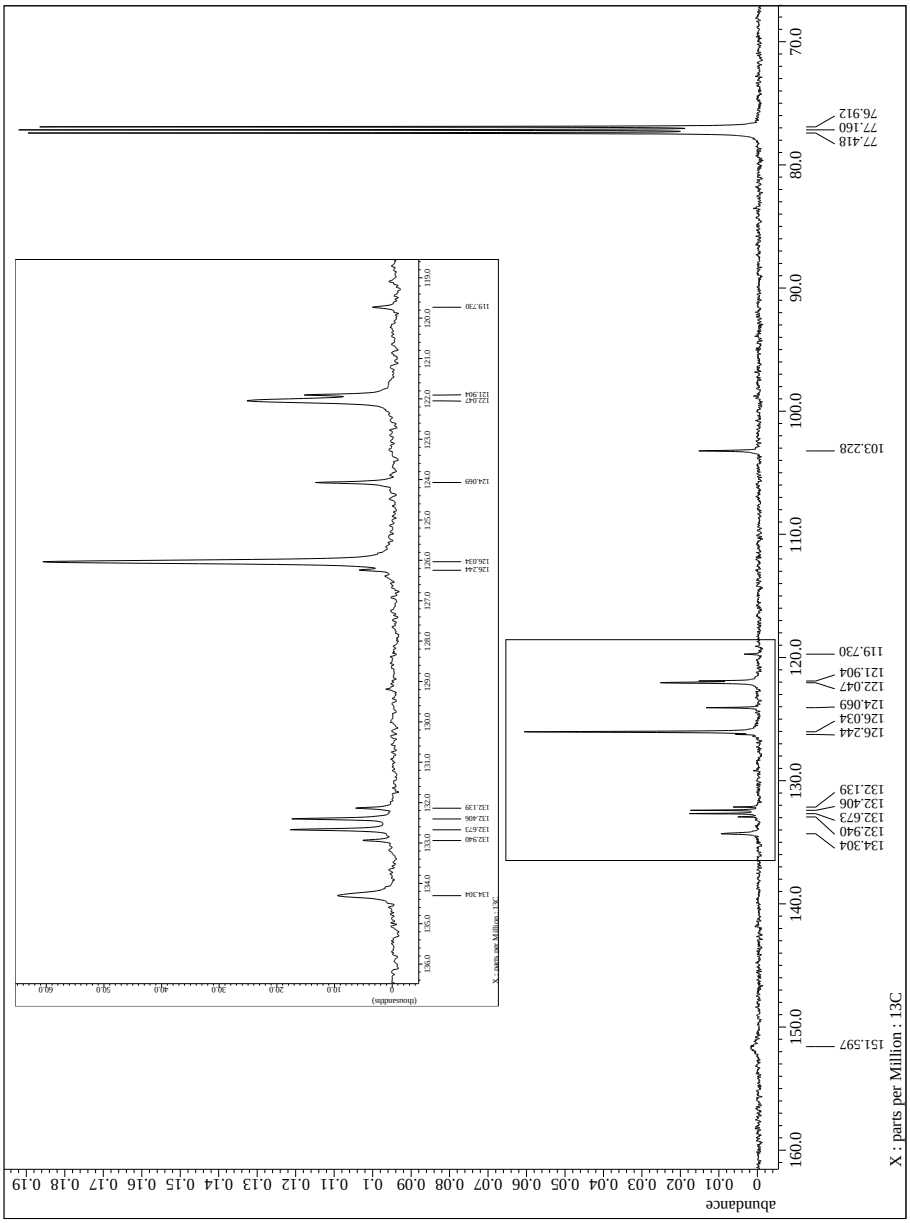

Figure A11: $^{13}C\{^{1}H\}$ NMR of $\{[3,5\text{-}(CF_3)_2Ph)_2Pz]Ag\}_3$.

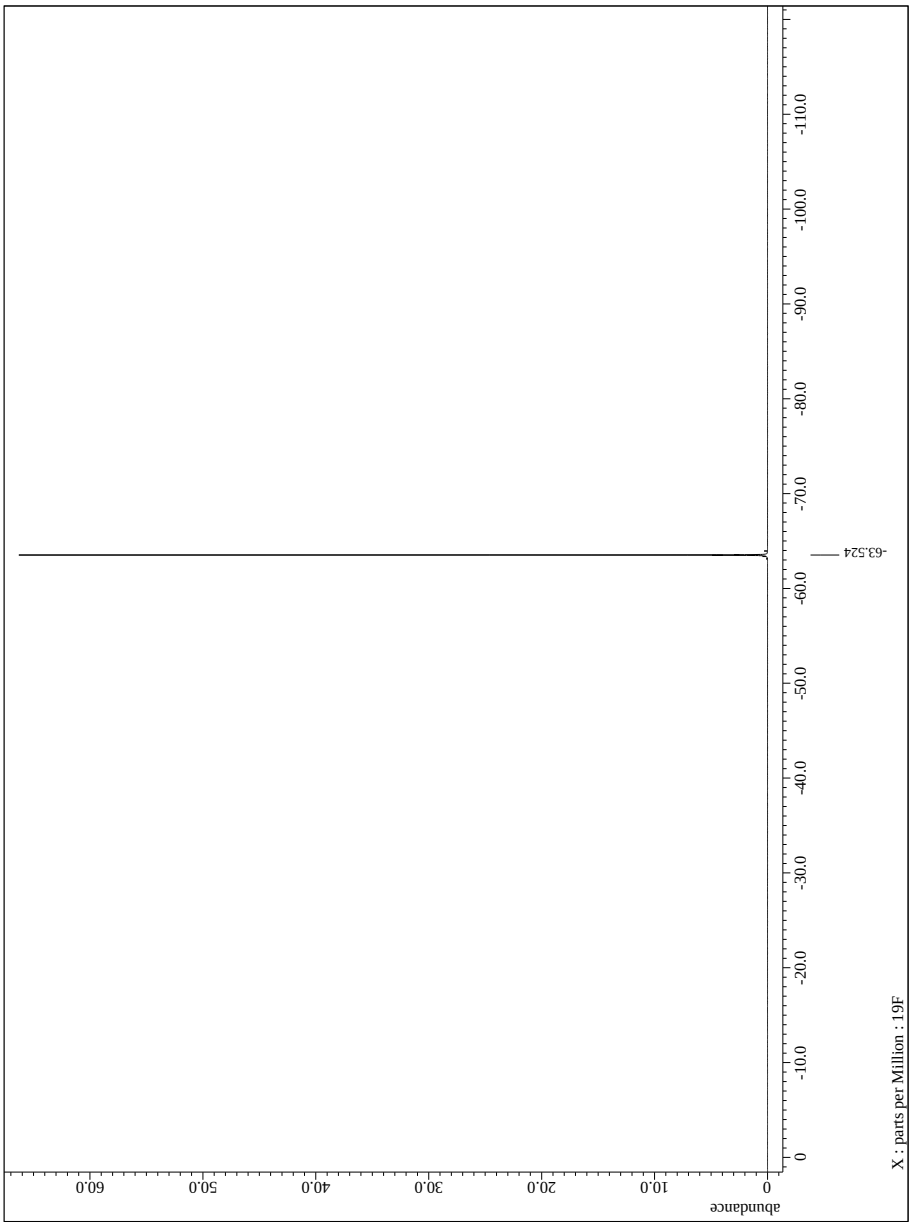

Figure A12: ^{19}F NMR of {[3,5-(3,5-$(CF_3)_2Ph)_2Pz$]Ag}$_3$.

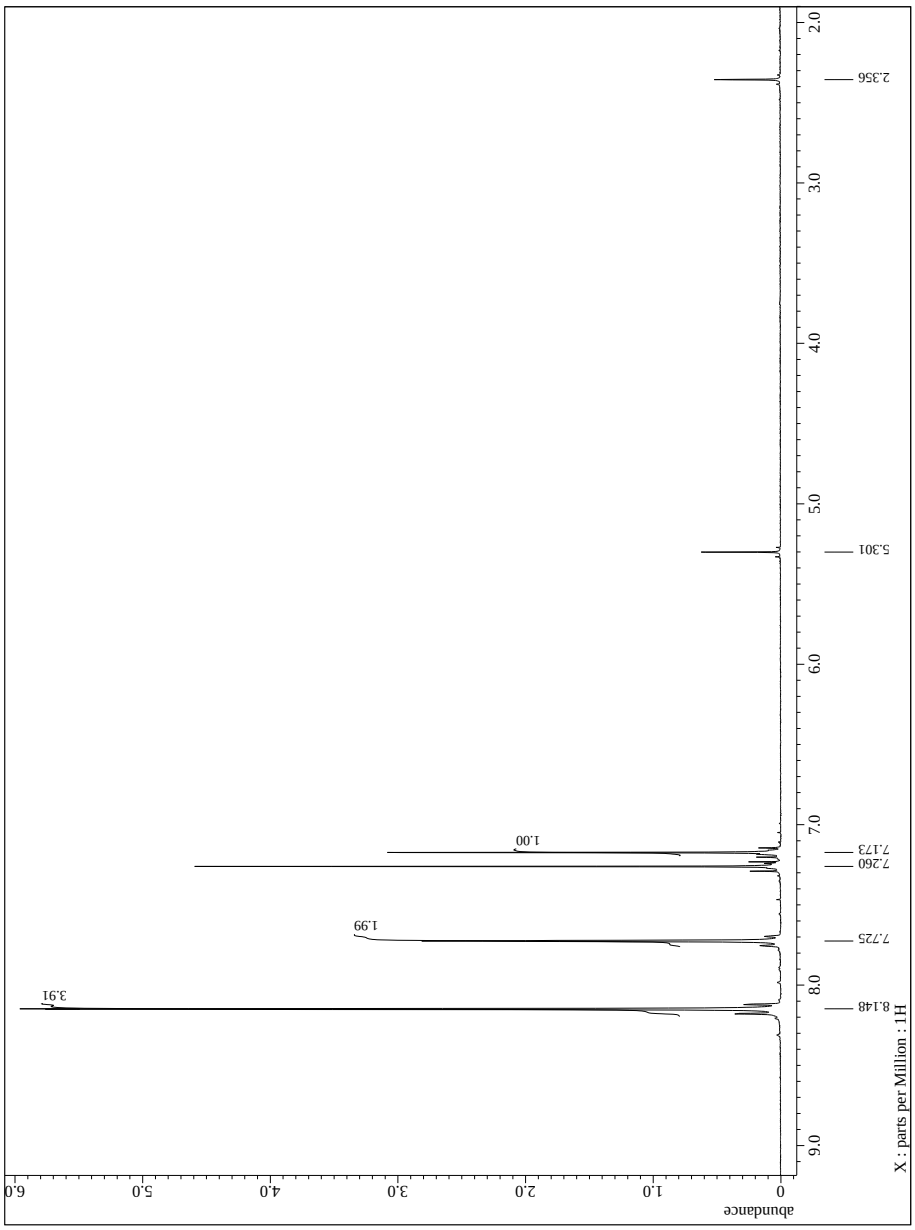

Figure A13: ^{1}H NMR of {[3,5-(3,5-$(CF_3)_2$Ph)$_2$Pz]Au}$_3$.

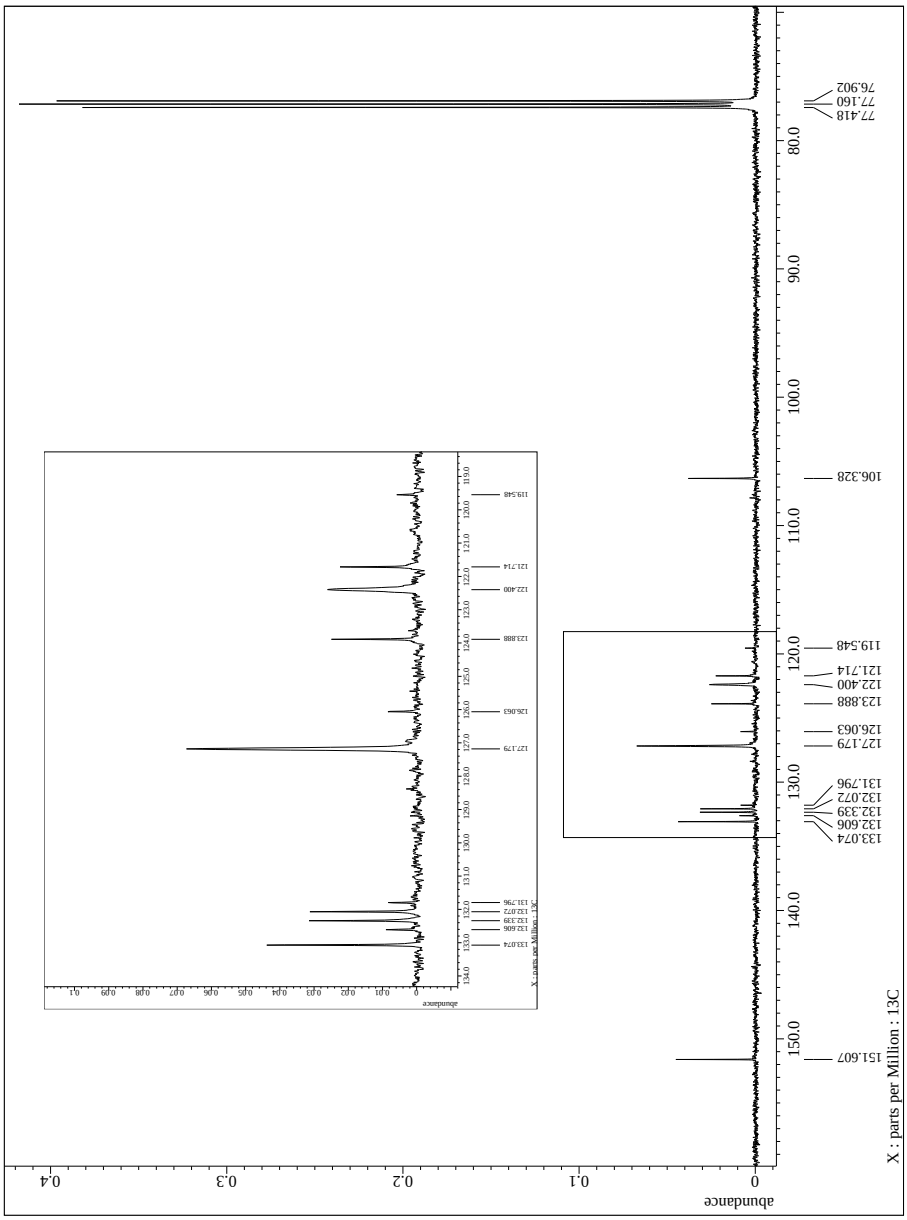

Figure A14: $^{13}C\{^{1}H\}$ NMR of $\{[3,5\text{-}(CF_3)_2Ph)_2Pz]Au\}_3$.

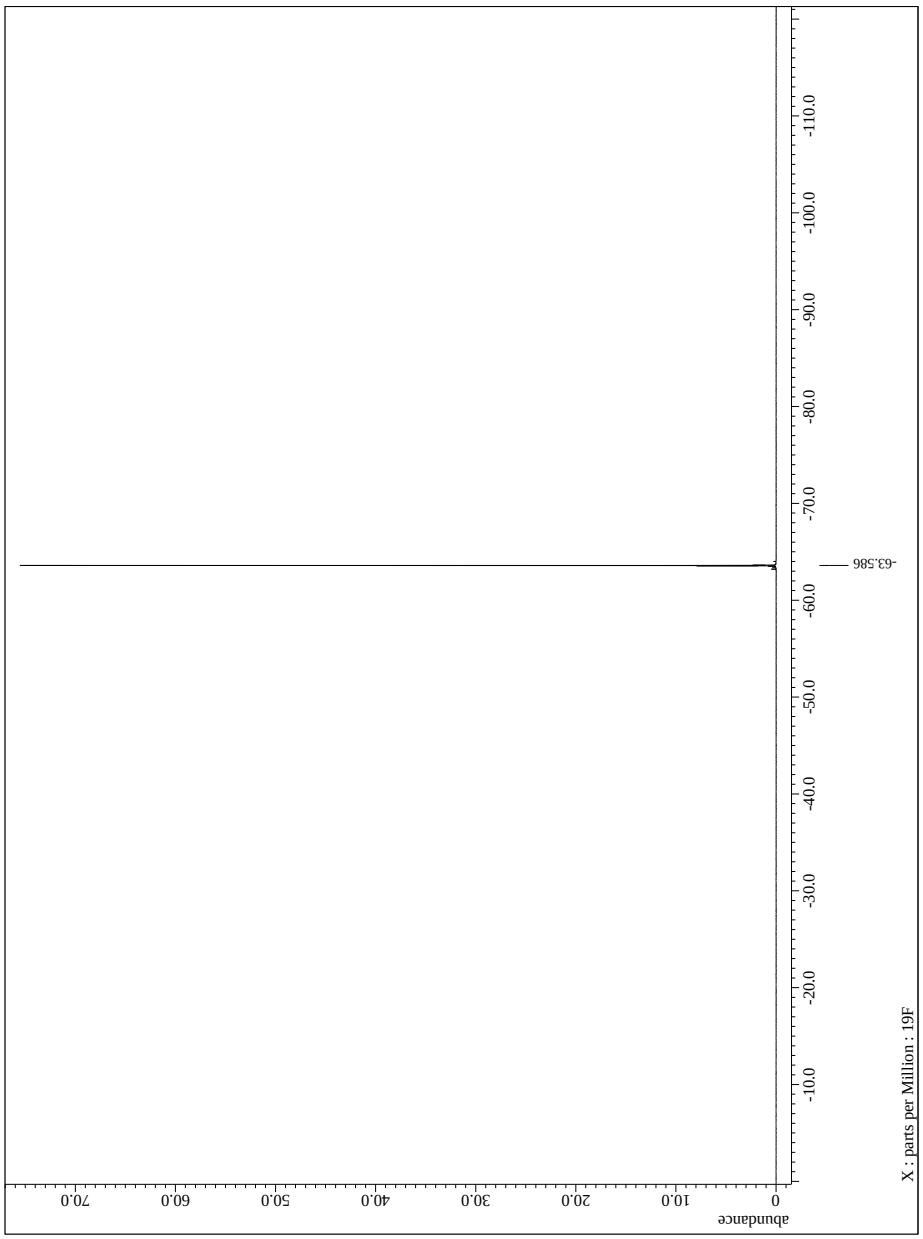

Figure A15: ^{19}F NMR of {[3,5-(CF$_3$)$_2$Ph)$_2$Pz]Au}$_3$.

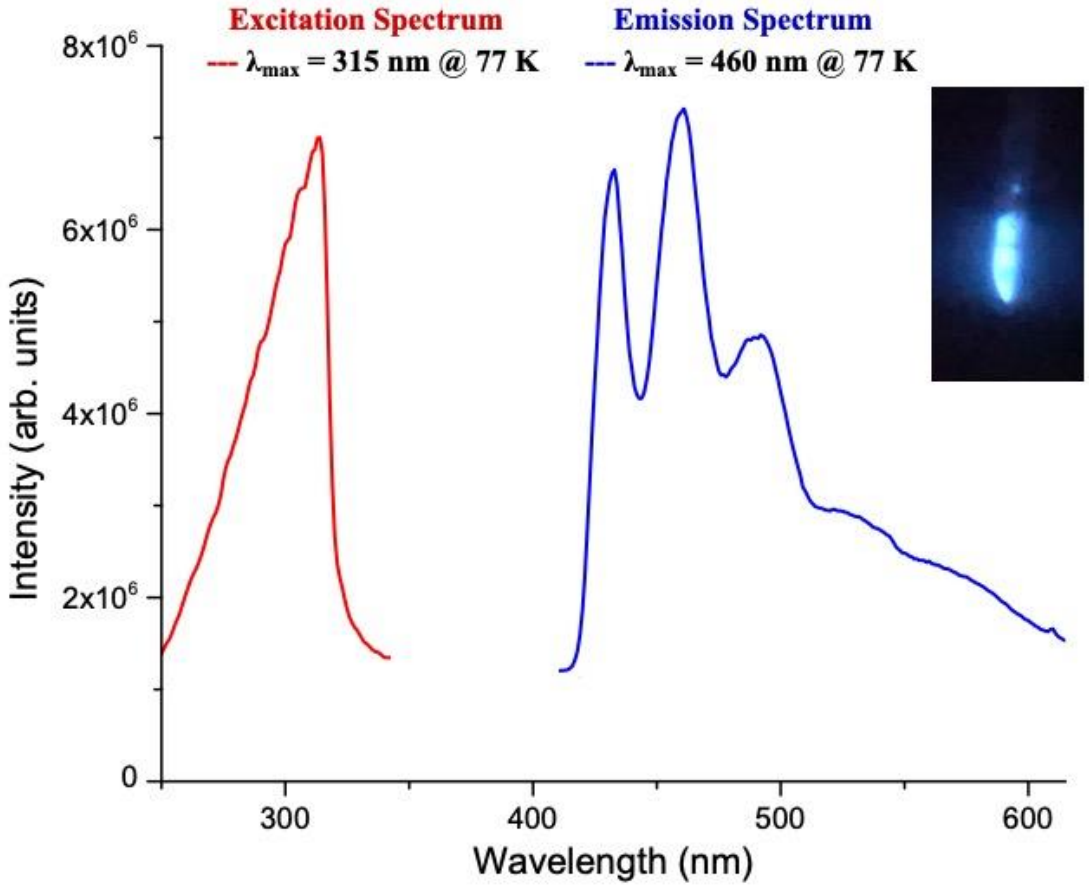

Figure A16: Luminescence Spectra of $\{[3,5\text{-}(3,5\text{-}(CF_3)_2Ph)_2Pz]Cu\}_3$ at 77 K.

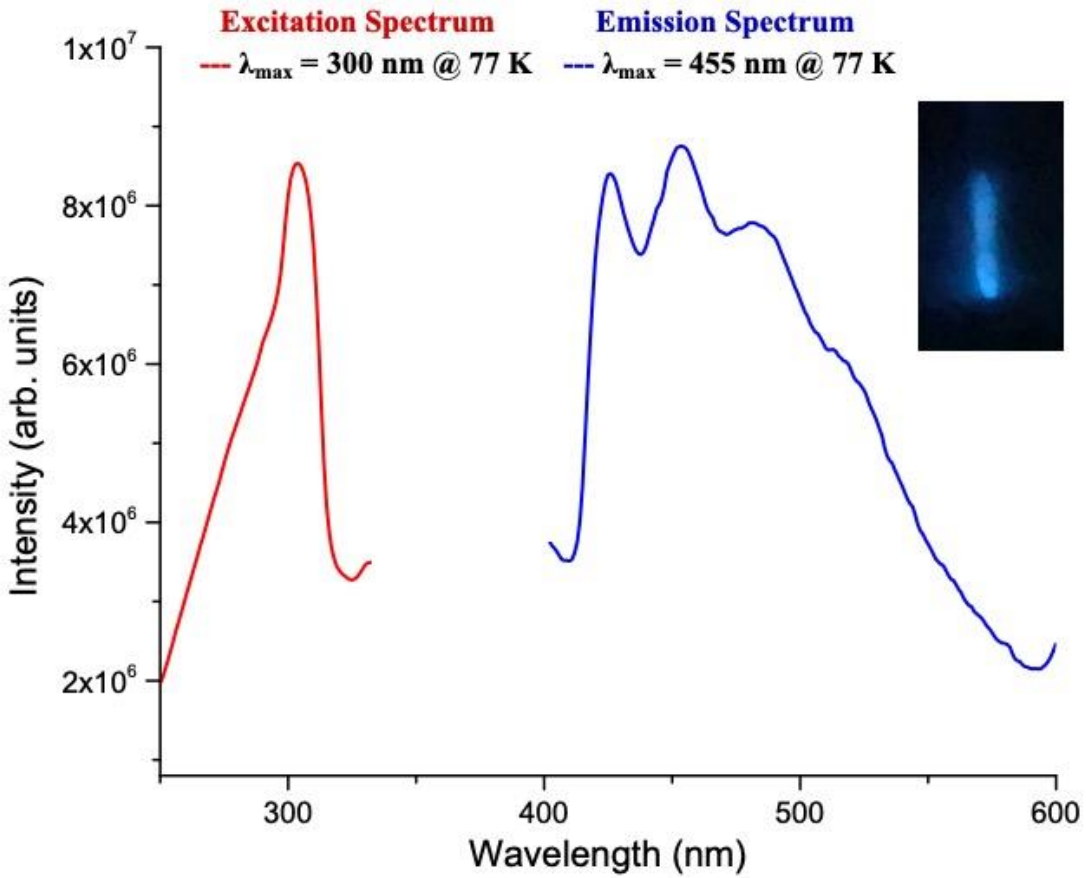

Figure A17: Luminescence Spectra of $\{[3,5\text{-}(3,5\text{-}(CF_3)_2Ph)_2Pz]Ag\}_3$ at 77 K.

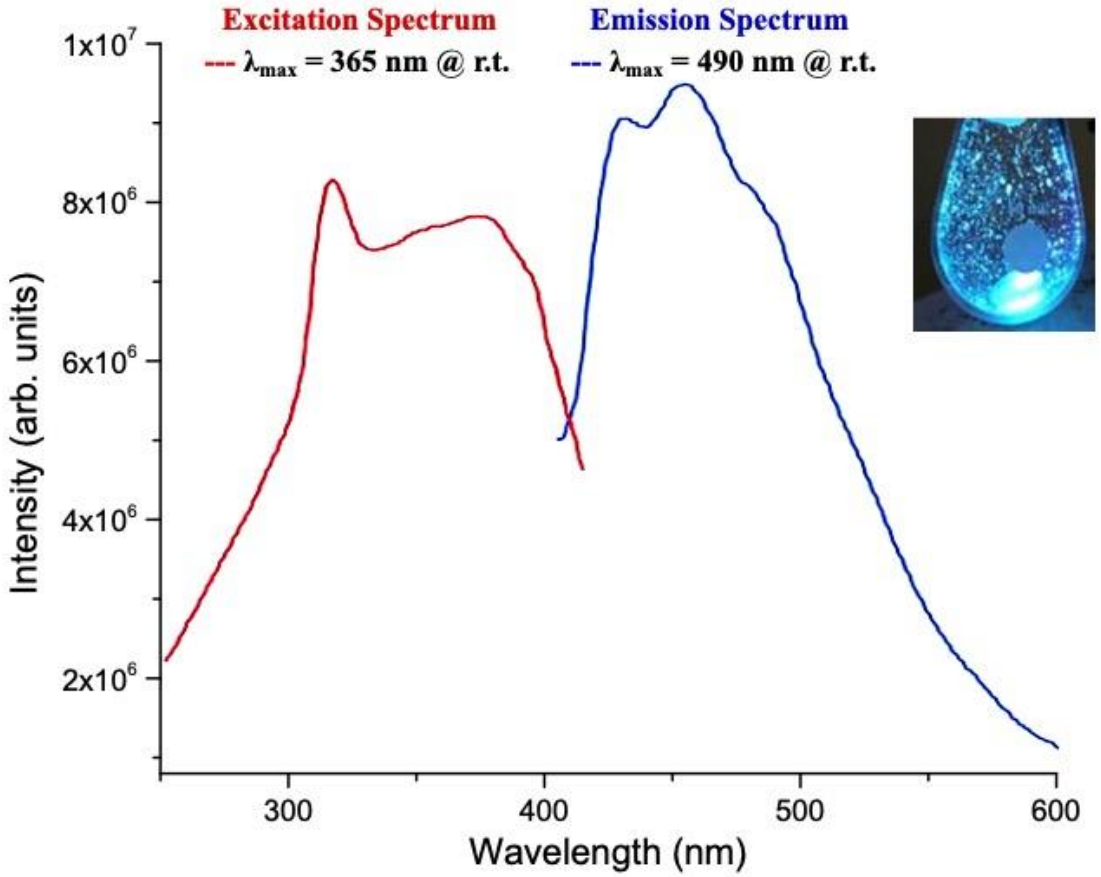

Figure A18: Luminescence Spectra of $\{[3,5\text{-}(3,5\text{-}(CF_3)_2Ph)_2Pz]Au\}_3$ at room temperature.

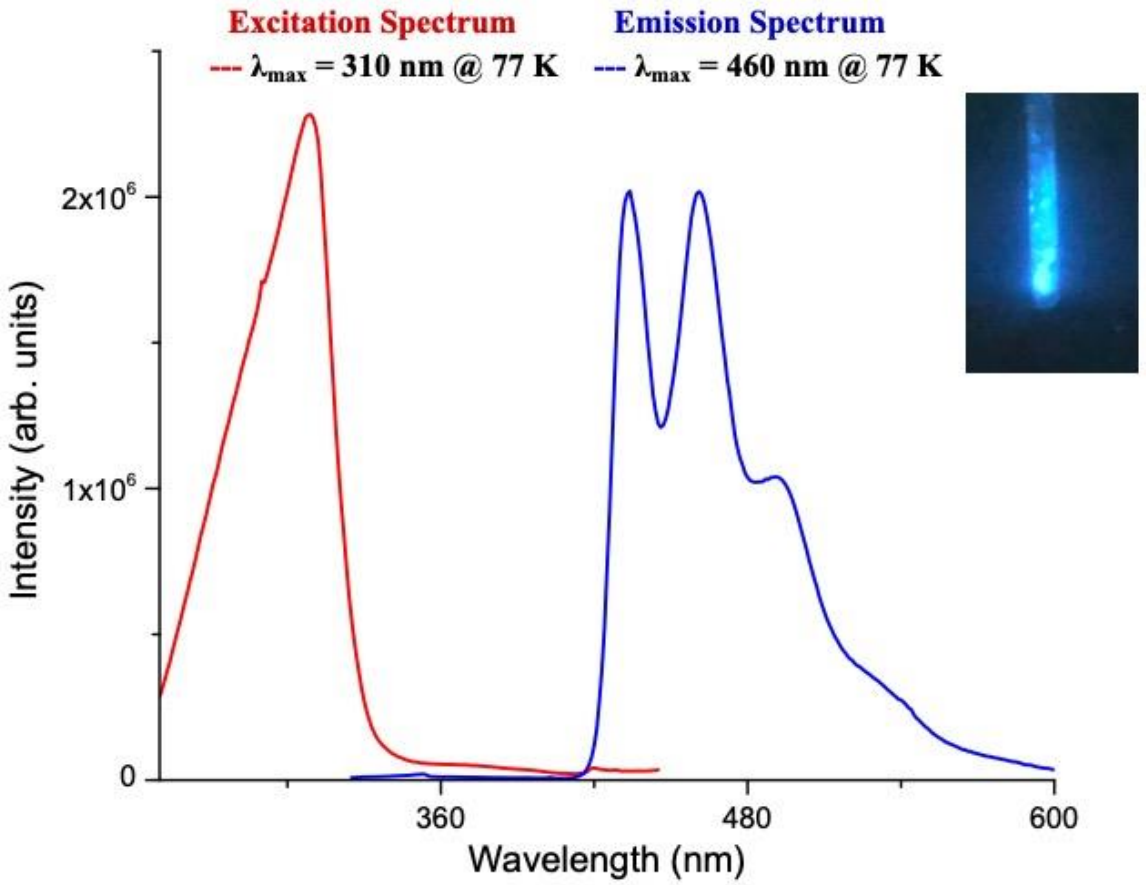

Figure A19: Luminescence Spectra of {[3,5-(3,5-$(CF_3)_2Ph)_2Pz$]Au}$_3$ at 77 K.

`

1-(*p*-tolyl)-4-hexyl-1*H*-1,2,3-triazole

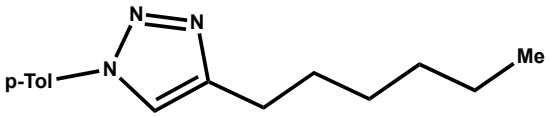

^{1}H NMR ($CDCl_3$, 500 MHz): 7.67 (s, 1H), 7.55 (d, 2H, J = 6.87 Hz), 7.23 (d, 2H, J = 6.87 Hz), 2.73 (t, 2H, J = 7.45 Hz), 2.35 (s, 3H), 1.65-1.71 (m, 2H), 1.33-1.37 (m, 2H), 1.26-1.29 (m, 4H), 0.85 (t, 3H, J = 6.87 Hz). ^{13}C{^{1}H} NMR ($CDCl_3$, 500 MHz): 149.0, 138.4, 135.0, 130.1, 120.2, 118.8, 31.6, 29.4, 29.0, 25.7, 22.6, 21.0, 14.1.

Reference: Devaborniny, P.; Ponduru, T.; Noonikara-Poyil, A.; Jayaranta, N.; Dias, H.V.R.; Acetylene and terminal alkyne complexes of copper(I) supported fluorinated pyrazolates: synthesis, structures, and transformations. *Dalton Transactions.* **2019**, *48*, 15782-15794.

1-(*p*-tolyl)-4-phenyl-1*H*-1,2,3-triazole

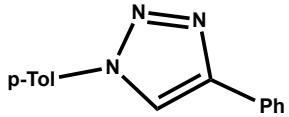

^{1}H NMR ($CDCl_3$, 500 MHz): 8.15 (s, 1H), 7.90 (d, 2H, J = 7.45 Hz), 7.65 (d, 2H, J = 8.60 Hz), 7.45 (t, 2H, J = 7.45 Hz), 7.30-7.36 (m, 3H), 2.42 (s, 3H). ^{13}C{^{1}H} NMR ($CDCl_3$, 500 MHz): 148.3, 139.0, 134.8, 130.4, 129.0, 128.4, 125.9, 120.5, 117.8, 21.2.

Reference: Meng, X.; Xu, X.; Gao, T.; Chen, B.; *Eur. J. Org. Chem.* **2010**, *2010*, 5409-5414.

`

Ethyl-2-phenylcyclopropane-1-carboxylate:

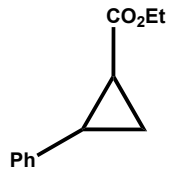

cis: ^{1}H NMR ($CDCl_3$, 500 MHz): 7.29-7.19 (m, 5H), 3.89 (q, 2H, J = 7.0 Hz), 2.60 (app q, 1H, J = 8.5 Hz), 2.10 (ddd, 1H, J = 9.3, 8.6, 5.0 Hz), 1.73 (ddd, 1H, J = 6.5, 5.0, 4.6 Hz), 1.35 (ddd, 1H, J = 8.6, 8.3, 4.6 Hz), 0.99 (t, 3H, J = 7.0 Hz). ^{13}C NMR ($CDCl_3$, 500 MHz): 171.0, 136.6, 129.3, 127.9, 126.6, 60.1, 25.4, 21.8, 14.0, 11.1.

trans: ^{1}H NMR ($CDCl_3$, 500 MHz): 7.33-7.11 (m, 5H), 4.19 (q, 2H, J = 7.0 Hz), 2.54 (ddd, 1H, J = 9.2, 6.5, 4.0 Hz), 1.92 (ddd, 1H, J = 8.2, 5.3, 4.0 Hz), 1.62 (ddd, 1H, J = 9.2, 5.3, 4.6 Hz), 1.33 (ddd, 1H, J = 8.2, 6.6, 4.6 Hz), 1.30 (t, 3H, J = 7.0 Hz). ^{13}C NMR ($CDCl_3$, 500 MHz): 173.4, 140.1, 128.5, 126.5, 126.2, 60.7, 26.2, 24.2, 17.1, 14.3.

Reference: Barrett, A.; Braddock, D.; Lenoir, I.; Tone, H.; *J. Org. Chem.* **2001**, *66*, 8260-8263.

`

Appendix B

Spectroscopic data of chapter 3

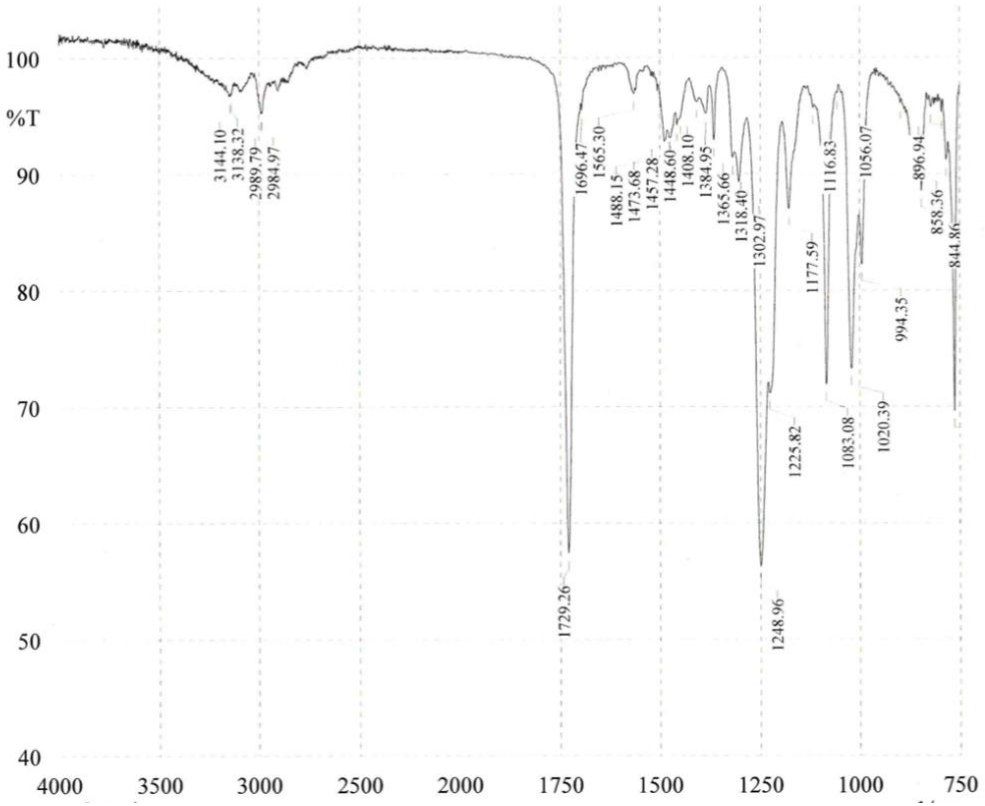

Figure B1: IR of {[3,5-$(CO_2Et)_2$PzH.

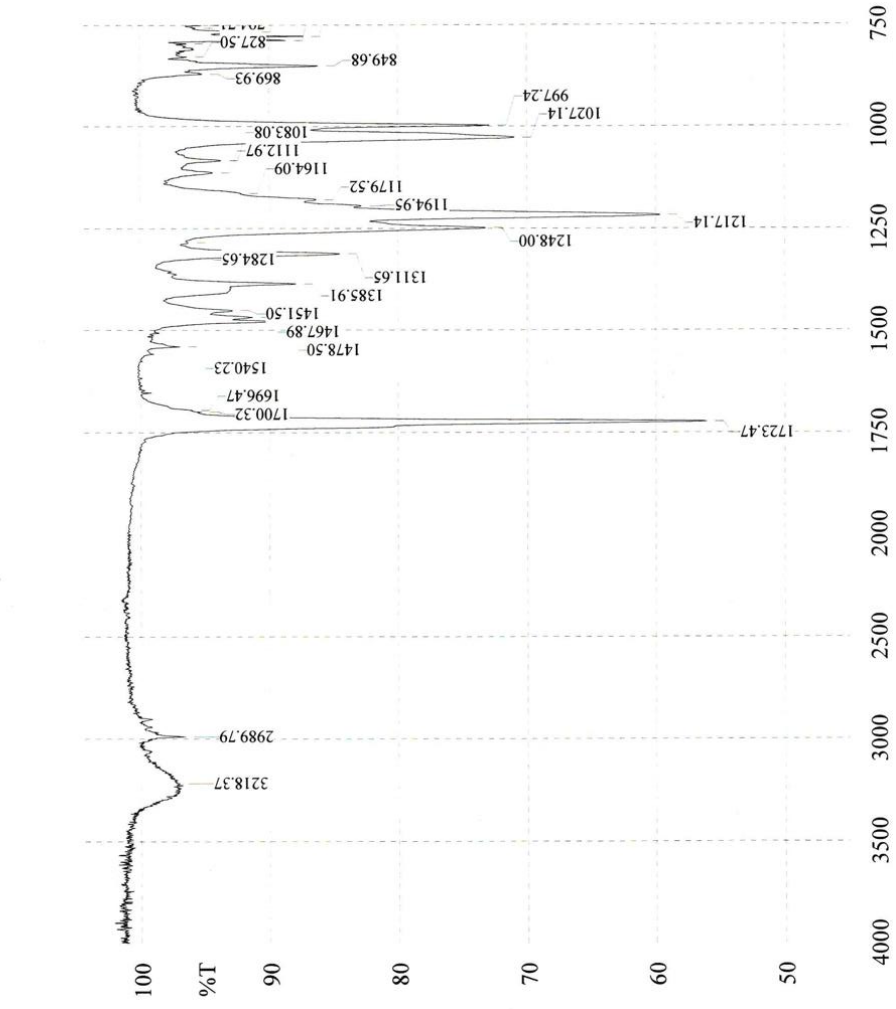

Figure B2: IR of {[4-Br-3,5-$(CO_2Et)_2$PzH.

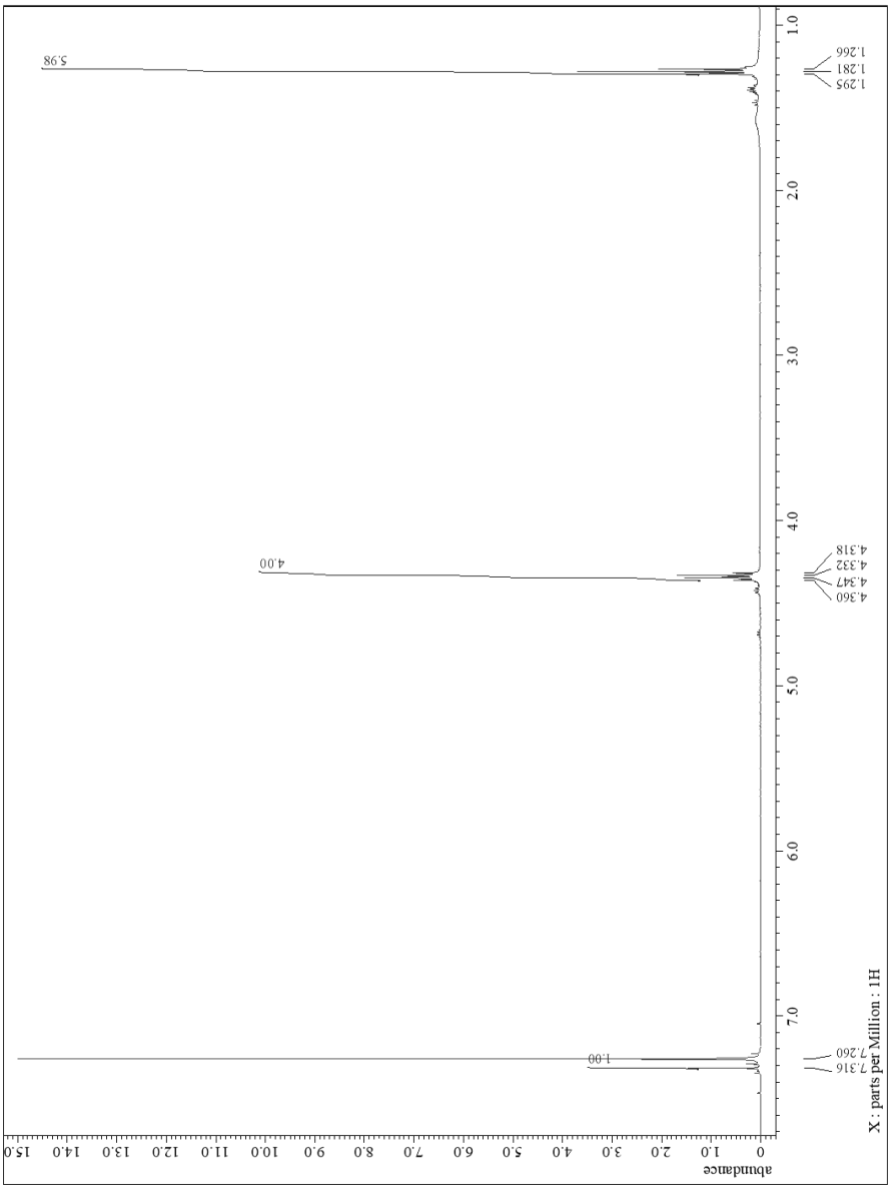

Figure B3: ^{1}H NMR of {[3,5-(CO$_2$Et)$_2$Pz]Cu}$_3$ in CDCl$_3$.

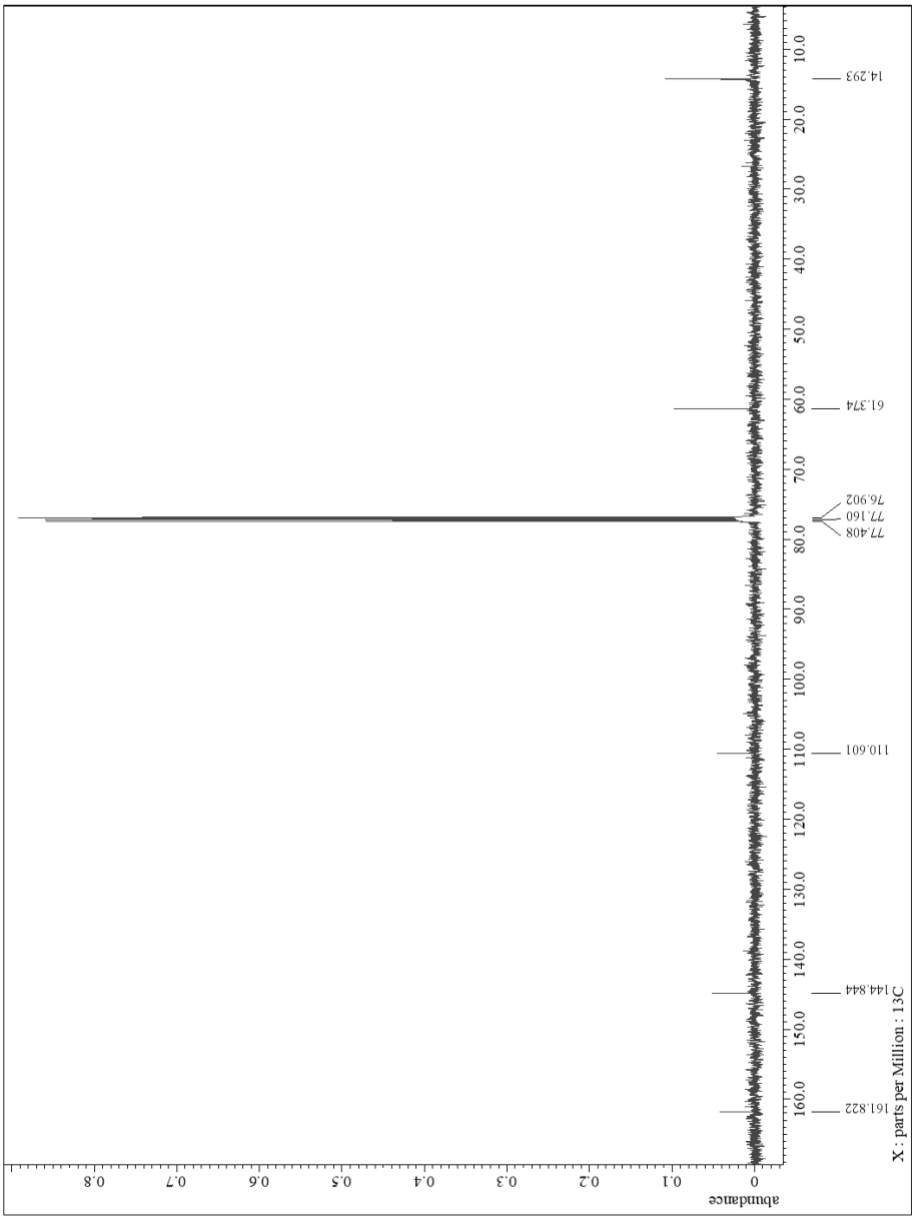

Figure B4: $^{13}C\{^{1}H\}$ NMR of $\{[3,5\text{-}(CO_2Et)_2Pz]Cu\}_3$ in $CDCl_3$.

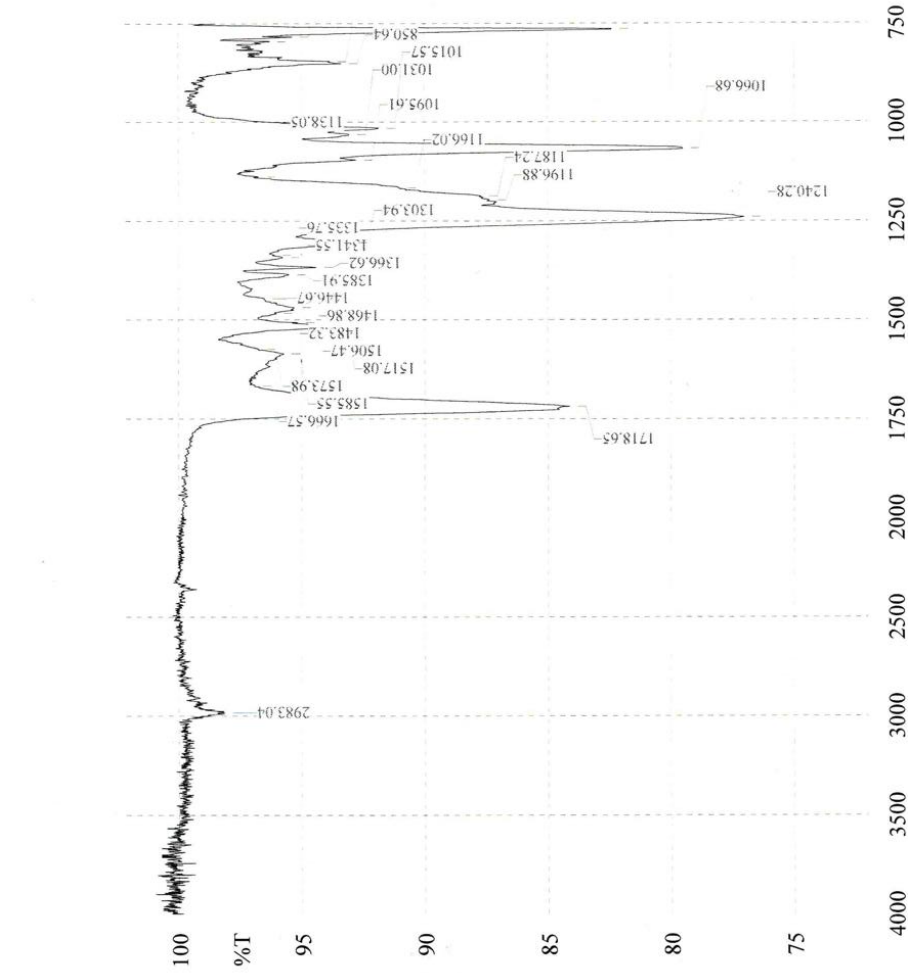

Figure B5: IR spectrum of {[3,5-$(CO_2Et)_2Pz$]Cu}$_3$.

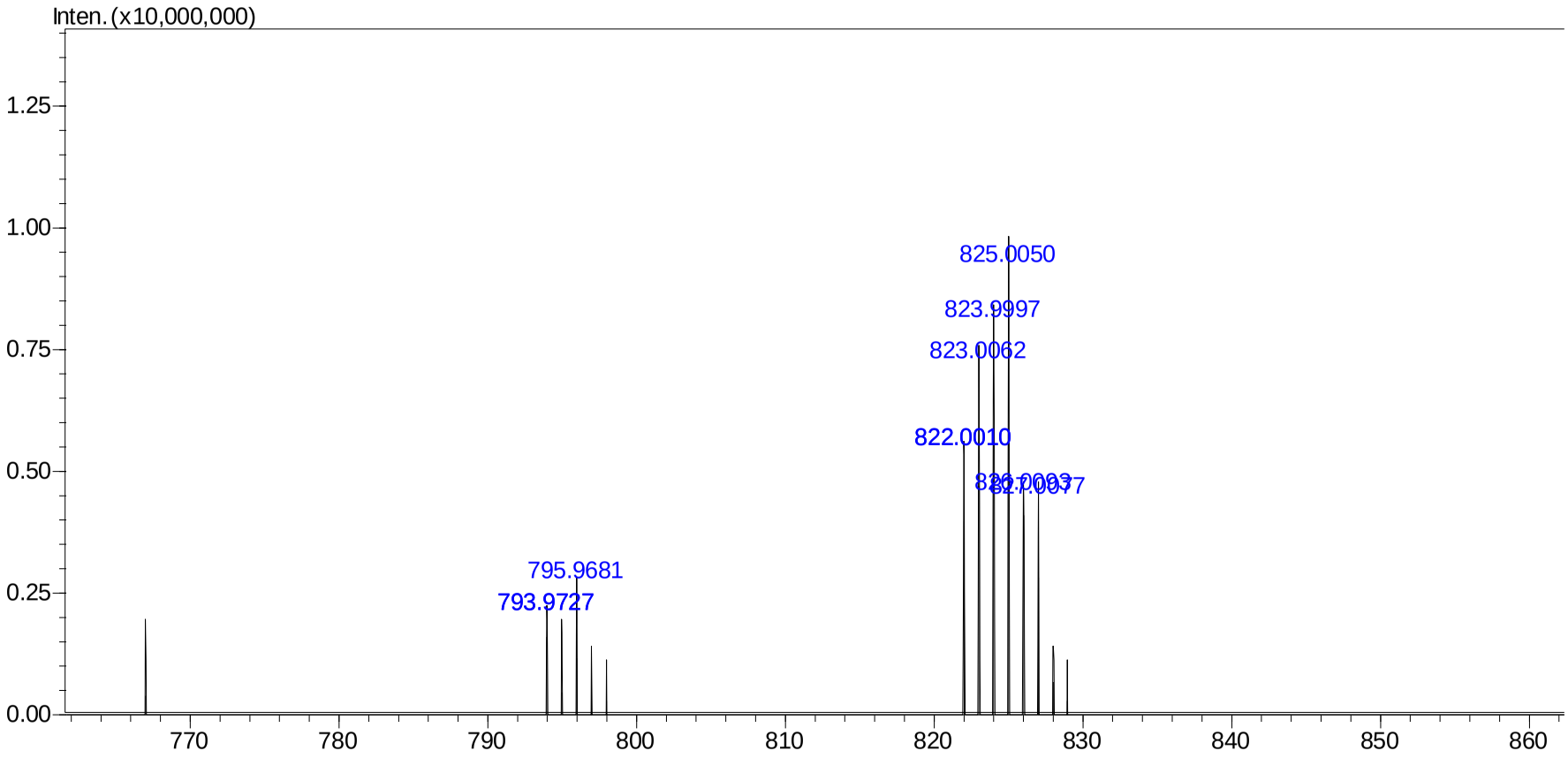

Figure B6: HRMS $[M+H]^+$ peaks of $\{[3,5\text{-}(CO_2Et)_2Pz]Cu\}_3$ in $CHCl_3$.

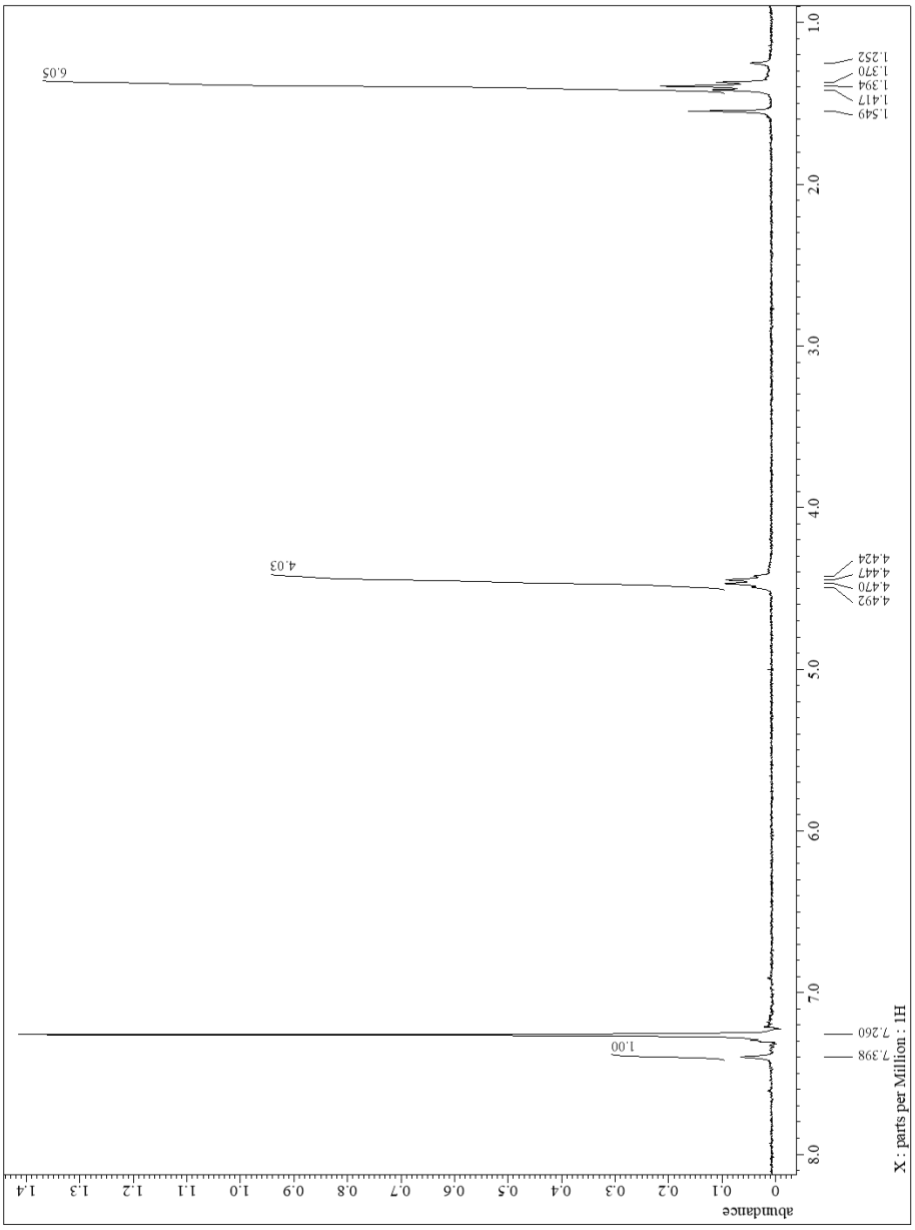

Figure B7: ^{1}H NMR of {[3,5-$(CO_2Et)_2$Pz]Ag}$_3$ in $CDCl_3$.

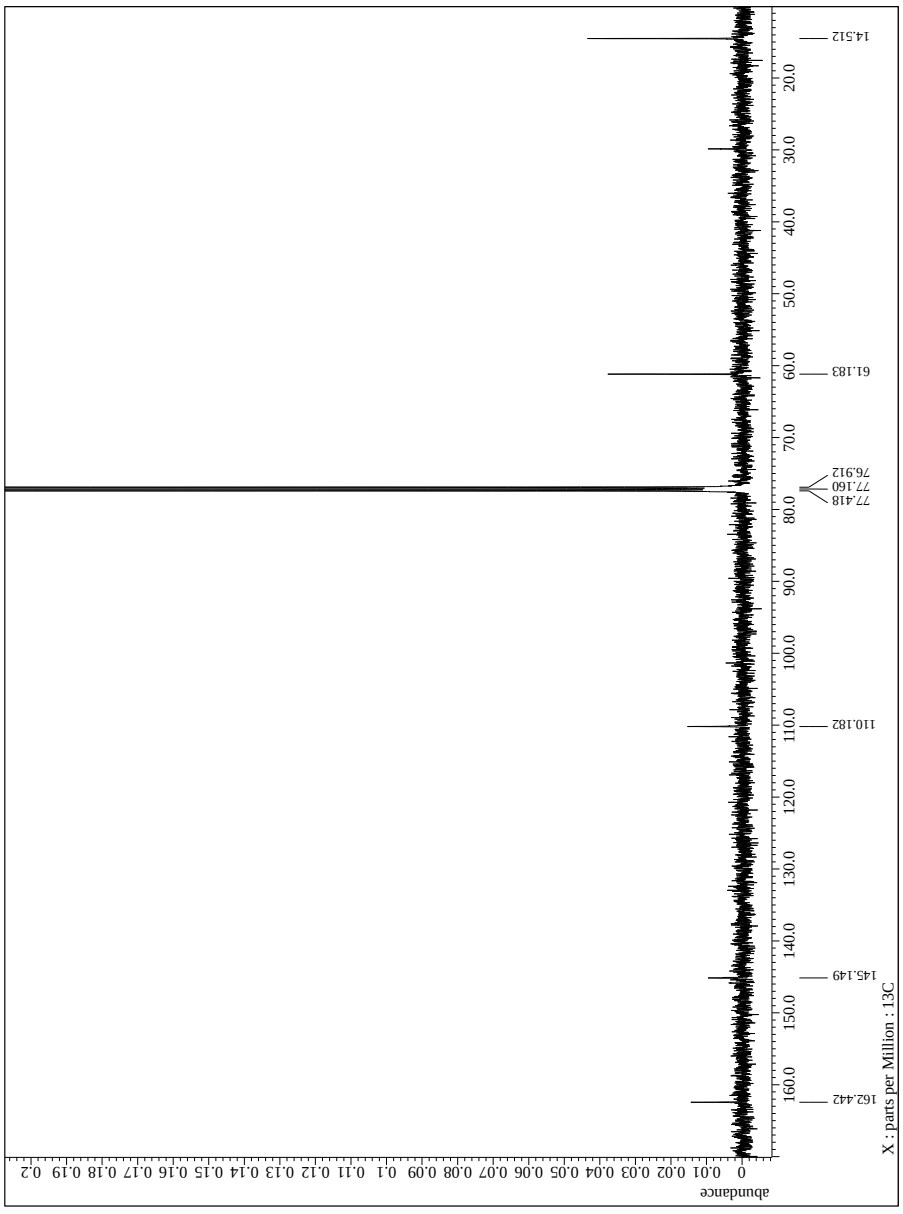

Figure B8: $^{13}C\{^{1}H\}$ NMR of $\{[3,5\text{-}(CO_2Et)_2Pz]Ag\}_3$ in $CDCl_3$.

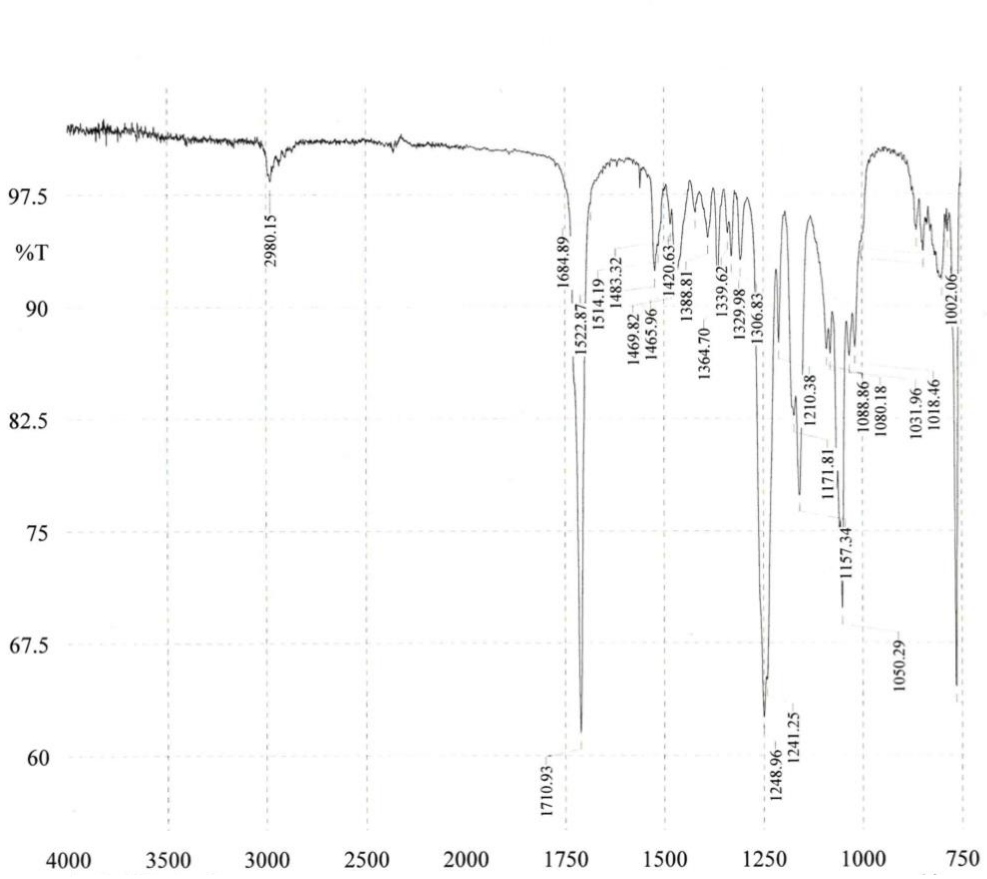

Figure B9: IR spectrum of $\{[3,5\text{-}(CO_2Et)_2Pz]Ag\}_3$.

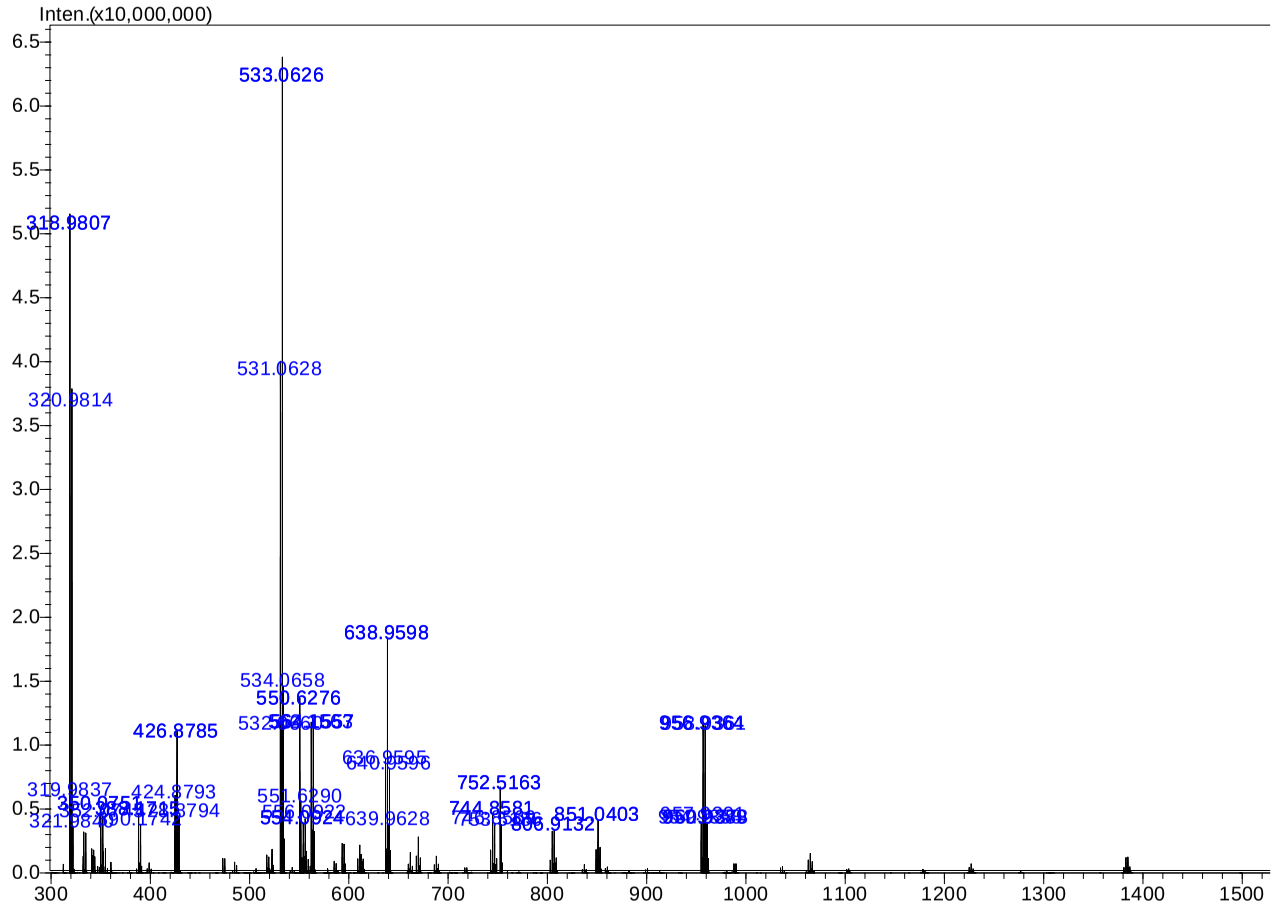

Figure B10: HRMS (full spectrum) of $[3,5\text{-}(CO_2Et)_2Pz]Ag\}_3$ in $CDCl_3$

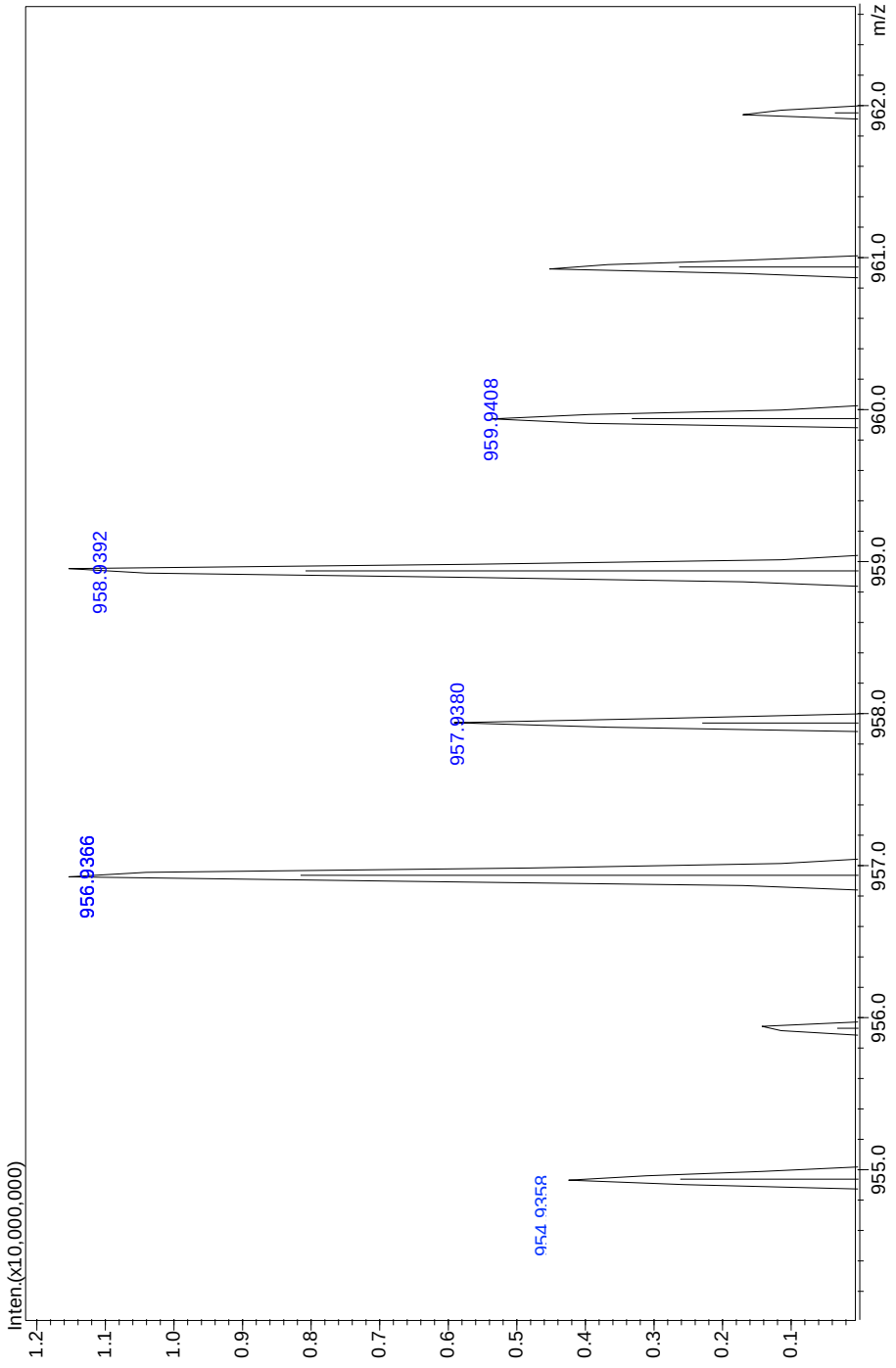

Figure B11: HRMS $[M+H]^+$ peaks of $[3,5\text{-}(CO_2Et)_2Pz]Ag\}_3$ in $CDCl_3$.

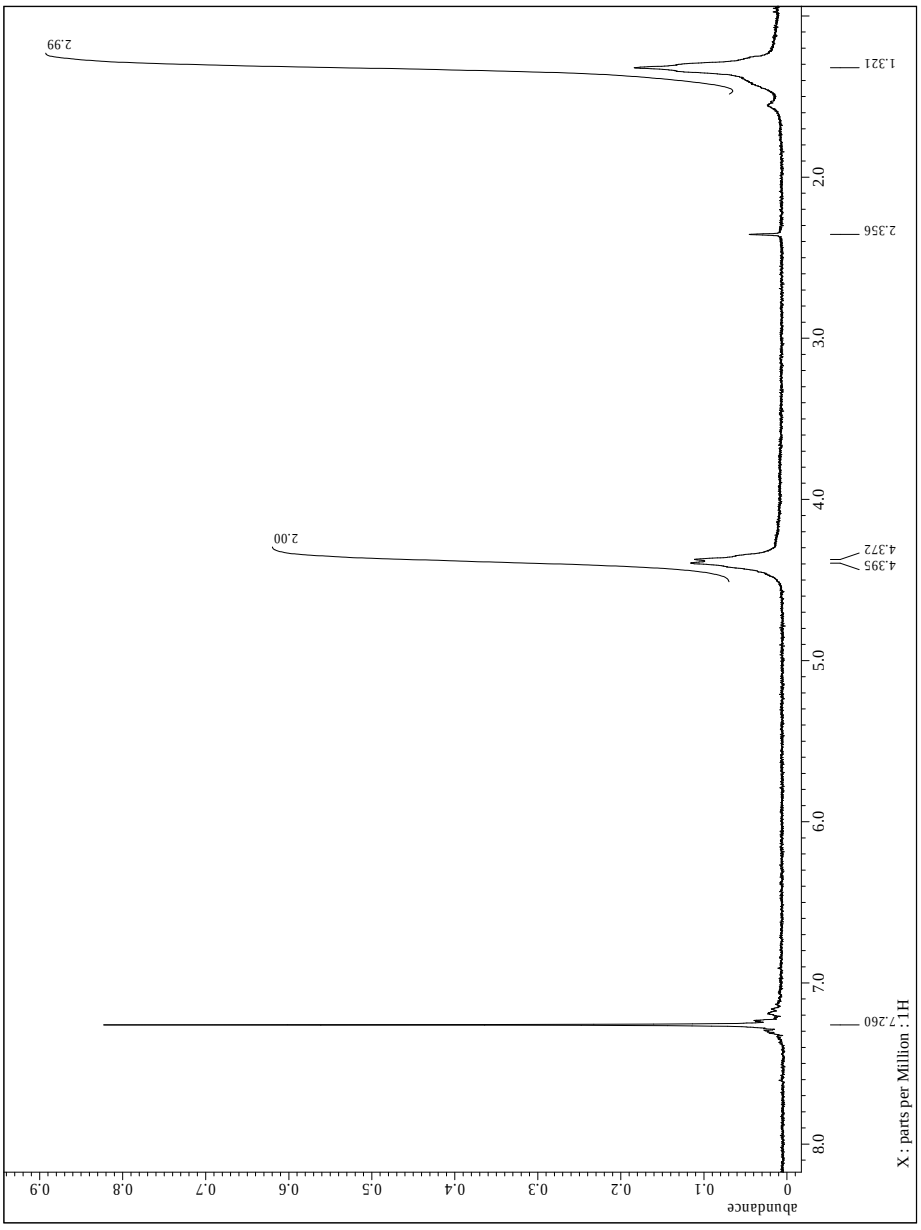

Figure B12: ^{1}H NMR of {[4-Br,3,5-$(CO_2Et)_2Pz$]Cu}$_3$ in $CDCl_3$.

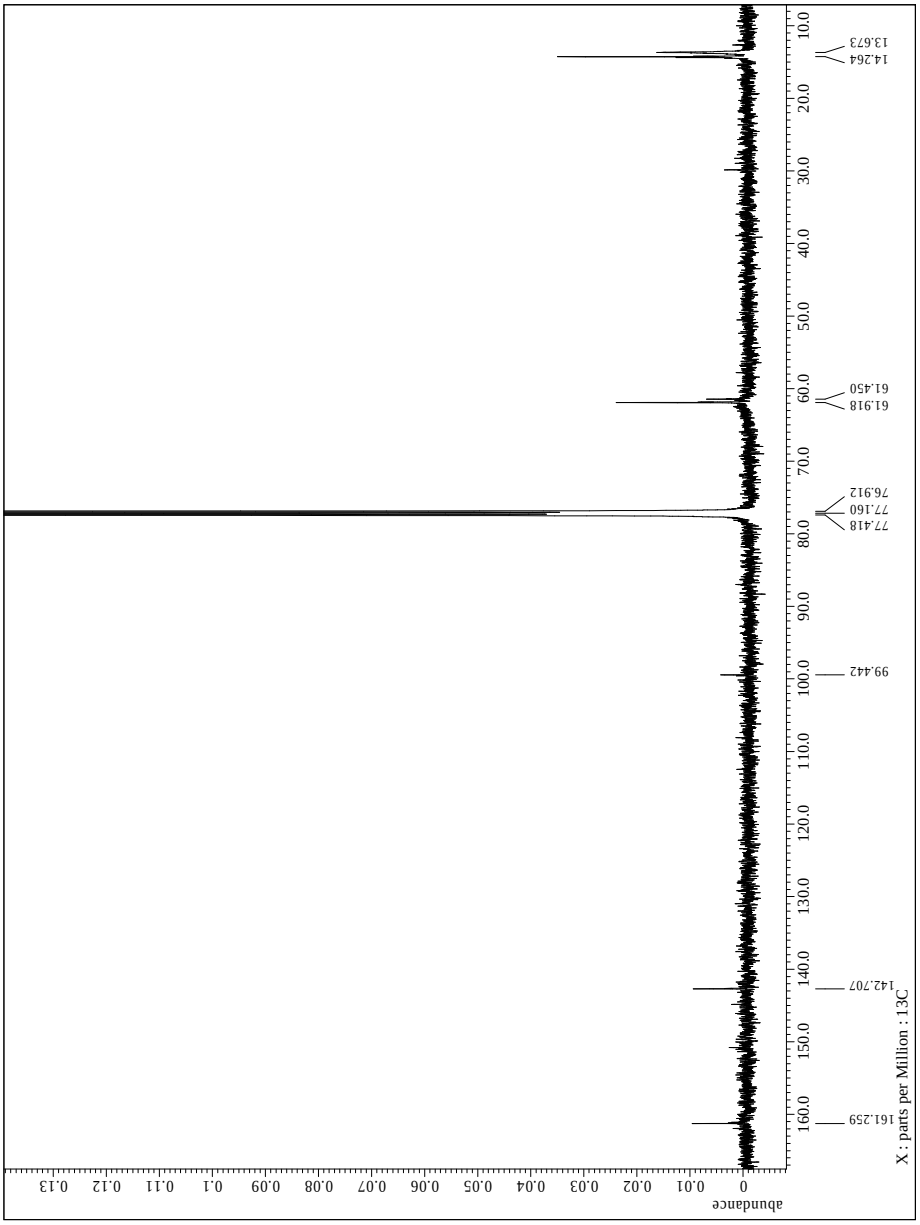

Figure B13: $^{13}C\{^{1}H\}$ NMR of $\{[4\text{-Br},3,5\text{-}(CO_2Et)_2Pz]Cu\}_3$ in $CDCl_3$.

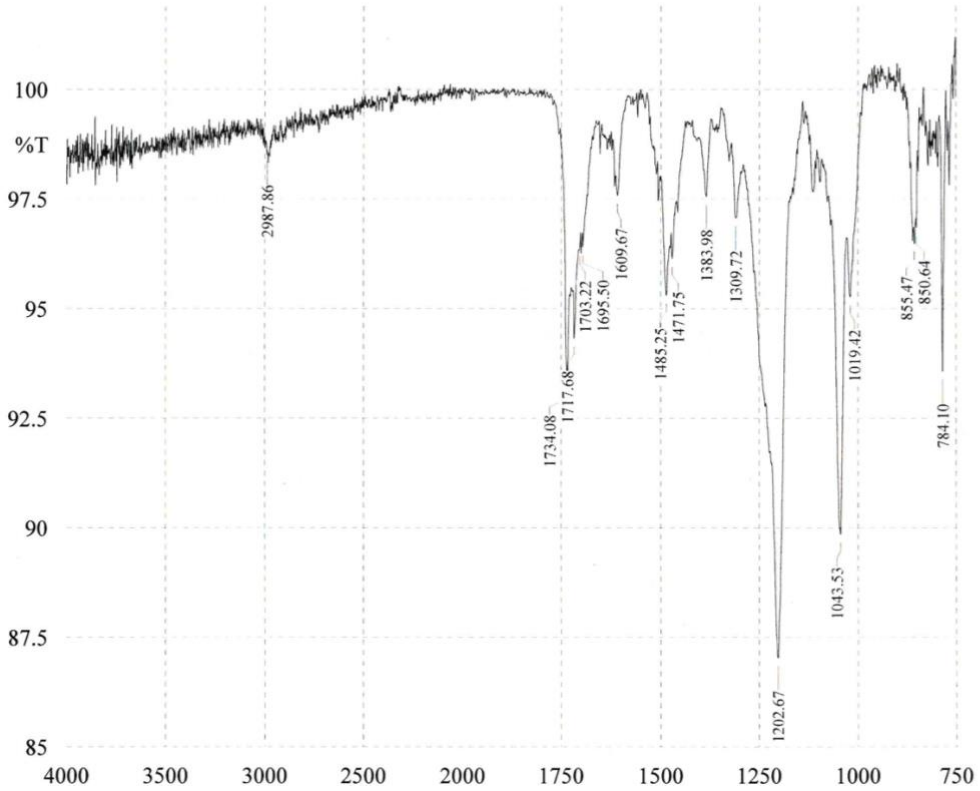

Figure B14: IR spectrum of {[4-Br,3,5-$(CO_2Et)_2$Pz]Cu}$_3$.

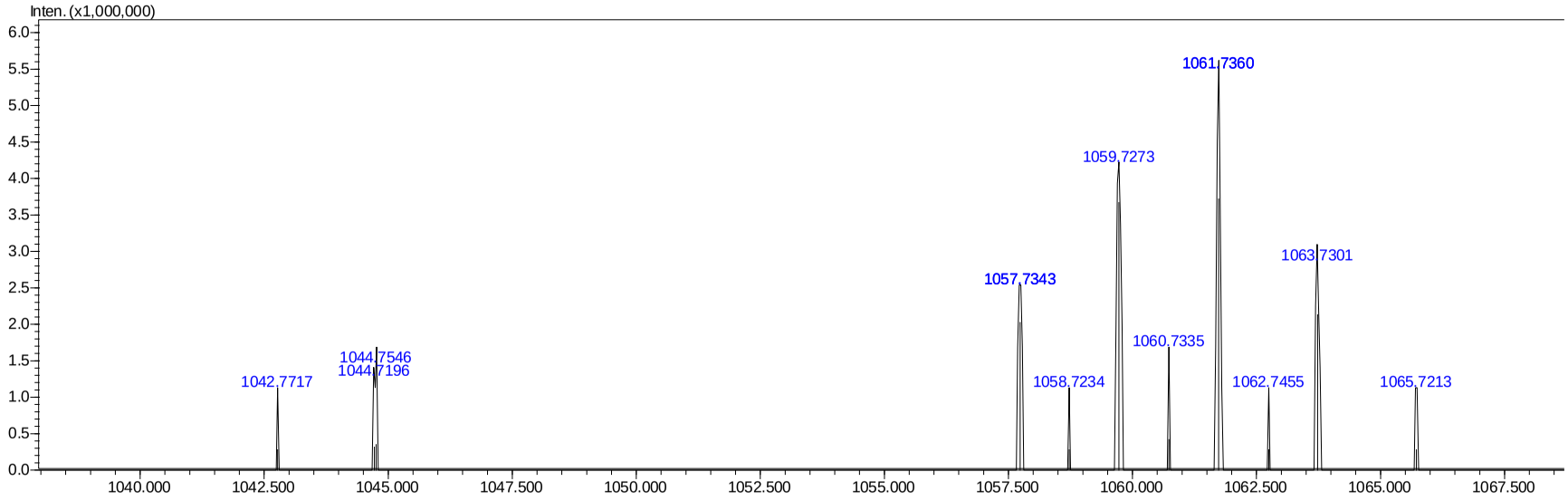

Figure B15: HRMS $[M]^+$ of $\{[4\text{-Br},3,5\text{-}(CO_2Et)_2Pz]Cu\}_3$.

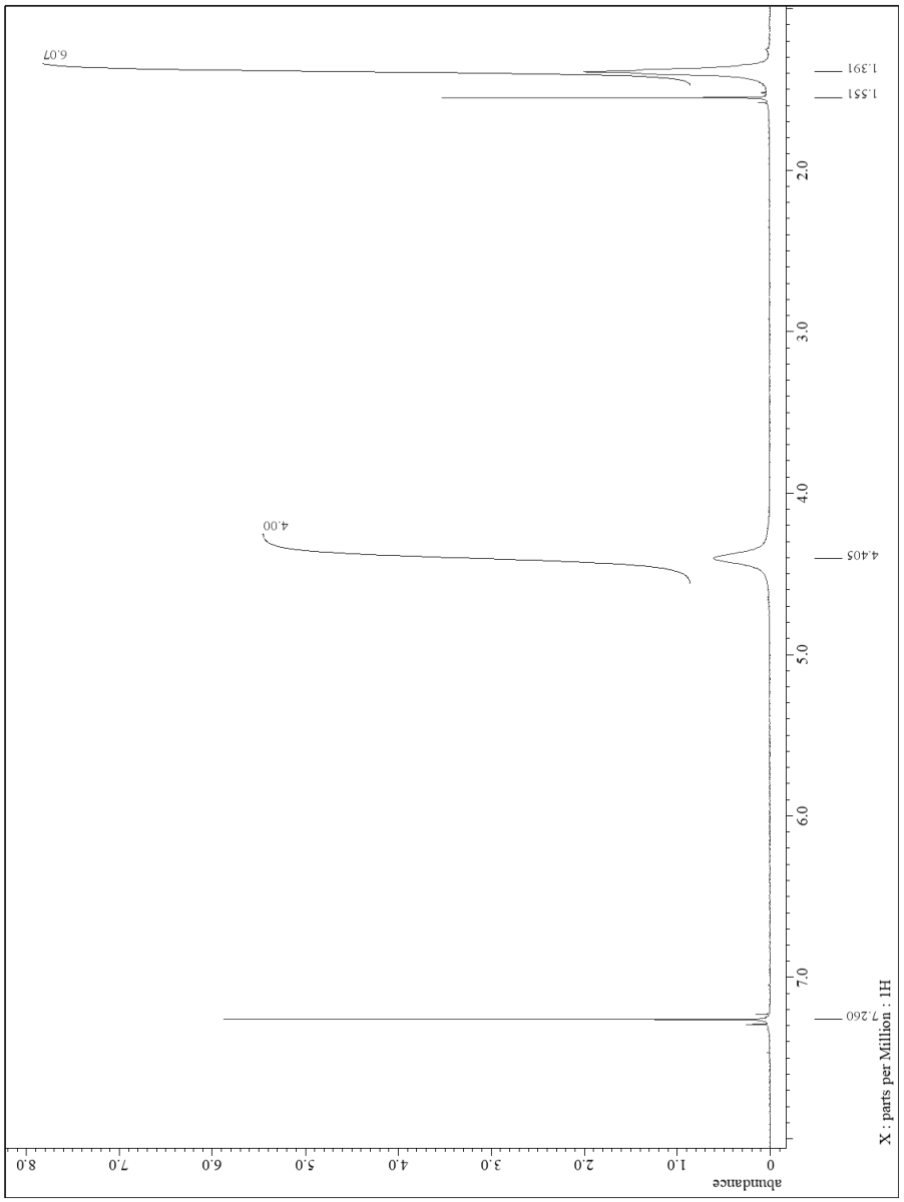

Figure B16: ^{1}H NMR of {[4-Br,3,5-(CO_2Et)$_2$Pz]Ag}$_3$ in $CDCl_3$.

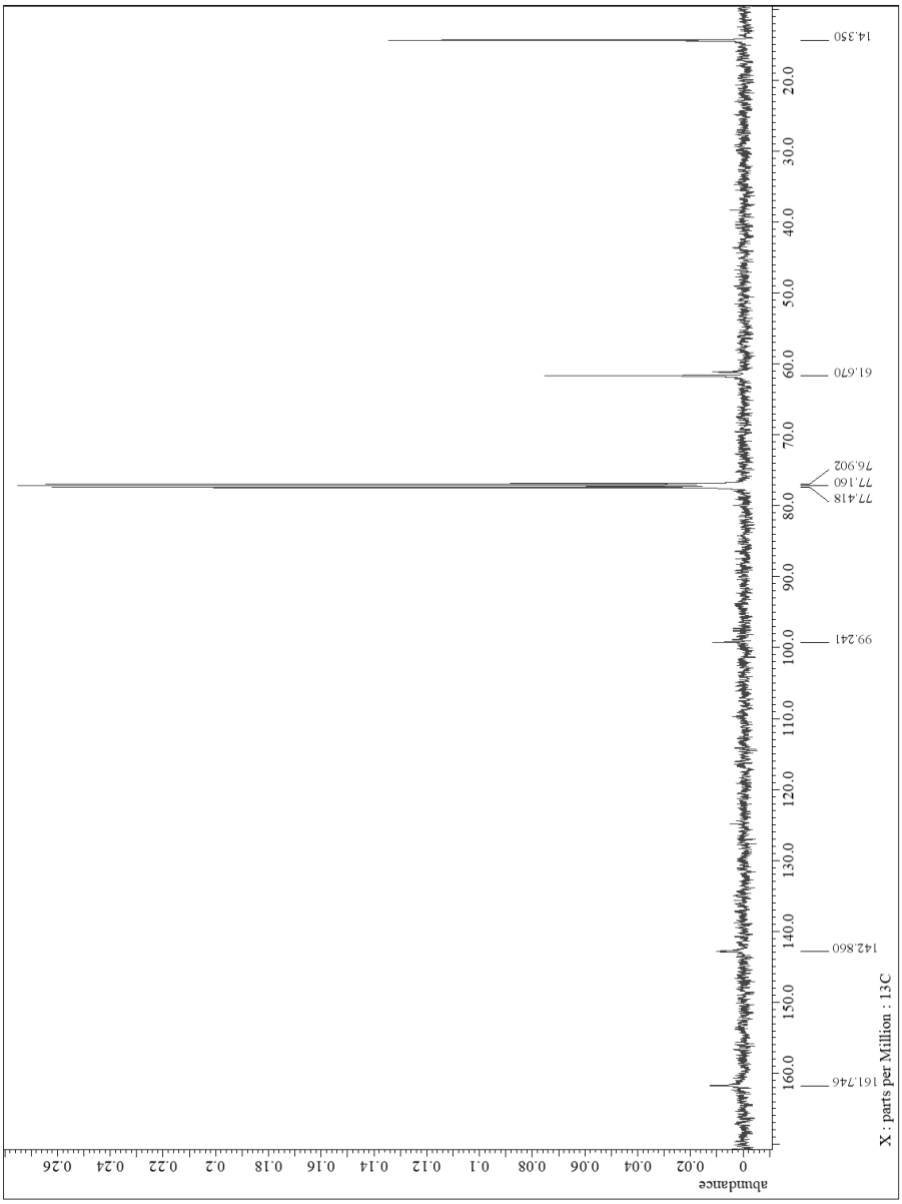

Figure B17: $^{13}C\{^{1}H\}$ NMR of $\{[4\text{-Br},3,5\text{-}(CO_2Et)_2Pz]Ag\}_3$ in $CDCl_3$.

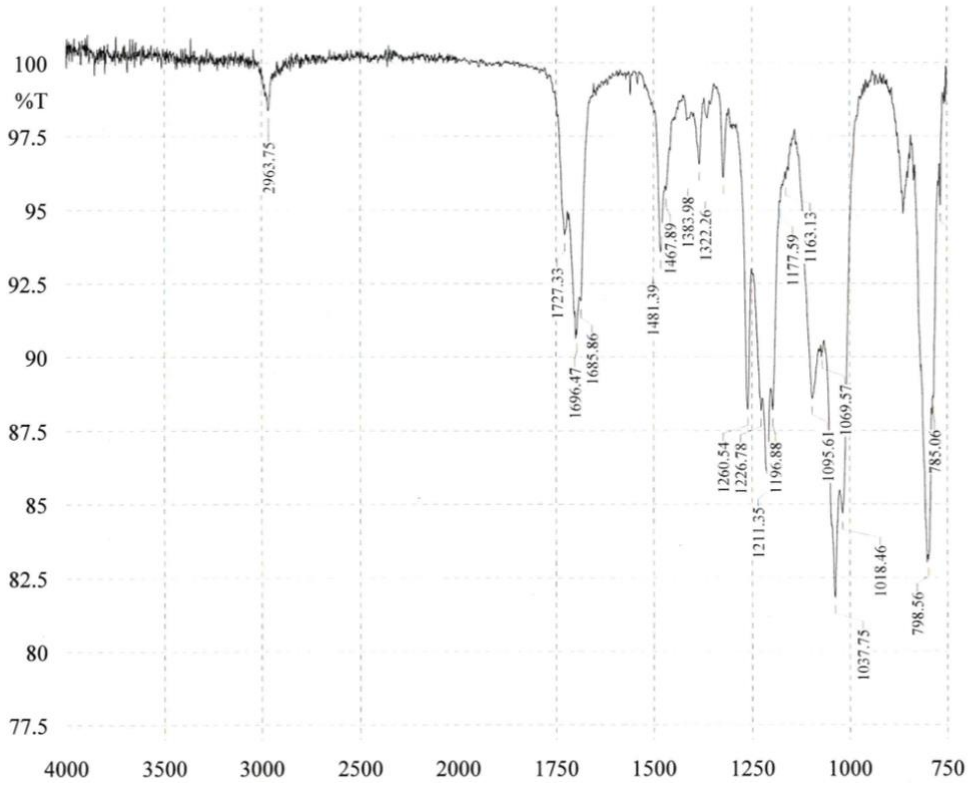

Figure B18: IR spectrum of {[4-Br,3,5-$(CO_2Et)_2$Pz]Ag}$_3$.

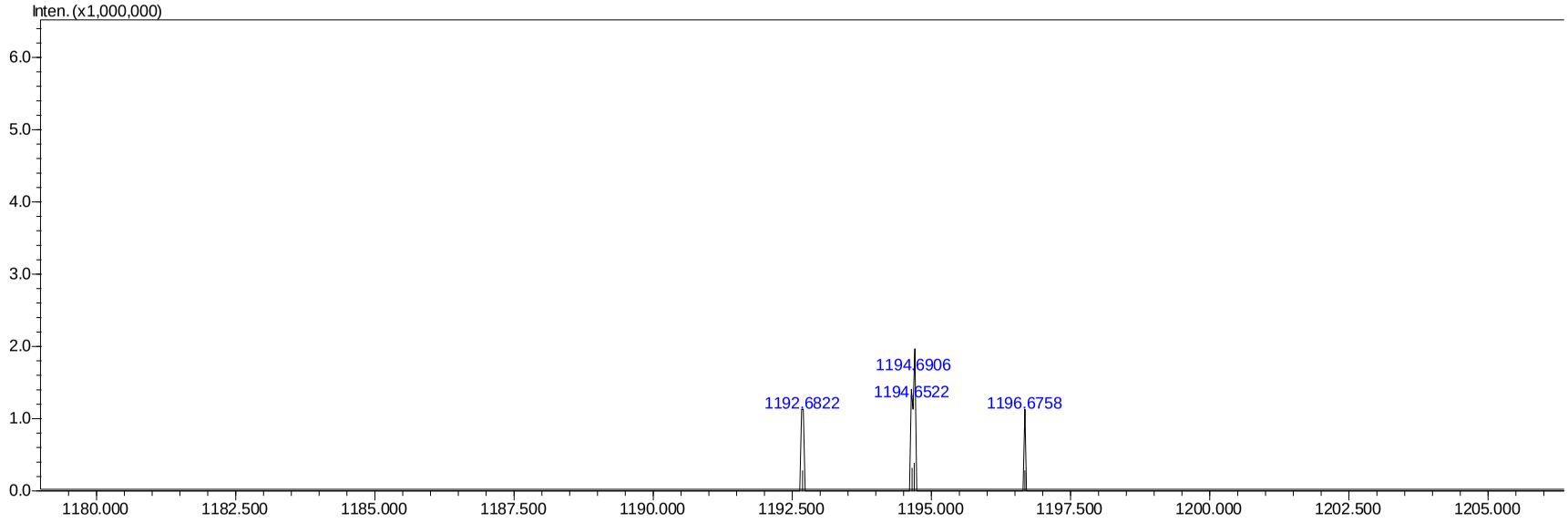

Figure B19: HRMS $[M+H]^+$ of $\{[4\text{-Br},3,5\text{-}(CO_2Et)_2Pz]Ag\}_3$.

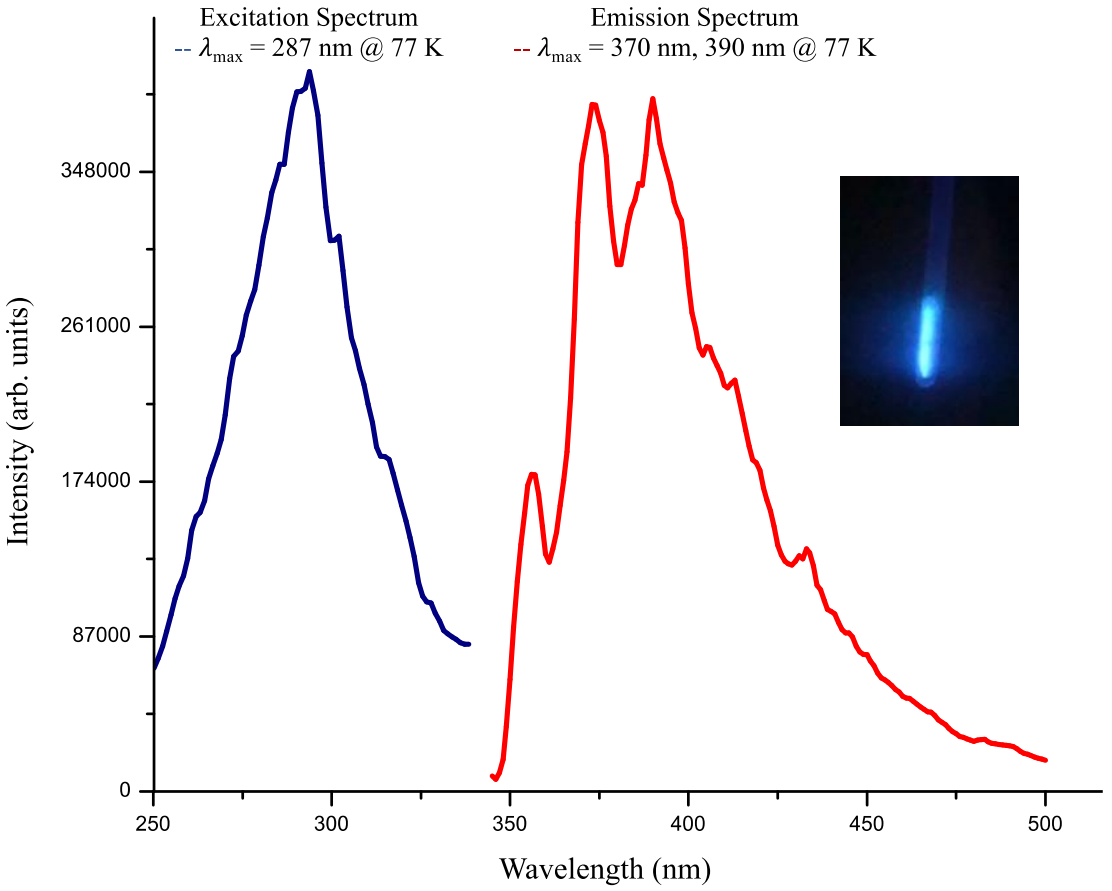

Figure B20: Luminescence Spectrum of $\{[(3,5\text{-}(CO_2Et)_2Pz]Ag\}_3$ at 77 K.

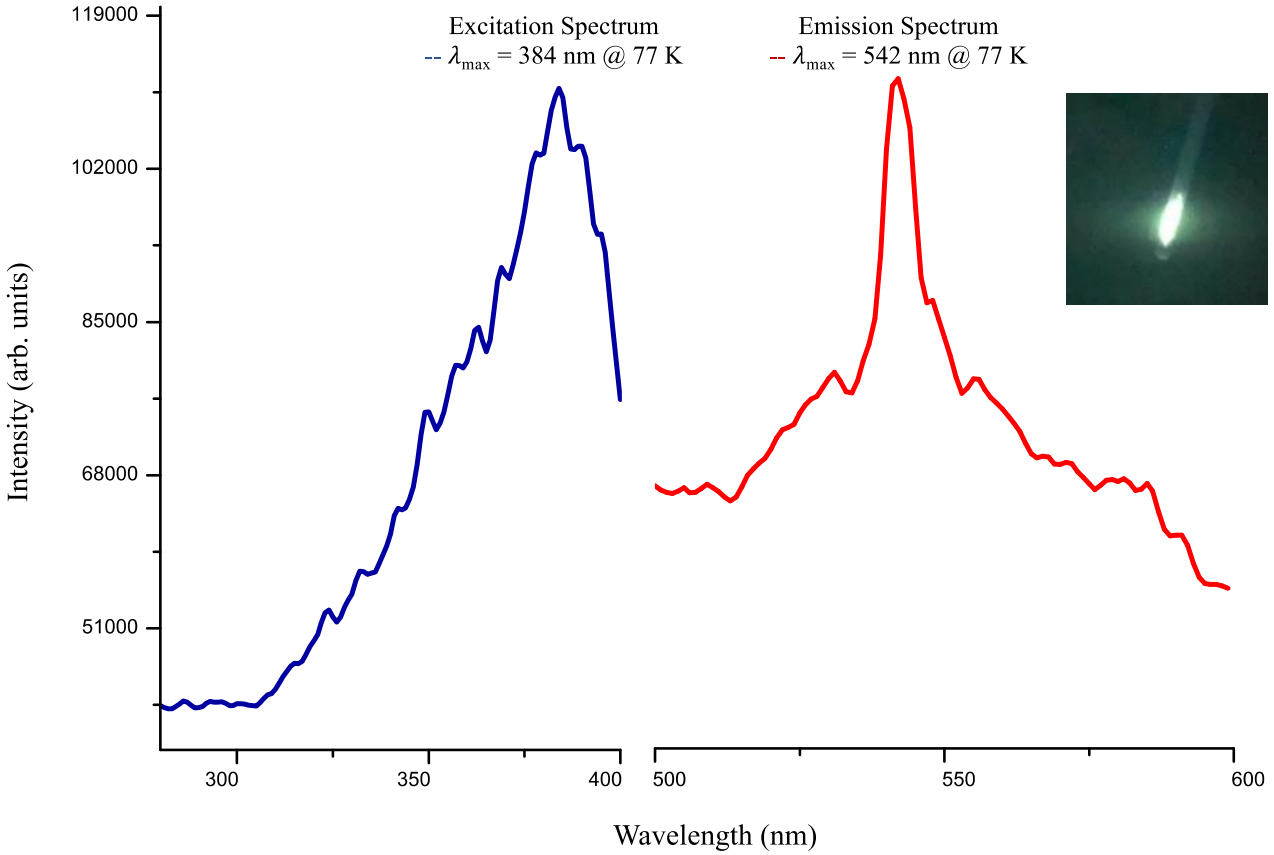

Figure B21: Luminescence Spectrum of $\{[(4\text{-Br-}3,5\text{-}(CO_2Et)_2Pz]Ag\}_3$ at 77 K.

`

Appendix C

Spectroscopic data of chapter 4

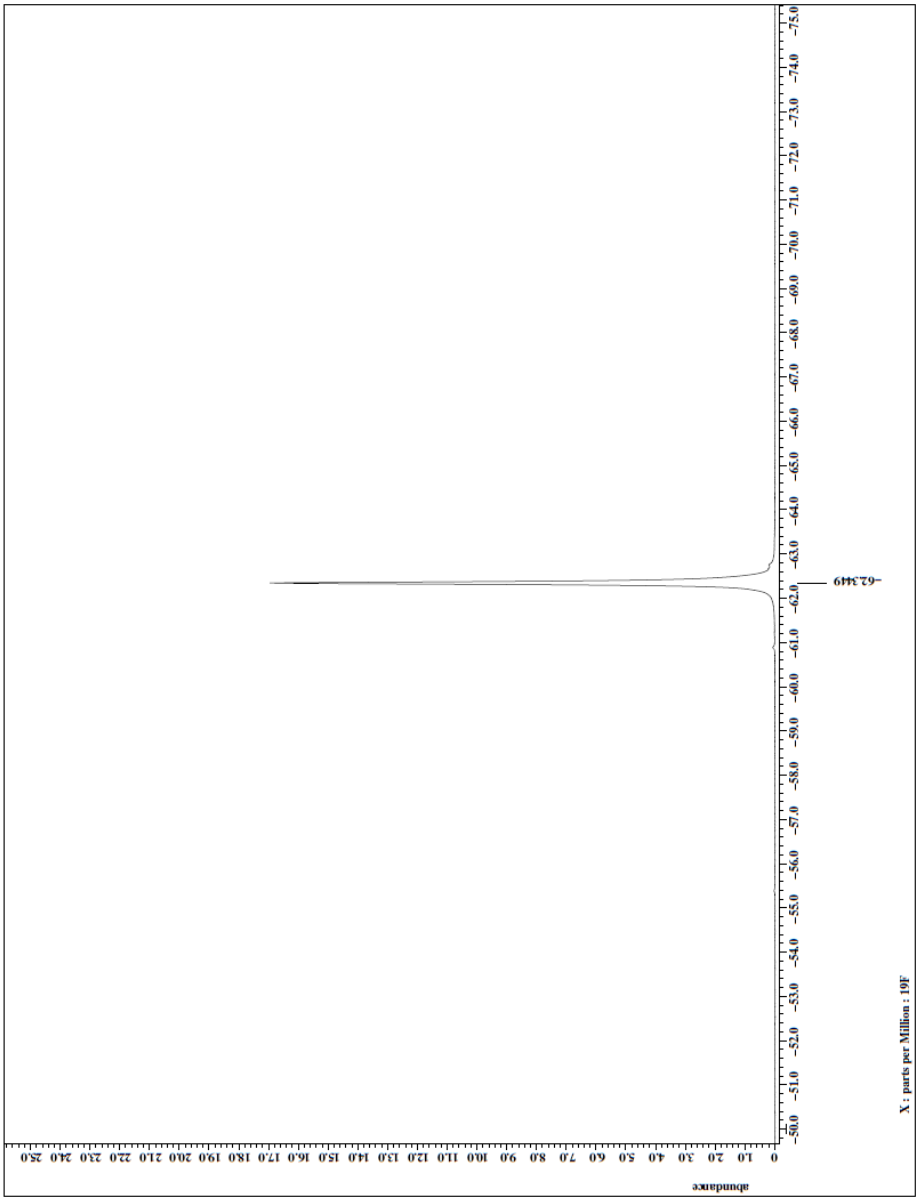

Figure C1: ^{19}F NMR spectrum of $\{[4\text{-}NO_2,3,5\text{-}(CF_3)_2Pz]Cu\}_3$ in $(CD_3)_2CO$.

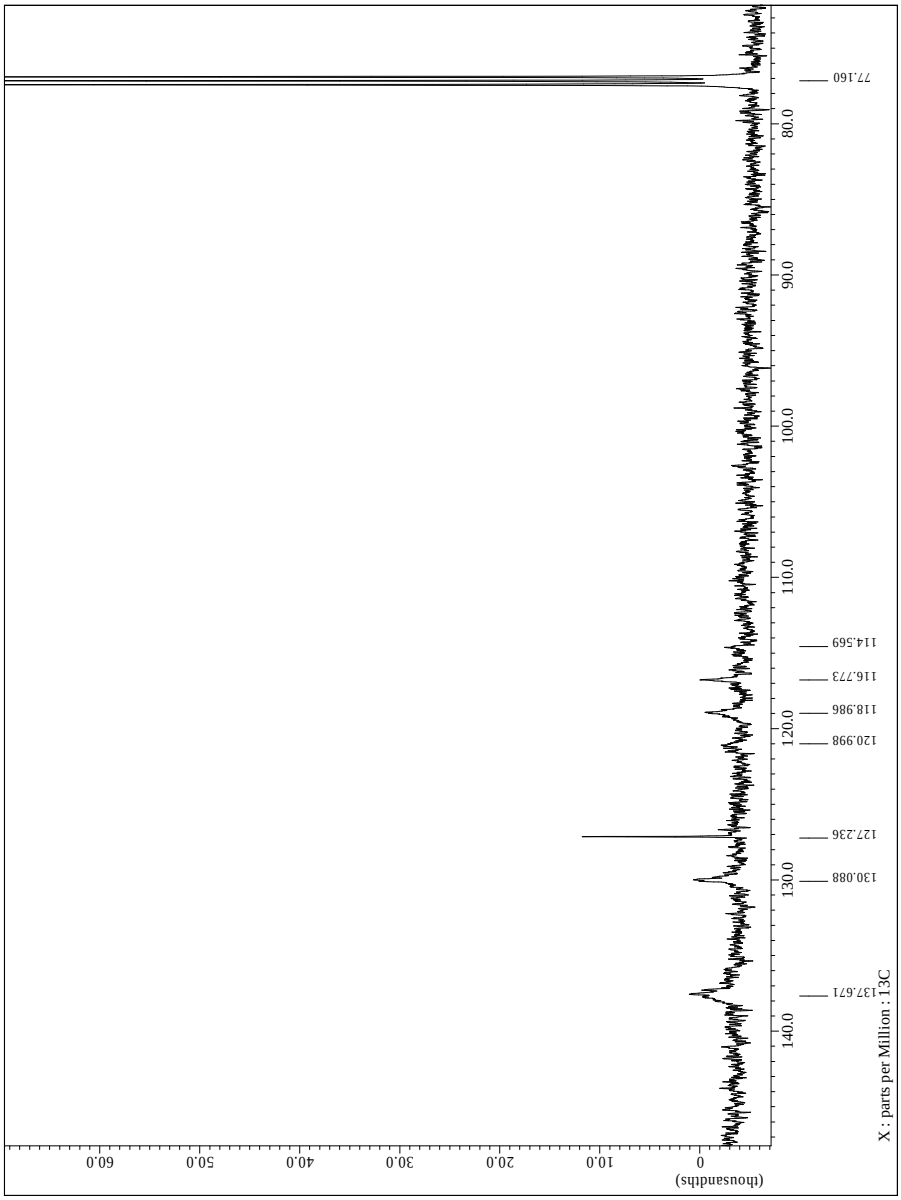

Figure C2: ^{13}C NMR spectrum of {[4-NO_2,3,5-$(CF_3)_2$Pz]Cu}$_3$ in $CDCl_3$/THF 1:1.

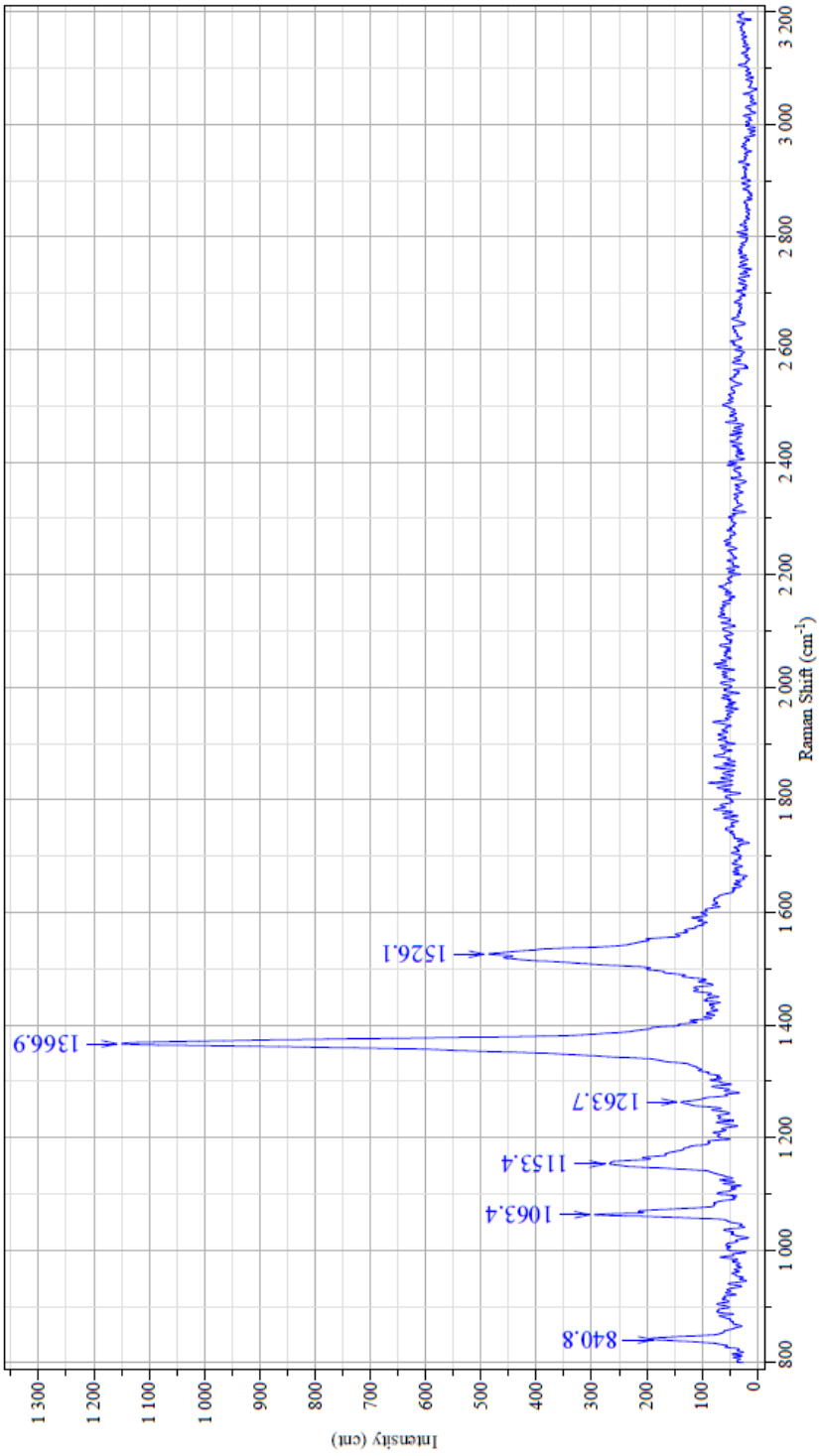

Figure C3: Raman spectrum of {[4-NO_2,3,5-$(CF_3)_2$Pz]Cu}$_3$.

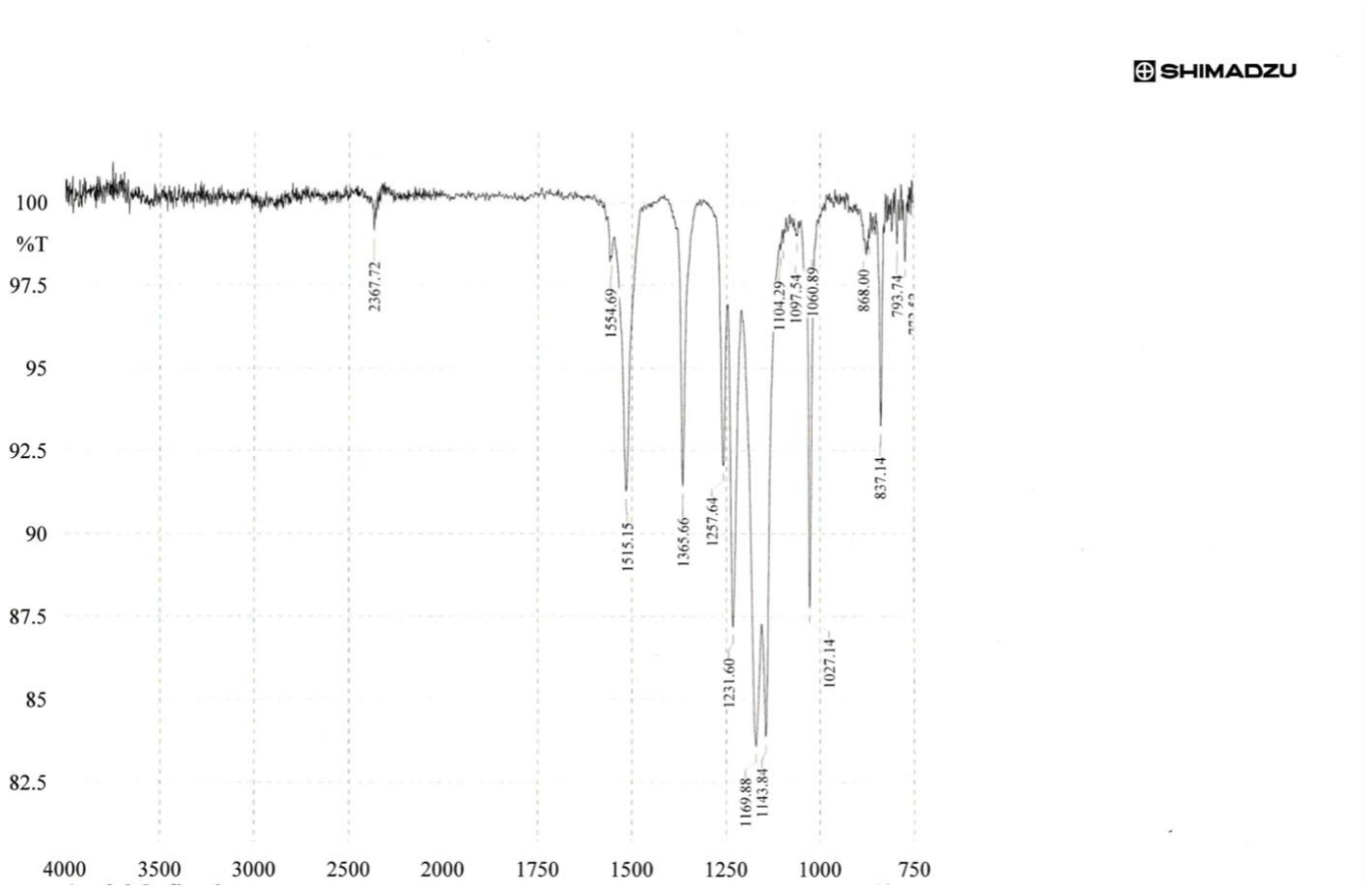

Figure C4: IR spectrum of {[4-NO_2,3,5-$(CF_3)_2$Pz]Cu}$_3$.

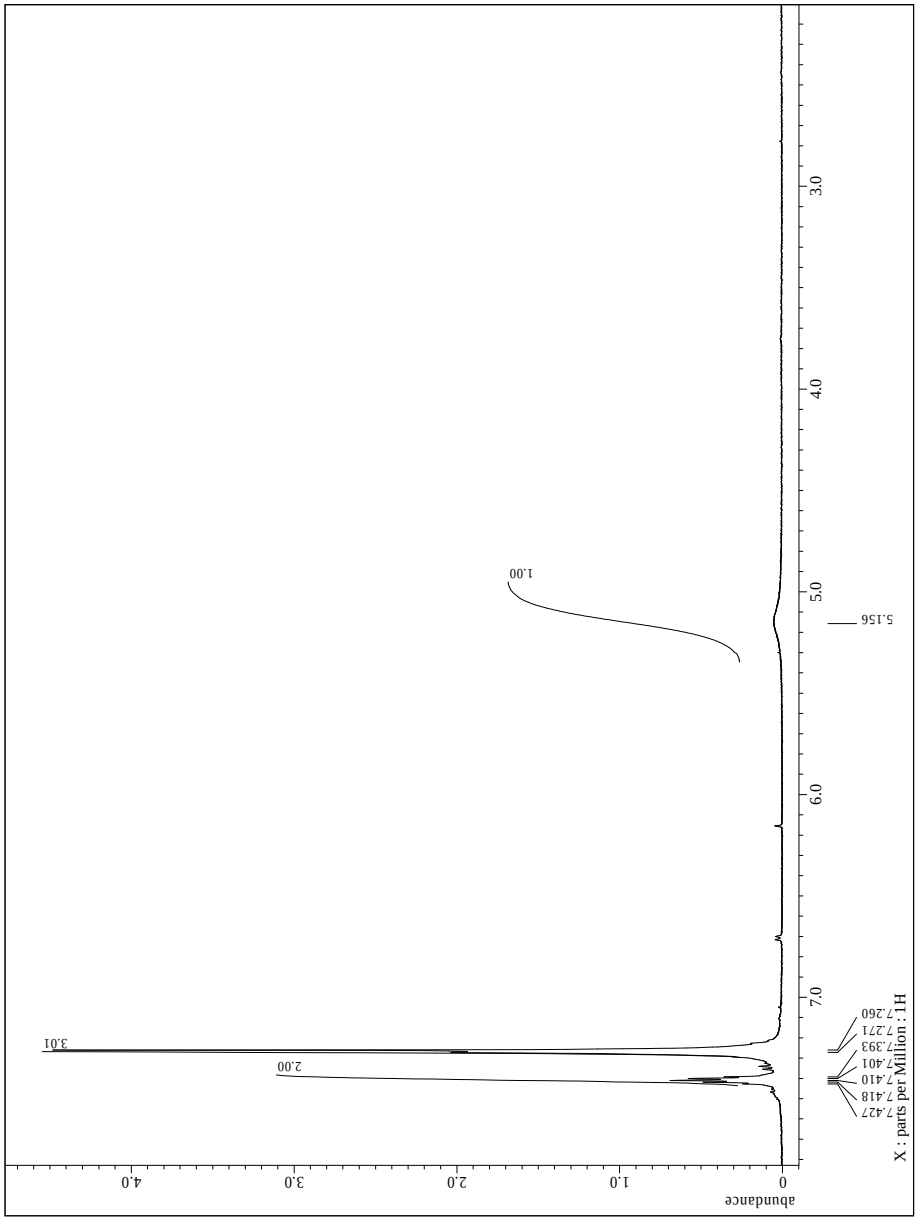

Figure C5: ^{1}H NMR spectrum of Cu2(μ-[4-NO_2-3,5-$(CF_3)_2$Pz])$_2$(HC≡CPh)$_2$ in $CDCl_3$.

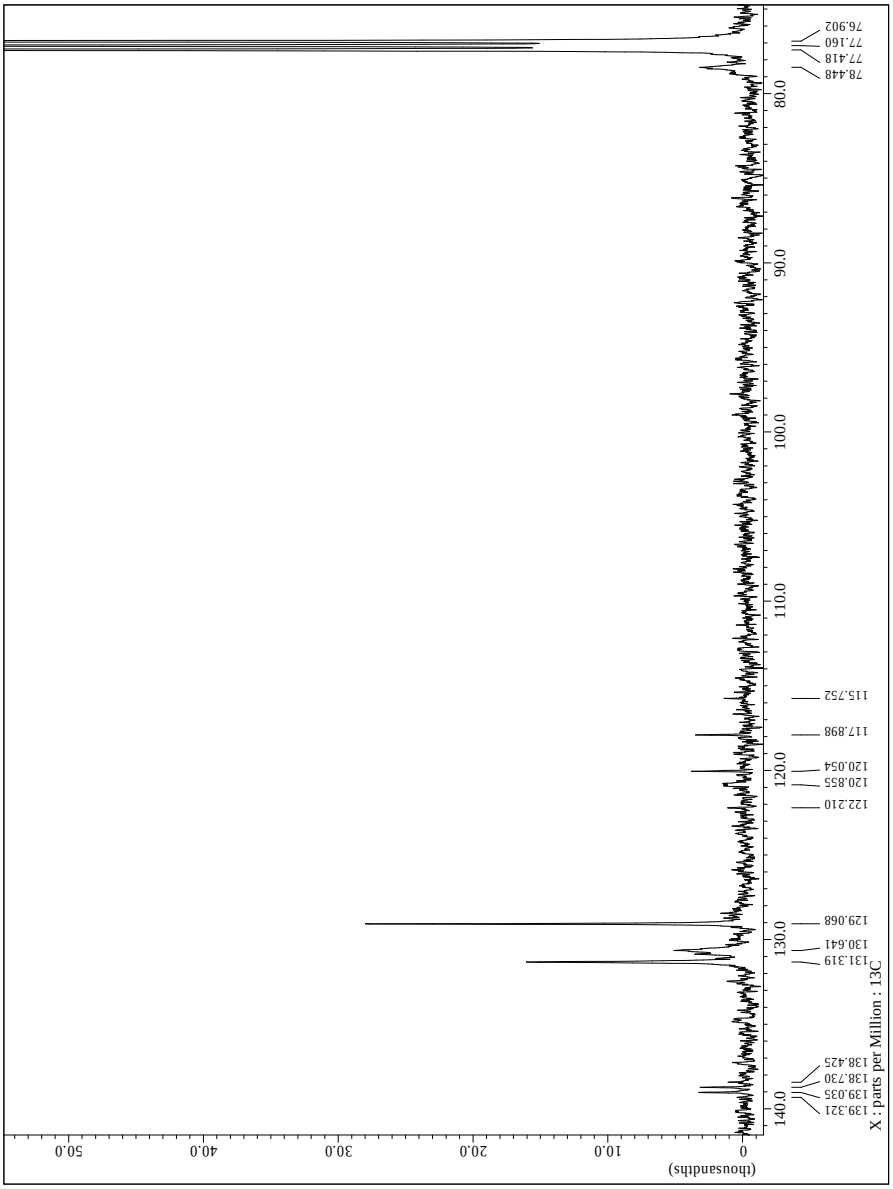

Figure C6: $^{13}C\{^{1}H\}$ NMR spectrum of $Cu_2(\mu\text{-}[4\text{-}NO_2\text{-}3,5\text{-}(CF_3)_2Pz])_2(HC{\equiv}CPh)_2$ in $CDCl_3$.

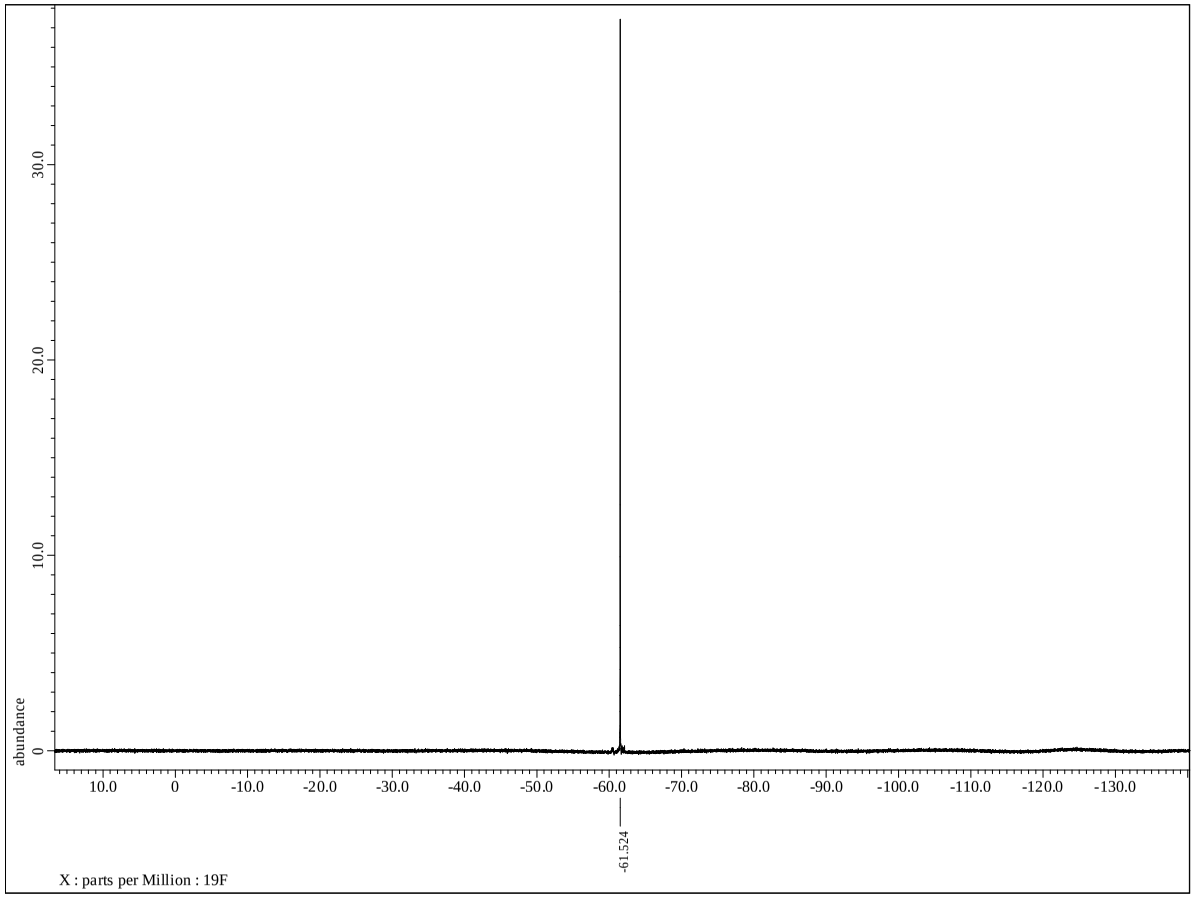

Figure C7: ^{19}F NMR spectrum of $Cu_2(\mu\text{-}[4\text{-}NO_2\text{-}3,5\text{-}(CF_3)_2Pz])_2(HC{\equiv}CPh)_2$ in $CDCl_3$.

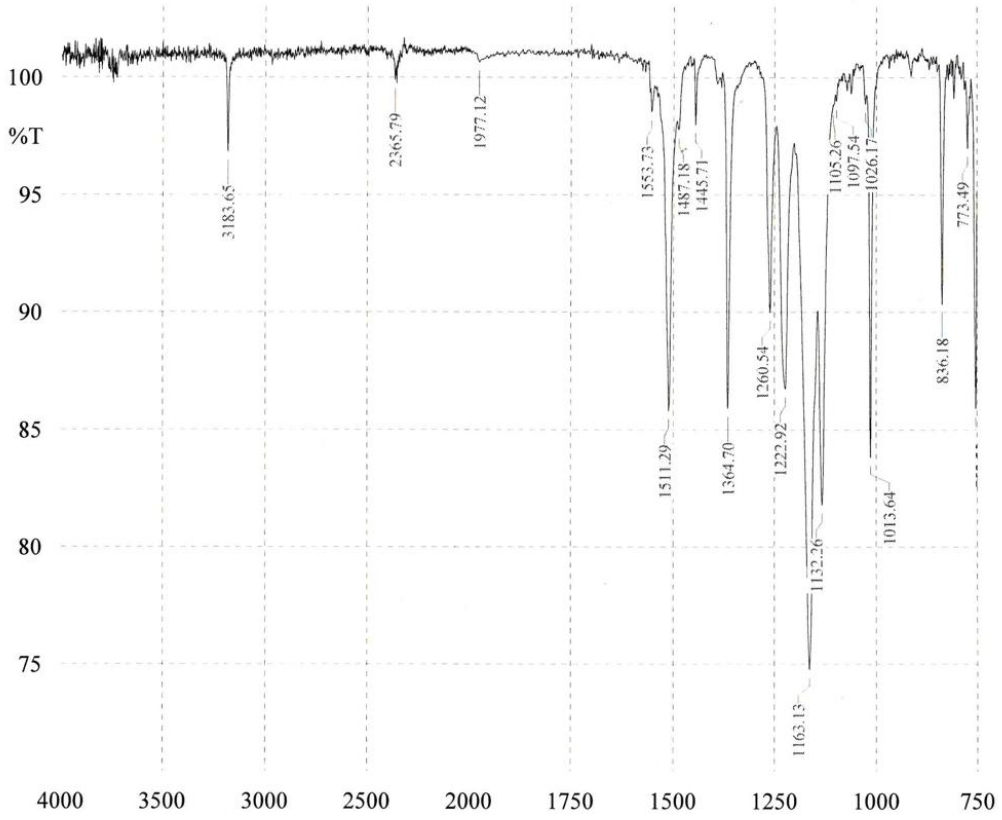

Figure C8: IR spectrum of $Cu_2(\mu\text{-}[4\text{-}NO_2\text{-}3,5\text{-}(CF_3)_2Pz])_2(HC{\equiv}CPh)_2$.

`

Appendix D

Spectroscopic data of chapter 5.1

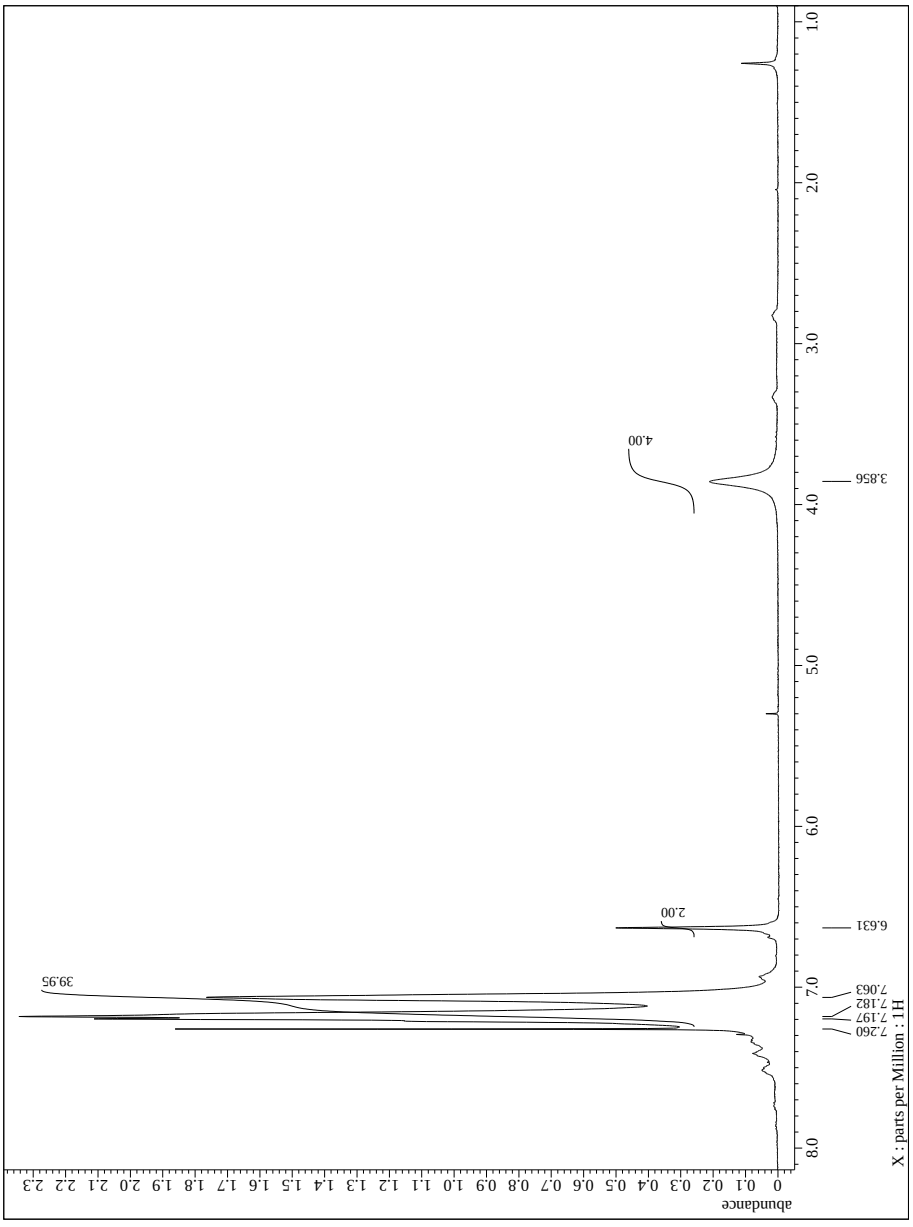

Figure D1: ^{1}H NMR spectrum of {Cu[3,5-$(CF_3)_2$Pz](μ-dppm)}$_2$.

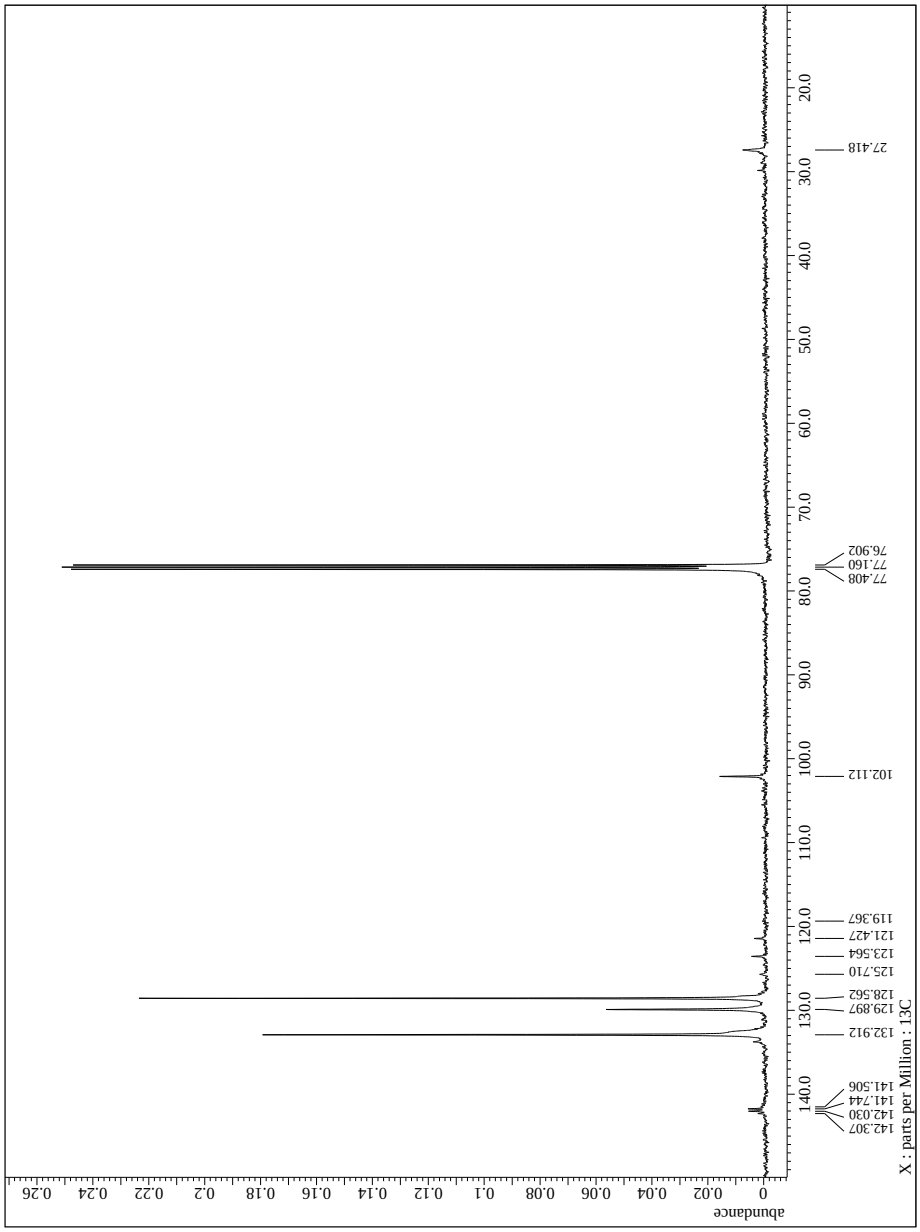

Figure D2: $^{13}C\{^{1}H\}$ NMR spectrum of $\{Cu[3,5\text{-}(CF_3)_2Pz](\mu\text{-dppm})\}_2$.

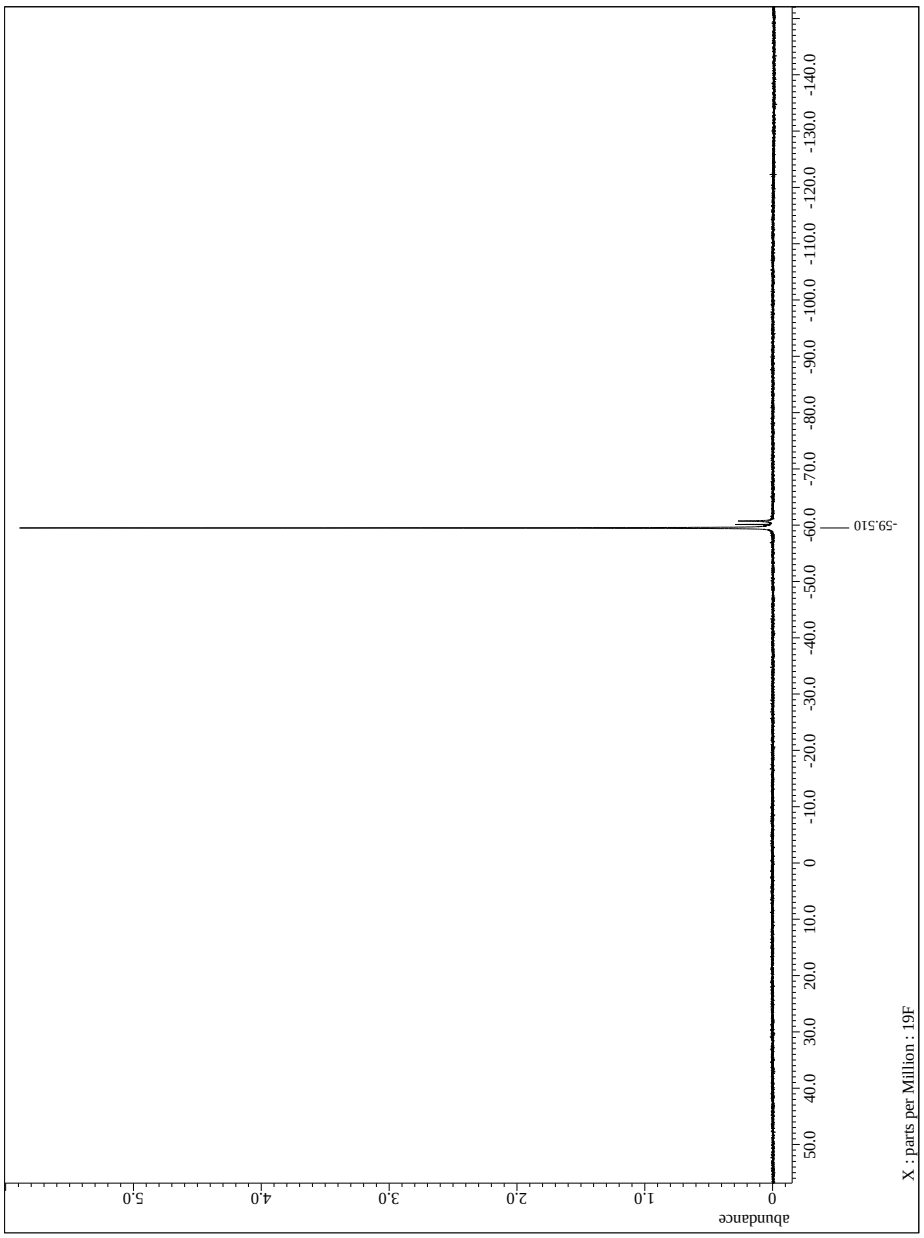

Figure D3: ^{19}F NMR spectrum of {Cu[3,5-$(CF_3)_2$Pz](μ-dppm)}$_2$.

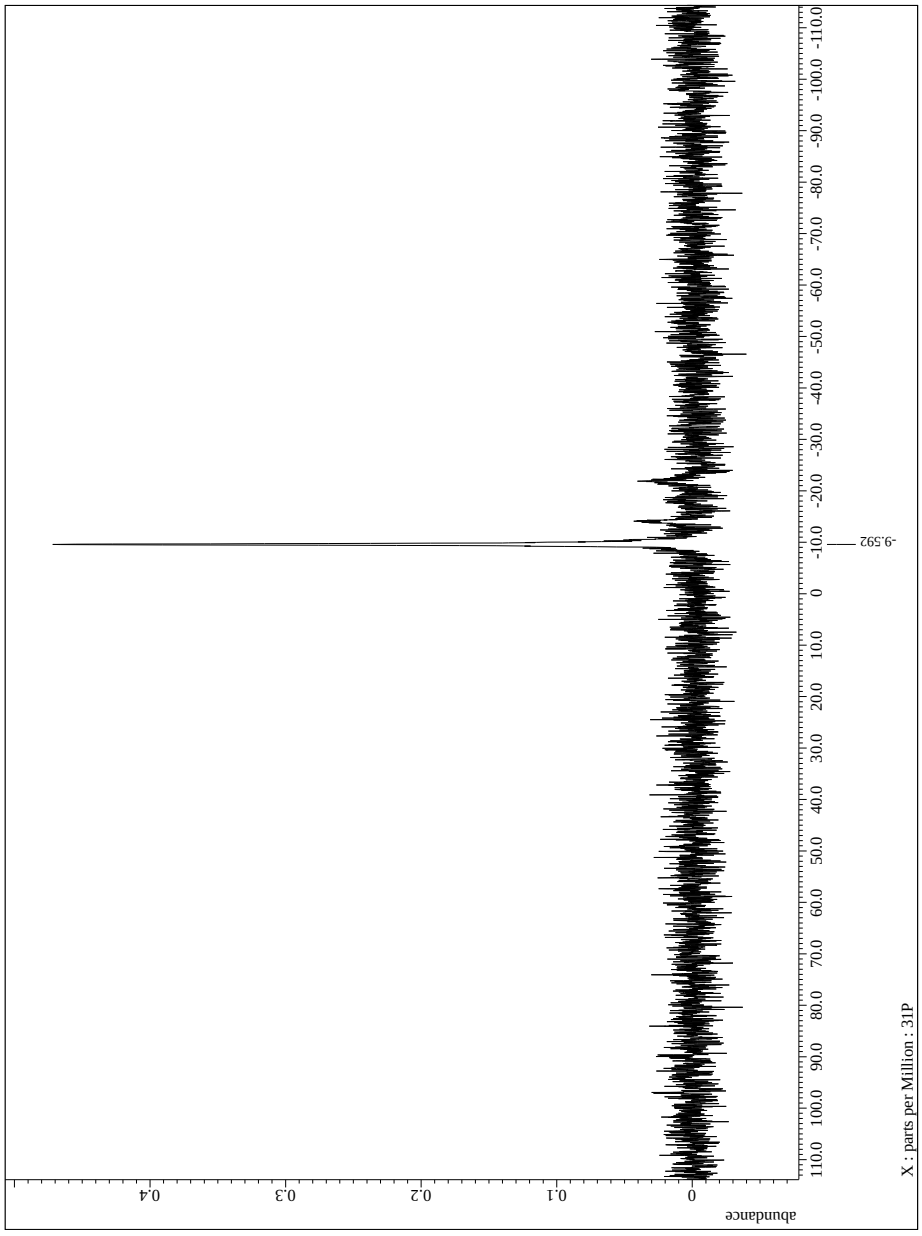

Figure D4: $^{31}P\{^{1}H\}$ NMR spectrum of $\{Cu[3,5\text{-}(CF_3)_2Pz](\mu\text{-dppm})\}_2$.

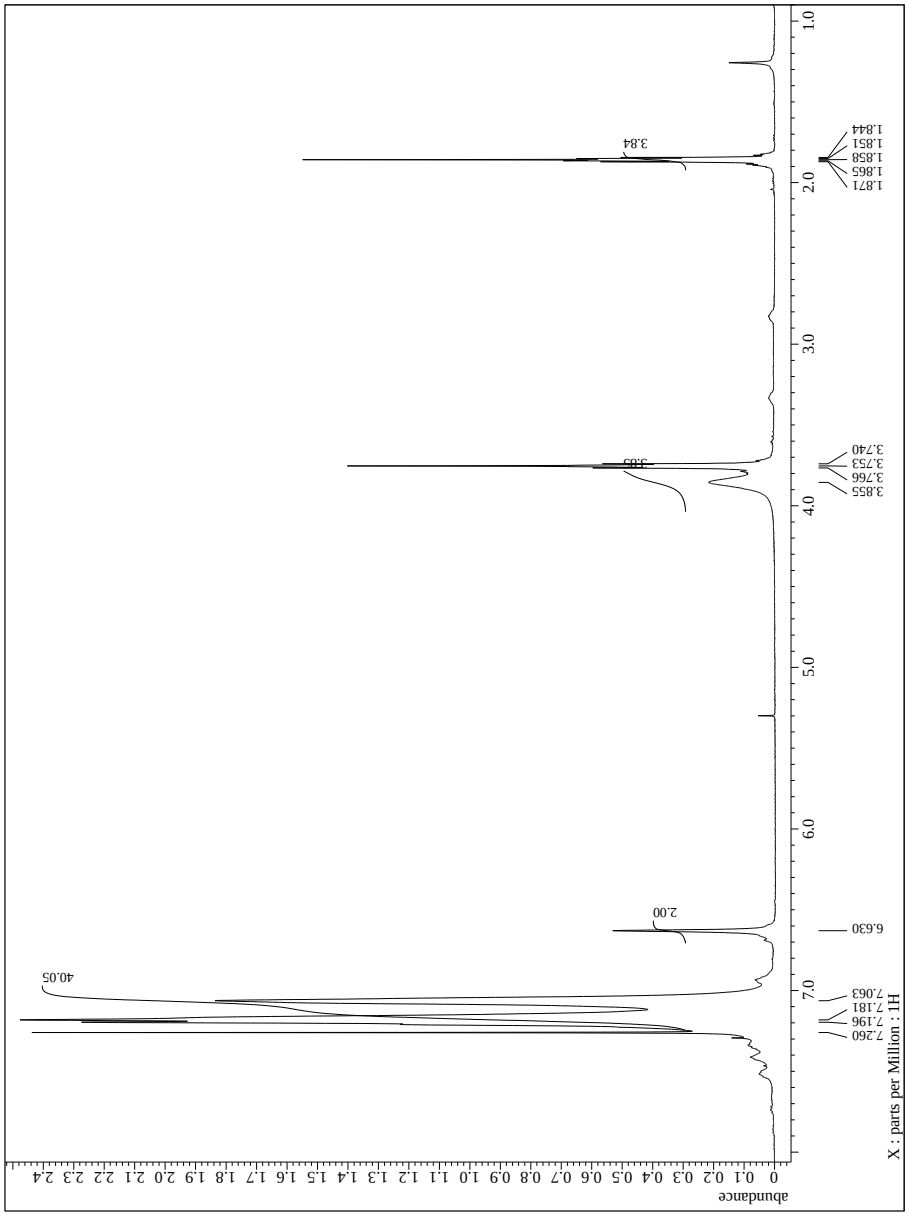

Figure D5: ^{1}H NMR spectrum of $\{Cu[3,5\text{-}(CF_3)_2Pz](\mu\text{-dppm})\}_2 \bullet 3THF$.

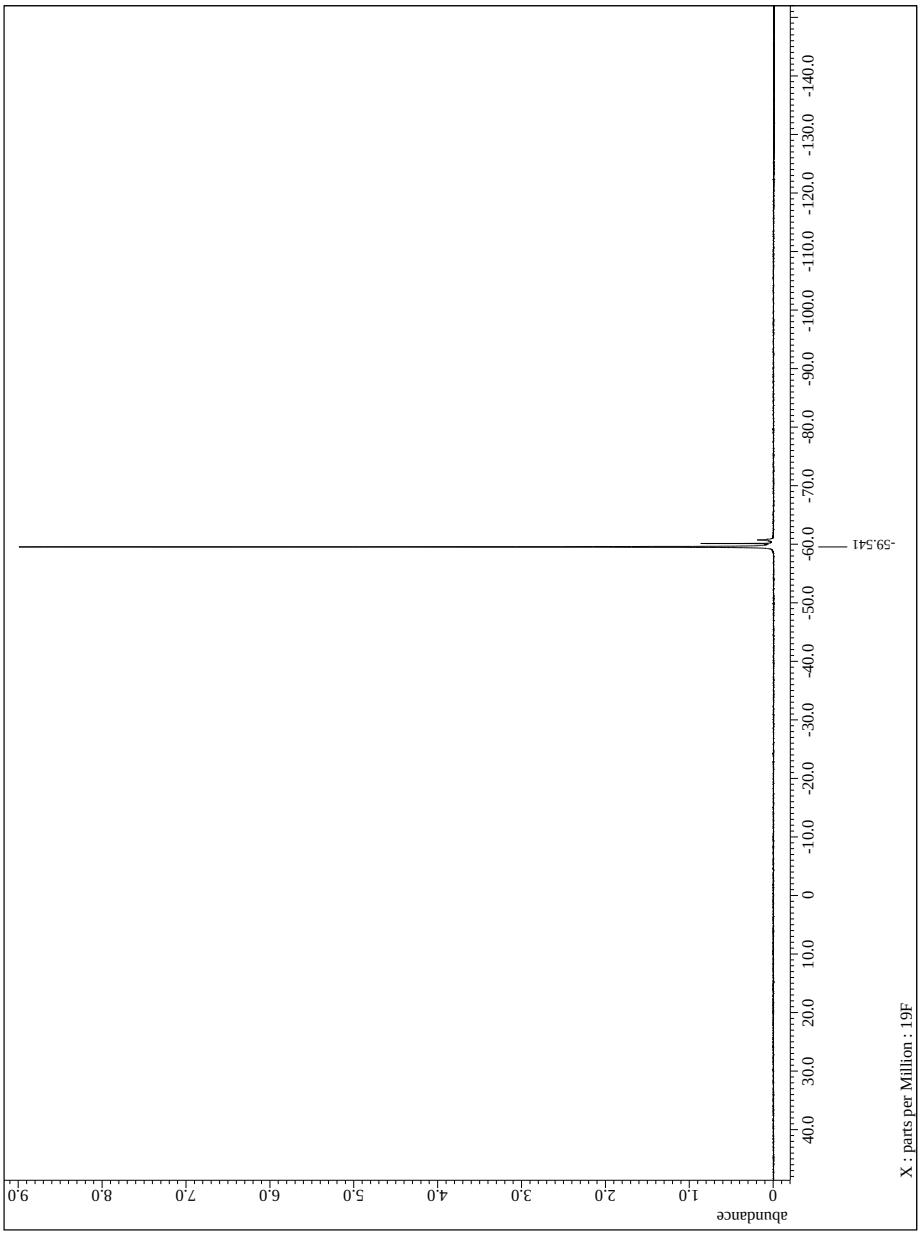

Figure D6: ^{19}F NMR spectrum of {Cu[3,5-$(CF_3)_2$Pz](μ-dppm)}$_2$•3THF.

`

Biographical Information

Monika Patterson was born in Arlington, Texas. She completed her high school education at Fort Worth Christian School in North Richland Hills, Texas in 2013. After high school she attended Texas Christian University where she received a Bachelors of Science in Chemistry with a minor in Spanish in 2017. She joined the Ph.D. graduate program in Chemistry at the University of Texas at Arlington in the fall of 2017 and joined Professor Rasika Dias' group in the spring semester of 2018. She completed her doctoral degree in inorganic chemistry in fall of 2021 and will start her industrial career at Uniwell Laboratories, a nutraceutical company, in Fort Worth, Texas as a Product Development Scientist in December of 2021.

`

References

1. P. K. Mykhailiuk, *Chemical Reviews*, 2021, **121**, 1670-1715.
2. D. W. Mariano Grünebaum and Annika Buchheit and Christina Günther and Hans, *Tetrahedron Letters*, 2016, **57**, 1555-1559.
3. M. G. La and G. Ardizzoia, *Prog. Inorg. Chem*, 1997, **46**, 151-238.
4. M. A. Halcrow, *Dalton Trans.*, 2009, 2059-2073.
5. H. V. R. Dias, H. V. Diyabalanage, M. G. Eldabaja, O. Elbjeirami, M. A. Rawashdeh-Omary and M. A. Omary, *Journal of the American Chemical Society*, 2005, **127**, 7489-7501.
6. K. Fujisawa, Y. Ishikawa, Y. Miyashita and K.-i. Okamoto, *Inorganica Chimica Acta*, 2010, **363**, 2977-2989.
7. K. Fujisawa, Y. Ishikawa, Y. Miyashita and K.-i. Okamoto, *Chemistry Letters*, 2004, **33**, 66-67.
8. G. Yang and R. G. Raptis, *Inorg. Chim. Acta*, 2007, **360**, 2503-2506.
9. H. H. Murray, R. G. Raptis and J. P. Fackler, Jr., *Inorg. Chem.*, 1988, **27**, 26-33.
10. K. a. I. Y. a. M. Y. a. O. K.-i. Fujisawa, *Chemistry Letters*, 2004, **33**, 66-67.
11. A. Maspero, S. Brenna, S. Galli and A. Penoni, *Journal of Organometallic Chemistry*, 2003, **672**, 123-129.
12. H. V. R. Dias, S. A. Polach and Z. Wang, *Journal of Fluorine Chemistry*, 2000, **103**, 163-169.
13. H. V. R. Dias, C. S. P. Gamage, J. Keltner, H. V. K. Diyabalanage, I. Omari, Y. Eyobo, N. R. Dias, N. Roehr, L. McKinney and T. Poth, *Inorg. Chem.*, 2007, **46**, 2979-2987.
14. H. V. R. Dias, H. V. K. Diyabalanage, M. A. Rawashdeh-Omary, M. A. Franzman and M. A. Omary, *Journal of the American Chemical Society*, 2003, **125**, 12072-12073.
15. H. V. R. Dias and H. V. K. Diyabalanage, *Polyhedron*, 2006, **25**, 1655-1661.
16. X.-P. Lv, D.-H. Wei and G. Yang, *Inorg. Chem.*, 2017, **56**, 11310-11316.
17. B. Chilukuri, R. N. McDougald, M. M. Ghimire, V. N. Nesterov, U. Mazur, M. A. Omary and K. W. Hipps, *The Journal of Physical Chemistry C*, 2015, **119**, 24844-24858.
18. C. V. Hettiarachchi, M. A. Rawashdeh-Omary, D. Korir, J. Kohistani, M. Yousufuddin and H. R. Dias, *Inorganic chemistry*, 2013, **52**, 13576-13583.
19. N. B. Jayaratna, M. G. Cowan, D. Parasar, H. H. Funke, J. Reibenspies, P. K. Mykhailiuk, O. Artamonov, R. D. Noble and H. R. Dias, *Angewandte Chemie*, 2018, **130**, 16680-16684.
20. M. A. Omary, M. A. Rawashdeh-Omary, M. A. Gonser, O. Elbjeirami, T. Grimes, T. R. Cundari, H. V. Diyabalanage, C. S. P. Gamage and H. R. Dias, *Inorganic chemistry*, 2005, **44**, 8200-8210.
21. M. W. Dodge, W. F. Wacholtz and J. T. Mague, *Journal of Chemical Crystallography*, 2005, **35**, 5-12.

`

22. H. V. R. Dias, H. V. K. Diyabalanage, M. M. Ghimire, J. M. Hudson, D. Parasar, C. S. P. Gamage, S. Li and M. A. Omary, *Dalton Transactions*, 2019, 14979-14983.
23. N. B. Jayaratna, M. M. Olmstead, B. I. Kharisov and H. V. R. Dias, *Inorg. Chem.*, 2016, **55**, 8277-8280.
24. N. B. Jayaratna, C. V. Hettiarachchi, M. Yousufuddin and H. V. R. Dias, *New J. Chem.*, 2015, **39**, 5092-5095.
25. D. Parasar, R. M. Almotawa, N. B. Jayaratna, Y. S. Ceylan, T. R. Cundari, M. A. Omary and H. R. Dias, *Organometallics*, 2018, **37**, 4105-4118.
26. D. Parasar, T. T. Ponduru, A. Noonikara-Poyil, N. B. Jayaratna and H. R. Dias, *Dalton Transactions*, 2019, **48**, 15782-15794.
27. D. Parasar, N. B. Jayaratna, A. Muñoz-Castro, A. E. Conway, P. K. Mykhailiuk and H. R. Dias, *Dalton Transactions*, 2019, **48**, 6358-6371.
28. D. Parasar, A. H. Elashkar, A. A. Yakovenko, N. B. Jayaratna, B. L. Edwards, S. G. Telfer, H. R. Dias and M. G. Cowan, *Angewandte Chemie International Edition*, 2020, **59**, 21001-21006.
29. A. Bondi, *J. Phys. Chem. A*, 1964, **68**, 441-451.
30. C. Hansch, A. Leo and R. Taft, *Chemical reviews*, 1991, **91**, 165-195.
31. J. S. Lakhi, M. R. Patterson and H. R. Dias, *New Journal of Chemistry*, 2020, **44**, 14814-14822.
32. R. Galassi, M. A. Rawashdeh-Omary, H. V. R. Dias and M. A. Omary, *Comments Inorg. Chem.*, 2019, **39**, 287-348.
33. J. Zheng, H. Yang, M. Xie and D. Li, *Chemical Communications*, 2019, 7134-7146.
34. J.-P. Zhang, Y.-B. Zhang, J.-B. Lin and X.-M. Chen, *Chemical Reviews*, 2012, **112**, 1001-1033.
35. P. Pyykkö, N. Runeberg and F. Mendizabal, *Chemistry – A European Journal*, 1997, **3**, 1451-1457.
36. F. Meyer, A. Jacobi and L. Zsolnai, *Chemische Berichte*, 1997, **130**, 1441-1447.
37. A. Titov, A., O. A. Filippov, L. M. Epstein, N. V. Belkova and E. S. Shubina, *Inorganica Chimica Acta*, 2018, **470**, 22-35.
38. A. C. Jahnke, K. Pröpper, C. Bronner, J. Teichgräber, S. Dechert, M. John, O. S. Wenger and F. Meyer, *Journal of the American Chemical Society*, 2012, **134**, 2938-2941.
39. A. A. Mohamed, A. Burini and J. P. Fackler, *Journal of the American Chemical Society*, 2005, **127**, 5012-5013.
40. B. Tu, Q. Pang, H. Xu, X. Li, Y. Wang, Z. Ma, L. Weng and Q. Li, *Journal of the American Chemical Society*, 2017, **139**, 7998-8007.
41. J.-P. Zhang and S. Kitagawa, *Journal of the American Chemical Society*, 2008, **130**, 907-917.
42. R. Hahn, F. Bohle, W. Fang, A. Walther, S. Grimme and B. Esser, *Journal of the American Chemical Society*, 2018, **140**, 17932-17944.
43. A. Kishimura, T. Yamashita, K. Yamaguchi and T. Aida, *Nat. Mater.*, 2005, **4**, 546-549.
44. G. A. Ardizzoia, S. Cenini, G. La Monica, N. Masciocchi, A. Maspero and M. Moret, *Inorg. Chem.*, 1998, **37**, 4284-4292.

`

45. A. A. Titov, V. A. Larionov, A. F. Smol'yakov, M. I. Godovikova, E. M. Titova, V. I. Maleev and E. S. Shubina, *Chemical Communications*, 2019, **55**, 290-293.
46. G. A. Ardizzoia, S. Cenini, G. La Monica, N. Masciocchi and M. Moret, *Inorg. Chem.*, 1994, **33**, 1458-1463.
47. N. Masciocchi, M. Moret, P. Cairati, A. Sironi, G. A. Ardizzoia and G. La Monica, *J. Am. Chem. Soc.*, 1994, **116**, 7668-7676.
48. Y. Morishima, D. J. Young and K. Fujisawa, *Dalton Trans.*, 2014, **43**, 15915-15928.
49. C. R. Groom, I. J. Bruno, M. P. Lightfoot and S. C. Ward, *Acta Cryst., Section B*, 2016, **72**, 171-179.
50. R. G. Raptis and J. P. Fackler, *Inorg. Chem.*, 1988, **27**, 4179-4182.
51. J.-H. Chen, D. Wei, G. Yang, J.-G. Ma and P. Cheng, *Dalton Trans.*, 2020, **49**, 1116-1123.
52. J.-H. Chen, Y.-M. Liu, J.-X. Zhang, Y.-Y. Zhu, M.-S. Tang, S. W. Ng and G. Yang, *CrystEngComm*, 2014, **16**, 4987-4998.
53. G. Yang, P. Baran, A. R. Martinez and R. G. Raptis, *Cryst. Growth Des.*, 2013, **13**, 264-269.
54. M. A. Omary, M. A. Rawashdeh-Omary, H. V. K. Diyabalanage and H. V. R. Dias, *Inorg. Chem.*, 2003, **42**, 8612-8614.
55. H. V. R. Dias, S. A. Richey, H. V. K. Diyabalanage and J. Thankamani, *J. Organomet. Chem.*, 2005, **690**, 1913-1922.
56. M. A. Rawashdeh-Omary, M. D. Rashdan, S. Dharanipathi, O. Elbjeirami, P. Ramesh and H. V. R. Dias, *Chem. Commun.*, 2011, **47**, 1160-1162.
57. D. M. M. Krishantha, C. S. P. Gamage, Z. A. Schelly and H. V. R. Dias, *Inorganic Chemistry*, 2008, **47**, 7065-7067.
58. I. Alkorta, J. Elguero, H. V. R. Dias, D. Parasar and M. Martin-Pastor, *Magn. Reson. Chem.*, 2020, **58**, 319-328.
59. H. V. R. Dias and C. S. Palehepitiya Gamage, *Angew. Chem., Int. Ed.*, 2007, **46**, 2192-2194.
60. M. A. Omary, O. Elbjeirami, C. S. P. Gamage, K. M. Sherman and H. V. R. Dias, *Inorg. Chem.*, 2009, **48**, 1784-1786.
61. R. M. Almotawa, G. Aljomaih, D. V. Trujillo, V. N. Nesterov and M. A. Rawashdeh-Omary, *Inorg. Chem.*, 2018, **57**, 9962-9976.
62. R. Galassi, M. M. Ghimire, B. M. Otten, S. Ricci, R. N. McDougald, R. M. Almotawa, D. Alhmoud, J. F. Ivy, A.-M. M. Rawashdeh, V. N. Nesterov, E. W. Reinheimer, L. M. Daniels, A. Burini and M. A. Omary, *P. Nat. Acad. Sci. USA*, 2017, **114**, E5042-E5051.
63. Y. Chi, E. Lay, T.-Y. Chou, Y.-H. Song and A. J. Carty, *Chem. Vap. Deposition*, 2005, **11**, 206-212.
64. K. Kumpan, A. Nathubhai, C. Zhang, P. J. Wood, M. D. Lloyd, A. S. Thompson, T. Haikarainen, L. Lehtiö and M. D. Threadgill, *Bioorg. Med. Chem.*, 2015, **23**, 3013-3032.
65. F. Aguilar-Parrilla, G. Scherer, H. H. Limbach, M. d. l. C. Foces-Foces, F. Hernandez Cano, J. A. S. Smith, C. Toiron and J. Elguero, *J. Am. Chem. Soc.*, 1992, **114**, 9657-9659.
66. C. Foces-Foces, I. Alkorta and J. Elguero, *Acta Cryst. Section B*, 2000, **56**, 1018-1028.

`

67. R. M. Claramunt, P. Cornago, V. Torres, E. Pinilla, M. R. Torres, A. Samat, V. Lokshin, M. Valés and J. Elguero, *J. Org. Chem.*, 2006, **71**, 6881-6891.
68. Q. Wang, L. He, K. K. Li and G. C. Tsui, *Org. Lett.*, 2017, **19**, 658-661.
69. L. R. Kadel, J. R. Kromer, C. E. Moore and D. M. Eichhorn, *Polyhedron*, 2017, **125**, 206-218.
70. B. Willy and T. J. J. Müller, *Eur. J. Org. Chem.*, 2008, **2008**, 4157-4168.
71. M. Tang, W. Zhang and Y. Kong, *Org. Biomol. Chem.*, 2013, **11**, 6250-6254.
72. B. Aegurla and R. K. Peddinti, *Org. Biomol. Chem.*, 2017, **15**, 9643-9652.
73. H. S. Jena, C. Krishnaraj, J. Schmidt, K. Leus, K. Van Hecke and P. Van Der Voort, *Chem. Eur. J.*, 2020, **26**, 1548-1557.
74. A. A. Mohamed, L. M. Perez and J. P. Fackler, *Inorg. Chim. Acta*, 2005, **358**, 1657-1662.
75. S. Alvarez, *Dalton Trans.*, 2013, **42**, 8617-8636.
76. B. Cordero, V. Gomez, A. E. Platero-Prats, M. Reves, J. Echeverria, E. Cremades, F. Barragan and S. Alvarez, *Dalton Trans.*, 2008, 2832-2838.
77. C. W. Tornøe, C. Christensen and M. Meldal, *J. Org. Chem.*, 2002, **67**, 3057-3064.
78. V. V. Rostovtsev, L. G. Green, V. V. Fokin and K. B. Sharpless, *Angew. Chem., Int. Ed.*, 2002, **41**, 2596-2599.
79. J. E. Moses and A. D. Moorhouse, *Chem. Soc. Rev.*, 2007, **36**, 1249-1262.
80. H. Lang, A. Jakob and B. Milde, *Organometallics*, 2012, **31**, 7661-7693.
81. C. Wang, D. Ikhlef, S. Kahlal, J.-Y. Saillard and D. Astruc, *Coord. Chem. Rev.*, 2016, **316**, 1-20.
82. J. E. Hein and V. V. Fokin, *Chem. Soc. Rev.*, 2010, **39**, 1302-1315.
83. A. Caballero, A. Prieto, M. M. Diaz-Requejo and P. J. Perez, *Eur. J. Inorg. Chem.*, 2009, 1137-1144.
84. W. Wu, Z. Lin and H. Jiang, *Org. Biomol. Chem.*, 2018, **16**, 7315-7329.
85. J. A. Hirsch, *Topics in Stereochemistry*, 1967, 199-222.
86. T. M. Laine, M. D. Karkas, R.-Z. Liao, T. Akermark, B.-L. Lee, E. A. Karlsson, P. E. Siegbahn and B. Akermark, *Chemical Communications*, 2014, **51**, 1862-1865.
87. B. G. a. D. M. a. S. T. a. G. P. a. A. P. Angelo Maspero and Giovanni, *Journal of Fluorine Chemistry*, 2012, **139**, 53-57.
88. R. Huisgen, G. Szeimies and L. Möbius, *Chemische Berichte*, 1967, **100**, 2494-2507.
89. M. Meldal and C. W. Tornøe, *Chemical Reviews*, 2008, **108**, 2952-3015.
90. H. C. Kolb, M. G. Finn and K. B. Sharpless, *Angewandte Chemie International Edition*, 2001, **40**, 2004-2021.

`

91. V. A. Larionov, A. R. Stashneva, A. A. Titov, A. A. Lisov, M. G. Medvedev, A. F. Smol'yakov, A. M. Tsedilin, E. S. Shubina and V. I. Maleev, *Journal of Catalysis*, 2020, **390**, 37-45.
92. M. Patterson and R. Dias, *Dalton Transactions*, 2021.
93. D. Dheer, V. Singh and R. Shankar, *Bioorganic Chemistry*, 2017, **71**, 30-54.
94. Y. H. Lau, P. J. Rutledge, M. Watkinson and M. H. Todd, *Chemical Society Reviews*, 2011, 2848-2866.
95. A. H. El-Sagheer and T. Brown, *Accounts of Chemical Research*, 2012, **45**, 1258-1267.
96. M. Breugst and H.-U. Reissig, *Angewandte Chemie International Edition*, 2020, **59**, 12293-12307.
97. C. W. Tornøe and M. Meldal, in *Peptides: The Wave of the Future*, Springer, 2001, pp. 263-264.
98. A. K. Agrahari, P. Bose, M. K. Jaiswal, S. Rajkhowa, A. S. Singh, S. Hotha, N. Mishra and V. K. Tiwari, *Chemical Reviews*, 2021, **121**, 7638-7956.
99. V. K. Tiwari, B. B. Mishra, K. B. Mishra, N. Mishra, A. S. Singh and X. Chen, *Chemical Reviews*, 2016, **116**, 3086-3240.
100. J. Elguero and I. Alkorta, *Molecules*, 2020, **25**, 5108.
101. J. Zheng, Z. Lu, K. Wu, G.-H. Ning and D. Li, *Chemical Reviews*, 2020, **120**, 9675-9742.
102. P. L. Golas, N. V. Tsarevsky and K. Matyjaszewski, *Macromolecular Rapid Communications*, 2008, **29**, 1167-1171.
103. S. Yoshida, A. Shiraishi and K. Kanno, *Scientific Reports*, 2011, **1**.
104. G. Chesnokov, M. Topchiy, P. Dzhevakov, P. Gribanov, A. Tukov, V. Khrustalev, A. Asachenko and M. Nechaev, *Dalton Transactions*, 2017, 4331-4345.
105. D. Parasar, T. T. Ponduru, A. Noonikara-Poyil, N. B. Jayaratna and H. V. R. Dias, *Dalton Trans.*, 2019, **48**, 15782-15794.
106. A. A. Titov, V. A. Larionov, A. F. Smol'yakov, M. I. Godovikova, E. M. Titova, V. I. Maleev and E. S. Shubina, *Chem. Commun.*, 2019, **55**, 290-293.
107. T. Furuya, A. Kamlet and T. Ritter, *Nature*, 2011, 470-477.
108. E. S. Bruce, *Journal of Fluorine Chemistry*, 2001, **109**, 3-11.
109. K. Fujisawa, T. Ono, Y. Ishikawa, N. Amir, Y. Miyashita, K.-i. Okamoto and N. Lehnert, *Inorganic Chemistry*, 2006, **45**, 1698-1713.
110. K. Fujisawa, Y. Masahiro, M. Yoshitaro and K.-i. Okamoto, *Polyhedron*, 2009, **28**, 1447-1454.
111. H. V. R. Dias and H.-L. Lu, *Inorganic Chemistry*, 1995, **34**, 5380-5382.
112. B. T. Worrell, V. V. Malik Ja Fau - Fokin and V. V. Fokin.
113. V. O. Rodionov, D. D. Presolski Si Fau - Díaz, V. V. Díaz Dd Fau - Fokin, M. G. Fokin Vv Fau - Finn and M. G. Finn.
114. B. F. Straub, *Chemical Communications*, 2007, 3868-3870.
115. L. Jin, D. R. Tolentino, M. Melaimi and G. Bertrand.
116. S. Neumann, M. Biewend, S. Rana and W. H. Binder, *Macromolecular Rapid Communications*, 2020, **41**, 1900359.
117. R. Berg and B. F. Straub, *Beilstein J. Org. Chem.*, 2013, **9**, 2715-2750.

`

118. Y. Fang, K. Bao, P. Zhang, H. Sheng, Y. Yun, S.-X. Hu, D. Astruc and M. Zhu, *Journal of the American Chemical Society*, 2021, **143**, 1768-1772.
119. H. V. R. Dias, S. A. Polach, S.-K. Goh, E. F. Archibong and D. S. Marynick, *Inorg. Chem.*, 2000, **39**, 3894-3901.
120. C. Dash, G. Wang, A. Muñoz-Castro, T. T. Ponduru, A. O. Zacharias, M. Yousufuddin and H. V. R. Dias, *Inorganic Chemistry*, 2020, **59**, 2188-2199.
121. V. O. Rodionov, V. V. Fokin and M. G. Finn, *Angewandte Chemie International Edition*, 2005, **44**, 2210-2215.
122. C. P. Seath, G. A. Burley and A. J. B. Watson, *Angewandte Chemie International Edition*, 2017, **56**, 3314-3318.
123. B. Venderbosch, J.-P. H. Oudsen, J. I. van der Vlugt, T. J. Korstanje and M. Tromp, *Organometallics*, 2020, **39**, 3480-3489.
124. A. Makarem, R. Berg, F. Rominger and B. F. Straub, *Angewandte Chemie International Edition*, 2015, **54**, 7431-7435.
125. H. Chen, C. Soubra-Ghaoui, Z. Zhu, S. Li, T. A. Albright and C. Cai, *Journal of Catalysis*, 2018, **361**, 407-413.
126. B. M. El-Zaatari, A. U. Shete, B. J. Adzima and C. J. Kloxin, *Physical Chemistry Chemical Physics*, 2016, **18**, 25504-25511.
127. M. A. Omary, J. J. Determan, C. S. Palehepitiya Gamage, P. Sinha, S. Li, M. R. Patterson, V. N. Nestero, A. K. Wilson and H. Rasika Dias, *Comments on Inorganic Chemistry*, 2020, **40**, 1-24.
128. B. Geffroy, P. le Roy and C. Prat, *Polymer International*, 2006, **55**, 572-582.
129. A. Chaskar, H.-F. Chen and K.-T. Wong, *Advanced Materials*, 2011, **23**, 3876-3895.
130. *Triplet Emitters for OLED Applications. Mechanisms of Exciton Trapping and Control of Emission Properties*, Springer Berlin Heidelberg, Berlin, Heidelberg, 2004.
131. D. Tanaka, H. Sasabe, Y. J. Li, S. J. Su, T. Takeda and J. Kido, *Japan Journal Applied Physics*, 2006, **46**, 10-12.
132. L. Xiao, S.-J. Su, Y. Agata, H. Lan and J. Kido, *Advanced Materials*, 2009, **21**, 1271-1274.
133. C. Adachi, M. A. Baldo, M. E. Thompson and S. R. Forrest, *Journal of Applied Physics*, 2001, **90**, 5048-5051.
134. M. A. Omary, R. M. Kassab, M. R. Haneline, O. Elbjeirami and F. P. Gabbaï, *Inorganic Chemistry*, 2003, **42**, 2176-2178.
135. C. Burress, O. Elbjeirami, M. A. Omary and F. P. Gabbaï, *Journal of the American Chemical Society*, 2005, **127**, 12166-12167.
136. C. Stoffers, S. Yang, F. Zhang, S. M. Jacobsen, B. K. Wagner and C. J. Summers, *Applied Physics Letters*, 1997, **71**, 1759-1761.
137. O. Elbjeirami, M. A. Rawashdeh-Omary and M. A. Omary, *Research on Chemical Intermediates*, 2011, **37**, 691.
138. M. Ikai, S. Tokito, Y. Sakamoto, T. Suzuki and Y. Taga, *Applied Physics Letters*, 2001, **79**, 156-158.
139. C. Adachi, M. A. Baldo, S. R. Forrest and M. E. Thompson, *Applied Physics Letters*, 2000, **77**, 904-906.

`

140. M. A. Baldo, M. E. Thompson and S. R. Forrest, *Pure and Applied Chemistry*, 1999, **71**, 2095--2106.
141. X. Gong, M. R. Robinson, J. C. Ostrowski, D. Moses, G. C. Bazan and A. J. Heeger, *Advanced Materials*, 2002, **14**, 581-585.
142. S. C. Lo, N. A. H. Male, J. P. J. Markham, S. W. Magennis, P. L. Burn, O. V. Salata and I. D. W. Samuel, *Advanced Materials*, 2002, **14**, 975-979.
143. S. Welter, K. Brunner, J. W. Hofstraat and L. De Cola, *Nature*, 2003, **421**, 54-57.
144. T. J. Meyer, *Accounts of Chemical Research*, 1989, **22**, 163-170.
145. F. Li, M. Zhang, J. Feng, G. Cheng, Z. Wu, Y. Ma, S. Liu, J. Sheng and S. T. Lee, *Applied Physics Letters*, 2003, **83**, 365-367.
146. M. Yuguang, Z. Houyu, S. Jiacong and C. Chiming, *Synthetic Metals*, 1998, **94**, 245-248.
147. X. Jiang, A. K. Y. Jen, B. Carlson and L. R. Dalton, *Applied Physics Letters*, 2002, **81**, 3125-3127.
148. M. A. Baldo, D. F. O'Brien, Y. You, A. Shoustikov, S. Sibley, M. E. Thompson and S. R. Forrest, *Nature*, 1998, **395**, 151-154.
149. G. E. Jabbour, J. F. Wang and N. Peyghambarian, *Applied Physics Letters*, 2002, **80**, 2026-2028.
150. A. Laguna and M. Laguna, *Coordination Chemistry Reviews*, 1999, **193-195**, 837-856.
151. H. Schmidbaur and A. Schier, *Chemical Society Reviews*, 2012, **41**, 370-412.
152. V. Wing-Wah Yam and K. Kam-Wing Lo, *Chemical Society Reviews*, 1999, **28**, 323-334.
153. K. Barakat and T. R. Cundari, *Chemical Physics*, 2005, **311**, 3-11.
154. K. A. Barakat, T. R. Cundari and M. A. Omary, *Journal of the American Chemical Society*, 2003, **125**, 14228-14229.
155. M. Hashimoto, S. Igawa, M. Yashima, I. Kawata, M. Hoshino and M. Osawa, *Journal of the American Chemical Society*, 2011, **133**, 10348-10351.
156. J. Zhang, C. Duan, C. Han, H. Yang, Y. Wei and H. Xu, *Advanced Materials*, 2016, **28**, 5975-5979.
157. D. M. Zink, M. Bächle, T. Baumann, M. Nieger, M. Kühn, C. Wang, W. Klopper, U. Monkowius, T. Hofbeck, H. Yersin and S. Bräse, *Inorganic Chemistry*, 2013, **52**, 2292-2305.
158. A. Schinabeck, J. Chen, L. Kang, T. Teng, H. H. H. Homeier, A. F. Suleymanova, M. Z. Shafikov, R. Yu, C.-Z. Lu and H. Yersin, *Chemistry of Materials*, 2019, **31**, 4392-4404.
159. Y. Li, Z. Li, Y. Hou, Y.-N. Fan and C.-Y. Su, *Inorganic Chemistry*, 2018, **57**, 13235-13245.
160. Y. Zhang, M. Schulz, M. Wächtler, M. Karnahl and B. Dietzek, *Coordination Chemistry Reviews*, 2018, **356**, 127-146.
161. S. Keller, F. Brunner, J. M. Junquera-Hernández, A. Pertegás, M.-G. La-Placa, A. Prescimone, E. C. Constable, H. J. Bolink, E. Ortí and C. E. Housecroft, *ChemPlusChem*, 2018, **83**, 217-229.
162. S. Keller, A. Prescimone, E. C. Constable and C. E. Housecroft, *Photochemical & Photobiological Sciences*, 2018, **17**, 375-385.

`

163. M. Alkan-Zambada, S. Keller, L. Martínez-Sarti, A. Prescimone, J. M. Junquera-Hernández, E. C. Constable, H. J. Bolink, M. Sessolo, E. Ortí and C. E. Housecroft, *Journal of Materials Chemistry C*, 2018, **6**, 8460-8471.
164. M. Washimi, M. Nishikawa, N. Shimoda, S. Satokawa and T. Tsubomura, *Inorganic Chemistry Frontiers*, 2017, **4**, 639-649.
165. D. Kakizoe, M. Nishikawa, Y. Fujii and T. Tsubomura, *Dalton Transactions*, 2017, **46**, 14804-14811.
166. H. Yersin, *Journal*, 2019.
167. V. Wing-Wah Yam, E. Chung-Chin Cheng and N. Zhu, *Chemical Communications*, 2001, 1028-1029.
168. Y. Sun, S. Zhang, G. Li, Y. Xie and D. Zhao, *Transition Metal Chemistry*, 2003, **28**, 772-776.
169. Q. Benito, X. F. Le Goff, G. Nocton, A. Fargues, A. Garcia, A. Berhault, S. Kahlal, J.-Y. Saillard, C. Martineau, J. Trébosc, T. Gacoin, J.-P. Boilot and S. Perruchas, *Inorganic Chemistry*, 2015, **54**, 4483-4494.
170. D. Li, Q. Feng, X.-L. Feng and J.-W. Cai, *Inorganic Chemistry Communications*, 2003, **6**, 361-364.
171. K. R. Kyle and P. C. Ford, *Journal of the American Chemical Society*, 1989, **111**, 5005-5006.
172. K. R. Kyle, J. DiBenedetto and P. C. Ford, *Journal of the Chemical Society, Chemical Communications*, 1989, 714-715.
173. K. R. Kyle, W. E. Palke and P. C. Ford, *Coordination Chemistry Reviews*, 1990, **97**, 35-46.
174. K. R. Kyle, C. K. Ryu, P. C. Ford and J. A. DiBenedetto, *Journal of the American Chemical Society*, 1991, **113**, 2954-2965.
175. A. Dossing, C. K. Ryu, S. Kudo and P. C. Ford, *Journal of the American Chemical Society*, 1993, **115**, 5132-5137.
176. M. Vitale, C. K. Ryu, W. E. Palke and P. C. Ford, *Inorganic Chemistry*, 1994, **33**, 561-566.
177. P. C. Ford, *Coordination Chemistry Reviews*, 1994, **132**, 129-140.
178. J. A. Simon, W. E. Palke and P. C. Ford, *Inorganic Chemistry*, 1996, **35**, 6413-6421.
179. P. C. Ford, E. Cariati and J. Bourassa, *Chemical Reviews*, 1999, **99**, 3625-3648.
180. M. Vitale and P. C. Ford, *Coordination Chemistry Reviews*, 2001, **219-221**, 3-16.
181. M. J. Leitl, V. A. Krylova, P. I. Djurovich, M. E. Thompson and H. Yersin, *Journal of the American Chemical Society*, 2014, **136**, 16032-16038.
182. M. A. Omary, P. Sinha, P. S. Bagus and A. K. Wilson, *The Journal of Physical Chemistry A*, 2005, **109**, 690-702.
183. J. J. Determan, M. A. Omary and A. K. Wilson, *The Journal of Physical Chemistry A*, 2011, **115**, 374-382.
184. J. J. Determan, P. Sinha, A. K. Wilson and M. A. Omary, *The Journal of Physical Chemistry C*, 2015, **119**, 7541-7541.
185. P. Pyykkö, *Chemical Reviews*, 1997, **97**, 597-636.

`

186. M. Wrighton and D. L. Morse, *Journal of the American Chemical Society*, 1974, **96**, 998-1003.
187. P. J. Giordano, S. M. Fredericks, M. S. Wrighton and D. L. Morse, *Journal of the American Chemical Society*, 1978, **100**, 2257-2259.
188. S. M. Fredericks, J. C. Luong and M. S. Wrighton, *Journal of the American Chemical Society*, 1979, **101**, 7415-7417.
189. R. Hamze, S. Shi, S. C. Kapper, D. S. Muthiah Ravinson, L. Estergreen, M.-C. Jung, A. C. Tadle, R. Haiges, P. I. Djurovich, J. L. Peltier, R. Jazzar, G. Bertrand, S. E. Bradforth and M. E. Thompson, *Journal of the American Chemical Society*, 2019, **141**, 8616-8626.
190. R. Hamze, L. Peltier Jesse, D. Sylvinson, M. Jung, J. Cardenas, R. Haiges, M. Soleilhavoup, R. Jazzar, I. Djurovich Peter, G. Bertrand and E. Thompson Mark, *Science*, 2019, **363**, 601-606.
191. Y. Nakayama, H. Inagi and M. Zhang, *Journal of Applied Physics*, 1999, **86**, 768-773.
192. J. Thomas, J. John, N. Parekh and W. Dehaen, *Angewandte Chemie International Edition*, 2014, **53**, 10155-10159.
193. G. Sheldrick, *Acta Crystallogr. Sect. C: Struct. Chem.*, 2015, **71**, 3-8.
194. O. V. Dolomanov, L. J. Bourhis, R. J. Gildea, J. A. K. Howard and H. Puschmann, *J. Appl. Crystallogr.*, 2009, **42**, 339-341.
195. A. Maspero, G. B. Giovenzana, D. Monticelli, S. Tagliapietra, G. Palmisano and A. Penoni, *Journal of Fluorine Chemistry*, 2012, **139**, 53-57.
196. F. Sebest, K. Lachhani, C. Pimpasri, L. Casarrubios, A. J. P. White, H. S. Rzepa and S. Díez-González, *Advanced Synthesis & Catalysis*, 2020, **362**, 1877-1886.
197. G. K. S. Prakash, M. A. Stephenson, J. G. Shih and G. A. Olah, *The Journal of Organic Chemistry*, 1986, **51**, 3215-3217.
198. M. J. Frisch, G. W. Trucks, H. B. Schlegel, G. E. Scuseria, M. A. Robb, J. R. Cheeseman, G. Scalmani, V. Barone, B. Mennucci and G. A. Petersson, *Journal*, 2009.
199. A. D. Becke, *The Journal of Chemical Physics*, 1993, **98**, 5648-5652.
200. J. P. Perdew, *Unified theory of exchange and correlation beyond the local density approximation*, Akademie Verlag, Berlin, Germany, 1991.
201. K. Burke, J. P. Perdew and Y. Wang, *Derivation of a Generalized Gradient Approximation: The PW91 Density Functional.*, Plenum, New York, 1998.
202. J. P. Perdew, J. A. Chevary, S. H. Vosko, K. A. Jackson, M. R. Pederson, D. J. Singh and C. Fiolhais, *Physical Review B*, 1993, **48**, 4978-4978.
203. J. P. Perdew, K. Burke and M. Ernzerhof, *Physical Review Letters*, 1996, **77**, 3865-3868.
204. G. Herzberg, *Journal*, 1950, **1**.
205. P. J. Hay and W. R. Wadt, *The Journal of Chemical Physics*, 1985, **82**, 270-283.
206. M. Couty and M. B. Hall, *Journal of Computational Chemistry*, 1996, **17**, 1359-1370.

`

207. M. M. Francl, W. J. Pietro, W. J. Hehre, J. S. Binkley, M. S. Gordon, D. J. DeFrees and J. A. Pople, *The Journal of Chemical Physics*, 1982, **77**, 3654-3665.